Universitat de Girona

IMPLEMENTATION OF A HIGH-PRESSURE RESIN TRANSFER MOLDING (HP-RTM) PROCESS TO INCREASE THE PRODUCTION RATE OF STRUCTURAL COMPOSITES AND CHARACTERIZATION OF SUSTAINABLE VITRIMER-MATRIX HIGH-PERFORMANCE COMPOSITES

Cristian Builes Cárdenas

Universitat de Girona

Doctoral Thesis

IMPLEMENTATION OF A HIGH-PRESSURE RESIN TRANSFER MOLDING (HP-RTM) PROCESS TO INCREASE THE PRODUCTION RATE OF STRUCTURAL COMPOSITES AND CHARACTERIZATION OF SUSTAINABLE VITRIMER-MATRIX HIGH-PERFORMANCE COMPOSITES

by

Cristian Builes Cárdenas

2022

eurecat
Centre Tecnològic de Catalunya

Doctoral Thesis

IMPLEMENTATION OF A HIGH-PRESSURE RESIN TRANSFER MOLDING (HP-RTM) PROCESS TO INCREASE THE PRODUCTION RATE OF STRUCTURAL COMPOSITES AND CHARACTERIZATION OF SUSTAINABLE VITRIMER-MATRIX HIGH-PERFORMANCE COMPOSITES

by

Cristian Builes Cárdenas

2022

Doctoral Program in Technology

supervised by

Dr. Josep Costa Balanzat and Dr. Daniel Casellas Padró

Thesis submitted to the University of Girona for the degree of Doctor of Philosophy

Para mi team: María, Fran y Juan Carlos

¡Gracias por tanto!

Para mis padres

Acknowledgements

All the work presented in this thesis was conducted in Eurecat, *Centre Tecnològic de Catalunya* (Department of Composite Materials) in Cerdanyola del Vallès, Barcelona, Spain. This thesis was part of the "*Vicente López*" industrial Ph.D. grant program funded by Eurecat in 2019. This work was financially supported by the Catalan Government (*Generalitat de Catalunya*) through the funding grant ACCIÓ-Eurecat projects: PRIV MARIETA 2.0 (2018-2020) "*Desenvolupament d'una nova tecnologia d'injecció de resina d'alta pressió i alta productivitat per la fabricació de components lleugers d'alta resistència mecànica 2.0".* And PRIV MARIETA 4.0 (2020-2022) "*Desenvolupament d'una nova tecnologia d'injecció de resina d'alta pressió i alta productivitat per la fabricació de components lleugers. Adaptació de la tecnologia a línia de producció a escala laboratori".*

Part of this thesis was financially supported by the EU Horizon 2020 research and innovation project AIRPOXY "thermoformAble, repaIrable and bondable smart ePOXY-based composites for aero structures" with grant agreement 769274 under the H2020-MG-2017-Two-Stage call.

To my advisors Dr. Josep Costa Balanzat and Dr. Daniel Casellas Padró for all their guidance, kindness, patience and knowledge. Thanks to them, I always could find the north in all the uncertainties presented in this thesis. "*Us agraeixo molt per totes les vostres paraules de suport i tot el temps que han estat al meu costat donant-me ànims i guia. Sense vosaltres, aquest no hauria estat possible."*

To the Composite Materials department of Eurecat for bringing me in and allowing me to grow as a professional and as a person, thanks to all the knowledge imparted during these 4 years. Thanks to Ma. Eugenia Rodriguez for allowing me to develop this thesis under an industrial environment, it was a privilege to work in this unit. "*Agradezco infinitamente a mis compañeros y amigos de composites, especialmente a Ángel Bermúdez, Nuria "Nurieta" Latorre, Vincent Gayraud, Ronan Lecouche, Francisco Lanzas, Juan Carlos Pérez y Victor Reinao, de quienes aprendí mucho y quienes estuvieron ahí en momentos de alegría, tristeza y hasta de sustos, echo de menos vuestra compañía. Y a todas las personas maravillosas que conocí durante estos 4 años: Daniel S, Jeannette, Valentina, Aitana, Irangeli y Vicenç."*

To all the Eurecat staff involved in the MARIETA projects and which helped me a lot and from who I learned a lot during these years. "*Un agraïment molt especial per Arcadi Castanyer, quin es un dels mes "cracks" de tot Eurecat: moltes gràcies maco per tota la teva ajuda i paciència amb la maquina i amb la meva persona, et dec aquesta vida i un altre. I a totes les persones involucrades en el projecte: Oscar Martí, Raquel Busqué, Albert Brigido, i totes les unitats implicades: direcció científica, robòtica, desenvolupament de producte i simulació, teixits funcionals, manufactura avançada AMS i scouting".*

To all the amazing, lovely and beautiful people that I met during my years in Eurecat: Fran Fernández, Maite Iriondo, Carlos Espinar, Adrià Llausàs, Emir Ben, Silvia Cruz, Manel DaSilva, Nekane Lozano, Enric Pascual, Enric Fontdecaba, Germán Pérez, Carles Rubio, Iuliana Constantin, Carles Moreu, Cristina Balcells, Ilef Tarhouni, Oscar Caramanza, Javier Ardanuy, Felix Torres, Rubén Ruiz and many more.

To Dr. Maria Ariño Palacín. "*Maria mi gran supervisora, compañera y amiga, y a quien debo mucho de lo que soy como profesional de los composites y de la investigación. Millones y millones de gracias por estar siempre ahí en las buenas y en las malas, por hacerme sentir un miembro más del quipo desde el minuto cero, por escucharme y por todas las horas que has pasado dándome consejos y ayuda. Por hacerme sentir siempre en casa y por convertirte en uno de los mayores referentes de mi carrera, te has convertido casi en una hermana mayor para mi y espero algún día llegar a ser tan grande como tú.*"

To Iván Sánchez Gómez. "*Ivan, mi otro gran supervisor y compañero. Muchas gracias por estar pendiente siempre de mi tesis y por involúcrate tanto en el desarrollo de la misma, ha sido un placer trabajar con una persona tan profesional y tan dedicada como tú. Eskerrik asko.*"

To Anni Lahti and Marc Valldeperes. "*Anni, Marc. Le estoy infinitamente agradecido a la vida por haberlos conocido. Mil gracias por abrirme vuestros corazones y vidas, por tantos momentos que pasamos en Castellbisbal, Cerdanyola, en todo el Vallès Occidental y en Catalunya. Gracias por hacerme un miembro más de vuestra familia y por compartir vuestro amor gatuno conmigo. Os adoro y extraño cada día. Os dedico a vosotros y a las rapaciñas Clara y Olivia, esta tesis. Kiitos paljon, moltes gràcies.*"

To my family. "*A mis padres María y Sigifredo quienes siempre se han sacrificado por mi futuro y por mi bienestar, a quienes debo y dedico toda mi trayectoria profesional. A quienes dejé atrás hace más de 5 años y a más 8000 km de distancia para perseguir mi futuro y quienes me apoyaron siempre, y que a pesar de la distancia siempre están ahí apoyándome y deseando lo mejor para mí. A mi hermano Andrés, Heidy y a mis sobrinos Jacob y Sebastián. A mi tía Dora y primos Juan Pablo, Diego y Santiago*"

To Dr. Francisco Restrepo "*Pacho cohetes*" and Dr. Julián Sierra who inspired me to follow this path.

Publications

Here are listed the publications generated during this thesis development:

Peer-reviewed journal articles:

- Builes Cárdenas, C.; Gayraud, V.; Rodriguez, M.E.; Costa, J.; Salaberria, A.M.; Ruiz de Luzuriaga, A.; Markaide, N.; Dasan Keeryadath, P.; Calderón Zapatería, D. Study into the Mechanical Properties of a New Aeronautic-Grade Epoxy-Based Carbon-Fiber-Reinforced Vitrimer. *Polymers* 2022, 14, 1223. https://doi.org/10.3390/polym14061223

It's planned to generate more publications regarding the development of the HP-RTM machine and mold, and the mechanical characterization of the materials produced by it.

Acronyms

OEM's	Original Equipment Manufacturers
CFRP	Carbon Fiber Reinforced Polymers
OoA	Out of Autoclave
HP-RTM	High-Pressure Resin Transfer Molding
DEA	Dielectric Analysis
EU	European Union
USA	United Stated of America
LRI	Liquid Resin Infusion
RTM	Resin Transfer Molding
EoL	End of Life
GFRP	Glass fiber reinforced polymers
SRIM	Structural Reaction Injection Molding
PU	Polyurethane
HP-IRTM	High-Pressure Injection Resin Transfer Molding
HP-CRTM	High-Pressure Compression Resin Transfer Molding
FVF	Fiber Volumetric Fraction
T-RTM	Thermoplastic Resin Transfer Molding
PA - PA6	Polyamide - Polyamide 6
RMCP	Rapid Multi-Injection Composite Process
NCF	Non-Crimp Fabric
LCM	Liquid Composite Molding
DBVI	Double Bag Vacuum Infusion
VAP	Vacuum Assisted Process
CAPRI	Controlled Atmospheric Pressure Resin Infusion
ILSS	Interlaminar Shear Strength
CAN's	Covalent Adaptative Networks
4-AFD	4-Aminophenyl disulfide
DGEBA	Diglycidyl Ether of Bisphenol A
DETDA 2	Diethyltoluenediamine
Vurea	Vinylogous Urea
PHT	Polyhexahydrotriazine
BAPP	2,2-bis4-4-aminophenoxyphenylpropane
BMI	Bismaleimide
THF	Tetrahydrofuran
HCl	Hydrochloric acid
HMTA	Hexamethylenetetramine
BPA	Bisphenol A
EDA	Ethylenediamine
GA	Glutaric Anhydride
MSMEV	Multi-shape Memory Epoxy Vitrimer
DGEBF	Diglycidyl Ether of Bisphenol F
APTS	γ-Aminopropyltriethoxysilane
D2000	Poly(propylene glycol) bis(2-aminopropyl ether)
PACM	diamine 4,4'-methylenebiscyclohexanamine
EIA	Itaconic acid-based Epoxy
MA	Maleic Anhydride

ESO	Epoxidized Soybean Oil
VA	Vanillin 4-Aminophenol
Gte	Glycerol Triglycidyl Ether
Van-H-OH	Vanillin + 1,6-hexylenediamime
Van-MOH	Vanillin + m-xylylenediamine
VARTM	Vacuum Assisted Resin Transfer Molding
AMS	Advanced Manufacturing Systems
5HS	5-harness satin woven
CP	Cross-ply configuration
UD	Unidirectional fabric
RT	Room temperature
RH	Relative humidity
HW70	Preconditioning until equilibrium at 70°/85% RH, testing at 70°
HW120	Preconditioning until equilibrium at 70°/85% RH, testing at 120°
PBS	Percent Bending Strain
IPS	In-Plane Shear
OHT	Open Hole Tension
OHC	Open Hole Compression
FHC	Filled Hole Compression
G_{IC}	Mode I interlaminar fracture toughness
G_{IIC}	Mode II interlaminar fracture toughness
DSC	Differential Scanning Calorimetry
TMM	Tool-mountable monotrode
AMS	Advanced Manufacturing Systems

Contents

List of figures

List of tables

Abstract

Transport industry, especially automotive, is one of the most pollutant in the world. Current environmental concerns demand original equipment manufacturers (OEM's) to reduce the amount of emissions released by their vehicles, requiring more green alternatives to mobility.

By reducing the overall vehicle weight, it will be diminished the total amount of pollution for conventional combustion engine vehicles, or increase the autonomy of electric – hybrid vehicles, being the carbon fiber reinforced polymers (CFRP) the best option to reduce overall structural weight.

Thermoset CFRP offer many advantages over traditional automotive materials as steel or aluminum due to their high mechanical strength, high chemical and thermal resistance, dimensional stability and high durability under harsh conditions. But production of high performance CFRP has been limited to time and energy consuming methods as autoclave. Out of autoclave (OoA) solutions as RTM have become interesting manufacturing processes, being cheaper and presenting energetical, economical and logistics savings in comparison.

However, these OoA processes have limitations as long cycle times (specially filling and curing times), limiting the use of high-reactivity resins and making these processes unreliable to be considered for high-volume industries as the automotive, which needs very short cycle times (≈5 minutes). Other process steps as preforming or mold preparation also are time consuming, in which automation becomes a key factor to reduce overall processing time.

Moreover, CFRP are very expensive compared with traditional materials, as the raw fibers alone represent almost half of the total component cost, requiring high-volume manufacturing alternatives to overcome this issue. Furthermore, the current demand of CFRP structures is creating concerns about the amount of waste that these materials would generate in the future, as thermoset polymers are very complex to recycle. Separating the fibers from the matrix implies damaging the reinforcement and reducing their mechanical properties. In addition to current disposal solutions also implying environmental and economic concerns.

This thesis aims to explore the high-pressure resin transfer molding process (HP-RTM) as a feasible alternative to produce high performance CFRP in short cycle times. Additionally, it is complemented by using a new high-performance vitrimer polymer that presents thermoset-like performance while being reprocessable, reconformable and recyclable.

In order to achieve this objective, first this work describes the design parameters, initial set-up and modifications of a proprietary HP-RTM prototype machine, built for high-speed processing. This study also embraces the design of an HP-RTM mold. CFRP are manufactured and characterized by testing different process parameters to evaluate their influence over the mechanical performance. Besides, we implement real-time monitoring of the injection process using on-line cavity pressure sensors and dielectric analysis (DEA) curing sensors, comparing the results with conventional RTM process.

Additionally, we describe the complete mechanical characterization of a new high-performance vitrimer formulation based on disulfide exchange reactions, designed to compete with current and widely used aeronautic thermoset resin formulations. Both vitrimer and aeronautical thermoset composites are processed by base RTM process and HP-RTM process.

Mechanical results indicate that the HP-RTM process improves the mechanical performance of CFRP, compared with base RTM process. Also reducing the injection and curing times, when curing at high temperature. The vitrimer characterization indicate that this formulation is mechanically equivalent to the current aeronautic thermoset resins. Therefore, it can be used as a matrix for high-performance composites, also presenting improvements when processed with the HP-RTM process in comparison with base RTM process.

Resumen

La industria del transporte, especialmente la automotriz, es una de las más contaminantes en el mundo. Las crecientes demandas medioambientales están haciendo que los principales fabricantes del sector (OEM's) reduzcan la cantidad de emisiones que producen sus vehículos, requiriendo alternativas más sostenibles para la movilidad.

Reducir el peso de los vehículos aminoraría la cantidad total de contaminantes que son emitidos a la atmosfera, en vehículos de combustión interna, o incrementaría la autonomía de vehículos híbridos o eléctricos, siendo los materiales compuestos reforzados por fibra de carbono (CFRP) la mejor opción para hacerlo.

Los materiales compuestos termoestables de fibra de carbono ofrecen muchas ventajas con respecto a materiales tradicionales de la industria automotriz, como el acero o el aluminio, gracias a su alta resistencia mecánica, resistencia química y térmica, estabilidad dimensional y alta durabilidad bajo condiciones severas. Pero la producción de materiales compuestos de alto rendimiento (CFRP) ha estado limitada por el uso de métodos con un alto consumo de tiempo y recursos como el autoclave. Alternativas fuera de autoclave (OoA) como el proceso de inyección de resina (RTM), se han convertido en procesos de manufactura de alto interés, gracias a sus ventajas sobre el consumo energético y su eficiencia logística, en comparación con el autoclave.

Sin embargo, estos métodos presentan limitaciones, como tiempos elevados de procesado (llenado y curado). Limitando así la implementación de resinas de alta reactividad, y haciéndolos poco interesantes para industrias con altos volúmenes de producción como la automotriz, que maneja tiempos de procesado muy cortos (≈5 minutos). Otras etapas del proceso como el preformado la preparación el molde también consumen tiempo, en estas la automatización se vuelve un factor necesario para reducir el tiempo total de proceso.

Además, los materiales compuestos de fibra de carbono son muy costosos si se comparan con materiales tradicionales. Las fibras mismas representan casi la mitad del coste total de los componentes, requiriendo de alternativas de producción con un alto volumen para contrarrestarlo. Es más, la creciente demanda de estos materiales incrementa las preocupaciones sobre la cantidad de desperdicios que se generarán en el futuro, ya que los materiales compuestos termoestables son muy difíciles de reciclar. Separar las fibras de la matriz implica daños en su estructura, reduciendo su resistencia mecánica. Adicionalmente, los procesos de reciclado actuales también crean inconvenientes medioambientales y económicos.

Esta tesis pretende explorar el proceso de inyección de resina a alta presión (HP-RTM) como una alternativa viable para la producción de materiales compuestos de alto rendimiento, en tiempos de procesado cortos. Adicionalmente, se complementa con el uso de un nuevo polímero vitrimérico de alto rendimiento, que combina la alta resistencia de los compuestos termoestables, con la reprocesabilidad, la reconformabilidad y la reciclabilidad.

Para cumplir este objetivo, primero describimos los parámetros de diseño, la puesta a punto y las modificaciones de un prototipo de maquina HP-RTM, creada para el procesado de materiales a alta velocidad. Este estudio también contiene el diseño de un molde apto para HP-RTM. Los materiales compuestos son fabricados y caracterizados probando diferentes parámetros de proceso para evaluar sus efectos sobre las propiedades mecánicas. Además, implementamos el

monitoreo en tiempo real del proceso de inyección usando sensores de presión y sensores dieléctricos (DEA) de curado, comparando los resultados con el proceso RTM convencional.

Adicionalmente presentamos la caracterización mecánica completa de una nueva formulación de vitrímero de alto rendimiento basado en reacciones de intercambio de disulfuros, diseñado para competir con las opciones actuales de resinas termoestables para el sector aeronáutico. Tanto los compuestos vitriméricos como los termoestables son fabricados mediante el proceso RTM base y el proceso HP-RTM.

Los resultados mecánicos indican que el proceso HP-RTM mejora el comportamiento mecánico de los compuestos de fibra de carbono, en comparación con el RTM base. Reduciendo adicionalmente los tiempos de inyección y de curado, cuando son implementados a alta temperatura. La caracterización del vitrímero indica que esta formulación es mecánicamente equiparable a su contraparte termoestable aeronáutica. Por tanto, pudiendo ser usada como matriz para materiales compuestos de alto rendimiento, adicionalmente presentando mejoras cuando se procesa mediante HP-RTM, en comparación con RTM.

Demostramos la capacidad del proceso HP-RTM para fabricar materiales compuestos con alta capacidad estructural, en tiempos de fabricación aceptables para la industria automotriz. Además de las ventajas de los materiales compuestos vitriméricos frente a los materiales compuestos termoestables tradicionales, ofreciendo nuevas posibilidades para un futuro más sostenible.

Resum

La indústria del transport, especialment l'automotriu és una de les més contaminants del món. Les creixents exigències mediambientals estan fent que els principals fabricants del sector (OEM's) redueixin la quantitat d'emissions que produeixin els seus vehicles, demandant alternatives més sostenibles para la mobilitat.

Reduir el pes dels vehicles minoraria la quantitat de contaminants que són emesos cap a l'atmosfera, en vehicles de combustió interna, o incrementaria l'autonomia dels vehicles híbrids o elèctrics, sent els materials compostos reforçats mitjanament fibra de carboni (CFRP) la millor opció per fer-ho.

Els materials compostos termoestables de fibra de carboni ofereixen molts avantatges respecte a materials tradicionals de la indústria automotriu, com l'acer o l'alumini, gràcies a la seva alta resistència mecànica, resistència química i tèrmica, estabilitat dimensional i alta durabilitat sota condicions severes. Però la producció de materials compostos d'alt rendiment (CFRP) han estat limitats per al ús de mitjans amb un alt consum de temps i recurs com l'autoclau. Alternatives fora d'autoclau com el procediment d'injecció de resina (RTM), s'han convertit en processos d'un alt interès, gràcies a els seus avantatges sobre el consum elèctric i la seva eficiència logística, en comparació amb l'autoclau.

No obstant això, aquests mètodes presenten limitacions, com temps de processament (ompliment i curat). Limitant així la implementació de resines d'alta reactivitat, fent-los poc interessants per a indústries amb elevats volums de producció com l'automotriu, que té temps de processament molt curts (≈5 minuts). Altres etapes de la manufactura com el preformat o la preparació del motlle també consumeixen temps, en aquestes, l'automatització es torna un factor necessari per a reduir el temps total del procediment.

Addicionalment, els materials compostos de fibra de carboni són molt cars, si són comparats amb materials tradicionals. Les fibres mateixes representen gairebé la meitat del cost total dels components, necessitant alternatives de producció amb una alta capacitat per contrarestar-ho. A més, la creixent demanda de aquests materials incrementa les preocupacions sobre la quantitat de rebuig que es produiran cap al futur, ja que els materials compostos termoestables són molt complicats de reciclar. La separació de les fibres respecte a la matriu implica danys en la seva estructura, reduint la seva resistència mecànica. Altrament, els processes de reciclatge actuals també generen inconvenients mediambientals i econòmics.

Aquesta tesi pretén explorar el procediment d'injecció de resina a alta pressió (HP-RTM) com una alternativa viable per a la introducció dels materials compostos d'alt rendiment, en temps de fabricació curts. A més a més, es complementa amb l'ús d'un nou polímer vitriméric d'alt rendiment, que combina l'alta resistència mecànica dels compostos termoestables, amb la reprocessabilitat, la comformabilitat i la reciclabilitat.

Per complir aquest objectiu, primer descrivim els paràmetres de disseny, la posta a punt i les modificacions d'un prototip de màquina HP-RTM, feta per a la fabricació de materials a alta velocitat. Aquest estudi també conté el disseny d'un motlle per HP-RTM. Els materials compostos són fabricats i caracteritzats provant diferents paràmetres de processament, per avaluar els seus efectes sobre les propietats mecàniques. A més, implementem el monitoratge

en temps real del procediment d'injecció fent ús de sensors de pressió i sensors dielèctrics (DEA) de curat, comparant els resultats amb el procediment d'injecció RTM convencional.

Addicionalment, presentem la caracterització mecànica completa d'una nova formulació de vitrímer d'alt rendiment basat en reaccions d'intercanvi de disulfurs, dissenyada per competir amb les opcions actuals de resines termoestables per al sector aeronàutic. Tant els compostos vitrimérics com els termoestables són fabricats mitjanament el procediment RTM base i el procediment HP-RTM.

Els resultats mecànics indiquen que el procediment HP-RTM millora el comportament mecànic dels materials compostos de fibra de carboni, en comparació amb el RTM base. Reduint addicionalment els temps d'injecció i curat, quant són implementats a alta temperatura. La caracterització del vitrímer indica que aquesta formulació és mecànicament comparable amb la seva contrapart termoestable aeronàutica. Per tant, podent ser usada com a matriu per a materials compostos d'alt rendiment, addicionalment presentant millores quan es processa mitjanament HP-RTM, en comparació amb el RTM.

Hem demostrat la capacitat del procediment HP-RTM per a la fabricació de materials compostos amb una alta capacitat estructural, en temps de fabricació acceptables per a la indústria automotriu. A més dels avantatges dels materials compostos vitrimérics en comparació amb els materials compostos termoestables tradicional, oferint noves oportunitats per a un futur més sostenible.

Chapter 1: Introduction

1.1. Background

Transport industry, specially automotive is one of the most pollutant, generating up to one quarter of the global CO_2 emissions [1], and representing up to one eight of the European Union (EU) emissions. For this, different governmental entities as the U.S.A. government or the European commission have been imposing regulations to the OEM's to reduce the total amount of CO_2 produced by their vehicles, with regulations on maximum emissions ranging from 130 g/km in 2015, 95 g/km in 2020 and an expected 60 g/km by 2025 [2]–[5]. The use of lighter materials will help to reduce the amount of pollutants emitted in conventional combustion engine vehicles, or increase the autonomy in electric/hybrid vehicles. A 7% of weight loss in vehicles could be achieved only by optimizing the vehicle structure, between 30% and 50% using lighter metal alloys as aluminum, and up to 70% could be achieved using composite materials as carbon fiber reinforced polymers (CFRP) [6]–[9]. This necessity is creating a demand of lightweight materials for automotive applications, implying a market increase of US $400 billion by 2030, representing an annual growth around 5% [10], [11].

Specifically, CFRP market was projected to grow 9.9% annually at the 2015-2020 period with the automotive industry becoming one of the most promising drivers for the carbon composite materials market [3], as displayed in Figure 1.1. The CFRP demand is concentrated mostly in regions as North America, Europe and Asia pacific, where Europe alone represents a 29% of the global demand. Other important sectors for the CFRP market are aerospace, wind turbine/energy sector, storage tanks and sports equipment [11]. Between the CFRP composites, thermosets represent a 80% of the total production due to their high-mechanical strength, high-chemical and thermal resistance, dimensional stability and high durability under aggressive conditions, replacing more traditional materials such as steel, aluminum and other metal alloys [11]–[14].

Figure 1.1. Building line for the BMW i3, a passenger car with a carbon fiber structure. [15]

Traditional manufacturing techniques for high-performance composites as autoclave present issues as the high-cost required for its operation, regarding energy consumption, required infrastructure and long manufacturing times [16], something that few industries are able to

manage, as the aerospace sector. Out of autoclave (OoA) techniques as liquid resin infusion (LRI) or resin transfer molding (RTM) have become interesting options due to their capacity to obtain cheaper composite parts in lesser times [17], [18], having low power requirements and logistic and material savings [19], [20]. Particularly, RTM stands out in the OoA process by having low capital investment, low operational cost, low exposure to volatiles compared with prepregs, final parts with tight dimensional tolerances, good surface finish in both sides of the component and the possibility to achieve high-fiber volume fractions, which implies better mechanical properties. [9]

1.2. Motivations

High-performance carbon fiber thermoset composite materials offer advantages as high mechanical strength and design flexibility, while having a very low weight compared with traditional automotive materials but presenting some disadvantages.

Component cost is one of the most important barriers for the CFRP implementation in the automotive industry, representing an increment up to ten times the cost of traditional materials [12], thus limiting the use of CFRP only for premium/luxury car makers [21], [22]. In addition, an important part of the total cost is associated with the raw materials [3], [23], as carbon fibers alone represent a 45% of the total cost [6].

Current OoA manufacturing techniques have limitations as long filling times, limiting the use of high-reactivity formulations as resin curing could represent up to 80% of the total process time [24]. Thus making these techniques unfeasible to implement in the automotive industry [9], [25], [26]

Current accepted production times for automotive parts round the 5 minutes limit [4], [6], [27], so reducing the manufacturing time would reduce total cost of the carbon fiber components balancing the cost of the raw materials [12], [24].

Moreover, the use of CFRP is creating concerns on the recyclability and the environmental impact of the composites waste [22], with no current cost-effective recycling and repairing methods [12], [22]. Composites recycling process is a challenge due to the disarming or debonding process, the complexity of the raw materials separation and the damage of the materials original performance [5].

The rapid rise in carbon fiber applications is creating challenges in the recycling process of waste: fiber cut-offs represent alone a 40% of the total waste, besides on the end-on-life (EoL) of CFRP, expecting to generate 20.000.000 kg of waste annually by 2025. As an example, only on the aeronautical industry, between 6000 and 8000 CFRP-based commercial aircrafts will reach the EoL by the end of 2030 [11], representing a challenge in order to dispose and recycle their materials.

Current solutions as pyrolysis (Figure 1.2), where the materials are burned, and landfilling where the materials are buried as leftovers create serious environmental an economical concerns [28], [29]. Since 2015, the EU is demanding to car makers a recovery of the 95% of the vehicle materials, with at least an 85% reuse and recycling [5], creating a necessity for a more sustainable structural materials in order to fulfil current environmental regulations.

Figure 1.2. Reclaiming of carbon fiber by pyrolysis in composite waste. [30]

Production of virgin carbon fiber is a very energy-intensive process, being up to ten times more than other synthetic fibers as glass [13], so implementing new methods for recovering and reuse CF materials from current components or structures will imply savings of resources and less waste production.

1.3. Objectives

This thesis aims to explore the possibilities to produce high-performance thermoset composites made with the high-pressure resin transfer molding (HP-RTM) technology in its injection variant, capable to improve the production rate of structural components for high-volume industries as automotive. In this case, is intended to prove that the HP-RTM process improves over standard RTM reducing mold filling time by increasing the injection pressure and reducing the curing time using high-reactivity formulations, which are only processable under high cadency manufacturing methods. Parallelly, prove that HP-RTM components present better mechanical properties than RTM due to the reduction of the internal porosity content caused by the high-pressure inside the injection cavity, forcing the resin to impregnate better the preform, and collapsing any remaining voids inside the laminate.

In addition, present a sustainable alternative for high performance composite matrices with the introduction of a new high-performance epoxy-based vitrimer formulation, aimed to compete with current thermoset resins for the aeronautic industry. In this case, characterizing mechanically this new vitrimer formulation to demonstrate that is comparable with an aero-graded thermoset resin, offering advantages as repairability, reprocessability and recyclability. It has to be highlighted that this particular vitrimer was produced by CIDETEC [31], and its development is not contemplated in this thesis.

To accomplish these goals, the specific objectives of this thesis are:

- Firstly, to tune and set-up a new prototype of a HP-RTM machine and its processing parameters, that was specifically designed and built in the Eurecat's facilities in order to produce high performance composites in short cycle times.
- Secondly, to characterize the mechanical properties of CFRP produced in the HP-RTM machine by evaluating the process parameters and their influence over the mechanical performance. In addition to compare the advantages of the HP-RTM process over conventional RTM by implementing on-line monitoring devices as cavity pressure sensors and cure monitoring sensors.
- Thirdly, to present a complete mechanical characterization of a new high-performance epoxy-based vitrimer composites based on disulfide exchange bonds that has been formulated with commercially available precursors, and it is aimed to compete with current aerospace grade thermoset formulations in order to introduce vitrimer advantages as reprocessability, reformability and recyclability in high performance industry sectors as aeronautics.
- Finally, to evaluate the possibility to produce carbon fiber composite materials using the HP-RTM process and the vitrimer resin to produce high-performance materials under allowable cycle times, while being sustainable.

1.4. Thesis lay-out

Chapter 2 presents the literature review of current HP-RTM technology. The process description, advantages, reported studies evaluating the process parameters, process issues and the mechanical properties of the composite materials produced by this technology. Additionally, it is also discussed the current state of vitrimer composites, what vitrimers are, their differences with current standard thermoset resins, as well the mechanical properties of current vitrimer-based fiber reinforced composites.

Chapter 3 presents the methodology for the thesis development. It describes all the materials, machines and test standards used for the HP-RTM and vitrimers characterization. As well the manufacturing procedures and the experimental proposals for both topics.

The core of this work is the HP-RTM process. This thesis used a new prototype HP-RTM machine, designed, built and implemented to study the material properties and its advantages over conventional RTM process. This machine is expected to be an alternative for high volume production of high-performance thermoset materials. Additionally, a HP-RTM mold was designed, built and tested for the technology implementation, bringing in process monitoring in real time by integrating cavity pressure sensors and dielectric (DEA) sensors for cure monitoring. Chapter 4 describes this process in detail, also exploring the initial set-up process and modifications of the HP-RTM machine prototype and the mold operation.

Results and discussions are presented in Chapters 5 and 6. Where Chapter 5 focuses on the HP-RTM process and the mechanical properties of the composites built by it, as well, the process analysis and optimization using the in-mold cavity sensors. Chapter 6 focuses on the carbon fiber composite materials produced by the new formulation of vitrimer, formulated to compete with current aerospace-grade thermoset resins and manufactured by conventional RTM and HP-RTM process.

Chapter 7 presents a general discussion on both thesis topics, bringing a summary on the most relevant findings during the thesis development. This thesis concludes on Chapter 8 by presenting overall conclusions over the HP-RTM machine and the composites produced by it, as well the findings on the new vitrimeric formulation and its mechanical performance. At the end are made some suggestions for future work.

Chapter 2: State of the art

This chapter describes the theoretical bases and the current state of the art for the HP-RTM technology, its related material properties and developments. Vitrimer polymers and their composites are also described in this chapter, considering their advantages over thermoset materials and their mechanical performance in fiber reinforced composites.

2.1. HP-RTM process

Nowadays, greenhouse effect gasses in the atmosphere are a serious subject in environmental awareness. Transport industry, especially automotive, has a major impact on the CO_2 emissions. Europe have been imposing regulations about CO_2 limits, making OEM's to consider the implementation for CFRP in order to lower the overall vehicle weight, increasing their efficiency and reducing their environmental impact [2], [5], [12]. Weight reduction could achieve 7% by applying a structure optimization, more by implementing high strength steel; aluminum structures reduce the overall weight between 30-50%, and implementation of continuous CFRP could lead to further weight reduction for vehicle structures [6], [7], [32].

Carbon fiber market is developing at the same rate as the carbon composite market. A big amount of fiber is used to produce prepreg materials, while other amounts are used in the production of fabrics and braids. Automotive industry is growing as an important driver for the carbon fiber market, where component cost for CFRP is very high. Fiber itself represents almost the half of the total price and cost of composite components are usually 10 times higher than conventional materials. Preforming also represents an important part of the total composite cost. Inside the composite market, most of the quote is determined by thermoset composites, compared to thermoplastic composites. [5], [6], [12]

For automotive industry, traditionally standard materials have been used: steel, aluminum and short glass fiber reinforced polymers (GFRP), having advantages on mass production capacity and low cost. Mayor efforts in research have been stablished for the implementation of high-performance composites in mass production. Use of continuous CFRP in automotive sector has been limited only for luxury/high-performance segment due to high cost, but offering high mechanical properties and low weight, also reducing the number of total components to be manufactured due to their design flexibility. The use of CFRP is also important for electric/hybrid vehicles in terms of weight reduction, meaning an increment on the overall range and autonomy, giving the possibility of reduction of the batteries weight while maintaining the same range. However, the implementation of CFRP in mass-production vehicles is limited by the cost of raw materials, and the lack of suitable manufacturing processes for high-volume production [3], [5], [24].

Liquid composite manufacturing techniques as RTM have been gaining attention due to the feasibility on producing continuous CFRP with short cycle times and low capital cost in comparison with autoclave. But presenting some limitations as long filling times, low production rates and a high porosity content related to low injection pressures [25], [26], [33].

RTM is an OoA process capable to produce high performance components by using continuous fiber reinforcements. It has the capability to obtain autoclave-like quality parts with complex shapes, good surface quality and good dimensional tolerances. Compared to autoclave, RTM presents reduced times of working and exposition to chemical volatiles, in addition to cost savings related to prepreg storage and logistics [20].

In RTM, dry fabric preforms are placed into a metallic rigid tooling that is closed to compress the preform until its final thickness. Use of binder (thermoplastic or thermoset) could be implemented to improve preform handling and to obtain net-shape preform geometries. Vacuum is applied and thermoset resins with low viscosities (0 – 300 mPa-s) are injected at low pressures (0.1 – 2 MPa, or 1 – 20 bar) through the mold vents. After curing, the mold is opened and the part is demolded [34], [35] (Figure 2.1 illustrates the process steps to obtain the final component by using RTM).

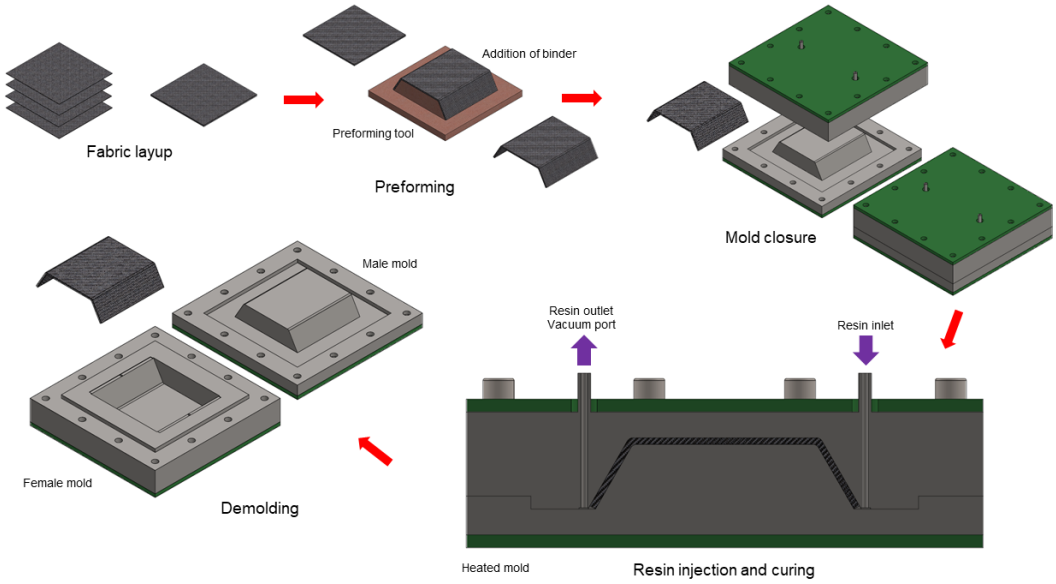

Figure 2.1. Detailed RTM process steps

But the RTM process presents some drawbacks: high investment costs on equipment and injection tooling (metallic). In addition to low impregnation rates, thus increasing the processing time and limiting its use under high-production environments [23], [27], [36].

HP-RTM is a modern and cost-efficient RTM process variant that enables the use of CFRP in the automotive industry, having high volume production capacity. The difference between HP-RTM and RTM is that resins are injected at high pressure, reducing mold filling times and enabling the use of high reactivity resins with short cycle times (≈5 minutes). As a consequence, main process defects that are usually presented on the final components are fiber washout (movement of the preform fibers) due to the amount of force that is created on the preform during the injection, displacing it from its original position, dry spots and race tracking effect [22], [37]–[39].

HP-RTM process was originally produced as a modification of the conventional RTM based on structural reaction injection molding (SRIM) for Polyurethane systems (PU). HP-RTM is conceived as a method to produce continuous FRP at industrial production rates (more than 25000 parts per year) [6], [7].

In this technology, resin and hardener are pumped separately at high pressures, more than 2 MPa (20 bars) by axial pistons, combining them inside a mixing device (mixhead) attached to the

injection mold. This means that components are only mixed at the final stage of injection, preventing premature curing reactions. In some cases, the mix head system allows to recirculate the resin and hardener to keep them at a constant temperature when the machine is not operative [6], [8].

When the injection starts, hydraulic pistons open the resin and hardener channels, allowing the components to mix and to be injected inside the mold cavity. Once this step is finished, pistons go back and close the resin and hardener channels, cleaning the system, reducing resin waste and avoiding the use of solvents. High-pressure pistons and the mix head system allow to have high flow rates (up to 200 g/s), reducing filling times and allowing the use of high reactivity resin systems (curing between 5 and 10 minutes). Moreover, it is possible to have a third channel for the injection of internal release agents for specific resin formulations. In order to improve further the process cycle time, hydraulic presses could be used to aid mold aperture and closure [6], [26].

HP-RTM process can be divided into two main variants: High-Pressure Injection RTM (HP-IRTM, Figure 2.2 a) and High-Pressure Compression RTM (HP-CRTM, Figure 2.2 b). HP-IRTM only differs from conventional RTM in the system pressure: mold is completely closed and the preform is compacted to reach final thickness (reduced permeability). In this method, high cavity pressures can be presented inside the mold. HP-CRTM is the combination of compression molding and RTM: mold is partially closed to leave a small gap, vacuum is applied, and resin is injected at high pressure to fill this gap and partially impregnate the preform. When the desired amount of resin has been injected, mold is completely closed, squeezing the resin and compacting the preform until its final thickness and intended fiber volumetric fraction (FVF). In this variant, the fiber preform is not compacted at the injection step, thus having more permeability. Impregnation is fast compared to the injection variant because is done in the out-of-plane direction of the preform ("z" direction). Use of process variants will depend on part geometry, complexity and technical requirements, HP-IRTM will require robust equipment (due to internal pressures), and HP-CRTM is preferred for larger and complex geometries. The use of binder in the preform could be necessary. [8], [27], [40], [41]

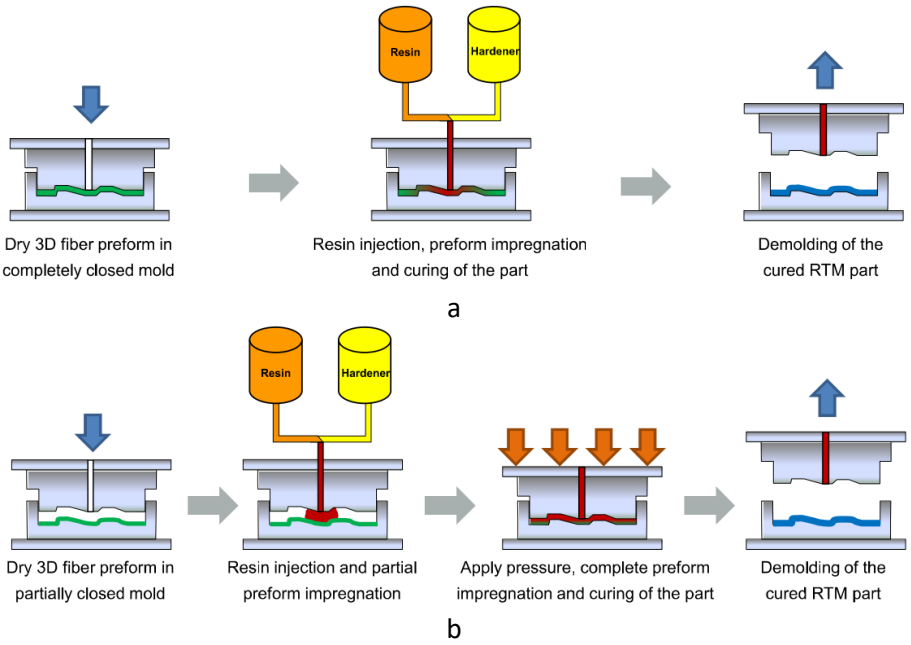

Figure 2.2. Resin injection sequence for HP-RTM process variants. (a) HP-IRTM. (b) HP-CRTM. Adapted from [6]

Early developers of the HP-RTM technology were KraussMaffei, Hennecke and Frimo (from Germany), and Cannon SpA (Italy) through modifications of PU metering machines. This development also pushed chemical developers to create highly reactive resin systems [42].

Conventional RTM was already used in the automotive industry with the Lotus Espirit in 1987 and in the Dodge Viper manufacturing. And more recently, HP-RTM was implemented for the production of CFRP parts in the i3 and i8 models of BMW where the short cycle time and the experience gained allowed them to reduce manufacturing cost up to 50%, where key factors have been stablished as reduced cycle time, automation and the use of continuous carbon fibers [43].

In HP-RTM process, one of the critical points in the cycle time is the preforming process where cutting, positioning and forming of the fabric layers take more time than the mold filling process, besides the time required for mold preparation and cleaning [23]. Automation is one of the key factors to overcome these problems, in addition to implement pressure and dielectric cure monitoring sensors, that could help to manage the process control and quality, reducing further the total process time. [42]

Currently, it is possible to find commercial solutions for HP-RTM machines (Table 2.1). KraussMaffei's RimStar series is one example: their metering machines cover a wide range of applications, being flexible for costumer specific requirements. Some of the models are EcoStar, Comet, Comet Nano (for PU processing) and RimStar CCM, RTM and PA (for epoxy, Polyamide (PA) and PU processing) [44], [45]. Cannon's E-System HP-RTM is another example, its main characteristics are processability and high resistance of different chemical components, precision on components metering and temperature control, easy maintenance and cleaning, and different customized configurations. [46]–[48]. The Streamline MK2 HP-RTM from Hennecke has the advantage of being compact and having an effective heating control for each component. This machine can process PU and Epoxy systems. [49]

Table 2.1. Main features for commercially available HP-RTM machines

Machine:	RimStar series	E-System	Streamline MK2
Manufacturer	KraussMaffei	Cannon SpA	Hennecke
Pressure system	Axial pistons	Axial pistons	Axial pistons
Pressure	-	-	-
Temperature	-	85° C/50° C for hardener. 35 °C release agent	100° C
Resin systems	Epoxy and PU	Epoxy	Epoxy and PU
Capacity	Up to 250 l	70 l for each component	Up to 150 l
Flow rate	N/A	Up to 140 g/s	Up to 250 cm^3/s
Vacuum assistance	Yes	Yes	Yes
Sensors	Volume flow, pressure and temperature	N/A	N/A
Additional characteristics	Different pump sizes for customer requirements, long service life, release agent integrated unit, modular design, energy efficient heating system (components enclosure)	Release agent dedicated unit, thermos regulated components with thermal jackets in tanks, possibility to connection directly to molds without adapters	Modular design, wireless operation, homogeneous temperature control, connection for press, addition of 2 more pressurized components

In Spain specifically, there is a patent for high-volume production of CFRP called Rapid Multi-Injection Composite Process (RMCP) [50] developed by the companies Carbures SA (now Airtificial [51]) and Sinatec SL [52]. This technology brings market competitivity on composite production compared with traditional automotive steel processing: resin is injected at high-pressure transversally to the fiber preform in multiple injection points to reduce the incident flow pressure, minimizing fibers deformation. In the process is integrated the fabric cutting and

positioning over the mold, control of heating and cure monitoring [51], [53]. There are no reports on this technology implementation under production environments.

In the HP-RTM process, mold design is important to determine the final component quality [6]. Good impregnation depends on the proper injection/vacuum strategy and optimum placing of sealings and fiber clamping mechanisms (pinch-off effect). In addition to aspects as the part geometry and production volume that will determine the final mold characteristics. Injection ports placement and injection strategy depends on the final part geometry and size. Ports' positions could be modified in aims to obtain less impregnation time to fix issues related to the preform impregnation as dry spots or void areas. Vacuum ports have the task of evacuating the air inside the mold cavity to produce high quality parts with low void contents. Vacuum ports must be placed in the last filling points of the preform.

Sealing strategies could be implemented in different ways but, it is recommended to seal in one plane as maximum sealing would be achieved when vacuum is applied. Conventional O-rings require good surface tolerances and sometimes could have the issue of trapped resin in the seal channel, while flexible or hollow tubes could perform better, especially in steel tooling. [6], [54]

Fiber clamping mechanisms (Figure 2.3) hold the reinforcement between the mold parts, producing a low permeability area, limiting the impregnation area and restricting the movement of the preform due to the drag force (fiber washout) produced by the advance of the resin under high pressure. In counterpart, fiber clamping strategies could create damage in the mold parts due to fiber abrasion, besides requiring trimming the final components to remove the excess of fibers and resin. Clamping could be done by using rubber elements, porous media as foams or with metal tooling [6], [37], [41].

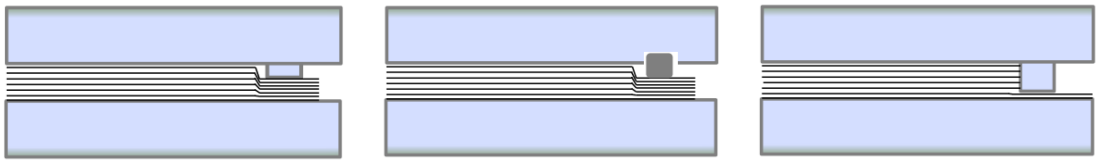

Figure 2.3. Fiber clamping/pinch-off mechanisms for RTM. a) Conventional pich-off. b) Rubber inserts. c) Partial pinch-off. Adapted from [6]

For the mold's materials, usually it is used steel and aluminum for high volume production, having advantages as good structural stability, flexibility for vacuum/pressure driven infusions, control of sample thickness and high fiber volume fraction. Steel molds specially, could maintain component dimensions during high-pressure impregnations. Mold heating could be implemented using high-capacity convective heaters that use oil or pressurized water [54]–[56].

2.1.1. Injection governing principle

Modeling of injection associated to the mold filling and preform infiltration is governed by Darcy's equation [57], that describes the speed of a fluid through a porous media or the flow rate per unit area:

$$v = \frac{\Delta P K}{l \mu} = \frac{Q}{A} \qquad 1$$

Where ΔP is the pressure differential in the system, K is the preform permeability tensor, l the flow length and μ is the fluid viscosity. Permeability is influenced by the fibers' direction (Figure 2.4), where is higher parallel to the fiber direction, compared to the perpendicular direction, and

FVF. If the pressure differential is assumed as constant, it's possible to calculate the injection time. [43], [54]

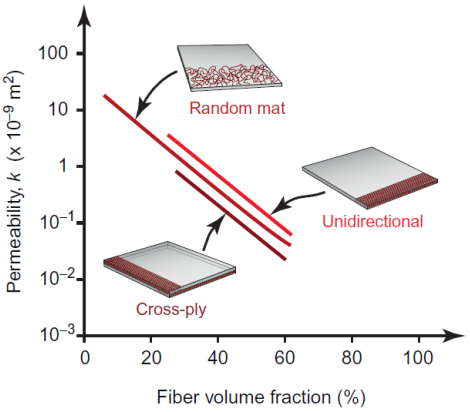

Figure 2.4. Relationship between fiber volume fraction, fiber orientation and permeability. [43]

$$t_{inj} = \frac{{L_{inj}}^2 \mu}{2\Delta P k} \qquad 2$$

Where L_{inj} is the injection length (shortest distance from the injection port to the vacuum vent).

Deviations of the theoretical approach can be presented when the resin has a non-Newtonian behavior or if in the reinforcement are presented defects as race tracking channels, wrinkles, fabric buckling, deflections at the resin inlet or movement during the mold filling.

In both cases (Equations 1 and 2), it is possible to reduce the injection time by increasing the injection pressure (the pressure differential), directly affecting the injection velocity.

2.1.2. Typical process defects

Main defects usually associated with the HP-RTM process are fiber washout (movement of fibers in a specific place in the preform), voids, race tracking and dry spots. Other associated defects are local changes in FVF, as well as local thickness changes.

Fiber washout means local movement of the reinforcement fibers due to fluid forces. It's associated with high-injection velocity or the high-pressure of the resin, that exceeds the friction forces between mold and the fabric causing a displacement of the fibers in the preform. It is reported that compression values in preforms with a bulk factor less than 1 (thickness of the dry reinforcement is less than the thickness of the mold cavity) will present fiber washout, so it is possible to reduce it by increasing the density of the fibers (adding more layers), or increase the compression forces over the fiber preform, having as a consequence the reduction of the permeability, thus increasing the filling time [37], [54].

Fiber movement could lead to local FVF changes in the final composite, modification of the resin flow creating resin reach zones or dry spots, lowering the mechanical properties of the composite part being produced [22], [38]. M. Bodaghi et al. [38] explained that washout could be prevented by implementing fiber clamping forces (pinching-off) in the preform, having risk for mold damage and the necessity of part trimming after the injection. Also, it's possible to

increment the mold closure force (normal force in the preform) to increase the fibers compaction, affecting the fibers permeability. Even it is possible to add binder agents to the fabrics to stabilize the preform, also having the risk of reducing the permeability of the fibers by chemical contamination. As, they explain, these proposals are only safeguards in the injection process, fiber washout can be prevented by knowing the friction forces in the preform layers (ply/ply) and the preform and the mold surface (ply/tool), generating preform in-plane stresses that oppose to the compression stress generated by the preform deformation due to inner fluid pressure. Moreover, they suggest that fiber washout can be neglected by applying a proper injection flow rate and pressure, especially in the early stages of the injection process.

Voids could be generated by air entrapment during the injection process due to components' mixing, interaction with contaminant particles or interaction with the fibers inside the preform. Voids also can be generated by volatiles present in the resin system. Main parameters that control void content are pressure and temperature, besides of vacuum level to avoid evaporation of volatiles (Table 2.2). Several techniques have been proposed to prevent voids formation: use of vacuum assistance in the injection, resin flushing/bleeding (allow more flow after mold filling is complete), control vacuum level when the resin presents evaporation of volatiles, resin degassing before injection, adequate selection of mold sealing mechanisms, increment of pressure during curing (post-fill), avoid excessive temperatures and selection of proper fabric, resin or binder agents. In any case, voids are believed to be inevitable, cannot be detected by visual inspection (when are located inside the laminate) and constitute one of the mayor causes for strength reduction in composite materials [25], [37], [54].

Table 2.2. Influence of process parameters on void content for a particular resin and fabric system. Adapted from [54], [58]

Parameter	Type of change	Average void content	Pore average length	Total void content
Cure pressure	+	-	No change	-
Vacuum level	+	-	-	-
Resin post filling distance	+	Unclear	+	+
Temperature	+	+	No change	+
Injection pressure	+	+	-	Unclear
Flushing time	+	+	-	-
Sizing	Removal	-	-	-
Lay-up	More 90°	+	No change	+

Race tracking is a deformation of the resin flow front (Figure 2.5). It is presented in zones with high permeability, in comparison with the average permeability of the reinforcement, these zones could be intentionally placed in the preform to improve the filling process or unintentionally presented. Resin flows faster in the high permeability areas, causing defects in the final part. Race tracking channels are more probable to appear in zones with large curvatures, corners, mold deflections and mold edges due to bad trimming of the preform layers. In addition to low reinforcement density zones or excessive fabric compaction during preforming. Race tracking is mainly a preform issue, it could be avoided by increasing the number of fabric layers, or the compaction forces in the race tracking channels to reduce local permeability, as well as change the injection strategy to avoid dry spots [54], [56], [59]. In vacuum bagged processes, race tracking could generate local thickness increments by influencing pressure gradients and the pressure distribution in the laminate. Dry spots in HP-RTM process are mainly caused by race tracking [36], [38].

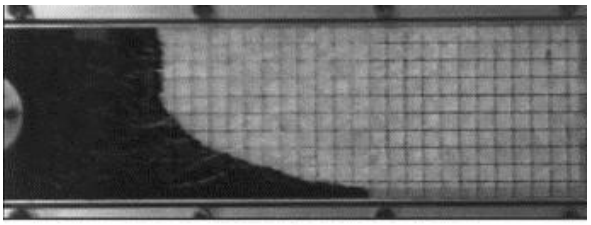

Figure 2.5. Example of race tracking in a permeability test. [59]

Dry spots represent large spots or zones with unimpregnated reinforcement. Dry spots are mainly generated by race tracking effect, but also can appear by inappropriate position of injection and vent gates inside the mold. Strategies as resin flushing/bleeding could help to solve the issue if the dry spot is located near to the vent gate. For composite molds, it could be required to manufacture new tooling in order to change the inlet/vent positions. For metallic tooling, it could be drilled new injection or venting ports and, if necessary, old ports could be sealed. Changes in the preform volumetric fraction due to fabric problems as overlapping also could generate dry spots [43], [54].

2.1.3. Process parameters and performance

Through other HP-RTM related studies, stablished main process parameters of HP-RTM process are: injection pressure or injection velocity, press force for mold closure, inlet and vent ports placement, injection temperature, reinforcement density, reinforcement architecture, vacuum application, mold gap size and the use of binder materials and their formulations [4], [8], [26], [27], [40], [41], [60].

R. Chaudhari [6] studied the HP-RTM process variants. For the injection variant (HP-IRTM), they detected that increasing the injection pressure led to fiber washout defects at the injection gate area. Initially, with the number of fabric layers used (5 layers), they detected a rise on the machine injection pressure, due to low permeability of the fiber preform (142 bar from 117 in the resin line set-up, and 132 bar form 124 bar in the hardener line set-up). By increasing the injection temperature was possible to reduce the incident force as the resin viscosity was lower.

In other publication about the HP-RTM process variants, R. Chaudhari et al. [7] described that in the injection variant there is a pressure rise during injection near the mold inlet (Figure 2.6). But during curing, pressure decreases due to resin shrinkage. Both process variants (HP-IRTM and HP-CRTM), have similar mechanical response. They observed that the properties of the composite material had more deviations under higher injection flow rates, and the use of vacuum during injection help to stabilize the mechanical response of the parts being produced.

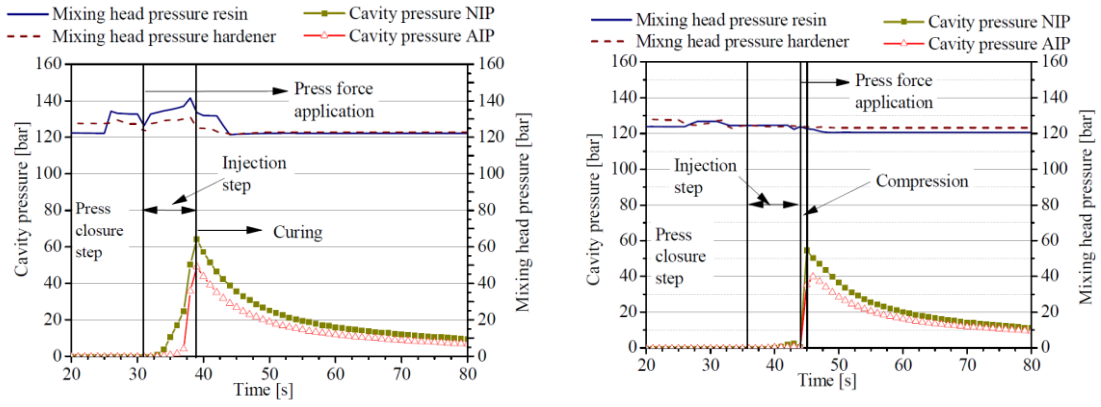

Figure 2.6. Comparison of the process parameters for both variants (a) HP-IRTM, (b) HP-CRTM. Flow rate of 80 g/s and pressure analyzed near to the injection gate (NIP) and away from it (AIP). [7]

P. Rosenberg et al. [32] analyzed the effect of pressure in the process variants. HP-CRTM has lower pressures during injection than the HP-IRTM due to the improved permeability using the mold gap. Maximum pressures were obtained near to the injection gate and lower near to the vacuum ports, pressure starts to decrease at the end of the injection step. Also, high pressures were recorded in the clamping areas during mold closure. Both process variants showed pressure decrease during curing due to resin shrinkage.

M. Bodaghi et al. [38] commented that the fiber washout zone tends to increase with the injection pressure, and all the preform deformation is concentrated at the injection point. By using two types of fabrics: non-crimp fabric (NCF) and satin wave, they showed that in the NCF wrinkles are induced with the injection pressure because these types of fabrics have more relative sliding and a weaker bond between the fiber tows compared with the crimped fabrics, thus increasing the washout area. Besides, they presented that race tracking channels generated dry spots inside the mold cavity. By adding more layers, the dry area increases due to local reductions of the reinforcement permeability.

Additionally, M. Bodaghi et al. [25] found that increasing the pressure during curing, it is possible to reduce void content. They made a comparison of void content in different manufacturing processes (Figure 2.7). In autoclave, it is possible to reduce void content by increasing the pressure, while the vacuum bag removes the air bubbles trapped inside the laminate. In HP-IRTM process variant, void content is almost minimal when is not used a gap in the mold. They also found that void content decreases when the voids size increases, and the void content is reduced when the resin flow advances. This is because as the flow front progresses, it decreases its velocity (reduction of the pressure differential), allowing more impregnation time inside the laminate, and reducing final voids size.

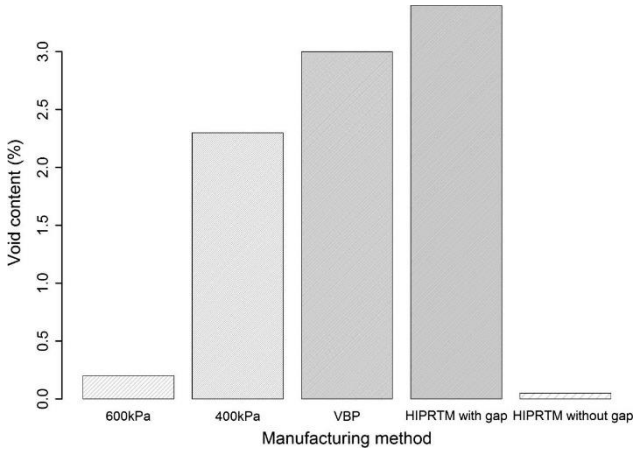

Figure 2.7. Total voids content for different manufacturing processes. Autoclave (600 kPa, 400 kPa), Vacuum Bag Processing (VBP) and HP-IRTM. [25]

In another study [36], they compared the HP-IRTM process with other liquid composite molding (LCM) techniques as double bag vacuum infusion (DBVI), vacuum assisted process (VAP) and controlled atmospheric pressure resin infusion (CAPRI). HP-IRTM is implemented with rigid tooling while the other processes depend on flexible tolling as vacuum bags. This translates less thickness variations unless fiber washout is presented. In the HP-IRTM process variant they observed slight differences in FVF due to fabric nesting and tow alterations induced by the resin pressure, as well as low void content. But the quantity of voids increased when the FVF also increased due to fabrics compression and nesting. They remarked that independently of the manufacture process, NCF presented more void content than satin woven fabrics.

Moreover, it's reported that by increasing the internal pressure of the mold cavity, the reaction rate also increases and accelerates the exothermic reaction [26]. G. P. Johari et al. [61] studied the effect of pressure and temperature in a DGEBA/Cyclo-hexylamine epoxy resin curing. They found that pressure increases the extent of reaction by increasing the equilibrium constant when the reaction products have less volume than the reactants, and thus increment the curing reaction rate. J. Ramos et al. [62] commented that the increment of pressure has similar effects as the increment of temperature during the curing process. They investigated the cure kinetics and shrinkage model for diglycidyl ether of bisphenol-A/ 4,40- methylenebis(3-chloro-2,6-diethylaniline) epoxy resin. Here, pressure increases the density of reacting groups, raising the probability of mutual approach and increasing the reaction rate. But in counterpart, pressure also lowers the molecular diffusion in the final stages of the curing reaction, reducing the reaction rate. They report that temperature has a stronger effect on the reaction rate compared to the effect of pressure.

$$\left(\frac{\partial \ln k}{\partial P}\right)_T = -\frac{\Delta v^*}{RT} + \frac{1}{V}\left(\frac{\partial V}{\partial P}\right)_T \qquad 3$$

Equation 3 presents the pressure dependence of the reaction rate constant k, where Δv^* is the activation volume for the reaction, and $(1/V)(\partial V/\partial P)$ is the compressibility factor and can be described as a linear function of pressure.

J. Cruz and T. Osswald [63] made a study for pressure influence over reaction rates in epoxy and unsaturated polyester resins. Pressure increases the reaction rate by the increment of the reaction constants. Specifically in epoxy resins, pressure also accelerates the reaction kinetics, but differences on the mechanical properties were not detected

Y. Huang and Y. Wen [64] also reported that for PU systems, a pressure increment favors the kinetic effect, but at the same time affects the reaction rate by decreasing the free volume available for the reactants, delaying the gel effect. This reduction of the free volume inside the polymer decreases the mobility of the growing molecules and reactants mobility, limiting the degree of cure [65].

Moreover, N. Gushurst et al. [66] commented that in traditional RTM processes, thermo-mechanical simulations only consider effects of degree of cure and temperature as the injection pressures are very low. (<0.8 MPa – 8 bar). But in HP-RTM process this cannot be neglected as they demonstrated that the increase of injection pressure leads to a higher degree of cure, glass transition temperature and ionic resin viscosity. The effect of pressure in the curing behavior can be described with the free-volume theory.

P. Rosenberg et al. [27], [32] remarked that if the HP-IRTM variant is done at a constant press force, the inner pressure of the injection would tend to open the mold cavity. While in the HP-CRTM variant, maintaining a predefined mold gap, the press has to apply more force in order to maintain it. At higher mold gaps, important pressure increments during injection were not detected. Also, the selected press force is translated directly to the inner cavity pressure. Similar mechanical response was obtained with both process variants.

R. Chaudhari [6] commented that for the compression variant, the mold gap has an influence over the final composite performance. Smaller gaps improve impregnation because big gaps led to air entrapment, in addition to avoiding fiber movement due to impregnation in the out-of-plane direction of the preform. During mechanical testing, tension and compression samples did not present remarkable variations, but flexural samples presented some variations influenced by fiber movement and presence of areas with poor impregnation due to different mold gaps. Fabric type had also an influence over the performance, bidirectional laminates (NCF) showed more fiber movement due to lower permeability if compared with UD laminates.

Related to injection strategies, R. Chaudhari [6] presented over-pressure issues in his HP-RTM machine, the mold used for his studies had a point-gate injection strategy (Figure 2.8 a). After trying to increase the injection temperature, he discovered that just by mechanizing a distribution channel in the injection gate (as a film-gate strategy, Figure 2.8 b) it was possible to reduce the incident pressure force in the fiber preform.

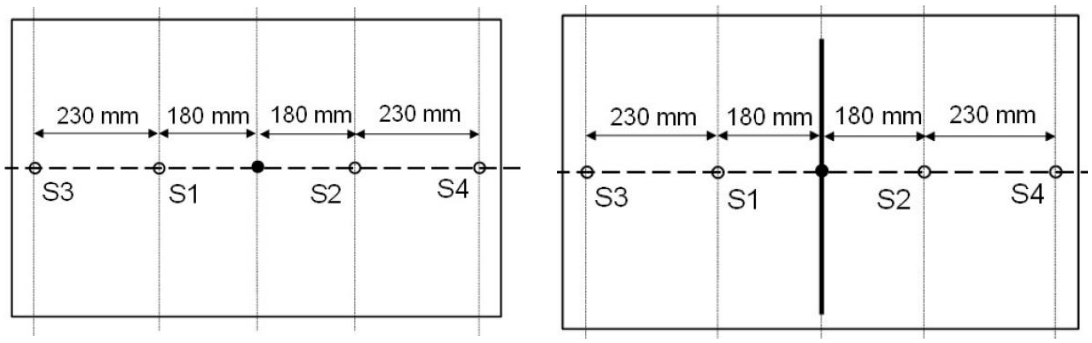

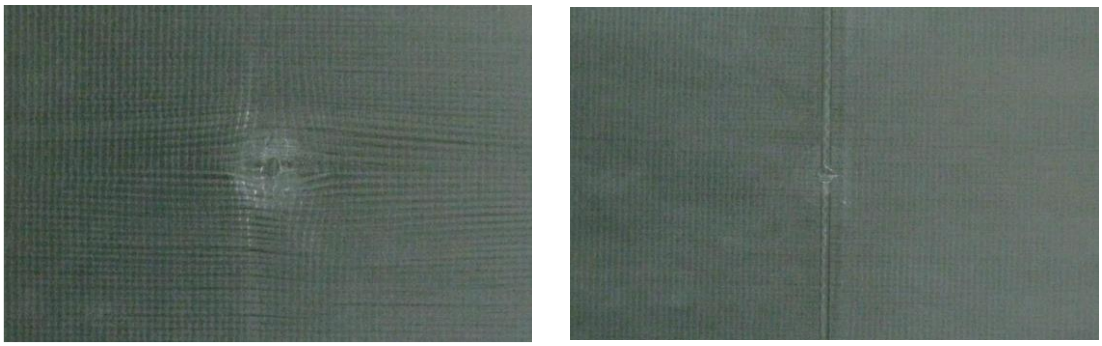

a b

Figure 2.8. Differences between injection strategies over fiber washout. (a) point gate strategy. (b) film gate strategy

This new injection strategy helped to avoid washout defects in the preform, allowing to increase the number of reinforcement plies and obtain composites with better FVF. Additionally, he reported that having less fiber washout helps to stabilize the mechanical performance of the final part.

In general It has to be remarked that the application of vacuum helps to reduce void content inside the laminates, improving mechanical properties as flexural and shear strength [7], [8].

B. Han et al. [4] observed that when vacuum is not correctly applied, resin injection becomes difficult to achieve. Trapped air (Figure 2.9) creates overpressure inside the mold cavity and the air is accumulated at the edges of the injection zone. Trapped air also has a detrimental impact over the mechanical properties: lower tension and flexural strength with more deviations, local thickness and preform compaction variations, besides of high void content and some distortions in the fiber laminate. They highlighted that the implementation of pressure and temperature sensors inside the mold cavity helped to monitor the injection process and curing state of the resin (exothermic temperature measurement), detecting a problem in the vacuum level of the mold by the parameter's response.

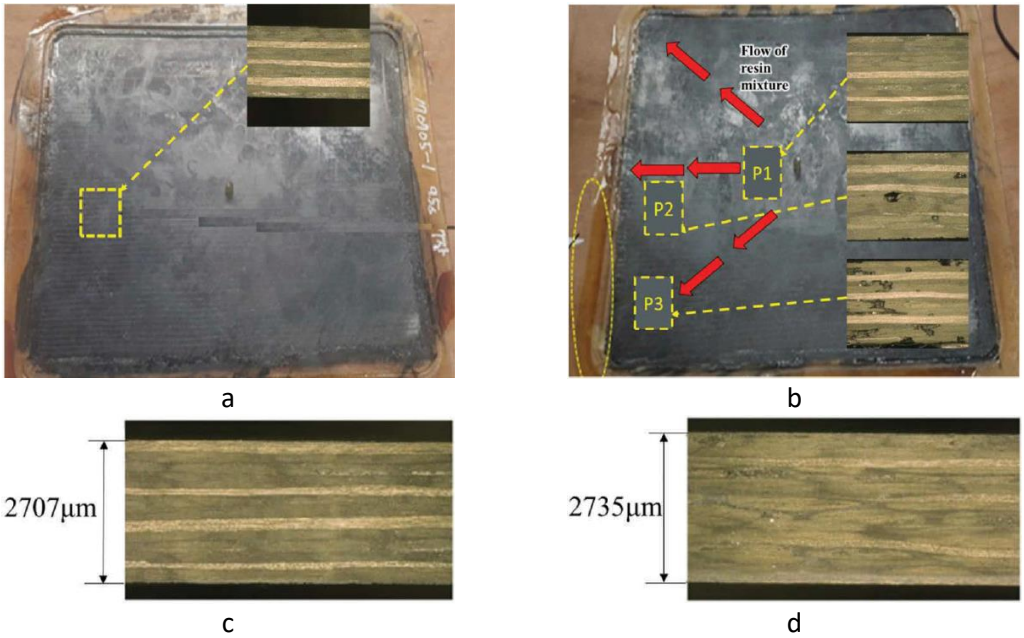

a b c d

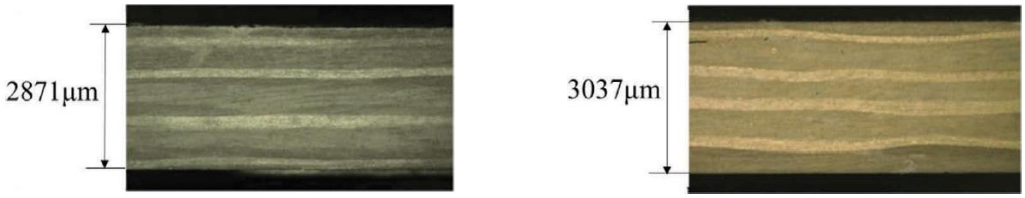

e f

Figure 2.9. Effect of the vacuum level on the final component response. (a, c, d) Normal vacuum level over voids, fiber distortion at inlet zone and fiber distortion at edge zone. (b, d, e) Abnormal vacuum level over voids, fiber distortion at inlet zone and fiber distortion at edge zone. [4]

R. Chaudhari [6] commented that the use of binders could lead into a reduction of the preform permeability. Hillermeier et al. [21] studied the influence of binder agents in the prevention of fiber washout during injection at high pressure (Figure 2.10). They remarked that is important that the binder agent has to be compatible with the matrix in order to not affect the preform permeability. They tested two types of binders: standard thermoplastic and thermoset. They found that the preform without binder presented more deformation at the injection point, compared with bindered preforms. Both binder systems presented good performance under the injection flow, but the thermoset binder presented better performance at higher flow rates.

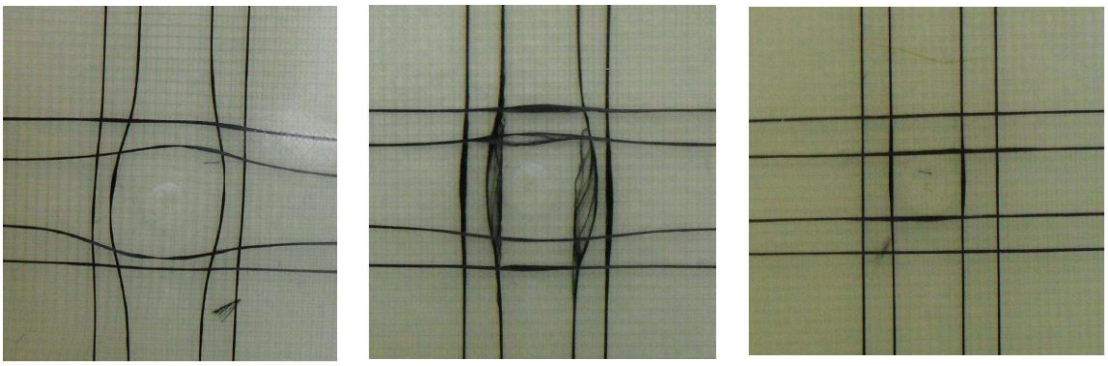

a b c

Figure 2.10. Effect of preform binder on the total fiber washout. (a) No binder, (b) Standard epoxy compatible binder. (c) Thermoset epoxy compatible binder. [21]

Khoun et al. [8] found that larger deformations of the fabric fibers are presented when a binder agent is not used in the preform, especially at high flow rates. Binder helped to improve this issue but still some misalignment was found, remarking that fiber movement is more dependent on the flow rate rather than the binder concentration. But also, it was found that binder concentration is the parameter that has a major influence over the mechanical properties: lower tensile properties, 20-30% lower flexural properties with binder concentrations of 4% in weight and 50% decrease from concentrations above 4%. This is due by the influence that the binder has over the preform permeability: outside fiber tows, binder can block the resin flow, but inside fiber tows can create a high void content.

P. Rosenberg et al. [41] studied the HP-RTM process for epoxy and PU systems. During injection, the PU resin required more pressure if compared with the epoxy resin due to differences in its viscosity, leading to a slower flow front progression, being affected also by the curing process, requiring more force to complete the mold filling. But, they detected a pressure drop in the areas away from the injection gate during curing, related to differences in the curing percentage compared with the last filling points inside the mold cavity (cure shrinkage). In general, both resin systems had similar FVF, but PU system presented slightly higher tensile strength than

Epoxy. PU systems also have the advantage of having similar properties than epoxy with less processing temperatures (Table 2.3).

Table 2.3. Summarized mechanical properties for both resin systems under HP-RTM process. Adapted from [41]

Test method	Resin type	Strength/Standard deviation [MPa]	Modulus/Standard deviation [MPa]	Elongation/Standard deviation [%]
Tensile properties (DIN EN ISO 527-4)	EP	741.7 ± 50.7	66.9 ± 4.3	1.09 ± 0.04
	PU	783.5 ± 36.6	63.6 ± 3.3	1.14 ± 0.04
Flexural properties (DIN EN ISO 14125:1998)	EP	970 ± 37.6	66.9 ± 2.8	1.66 ± 0.09
	PU	950 ± 13.9	63.9 ± 4.1	1.75 ± 0.21
Interlaminar shearing properties (DIN EN ISO 14130:1998)	EP	67.5 ± 2.19	-	-
	PU	64.3 ± 1.25	-	-
		Impact strength [kJ/m²]		**Energy absorbed at max force [J]**
Charpy impact strength (DIN EN ISO 179-1:2000)	EP	47.1 ± 2.63		1.61 ± 0.10
	PU	53.9 ± 2.99		1.90 ± 0.11

I. Swentek et al. [40] also made a study for the process parameters for Epoxy and PU. The compression force during injection and curing had no relevant influence over the final mechanical properties. By varying the injection flow rate, they detected that for the PU system it was not possible to rise it above 60 g/s due to a fast increase of the resin viscosity. Increments of the flow rate leads to an increase in the final mechanical properties due to removal of trapped air inside the laminate during injection. Both resin systems have similar processing parameters and mechanical properties. They recommend using gentle processing parameters because no improvements were detected with higher processing values during the HP-RTM processing.

F. Behnisch et al. [67] investigated the Interlaminar shear strength and impact behavior for Epoxy and PU resin systems in HP-RTM processing (Figure 2.11). PU resins presented more interlaminar shear strength (ILSS), energy absorption, elongation at break point and higher ductility than epoxy resin.

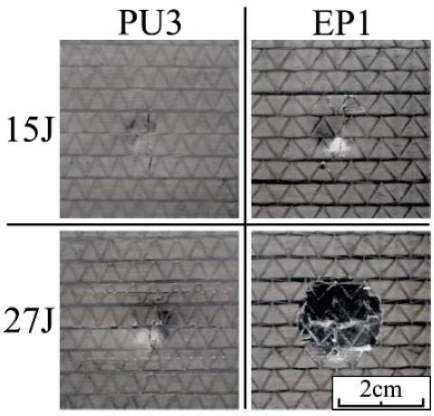

Figure 2.11. Comparison of the impact behavior for a PU resin system (PU3) and an Epoxy system (EP1) under different impact energies. [67]

S. Nonn et al. [37] studied the effect of the fiber clamping areas and their impact on the overall composite performance. When compression is applied in just one side of the preform, fibers eccentricity is created in the final composite, presenting bending moments when tensile loads are applied. Fiber waviness is created at the edges of the compacted zone, leading to early matrix damage and delaminations. They recommend applying symmetrical compaction forces

on both sides of the preform in order to generate fiber clamping and avoid fatigue failure. Fiber waviness is more detrimental than voids and this could generate a change on the out of plane permeability, altering the flow pattern in the lower part of the preform and possibly generating voids and dry spots.

Other investigations as R. Kim et al. [26] and M. Etchells and C. Lira [68] presented the importance of process monitoring in HP-RTM. Pressure and temperature sensors help to understand the effect of process variables over the performance and quality of the final component. Degree of curing sensors as ultrasonic, optical o dielectric help to optimize the process time and part quality, while providing information about resin arrival to different points and its viscosity state during injection.

But in some cases, sensors have to be isolated when conductive fibers are used (as carbon fiber). They highlighted that in some cases, implementation of sensors for process monitoring is limited for research and could not have applicability in the production field.

The HP-RTM process becomes an interesting alternative to high-performance high-volume production composite materials. Control of process parameters such as injection pressure, temperature, injection and vacuum strategies and process monitoring are key parameters to obtain a composite part with high quality, by preventing related process defects.

Table 2.4 summarizes all the process variables used for other authors in the HP-RTM processing. And Table 2.5 summarizes the mechanical characterization of HP-RTM composite materials under its injection variant (the HP-RTM compression variant is not considered in this study).

This thesis aims to go beyond the state of the art in providing a new alternative to HP-RTM processing, presenting a lab-scale prototype for high-pressure injected composites, possibly opening a market for small scale-low volume capacity machines, fitted more for research purposes a materials testing.

Table 2.4. Summary of the process variables for HP-RTM processing

References	Fiber / Fabric	Resin	Injection pressure [MPa] (Bar)	Injection flow [g/s]	Binder	Fiber volume content	Injection temperature [° C]	Curing temperature [° C]	Curing time [seg]
Chaudhari et al. [7]	CF Biaxial NCF 300 gr/m^2	Epoxy Dow Automotive (Possibly Voraforce)	12 (120)	40, 60, 80	Not specified	47-50%	80	-	300
Rosenberg et al. [32]	CF UD 335 g/m^2	Epoxy Sika Biresin CR170	12 (120)	40	Not specified 8 g/m^2	50-56%	80	120	300
Cherniaev et al. [1]	CF UD NCF 333 g/m^2	Epoxy Epikote RT 06150	12 (120)	40	Thermoset	45%	120	120	300 to 600
Swentek et al. [40]	GF UD 1218 g/m^2 & CF UD 300 g/m^2	Epoxy Epikote 05475 & PU Huntsman Rimline SK97014	12 (120)	20, 40, 60	Not specified	60%	60 EP 50 PU	120 EP 95 PU	300
Etchells and Lira. [68]	CF NCF 600 g/m^2	Epoxy Araldite LY3585	-	85	Thermoset Araldite LT3366 14 g/m^2	-	N/A	110-120	180, 240, 600
Hillermeier et al. [21]	-	Epoxy Epikote 05475	12 (120)	200	Thermoplastic Epikote 05390 12 g/m^2 & Thermoset Epikote System 620 12 g/m^2	-	120	120	300
Rosenberg et al. [41]	CF Biaxial 300 g/m^2	Epoxy Sika Biresin CR170 & PU Puromer Purorim 185 IT	12 (120) EP 15 (150) PU	40	Not specified	52.9% EP 51.5% PU	80 EP 70 PU	120 EP 90 PU	300
Khoun et al. [8]	GF Quad NCF 1205 g/m^2	Epoxy DOW Voraforce	-	35 - 85	Thermoset epoxy binder 0%, 4%, 5%, 6%	-	-	100	250
Rosenberg et al. [27]	GF UD NCF 1218 g/m^2	Epoxy Sika Biresin CR170	12 (120)	40	Not specified	57.85%	80	125	300
Bodaghi et al. [25]	CF 2x2 Twill 280 g/m^2	Epoxy Sika Biresin CR120	2 (20)	-	Thermoset Airtech epoxy binder	-	-	-	-
Behnisch et al. [67]	CF Biaxial NCF 300 g/m^2	Epoxy and PU systems	12 (120)	40	Not specified	52.40%	80 EP 80 PU1 80 PU2 45 PU3	120 EP 110 PU1 90 PU2 90 PU3	-
Bodaghi et al. [38]	CF 5 Satin woven 370 g/m^2 & CF NCF 392 g/m^2	Epoxy Prism EP2400 Monocomponent	2 (20)	-	Not specified	60%	90	180	7200 (Aerospace resin)
Han et al. [4]	CF	Epoxy Kumho KER 9610	12 - 13 (120 – 130)	-	Not specified	38%	80	114	300
Kim et al. [26]	CF	Epoxy Kumho KER 9610	125	64.7	Binder used, not specified	40%	80	110	500 - 600

Table 2.5. Summary of reported properties for HP-RTM composites

References	Process variations	Tensile modulus [GPa]	Tensile strength [MPa]	Flexural modulus [GPa]	Flexural strength [MPa]	ILSS [MPa]	IPS Modulus [GPa]	IPS Strength [MPa]	Charpy Impact strength [kJ/m²]	CAI [J]
Chaudhari et al. [7]	HP-IRTM + Vacuum	-	-	51	751	66	-	-	-	-
Cherniaev et al. [1]	Longitudinal properties	102.6 ± 3.8	1204 ± 50.1	-	-	-	3.1 ± 0.1	65.3 ± 1.3	-	-
Swentek et al. [40]	Carbon fiber + epoxy resin	121 ± 5	1370 ± 30	86.7 ± 3	1380 ± 50	-	-	-	-	-
Rosenberg et al. [41]	HP-IRTM + epoxy resin	66.9	741.7 ± 50	66.9	970 ± 37	67.5 ± 2	-	-	47.1 ± 2.6	-
Khoun et al. [8]*	Glass fiber + Vacuum + 45 g/s	≈ 23	≈ 400	35	900	-	-	-	-	-
Rosenberg et al. [27]	HP-RTM + Glass fiber	34.2 ± 1.15	621 ± 35	42.4 ± 2.4	1211 ± 114	46.4 ± 5.3	-	-	-	-
Behnisch et al. [67]	Epoxy resin. ILSS with short beam shear configuration	-	-	-	-	62	-	-	-	27
Han et al. [4]	Carbon fiber	-	432	-	512	-	-	-	-	-

* No given explicit data, approximated results.

2.2. Vitrimeric polymers and their composites

Thermoset fiber-reinforced composites have been widely used in numerous structural applications, particularly in the aerospace, automotive and wind power industries. Epoxies have excellent thermal and dimensional stability, good mechanical strength, creep and chemical resistance and good electrical isolation thanks to their permanent covalent cross-linked networks. That said, thermosets have long curing times, thus limiting their production to low-medium volume series, for which there is an increasing demand. In addition, thermosets have poor or complex reparability, are non-recyclable and cannot be reshaped after being cured, therefore generating a great deal of waste when components reach the end of their lifespans. The current and most common disposal solutions are pyrolysis and land filling, both of which imply serious environmental and economic issues [28], [69]–[74].

Back in 2011, Leibler et al [75] presented a new kind of polymer with outstanding properties called covalent adaptative networks (CANs), dynamers or vitrimers, that combine the performance of traditional thermosets with the versatility of thermoplastics due to characteristics such as processability, weldability, self-healing capacity and recyclability. Vitrimers, having associative dynamic networks (Figure 2.12), behave like traditional thermoset resins at service temperatures due to their frozen network topology. However, under certain stimuli, such as heat or light, they are able to reorganize their networks while maintaining a constant number of chemical bonds. In counterpart, dissociative formulations reduce their network crosslinking density, thus diminishing polymer dimensional stability and viscosity during reprocessing. Some vitrimer formulations need the addition of external catalysts to create the bond exchange reactions, as the material is heated above the vitrimeric transition temperature, therefore presenting issues with the vitrimer stability, its manipulation and mechanical response. Some studies present new formulations of catalyst-free vitrimers that can be processed with commercially available precursors, maintaining their properties during reprocessing and are more easily implemented on an industrial scale [70], [71], [76]–[85][86], [87].

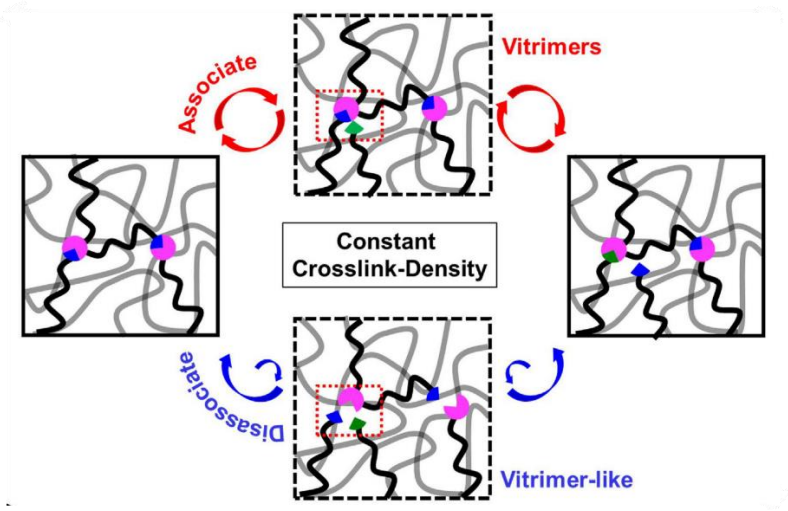

Figure 2.12. Dissociative vitrimer vs associative vitrimer [88].

Since then, different vitrimer formulations with variated dynamic mechanisms have been formulated and studied. Some of the reported dynamic mechanisms are: Diels-Alder adducts, alkoxyamines, urethanes and urea vitrimers, triazolinediones, 1-2-3-triazoliums, aniliniums,

coumarin dimers, trithiocarbonates, disulfides, diarylbibenzofuranones, boronic esters, acylhydrazones, imines and acetals, transesterification, transcarbamoylation, siloxane-silanols, olefin metathesis [74], [89]–[91]

Inside dynamic networks, disulfide-based formulations have been studied due to their advantages over other dynamic formulations as these systems can integrate the exchangeable bonds directly on the polymer structure, facilitating the formation of small fragments during a dissolution process and being facile and rapid to recycle [90]. Some examples of disulfide-based dynamic chemistries are Thiol-disulfide exchange, disulfide exchange, transthioesterification, thioacetal exchange, hemithioacetal formation and conjugate thiol addition. Particularly, dynamic sulfur species based on disulfide exchange are one of the most studied, especially for self-healing materials in which exchange reactions can be triggered by chemicals, heat or UV light [92], [93]. Disulfide exchange.-based formulations can be also used in vulcanized rubbers for the chemical industry [71]. Moreover, aromatic disulfide exchange-based vitrimers have been applied on different studies, having advantages on being catalyst free formulations. They are very versatile and easy to implement in polymer networks as polyurethanes, poly(urea-urethanes), polyimides and epoxy resins, and can be found in commercially available resources [74].

2.2.2. Fiber-reinforced vitrimer composites

Vitrimers present new possibilities for fiber-reinforced polymers such as post-curing reprocessing without losing performance, welding composite layers to form new monolithic and multi-layered materials or allowing composites to be welded to generate structural joints between parts. Additionally, the fibers and the matrix can be separated for reuse in other applications. Furthermore, vitrimers allow for the implementation of “enduring” prepregs that could be fully cured and still enable the processing of multi-layered laminates, thus avoiding the need for refrigerated storage and the multiple consumable materials for prepreg protection, in addition to offering a longer shelf life. Vitrimers offer the potential to create reprocessable and reparable thermoset composites, something which currently is a slow and expensive process requiring highly qualified personnel [29], [78], [80], [90], [94]–[96].

A pioneering publication on fiber-reinforced vitrimers by Ruiz de Luzuriaga, A. et al. [78] presented a glass fiber reinforced vitrimer based on diglycidyl ether of bisphenol A (DGEBA) epoxy monomer and a 4-aminophenyl disulfide (4-AFD) dynamic hardener. This is a catalyst-free formulation that presents fast stress relaxation at high temperatures. Compared to a traditional DGEBA epoxy with diethyltoluenediamine (DETDA, 2) hardener, the disulfide vitrimer showed comparable values of glass transition temperature (T_g), storage modulus (E’) and thermal stability, albeit with a slightly lower degradation temperature (T_d), possibly due to the disulfide species that are less energetically stable than other species in the formulation. Both the vitrimer and the thermoset showed comparable traction strength, suggesting that the use of dynamic formulations on composites will not affect their mechanical performance. The authors demonstrated the possibility of reshaping a cured composite sample manufactured by RTM and thermoforming it in a hot press (Figure 2.13). The reparability of the vitrimer formulation was illustrated by inducing delamination during an ILSS test and healing it by means of heating and pressure.

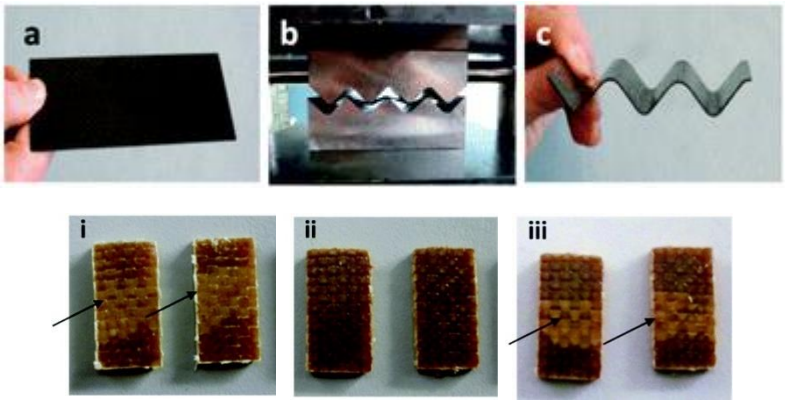

Figure 2.13 Demonstration of dynamic properties for a disulfide vitrimer formulation a-c) thermoforming of a cured CFR vitrimer. i-iii) Repairability of ILSS vitrimer samples. Demonstration of mechanochromy in vitrimers [78].

In another work of the same team [97], they proved that by using 4-Aminophenyl disulfide vitrimer, it was possible to confer visual indications of damage in composites by mechanochromy (change of color due to mechanical stimuli), mostly in cases when the matrix is broken, as in impacts (Figure 2.14).

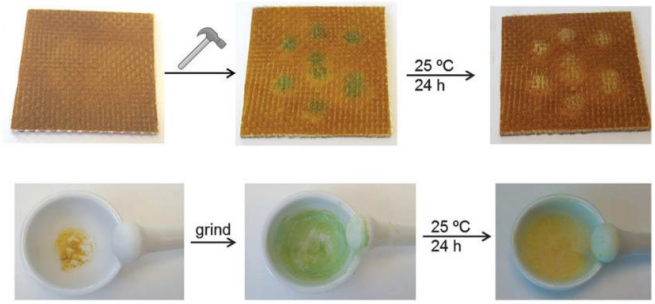

Figure 2.14. Demonstration of mechanochromy in vitrimers [97].

J. Markwart et al. [98] prepared a GFR vitrimer. In their case, the dynamic formulation was composed by vinylogous polyurethane and a dynamic phosphonate-based hardener, having the advantage of presenting flame-retardant properties, as other vinylogous polyurethane formulations probed to be very flammable. This formulation is also recyclable and its mechanically comparable to analogous phosphonate-free vitrimers.

W. Denissen and I. De Baere [99], [100] also prepared GFR composites with a resin based on vinylogous urea (vurea) moieties and dynamic amine exchange reactions that showed fast intrinsic exchange kinetics with good neat mechanical properties. This vitrimer formulation had very short relaxation times after the formulation passed its T_g, indicating good thermoforming capabilities. Tensile properties were comparable with other thermoset materials, while matrix-dominated properties, as in-pane shear strength, were similar in terms of stiffness but lower in strength. Thermoforming and recyclability were also investigated after curing, giving positive results.

K. Yu et al. [101] created a recyclable CFRP using a DGEBA epoxy resin and a dynamic system based on fatty acids and a $Zn(Ac)_2$ catalyst. This system can be fully dissolved in alcohol at temperatures between 160° C and 180° C. These temperatures were far lower of the degradation temperature of the epoxy matrix (≈350° C) and the carbon fiber (≈500° C), allowing the evaporation of the solvents to recover the epoxy matrix and the reinforcements without any

damage. The mechanical properties of the recovered materials were almost identical to the pristine ones.

H. Si et al. [79] reported that disulfide-based vitrimers have advantages of being catalyst-free formulations and have a rigid polymer structure and long term stability but, reprocessing and degradation of these dynamic systems are time consuming due to their high cross-linking density. They studied a high-content disulfide vitrimer (called dual disulfide-based formulation) that accelerates the cross-linking exchange rate, improving reprocessing and recyclability, in addition to present a rapid release of internal stresses when compared with single-based disulfide vitrimers. This formulation presented excellent solvent resistance and recovered fibers retained most of the original properties.

Disulfide-based dynamic formulations can be extended to polyurethane resins with advantages on easy reprocessability and recyclability, clean and safe manipulation by having isocyanate-free formulations, and improvement of impact resistance properties when combining them with pure epoxy composites. [102], [103]. Particularly, M. K. Bangash et al. [104] developed a bi-phase vitrimer formulation by joining epoxy-based vitrimers and PU-based vitrimers composites, both formulated with dynamic disulfide hardeners. By arranging the epoxy and PU vitrimers in different ways, it was possible to enhance the impact resistance of the composites compared with pure epoxy composites.

Y. Yuan et al. [73] studied unidirectional and cross-ply carbon reinforced vitrimers made of a high-performance polyhexahydrotriazine (PHT) and 2,2-bis4-4-aminophenoxyphenylpropane (BAPP). This vitrimer presented a high glass transition temperature and good thermal stability due to its strong and stable C-N bonds and crosslinking structures. This formulation also presented good resistance to solvents, oils, alkaline and salt solutions, strong oxidizing agents and acids. Moreover, this vitrimer was mechanically comparable to commercial high-performance epoxy – Bismaleimide (BMI) resins. They demonstrated that is possible to recycle and recover the carbon fibers (Figure 2.15) by dissolution on tetrahydrofuran (THF) solvent with Hydrochloric acid (HCl), even at room temperature in high acidic concentrations, with no visible damage on the fibers.

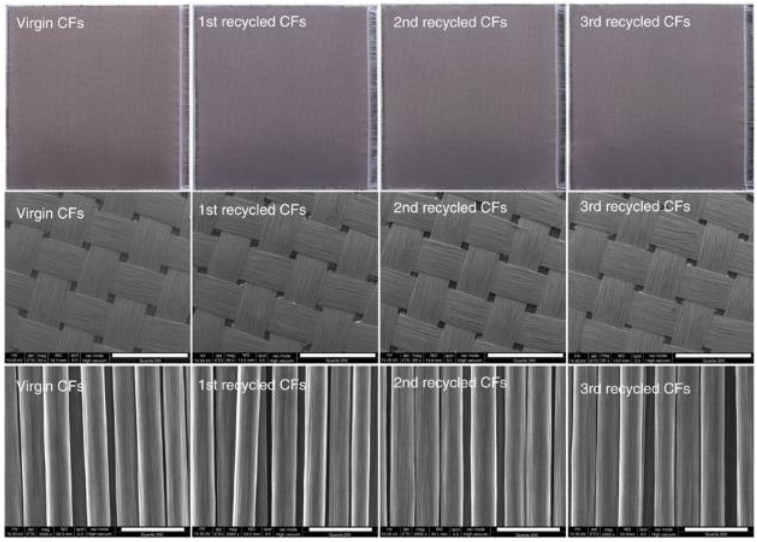

Figure 2.15 Sequence of multiply recycled CF/PHT vitrimer composites (SEM images). [73]

P. Taynton et al. [105] developed a fully recyclable CFR vitrimer using dynamic polyimine networks as a binder material, presenting high-performance in comparison with other self-

reinforced composites. This polyimine formulation presented good weldability between composite layers with no discernible interfaces between them, showing high efficiency in the crosslinking process. Flexural properties (modulus and strength) were comparable with commercially available composites for structural components. Authors reported good recyclability of the vitrimer binder in a solution with excess of diamine monomers without consuming important chemical or energetic resources, recovering carbon fibers with their original length and woven structure. This same group [80] later created the company Mallinda [106] which commercialize prepreg vitrimer composites that could be stored indefinitely at room temperature and processed by compression molding, even scraps could be repurposed for other applications or recycled.

L. Yu et al. [107] prepared a diamine-based CFR vitrimer with the advantage of having very short cycle times (4 minutes), producing fiber reinforced composites by impregnating the fibers with the vitrimer formulation in a powder state under compression molding. Moreover, their vitrimer composites can be repaired in-situ (mold-free) by means of pressure and temperature. Carbon fibers can be recovered from the vitrimer matrix with the original woven state and obtaining near 100% the fibers and the polymer.

S. Wang et al. [108] presented a high-performance CFR vitrimer with phenol-formaldehyde resin (Novolac), and boronic-ester dynamic bonds, presenting advantages on availability of neat materials and possibility of large-scale production, also having good solubility in organic and green solvents. This dynamic formulation had high interlaminar shear strength and flexural strength, with the advantage of having good reprocessability and almost full retention of the mechanical properties from the pristine material (95%), compared with thermoset phenol formaldehyde resins cured with hexamethylenetetramine (HMTA).

X. Liu et al. [109] prepared a catalyst-free phenolic-toluene diisocyanate vitrimer composites from commercially available resources. Their formulation had the advantage of preserving the mechanical strength of conventional phenolic resins while having efficient stress relaxation, good recyclability and a very high glass transition temperature (up to 200° C) due to the formation of higher molecular species in comparison with pristine phenolic resins. GFRP composites prepared with this vitrimer formulation presented comparable mechanical performance to other phenolic-based composites.

T. Liu et al. [110] proposed a catalyst-free epoxy vitrimer made of Bisphenol A (BPA) resin and ethylenediamine (EDA) prepolymers, with a dynamic glutaric anhydride (GA). This formulation presented better mechanical performance than reported similar CFR epoxy vitrimers. Additionally, this CFR vitrimer could be dissolved in water at high temperature by the hydrolysis of ester bonds in the cross-linked network. Recovered fibers from the recycle process presented comparable tensile strength to the pristine material.

H. Wang et al. [111] demonstrated that vitrimers allow multi-shape memory effects in CFR composites. They formulated a multi-shape memory epoxy vitrimer (MSMEV) based on Diglycidyl ether of bisphenol F resin (DGEBF) with 4-AFD, γ-aminopropyltriethoxysilane (APTS) and poly(propylene glycol) bis(2-aminopropyl ether) (D2000), where disulfide bonds and ether linkages allowed the network malleability. Silyl-ether linkages led to multi-shape memory behavior, and D2000 component led to fixity in the different states. The formulated vitrimer composites could reorganize and form new shapes under defined temperatures, presenting high repeatability under multiple cycles. Additionally, reinforcements could be recycled and reused. These characteristics can diversify the use of CFRP in transport industry by making shape

memory structures (Figure 2.16) capable of maintaining high mechanical properties as for example, a lot of space can be saved during storage and transportation of aerospace vehicles.

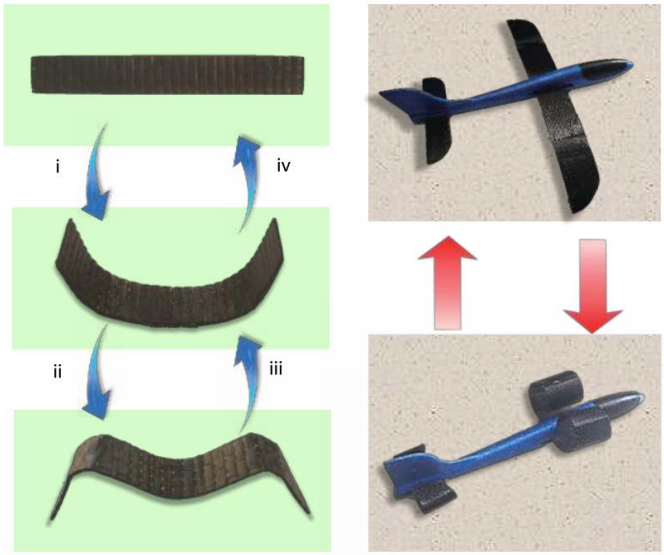

Figure 2.16 Demonstration of multi-shape memory in carbon fiber reinforced vitrimers. [111]

S. Wang et al. [95] investigated a CFR vitrimer from vanillin-based epoxy and a Schiff-based diamine 4,4'-methylenebiscyclohexanamine (PACM) dynamic hardener, being simple to prepare, economical and environmentally friendly. This vitrimer formulation had a slightly higher T_g and thermal stability than its thermoset counterpart by its high content of Schiff-based dynamic structure. It also had better tensile modulus and higher elongation at break compared with a thermoset Bisphenol-A epoxy resin (DER331-PACM). In counterpart, the tensile strength of this formulation was lower, possibly related to its lower cross-linking density. In a recent study of the same authors [87], they formulated a bio-based catalyst free epoxy vitrimer formulation with itaconic acid-based epoxy monomer (EIA), maleic anhydride (MA) and glycerin that present comparable mechanical properties as thermoset DGEBA epoxy resins, having improved malleability attributed to a high concentration of ester bonds and the glycerin in the formulation, and complete degradation under mild-alkaline conditions at room temperature that maintain the chemical structure and mechanical properties of recovered carbon fibers.

Y. Y. Liu et al. [112] presented the first formulation of a biobased epoxidized soy bean oil (ESO) and a Vanillin-4-aminophenol (VA) dynamic Schiff-based hardener, being an environmentally friendly and a safe substitute to traditional fossil-derived and toxic epoxy resins such as DGEBA. In comparison with a thermoset ESO-based resin formulation, this vitrimer had better neat tensile properties, attributed to the high stiffness of the network structure, and more elongation at break, possibly related to its low cross-linking density. ESO-VA vitrimer presented a high rate of stress relaxation while increasing temperature, this is done thanks to the acceleration of the rearrangement rate of the network topology. This vitrimer could be fully recycled by means of heat due to its imine exchange reactions, or under acidic conditions. In a more recent publication [113], they formulated an epoxy-based vitrimer of glycerol triglycidyl ether (Gte) an imine-containing vanillin and 4-aminophenol dynamic hardener, that also had good mechanical properties, and good recyclability, but with the ability of blocking the full range of UV light (200 – 400 nm) due to its C-N structure, thus possibly preventing aging to composite structures caused by long-term exposure to outdoor environments.

X. Liu et al. [114] prepared two bio-based imine vitrimers by taking DGEBA resin with two dynamic hardeners based on Vanillin + 1,6-hexylenediamime (Van-H-OH), and Vanillin + m-xylylenediamine (Van-MOH). Both bio-based vitrimers proved to be thermally stable, solvent resistant and mechanically comparable to conventional DGEBA formulations. The CFR vitrimers presented good recyclability under weak-mid acidic conditions and the fiber cloths used in their study maintained the textile structure, chemical structure, surface morphology and the mechanical properties of the pristine ones.

Y. Xu et al. [115] prepared a catalyst-free bio-based vitrimer by mixing epoxidized menthane diamine and adipic acid. In this case, their dynamic formulation proved to be fully recyclable, allowing to recover the reinforcement with the same mechanical properties as the original materials. Additionally, the prepared CFRP could be reprocessed, healed and exhibited shape memory and self-adhesive properties.

P. Li et al. [116] formulated three different benzyl cyclic acetal epoxy monomers. Due to low viscosities and a liquid state, one of these monomers can be processed via vacuum assisted RTM process (VARTM) to produced CFRP with good pristine and recycled mechanical performance, with no damage on the reinforcements after recovered under mild acidic conditions.

X. An et al. [117] manufactured a vitrimeric binder based on diglycidyl ether of bisphenol A resin, 4,4’-diselanediylbis(4-amino-N-benzylbutanamide) and selenolactone which can be used with carbon fiber, having fast relaxation times, high glass transition temperature and good reparability.

Y. Wang et al. [118] prepared four different lignin bio-based vitrimer formulations using a Vanillin epoxy monomer and combine it with different curing agents. One vitrimer based on Isophoronediamine presented the best tensile properties when compared to a conventional thermoset Bisphenol-A epoxy resin. Most of the formulated vitrimers could be easily degraded at room temperature under acidic conditions, and the recovered reinforcements conserved their original morphology and chemical structure.

In summary, vitrimers present comparable or, in some cases, better performance than traditional thermoset formulations, while presenting groundbreaking properties such as reprocessability, repairability, recyclability, weldability and shape memory, conserving a thermoset-like behavior whereas their topology is frozen. Some vitrimer formulations can be processed without the need of external catalyst that maintain mechanical properties trough time, also being safe for processing. And moreover, vitrimers can be developed with currently available precursor materials or be partially or fully biobased [119]–[121], additionally being soluble in organic solvents or even in water [122], becoming an environmentally friendly solutions. Theoretically, waste generation can be avoided and solvents or other chemical derivates can be recovered and used again.

Vitrimers have proved that can be processed under traditional manufacturing methods as RTM or resin infusion, and further reprocessed by compression molding, or in continuous production methods as pultrusion [123]. Besides apporting new or additional properties to conventional fiber reinforced polymer such as mechanochromy to obtain visual indications of damage, UV, electromagnetic or microwave shielding [124], [125] fire protection/resistance [84], [126], o create a new class of intelligent materials with the possibility of shape memory and shapeshifting abilities.

However, there is still a gap between their performance and current aerospace-grade structural thermoset composites, with no reported aerospace-capable vitrimer formulations yet. No detailed mechanical studies on vitrimer-based composites relevant to the aviation industry are available for use in evaluating the possible implementation of high-performance fiber-reinforced vitrimers in real structures.

Having this in mind, The EU H2020 project AIRPOXY (thermoformAble, repaIrable and bondable smart ePOXY-based composites for aero structures) [127], [128] was funded with the aim of introducing vitrimer advantages into the aeronautic industry to reduce production and maintenance costs of aeronautic composite parts. This thesis is related to this project in the use of a new high-performance vitrimer formulation and its use in the HP-RTM process, offering new possibilities to structural automotive materials.

This thesis goes beyond the state of the art by presenting a new high-performance vitrimer formulation, capable to substitute current thermoset matrices used in the aeronautical field having comparable performance.

Table 2.6 summarizes the mechanical performance of some fiber reinforced vitrimer formulations and some base thermoset aeronautic references.

Table 2.6 Summary of reported properties for vitrimer composites and some thermoset aeronautic-grade references

Reference	Fiber / Fabric	Resin / Monomer	Dynamic system / Hardener	Tensile modulus [GPa]	Tensile strength [MPa]	Compression strength [MPa]	Flexural Modulus [GPa]	Flexural strength [MPa]	ILSS [MPa]	Single lap shear strength [MPa]	Impact strength [kJ/m²]	Tg [° C]
A. Ruiz de Luzuriaga et al. [78], [97]	Glass	Diglycidyl ether of bisphenol A Epoxy	4-aminophenyl disulfide	-	88	292 ± 16	-	595 ± 39	37 ± 3	-	194 ± 18	130
W. Denissen et al. [99], [100]	Glass – plain weave (hot-pressed)	Vinylogous urethane	Amine	33.2	336	-	-	-	-	-	-	110
J. Markwart et al. [98]	Glass (62.2% wt fiber content)	Vinylogous polyurethane	Phosphonate	-	-	-	20.7 ± 0.7	387 ± 16	-	-	-	70
X. Liu et al. [109]	Glass (60% wt fiber content)	Phenol formaldehyde	Urethane	-	-	-	-	184.1	12.93	-		200
K. Yu et al. [101]	Carbon - plain weave	Diglycidyl ether of bisphenol A Epoxy	Fatty acid + $Zn(Ac)_2$ catalyst	≈2	≈100	-	-	-	-	-	-	-
H. Si et al. [79]	Carbon	Bis(4-hydroxyphenyl) disulfide	4-aminophenyl disulfide	10.5	334.5 ± 87.7	-	-	-	-	-	-	147
M. K. Bangash et al. [104]	Carbon – plain weave 200 g/m² FVF 43.36%	Diglycidyl ether of bisphenol A Epoxy	4-aminophenyl disulfide	-	-	-	51.8 ± 3.2	818 ± 64.82	53.2 ± 1.3	-	-	-
Y. Yuan et al. [73]	Carbon woven	Poly(hexahydrotriazine)	2,2-bis[4-(4-aminophenoxy)phenyl]propane	68.3	741.2	351.5	54.8	829.7	75.5	-	-	198.2
	Carbon UD			141.7	1806.6	343.3	127.4	1241.2	69.1	-	-	199.5
P. Taynton et al. [105]	Carbon – twill weave	Diamine-	Polyimine	14.2 ± 1.1	399 ± 85	-	32.4 ± 3.7	255 ± 56	-	-	-	145
L. Yu et al. [107]	Carbon (57 wt% fiber content)	Terephthaldehyde	Diethylenetriamine + tris(2-aminoethyl)amine	13.1	185	-	-	-	-	-	-	59.8
S. Wang et al. [108]	Carbon	Phenol formaldehyde	Boronic Ester	-	-	-	24.2 ± 0.3	411.6 ± 5.3	48 ± 2.5	-	-	153
Y. Liu et al. [87]	Carbon	Itaconic acid-based Epoxy	Maleic acid + glycerin	31.3	417	-	-	-	45	-	-	54
S. Wang et al. [95]	Carbon – plain weave	Vanillin Epoxy	Diamine 4,4'-methylenebiscyclohexanamine	35.3 ± 2.4	763 ± 71	-	-	-	-	-	-	172
Y. Y. Liu et al. [112]	Carbon	Bio epoxidized soybean oil	Vanillin + 4-aminophenol	1.18 ± 0.14	145.4 ± 17.13	-	-	-	-	-	-	27.6
Y. Y. Liu et al. [113]	Carbon – plain weave	Glycerol triglycidyl ether	Vanillin + 4-aminophenol	12.9	449	-	-	-	-	-	-	70
X. Liu et al. [114]	Carbon plain weave	Diglycidyl ether of bisphenol A Epoxy	Vanillin + 1,6-hexylenediamime	16.8	584	-	-	-	-	-	-	83

			Vanillin + m-xylylenediamine	19.3	622	-	-	-	-	-	-	96
Y. Xu et al. [115]	Carbon (60% wt fiber content)	Bio epoxidized menthane diamine	Adipic acid	-	465					3.8		86
P. Li et al. [116]	Carbon – woven (60% wt fiber content)	Benzyl cyclic acetal epoxy	Trimethylolpropane	25.5 ± 0.7	635.9 ± 24.1			62.4 ± 0.9				143
X. An et al. [117]**.**	Carbon – plain weave (200 g/m^2)	Diglycidyl ether of bisphenol A + 4,4′ - Methylenebis(N,N-diglycidylaniline)	4,4′ - diselanediylbis(4-amino-N-benzylbutanamide)	-	≈600 - 650	-	-	-	-	-	-	113 - 144
Y. Wang et al. [118]**.**	Carbon-woven (198 g/m^2) 36.3% FVF	Vanillin Epoxy	4,4′-Diaminodiphenylmethane	≈3.5	≈500	-	-	-	-	-	-	143
	Carbon-woven (198 g/m^2) 36% FVF		Diethylenetriamine	≈6	350	-	-	-	-	-	-	58
	Carbon-woven (198 g/m^2) 34.8% FVF		Isophoronediamine	11.7	571	-	-	-	-	-	-	132
	Carbon-woven (198 g/m^2) 30% FVF		Isophoronediamine + Polyetheramine	≈6	≈500	-	-	-	-	-	-	84
H. Memom et al. [29]	Carbon	Trifunctional epoxy	Imine Vanillin-HTDA	-	-	-	56	1028	52	-	-	131
T. Liu et al. [110]	Carbon	Bisphenol A + Ethylenediamine	Glutaric anhydride	17.1 ± 2.5	356 ± 28.7	-	-	-	-	-	-	95
H. Wang et al. [111]	Carbon (low wt%)	Diglycidyl ether of bisphenol F	4-Aminophenyl disulfide + Aminopropyltriethoxysilane + Poly(propylene glycol)bis(2-aminopropyl ether)	10.18	320	-	-	-	-	-	-	97.4
Aeronautic standard reference. [73]	Carbon – 5h satin (prepreg)	Hexply 914	-	70	631	-	61	912	64	-	-	190
Aeronautic standard reference [129]	Carbon 8H satin 6K (prepreg)	Hexply 8552	-	86	1014	-	-	-	90	-	-	200
Aeronautic standard reference [130]	Carbon UD (prepreg)	Epikote 475	-	-	-	-	60	1020	65	-	-	190
Aeronautic standard reference (approximated results) [131]	Carbon - 5H satin	RTM6	-	69	1180	950	-	-	67.5	-	-	-

Chapter 3: Methodology

In this chapter we describe the materials, equipment, standards and the manufacturing processes for the HP-RTM and vitrimer composites testing.

As commented previously, the objective is to prove that HP-RTM can overcome current RTM process flaws increasing the injection time by effect of pressure, making possible to use high-reactivity resin formulations, cutting more the processing time. For this, the implementation of the on-line monitoring systems will be crucial as through by different injection tests, in RTM and HP-RTM, we are going to measure the filling time, impregnation quality and curing behavior.

Based on the state of the art, high pressure can also improve the mechanical behavior of the composites produced by this technology by the reduction of the internal porosity. For that we are going to evaluate the mechanical properties for composites produced by RTM and HP-RTM, especially measuring properties that depends more on the interaction between matrix and reinforcement, making them especially prune to be affected by the internal porosity content as: flexion, compression and interlaminar shear strength [132]–[134]. These properties are going to be compared with the measurement of the porosity content between RTM samples and HP-RTM samples injected at different pressures.

In the AIRFPOXY project [1], different mechanical properties were defined for of a widely used aeronautic thermoset resin and the idea is to evaluate the epoxy-based new vitrimer formulation under the same properties to compare it and determine if can be implemented as a possible substitute for thermoset fiber reinforced composites, providing new characteristics and bringing new advantages in sustainability. For proving this, thermoset and vitrimer composites are produced under the same process (RTM) and with the same reinforcements to test the performance of the vitrimer matrix, in this case, different moisture and temperature conditions are implemented. In addition, both aero-grade thermoset and vitrimer resins are processed by HP-RTM process to demonstrate also that this technology can also be implemented in sectors such as aeronautics, improving the mechanical properties and helping to reduce processing time.

3.1. Materials

3.1.1. Reinforcements

Carbon fibers are used as reinforcement for both HP-RTM and vitrimer composites. A bidirectional 0/90 NCF is used in the HP-RTM samples. This fabric is composed by Aksa A-42 12K fibers (tensile strength and modulus of 4200 MPa and 240 GPa respectively [135]) with fibers density of 1.76 g/cm^3, areal weight of 205±5 g/m^2 in 0° direction (Figure 3.1 a) and 205±5 g/m^2 in 90° (410 g/m^2 in total, Figure 3.1 b). The fibers are hold by a 6 ± 1 g/m^2 trikot polyester yarn, this fabric was provided by Saertex GmbH [136].

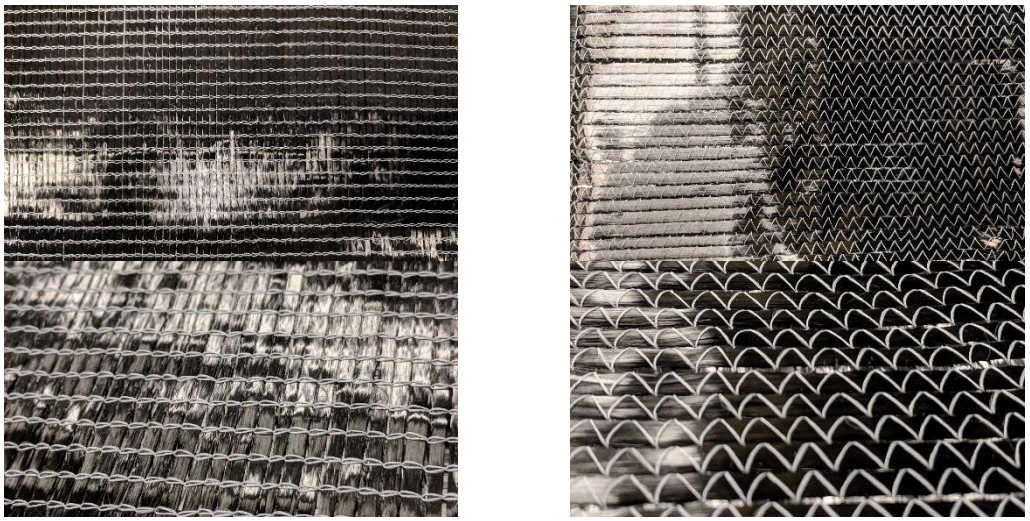

a b

Figure 3.1. CF NCF 410 g/m^2 (a) 0° direction. (b) 90° direction

The stacking sequence was defined as a cross-ply configuration with 5 layers of bidirectional fabrics (0/90, 0/90, 0/90, 90/0, 90/0), reaching an intended thickness of 2.00 mm with a theoretical fiber volume fraction (V_f) of 58.23%.

$$V_f = \frac{nA_w}{h\rho_f} \quad (4)$$

In this equation, n is the number of layers, $A_w$is the fabric aerial weight, h is the thickness and ρ_f is the fibers density. [36]

Other glass fiber reinforcements were used to check the function or validate the modifications of the HP-RTM machine: bidirectional NCF of 500 g/m^2, MAT of 200 g/m^2 and a veil of 50 g/m^2.

Additionally, two different carbon fiber reinforcements were used in the vitrimers characterization. These fabrics were provided by Chomarat. One was C-WEAVE™ 280SA5 (Figure 3.2 a), which is a 5-harness satin (5HS) woven fabric with T800HB 6K intermediate modulus fibers and an aerial weight of 280 g/m^2. [137]. The other reinforcement was C-PLY™ SP U268S5 (Figure 3.2 b), which is a unidirectional (UD) fabric with T800H 24K intermediate modulus fibers and an aerial weight of 284 g/m^2. Both reinforcements were manufactured with a custom-made PA stabilization veil (Figure 3.2 c), with an aerial weight of 8 g/m^2, intended to improve the interlaminar toughness of the final vitrimer composites. The FVF for both vitrimer composites and thermoset baseline was set to 58%, considering fabrics characteristics, samples thickness and number of fabric plies [138], [139].

a b c

Figure 3.2. Fabric reinforcement structures. a) 5-Harness satin weave. b) UD fabric. c) Detail of co-PA binder veil

To characterize the 5HS fabric, we tested cross-ply configurations (CP), while for the UD reinforcement, 0° and 90° configurations were used. Laminate tests were performed over a quasi-isotropic configuration.

Testing of the HP-RTM vitrimer and the high-performance resin was made using the NCF reinforcements.

3.1.2. Resins

Sicomin epoxy resin (SR 1331) [140] was used for the HP-RTM testing as the standard formulation. This is a 3-part resin system with an anhydride-based hardener (SH 166) and accelerator (SX AC 1MI), intended for pultrusion and filament winding processes, having the advantage of presenting very low viscosity at injection temperatures: from 135 ± 25 mPa-s at 40° C to 42 ± 8 mPa-s at 60° C, making it appropriate for liquid injection processes. In addition to working at different temperatures to reduce its curing time: from 240 min at 80° C to 4 min approximately at 140° C, while having long pot life, making it suitable to process in the HP-RTM machine without having risk of curing during the operation. Mixing ratio is fixed as 100:90:2 in weight (52.1% - 46.9% - 1% in volume).

Hexcel RTM6 [141] was used as the high-performance thermoset reference, which is a widely used epoxy system for aeronautic structures. This is a mono-component formulation intended to injection processes as RTM or LRI, having low viscosity at injection temperatures (from 200 mPa-s at 80° C to 33 mPa-s at 120° C approximately).

For the vitrimer testing, we used a new formulation of an aeronautical-grade epoxy-based vitrimer (referred as AIR-3R) that has low viscosity at processing temperatures, so that it can be processed by infusion and RTM processes. It consists of a catalyst-free formulation composed of commercially available functional epoxy groups and a new hardener with dynamic crosslinks based on aromatic disulfide species, also commercially available. This is a patented formulation, created, characterized and provided by Cidetec [31], [142], [143].

3.1.3. Other materials

We used a peel ply layer in the HP-RTM processing in order to help the demolding of the composite panels from the HP-RTM mold (upper part). This peel-ply layer consist on a Nylon-66 fabric of 85 g/m^2 with a maximum operative temperature of 190° C. Material provided by INP96 [144].

We applied semi-permanent demolding agents on the mold surfaces, injection nozzles and mixhead closing mechanisms prior each injection (Chemlease 15 Sealer EZ and Chemlease 41-90 EZ). Both provided by Uneco – Gazechim [145].

Additionally, we used the Huntsman Araldite LY 3585 (XB 3585) fast-curing system in the initial bi-component HP-RTM injection trials. It's a epoxy formulation specially designed for automotive industry. This resin was mixed with Aradur 3475 CH amine hardener in a 100:25 parts by volume (mix ratio of 80% - 20%). This resin system was provided by Antala chemicals [146], [147].

Mold closing bolts were lubricated with high-temperature aluminum-base grease to prevent gripping at the mold closure. Grease supplied by Cronaser Sl [148].

3.2. Manufacture procedure

Prior injections, all mold surfaces, injection nozzles and closing accessories were coated with the semi-permanent demolding agents: all parts were cleaned with acetone and then, 4 layers of sealer (Chemlease 15) were applied using a clean cotton cloth, with a space of 10 minutes between each layer. After drying for 30 minutes, we applied 6 layers of the demolding agent (Chemlease 41-90 EZ) with another cloth, again waiting 10 minutes between applications. Release agents were applied additionally in the cavities of the injection nozzles using a cotton tip (Figure 3.3).

The molds were cleaned between injections with a dry cloth to remove any solid residue of resin. Then, we scrapped the mold surfaces with a copper tool to detach any resin remains if necessary (in order to avoid any surface indentation). After this, two more layers of demolding agent were applied before the following injection.

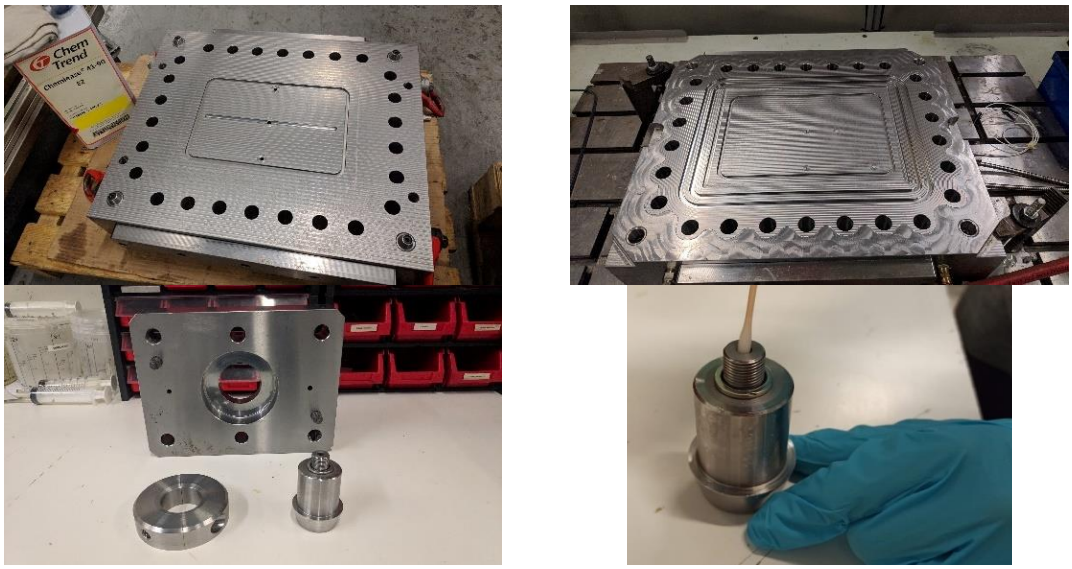

Figure 3.3. Treatment with demolding agents to the different mold parts

3.2.1. HP-RTM manufacturing process

Dry NCF reinforcement was extended above the cutting table and manually stretched to ensure the fibers had a proper alignment. The NCF layers were cut using a manual blade and a plastic template with the same dimensions as the injection cavity. Reference directions were defined following the polyester stich yarn to know the CF directions (Figure 3.4).

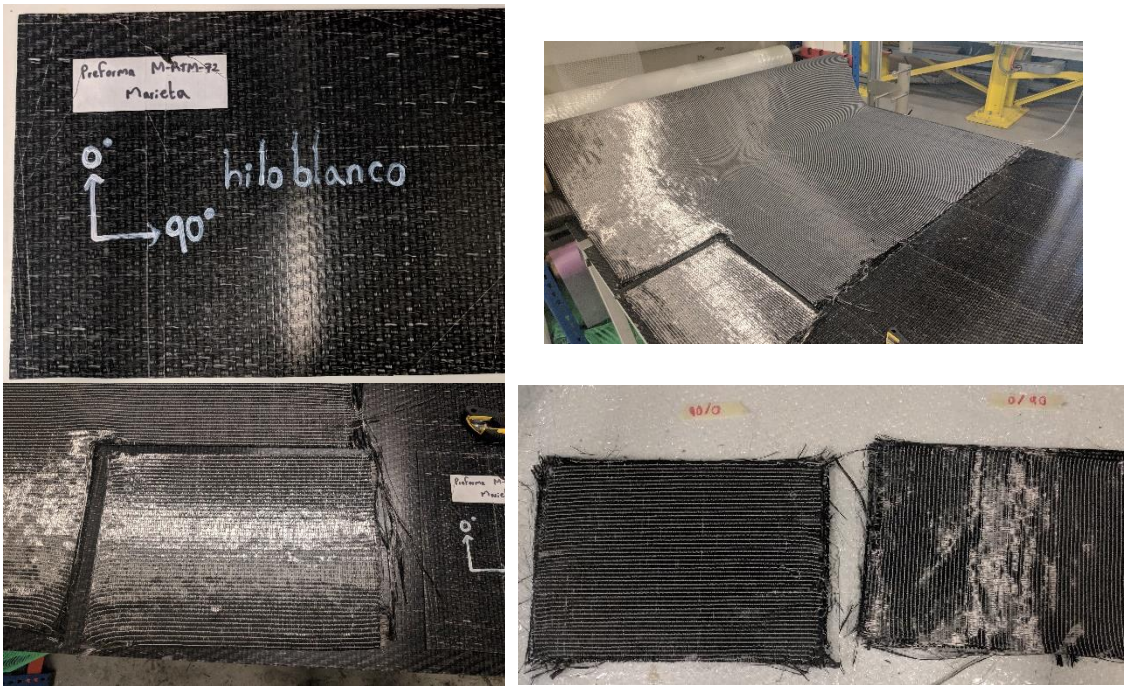

Figure 3.4. Cutting of individual fabric layers using the plastic template and the defined reference directions

Carbon NCF layers were stacked in the final lay-up to give them a final trim with scissors. No binders or adhesives were applied between the fabric layers and neither pressure or temperature was applied during the preforming process. The fabric preform was manually placed inside the injection cavity and the HP-RTM mold was closed applying a pretension of 200 Nm, and a final closing torque of 400 Nm, following a cross-path method to ensure a uniform force distribution over the mold structure. Injection and vacuum nozzles were introduced into the mold and maintained in place by the mold holding plate, applying a closing torque of 265 Nm on the holding plate bolts. Injection and vacuum valves were adapted above the mixhead holding plate in their respective thread. Finally, the machine injection hose and the vacuum hoses were attached to the valves (Figure 3.5).

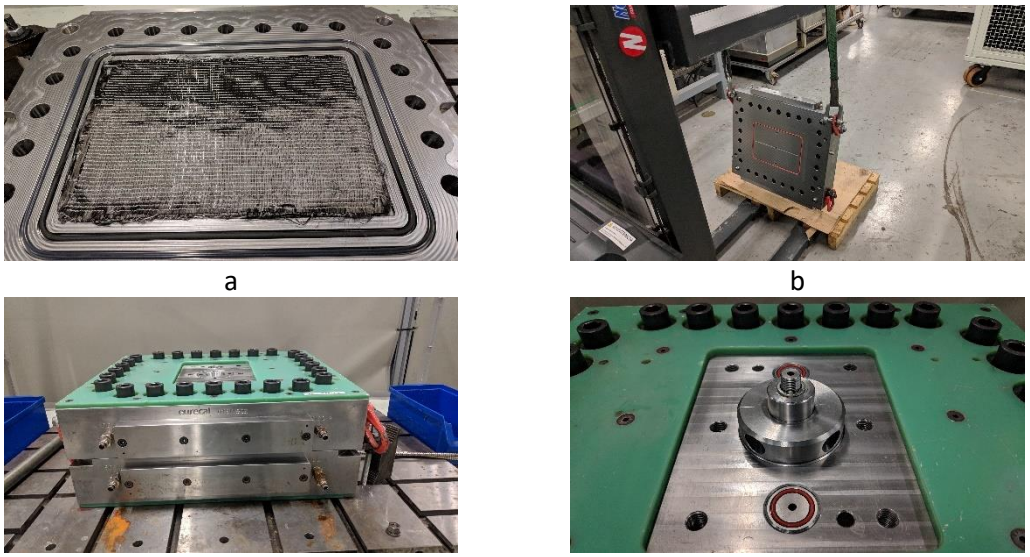

a b c d

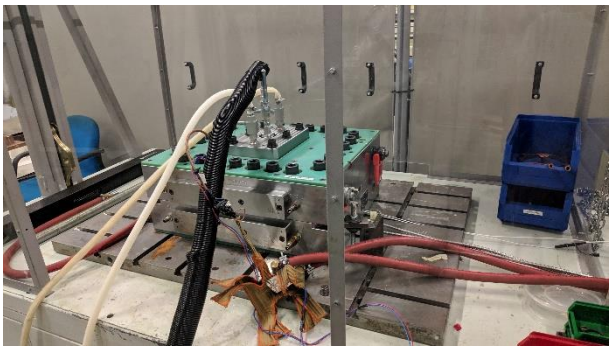

e

Figure 3.5. Mold closing for HP-RTM injection. a) Preform placement on cavity. b) Upper mold part manipulation for closing. c) Closing of both mold parts using the DIN 912 M24 bolts. d) Placement of the modified injection nozzle and the metal ring prior closing with the holding plate. e) final injection assembly (mono-component injection)

400 g of resin were measured and heated inside a convection oven at 80° C while the HP-RTM was set to prepare the injection, heating its tanks to 75° C to ensure at least 60° C in the fluid (based on the set-up tests performed in the machine). The hardener and accelerator (Sicomin) were maintained at room temperature. When the machine tanks reached the operational temperatures, the resin was extracted from the oven, and the hardener and accelerator were mixed in the corresponding quantities: 360 g of hardener and 8 g of accelerator. The mixture was immediately poured inside the machine tank (mono-component injection) to start the degassing process for 10 minutes at 60° C. When finished, the injection tank was pressurized to the intended injection pressure by maintaining the dosing valves closed (Figure 3.6).

Figure 3.6. Pouring of the resin mixture inside the injection tanks.

Prior injection, vacuum was applied in the mold to evacuate air inside the cavity. Vacuum leaks were measured first at room temperature and after reaching the injection temperature in the mold. Allowable leaks values were defined based on the Eurecat Technological Center experience in other projects [149], [150]. Maximum leaks were set to 5 x 10^{-4} MPa (5 mbar) per minute inside the mold cavity, injections with leaks above this value were no recommended (possible failures on mold closure, sealing joints or accessories that might cause resin infiltrations or induce porosity inside the composite).

After checking vacuum leaks, the mold valves were closed and the machine dosing valves were opened to allow resin mixture to arrive at the mold inlet, without entering in the mold cavity to make sure that the machine will only measure the resin that is inside of it. After this, the injection valve was opened, and the injection was carried manually until the entire mold cavity is pressurized (readings of the machine pressure sensor and the mold pressure sensors). Then, the injection valve was closed, and the machine was detached and cleaned while the composite was being cured inside the mold. The mold cavity was opened after reaching curing time and the composite was demolded. Machine, mold and accessories were then prepared for the following injections. (Figure 3.7)

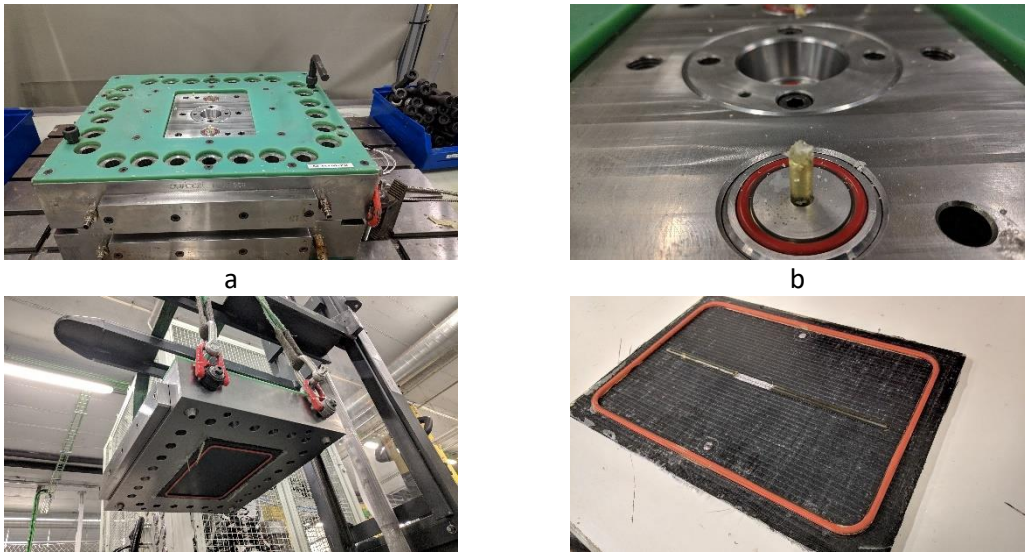

a b c d

Figure 3.7. Demolding process. a) Mold opening using extraction bolts. b) Detail of remanent resin at the channels of vacuum. c) Opening of the mold using a hydraulic elevator. d) Final part detachment

We set different curing times depending on the injection temperature as the HP-RTM trials were manufactured under different pressures and temperatures, this is displayed in Table 3.1:

Table 3.1. Curing times for the different process parameters in the HP-RTM samples

Pressure [MPa] (bar)	Injection Curing temperature [C]	In mold curing time [min]
2 (20)	80	240
5 (50)		
8 (80)		
5 (50)	120	120
	140	12

HP-RTM samples for the vitrimer and the high-performance resin were manufactured in the same way as described before. Both RTM6 and vitrimer were heated and maintained inside the injection tank at 80° C. RTM6 resin was injected at a mold temperature of 120° C, while the vitrimer was injected at a mold temperature of 130° C. Curing of the RTM6 samples was done increasing the mold temperature up to 180° C at 1° C/min, maintaining the curing temperature for 2 hours. Curing of the vitrimer samples was performed following the vitrimers RTM procedure (3.2.2)

Dimensional, visual and C-Scan ultrasonic inspections were performed in each composite before testing. Thickness measurements were performed following a predefined grid of points every 20 mm, giving to a total of 14 measuring points in the length direction, and 8 measuring points

in the width direction, avoiding the central part of the composite panel where it was located the resin distribution channel (Figure 3.8 and Figure 3.9).

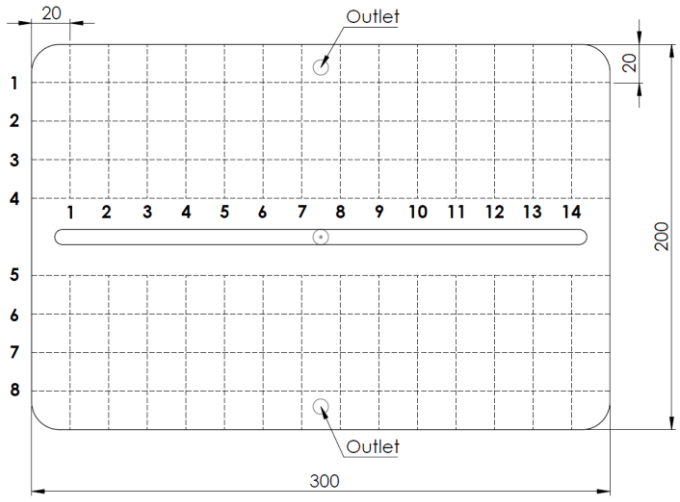

Figure 3.8. Grid of thickness measurement points on the HP-RTM panels. Dimensions in mm

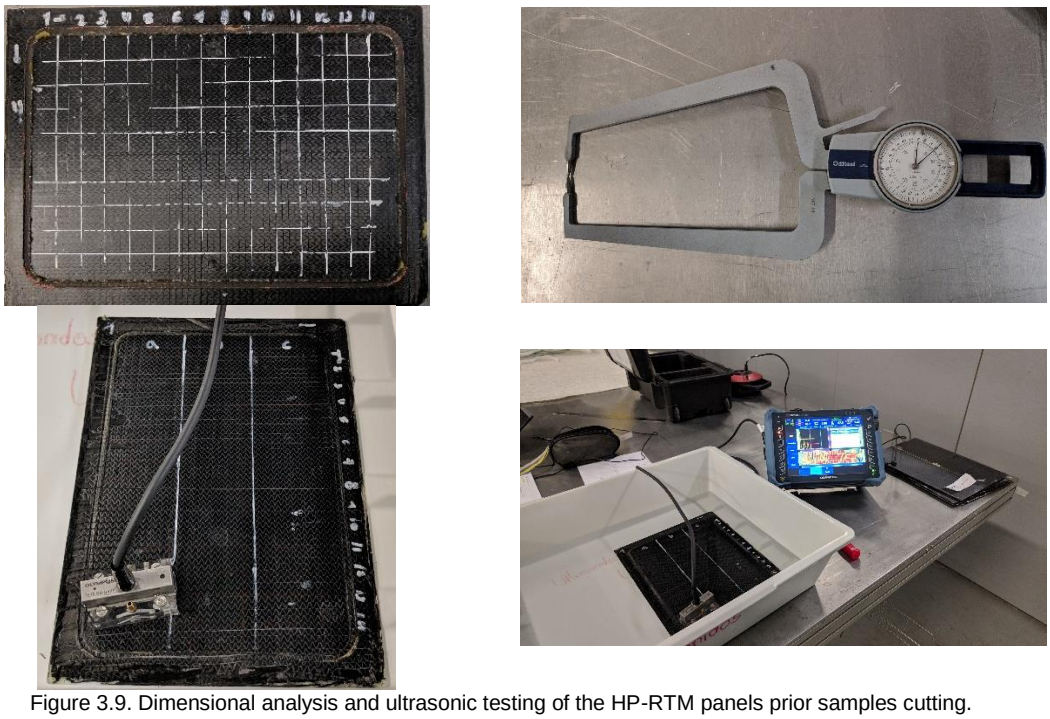

Figure 3.9. Dimensional analysis and ultrasonic testing of the HP-RTM panels prior samples cutting.

The mechanical testing coupons were cut using waterjet, ensuring that all coupons were extracted from the same position in every panel. We marked a reference point on all the samples to guide the cutting process (Figure 3.10), giving a distance of 5 mm between coupons, 5 mm from the injection distribution channel and 15 mm from the fiber clamping areas.

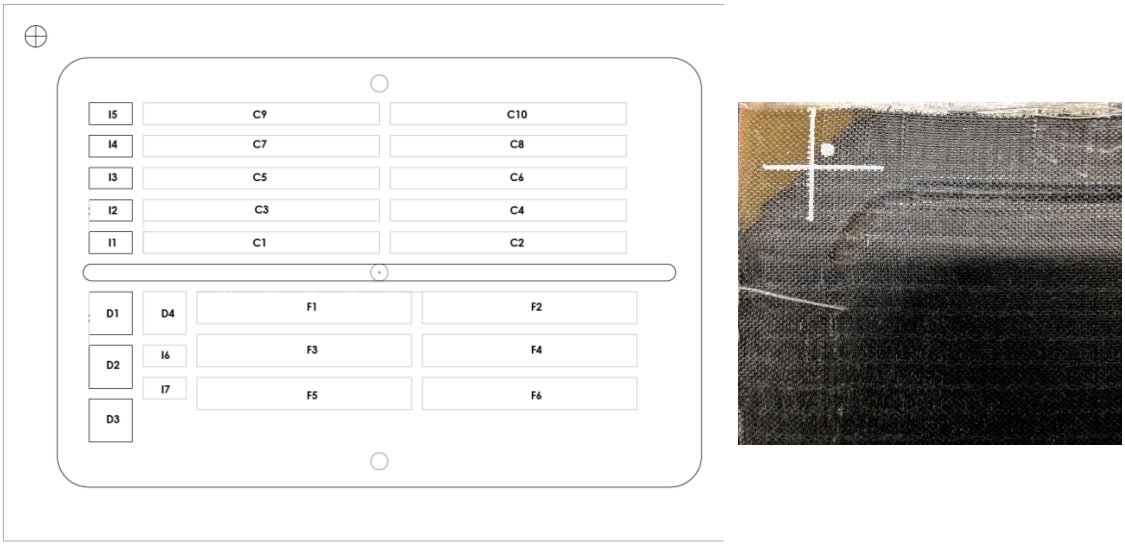

Figure 3.10. Cutting map and reference point for testing coupons. C: Compression coupons. D: Fiber, resin and porosity content coupons. I: ILSS coupons. F: Flexion coupons

3.2.2. Vitrimer RTM composites

Vitrimer composite panels were manufactured by conventional RTM using three-part metallic molds: upper and lower mold parts with an intermediate spacer, which gives the samples their final thickness required for the mechanical tests. Cavity dimensions were 505 mm x 605 mm for a steel mold and 380 mm x 220 mm for an aluminum mold. One of the two molds was selected depending on the test preparation, specimen dimensions or availability (Figure 3.11).

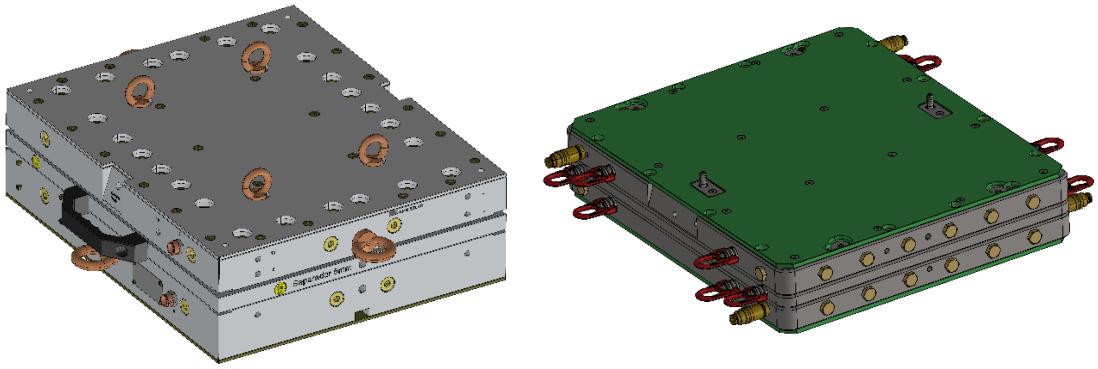

a b

Figure 3.11. Molds for conventional RTM. a) Aluminum mold of 380 x 220 mm cavity. b) Steel mold of 505 x 605 mm cavity

Dry fabrics were cut and manually placed inside the mold cavity with the specific reinforcement type and stacking sequence for each test. No pressure or temperature change was applied to the laminate during the preforming process. Prior injection, resin was degassed inside the RTM machine tank during 30 minutes at 80° C under vacuum, while the mold was being heated at 130° C, having a heating slope of 2° C/min. Injection was carried out at a constant rate of 50 g/min, maintaining a maximum pressure of 0.1 MPa (1 bar). When the mold cavity was full, a post-filling step was applied, thus increasing the cavity pressure up to 0.4 MPa (4 bars) to ensure full preform impregnation, constant fiber volumetric fraction and less void content [151], [152]. Mold temperature was maintained during 60 min. Then a second curing step was applied

increasing mold temperature up to 180° C at 1.5 °C/min and maintained it for 30 minutes more. After this, the mold was opened, and the part demolded (Figure 3.12).

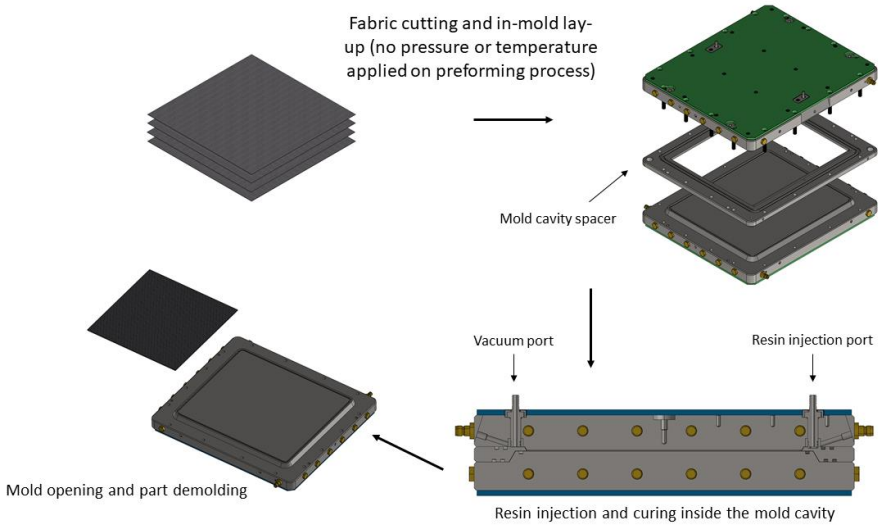

a

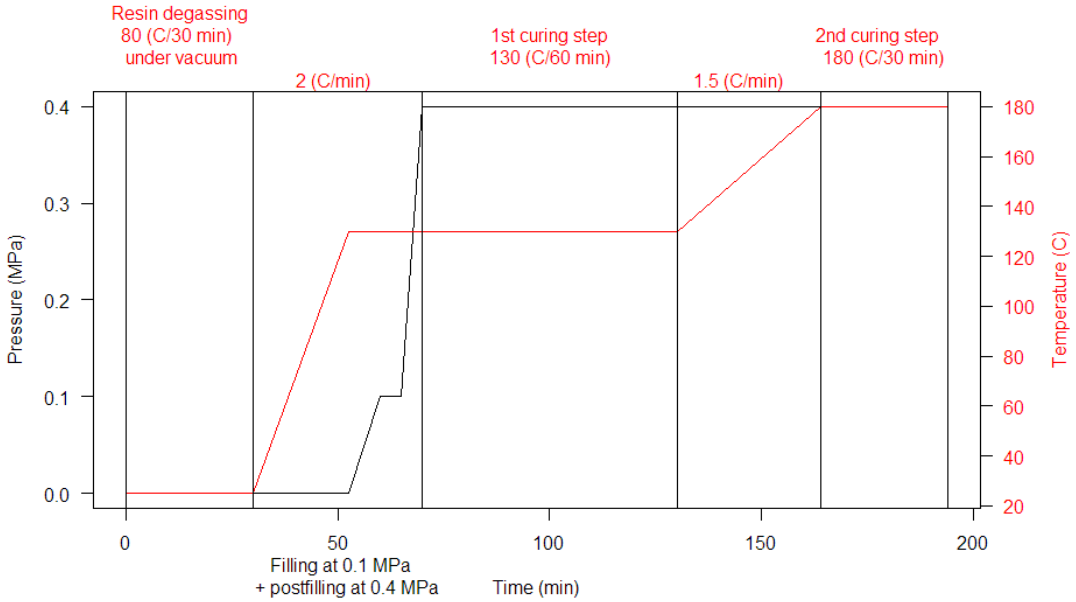

b

Figure 3.12. Detail of manufacturing procedure for vitrimer composites. (a) Process steps for composite manufacture. (b) Process conditions for injection and curing.

Samples were also validated prior machining through visual inspection and C-scan ultrasonic inspection (Figure 3.13 a and b), cutting was done by waterjet.

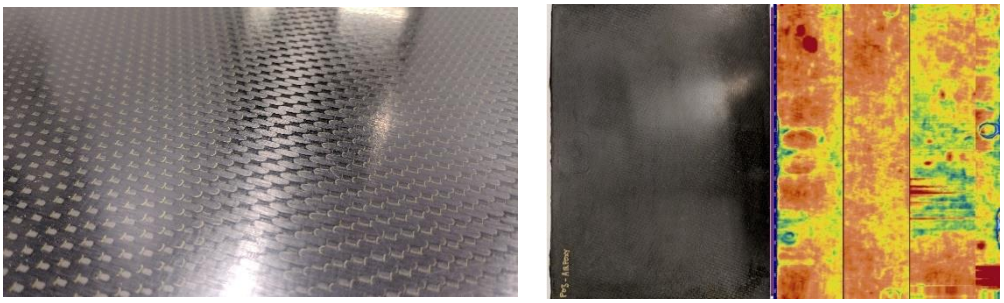

a b

Figure 3.13 Preparation of vitrimer composite test samples. a) visual inspection on the CF samples b) C-Scan inspection.

3.3. Parametric study

3.3.1. HP-RTM process

Main operational parameters for the HP-RTM process in its injection variant were defined in the state-of-the-art chapter. Injection pressure and injection rate, injection temperature, composite fiber fraction and fabric architecture can affect the process, as well as vacuum level and the inclusion of bindering materials inside the preform [4], [6], [8], [26], [27], [40], [41], [60].

Injection pressure and injection rate can affect the final composite quality more than other variables. At high-pressure, HP-RTM can overcome autoclave parts quality and reduce drastically the porosity content on the final material. In counterpart, reported risks of high injection pressure/rate are mainly fiber deformation or washout in the fabric preform due to the incident force in the preform fibers, also adding the possibility of mold opening [24], [25]. For this study, we only considered the injection pressure as the main difference with conventional RTM process., as by following Darcy's equation (Equation 1) [57], [153], both injection pressure (P) and flux (injection rate - Q) have an direct effect of the fluid velocity, so by studying both parameters simultaneously could have the same effect on the composite quality. Pressure is studied to see the effect on the composite final quality and the improvement of the process time.

Mold injection temperature is evaluated mainly for the process cycle reduction as the resin system allows to change the curing temperature. Temperature influence over other parameters as viscosity and its influence over the permeability are not considered.

This study also considers the use of three different resin formulations: a standard epoxy resin (Sicomin), a high-performance resin formulated for aeronautical structures (RTM6) and a state-of-the-art epoxy-based vitrimer based of disulfide exchange networks, in order to evaluate the influence of the process parameters on the final performance of the resin formulations.

Vacuum and the use of binders are no considered into this study. Vacuum is a standard parameter in injection processes as RTM or HP-RTM, avoiding its application can induce porosity inside the laminates by trapped air. Binder is used in cases with complex geometries that require special manipulation before the injection, and its presence can lower the overall preform permeability, also penalizing the final composite quality [6], [41]. The use of binder is discarded for this study as only flat panels are manufactured, in addition to avoid possible influences of

external materials in the final composite quality. The number of layers and stacking sequences are maintained as constant in order to ensure that the final mechanical properties are comparable. Fiber architecture is also maintained.

The experimental proposal for HP-RTM composites is summarized in Table 3.2.

Table 3.2. Experimental proposal for HP-RTM materials testing

Study	Resin	Process	Pressure [MPa] (bar)	Injection temperature [° C]
Baseline	Standard EP	RTM	0.1 + 0.6 (1 + 6)	80
	RTM6			As defined in datasheet
	AIR-3R			
Process parameters	Standard EP	HP-RTM	2 (20)	80
	Standard EP	HP-RTM	5 (50)	80
	Standard EP	HP-RTM	8 (80)	80
	Standard EP	HP-RTM	5 (50)	120
	Standard EP	HP-RTM	5 (50)	140
New materials	RTM6	HP-RTM	5 (50)	As defined in datasheet
	RTM6	HP-RTM	8 (80)	
	AIR-3R	HP-RTM	5 (50)	
	AIR-3R	HP-RTM	8 (80)	

In this study we used reinforcements of carbon fiber NCF. In all cases, injection time is recorded.

RTM and HP-RTM samples were evaluated under the same conditions. Testing was performed in a controlled environment; materials were tested as received at room temperature.

3.3.2. Vitrimer composites

This part of the current thesis was developed as part of the Airpoxy project described before. It is presented a full mechanical characterization of a new carbon fiber reinforced vitrimer, based on disulfide exchange bonds. This vitrimer was designed to compete in performance with current aerospace-grade thermoset epoxy resins.

Here, we only focus on the vitrimer composites properties, as details of the vitrimer formulation and its dynamic properties will be published in separated works under the Airpoxy project.

A set of baseline material properties relevant for aeronautical applications were defined in order to compare the AIR-3R resin behavior as a matrix for fiber reinforced composites [138]. The objective of this vitrimer composite is to be mechanically comparable and compete to one of the most widely used thermoset resin systems in the RTM process in the aeronautical industry, such as the HexFlow® RTM6 from Hexcel [141]. Baseline data was scaled up to 10% to account for the fact that the reference composite properties has been obtained with a standard modulus fiber, whereas in this work we used an intermediate modulus fiber (around 20% difference in

the respective tensile modulus [154]–[157]). All conventional thermoset values were collected with samples manufactured by RTM using the RTM6 resin (referred to as STD-AR from here on). Baseline values are summarized in Table 3.3.

Table 3.3. Baseline specifications for the AIR-3R resin based on conventional STD-AR. Adapted from [60]

Material	Specification	Unit	Fabric configuration and test conditioning					
			CP			UD		
			RT	HW70	HW120	RT	HW70	HW120
Neat resin	Glass transition temperature	° C	> 170					
	Tensile modulus	GPa	3					
	Tensile strength	MPa	75					
	Flexural modulus	GPa	3.3					
	Flexural strength	MPa	132					
Ply properties	Tensile modulus – warp direction	GPa	> 70			> 155		
	Tensile modulus – weft direction	GPa	> 70			> 8.5		
	Tensile strength – warp direction	MPa	> 980			> 2325		
	Tensile strength – weft direction	MPa	> 980			> 47.6		
	Compression modulus – warp direction	GPa	> 68			> 140		
	Compression modulus – weft direction	GPa	> 68			> 8.5		
	Compression strength – warp direction	MPa	> 646			> 1386		
	Compression strength – weft direction	MPa	> 646			> 255		
	Interlaminar shear strength	MPa	> 60	> 42	> 30	> 70	> 42	> 30
	In-plane shear modulus	GPa	> 4.5	> 3.6	> 2.3	> 4.4	> 3.5	> 2.2
	In-plane shear strength	MPa	> 86	> 73	> 49	> 82	> 65	> 41
Material	Specification	Unit	Quasi-isotropic laminate					
			RT		HW70		HW120	
Laminate properties	Fracture toughness GIC*	J/m2	> 700					
	OHT strength	MPa	> 490		> 380		> 360	
	OHC strength	MPa	> 340		> 250		> 180	
	FCH strength	MPa	> 430		> 300		> 275	

*Fracture toughness mode II (G_{IIC}) is not available on the baseline data.

Materials were tested as received at room temperature (RT) or preconditioned until equilibrium at 70° C and 85% relative humidity (RH) and then tested at two different temperatures, 70° C (HW70) and 120° C (HW120).

3.4. Tests and equipment

3.4.1. Materials characterization

Neat vitrimer tensile tests were performed following the ISO 527-2:2012 standard [158] on five dumbbell-shaped specimens (type 1B) of 150 mm in total length, and 20 mm in total width and a thickness of 4 mm. The testing area had a length of 50 mm and a width of 10 mm. Test were carried out at a speed rate of 1 mm/min.

Neat vitrimer flexural tests were performed following the ISO 178:2019 standard [159] in a three-point test configuration. The specimen dimensions were 80 mm length, 10 mm width and 4 mm thickness. Five specimens tested at a speed rate of 2 mm/min

Tensile tests were performed following ISO 527-4:1997 standard [160] on specimens of 250 mm x 25 mm with 2 mm thickness (tabbed type 3) for the vitrimer samples with the 5HS

reinforcement, and 250 mm x 15 mm and 1 mm thickness for the vitrimer samples with the UD reinforcement. Five specimens were tested for each reinforcement. Tests were carried out at a speed of 2 mm/min.

Compression tests were performed following the ISO 14126:1999 standard [161] for the vitrimer 5HS fabric and the NCF HP-RTM samples, at the speed of 0.5 mm/min. Ten 110 mm 10 mm specimens with 2 mm thickness (tabbed type A for the AIR-3R samples and non-tabbed type B1 for HP-RTM samples) were tested. The UD tests were performed following the ASTM D3410/B standard [162] with specimen dimensions of 150 mm x 10 mm x 3 mm. Strain gages were bonded in the vitrimer coupons (both sides).

A percent bending strain (PBS) [162] of 10% section threshold of 10% was established for the vitrimer composites tests to be considered as valid. Above this value, the coupon experiences undesirable load modes such as bending, buckling or torsion. This value is computed as indicated in equation 5, by taking the stress-strain slope from the two strain gauges placed in both faces of the compression sample.

$$B_y = \frac{\varepsilon_1 - \varepsilon_2}{\varepsilon_1 + \varepsilon_2} * 100 \qquad 5$$

Where B_y is the PBS, ε_1 is the indicated strain from the gage in one sample side (1), and ε_2 is the strain from the other sample side (2). An anti-buckling device was used following the requirements from the ASTM standard (ITTRI test fixture).

To align the compression samples inside the ITTRI, two metallic stoppers were machined in order to align the compression samples in the longitudinal direction, in this way coupons were positioned between the stoppers. Masking tape was used as an alignment method for the transversal direction, the tape edge gave a visual indication were to place the coupons. The ITTRI test fixture was closed first in one side to maintain the coupon in position, and then the other side (Figure 3.14).

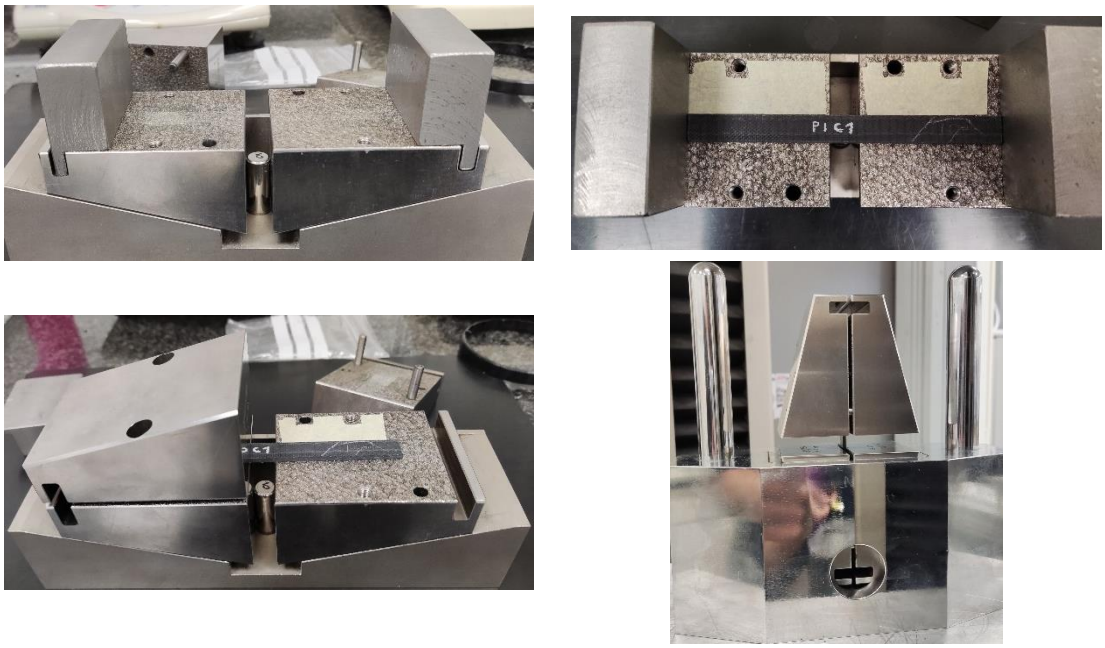

Figure 3.14. Alignment and preparation of the compression coupons for testing

3-point flexural tests were performed following the ISO 14125:1998 standard [163] on 5 samples of 100 mm in length, 15 mm in width and a thickness of 2 mm (type 4). Testing span was fixed

at 80 mm, with a loading element radius of 3 mm and support element radius of 3 mm (out of standard). All specimens were tested under the same conditions. Test speed rate was fixed at 5 mm/min, following test velocity suggested by the standard, considering sample dimensions for three-point bending test. (Equation 6)

$$v = \frac{\varepsilon' L^2}{6h} \qquad 6$$

We marked the width of the flexural coupons on the testing tool to align them. We also marked on the coupons surface the position of the support radius and the position of the load center (Figure 3.15).

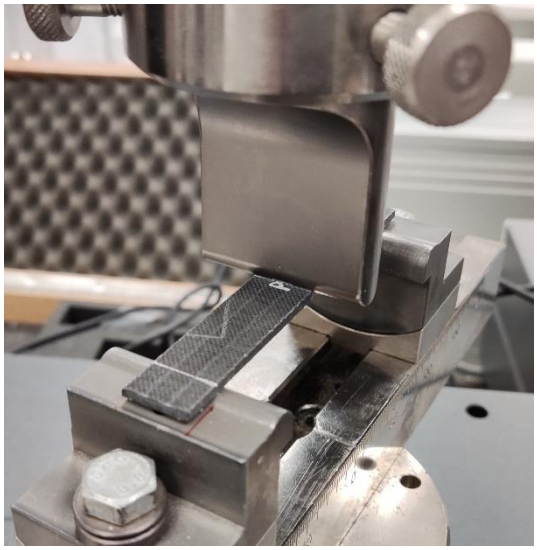

Figure 3.15. Alignment of flexural coupons for testing

Interlaminar Shear Strength (ILSS) tests were performed following ISO 14130:1997 standard [164] at a loading rate of 1 mm/min. Specimen dimensions were 20 mm x 10 mm with 2 mm thickness. Coupons were aligned using the same method as the described in the flexural testing (Figure 3.16).

Figure 3.16. Positioning of ILSS coupons for testing

In-Plane Shear (IPS) tests were performed following ISO 14129:1997 standard [165] with a loading rate of 2 mm/min. Specimen dimensions were 250 mm x 25 mm with 2 mm thickness, (tabbed specimens). Deformations were measured using a biaxial extensometer.

Open Hole Tension (OHT) and compression (OHC) tests were performed following ASTM standards D5766M [166] and ASTM D6484M [167] respectively. Specimens were 3 mm in thick, 300 mm long and 36 mm wide. The hole diameter was 6 mm. Tests were carried out at speeds of 2 mm/min (OHT) and 1 mm/min (OHC).

Filled Hole Compression (FHC) tests were performed following the ASTM D6742M standard [168]. Specimen dimensions were 300 mm x 36 mm with 3 mm thickness and 6 mm hole diameter. The specimen was mounted with a titanium protruding-head HI-LOK DAN 7-8-3 fuse pin. Test were carried on five specimens at a speed of 1 mm/min.

Mode I fracture toughness (G_{IC}) tests were performed following the EN 6033:2015 standard [169]. Sample dimensions were 250 mm x 25 mm x 3.2 mm thickness. Inside the specimens 0.01 mm thick PTFE release film was used to create a crack in the laminate. Test carried out at a speed of 10 mm/min under interlaminar configuration.

Mode II fracture toughness (G_{IIC}) test were performed following the EN 6034:2015 standard. [170]. The sample dimensions were 115 mm long, 25 mm wide and 3 mm thick. The same PTFE film of G_{IC} test was used. Test carried out at a speed of 1 mm/min under interlaminar configuration.

The glass transition temperature (T_g) was measured following the ISO 11357-2:2013 standard, using the differential scanning calorimetry method (DSC) [171]. The RTM6 and vitrimer samples were heated until 230° C, while the Sicomin resin was heated until 200° C. Two heating steps were applied to all samples at a speed of 10° C/min, applying an intermediate cooling step using nitrogen with a flow rate of 20 ml/min. A second batch of DSC tests were performed for the Sicomin resin as it was difficult to determine the T_g using the 10° C/min slope. We decided to apply a 20° C/m heating slope in order to catch the T_g, as the 10° C/min slope was better to see

the residual enthalpy from the samples [172]. For this resin formulation, we tested an uncured sample with carbon fibers to have a more similar material to the final cured samples.

Fiber volumetric fraction (FVF) and porosity content was evaluated following standard UNE-EN 2564:2018 [173] using sulfuric acid at 98% and a solution of 30% hydrogen peroxide under method B (sand bath). Samples were prepared prior testing by heating them inside an oven at 90° C for 24 hours, and inside a desiccator for 170 hours. In order to avoid possible negative results on the porosity measurement, as described in the ASTM counterpart standard (ASTM D 3171-06 [174]), densities of the cured resin and dry fabrics were measured following standard ISO 1183-1:2019, method A [175]. Sample dimensions were 20 x 20 mm with 2 mm thickness to adjust samples weight close to 1 g, cured resin samples were manufactured using the same process parameters as the respective composites, degassing the resin mixtures before curing. Acid temperature was adjusted to overpass the curing temperature of each sample, acid exposure time was defined in order to ensure a proper dissolution of the cured matrix before oxidizing it with the hydrogen peroxide, maintaining the samples under constant stirring.

Table 3.4 summarizes the test applied on the specific thesis topic:

Table 3.4. Summary of tests applied on the thesis topics

Test	**Standard**	**Thesis topic**	
		HP-RTM	**Vitrimer composites**
Neat polymer tension	ISO 527-2:2012	×	✓
Neat polymer compression	ISO 178:2019	×	✓
Tension	ISO 527-4:1997	×	✓
Compression	ISO 14126:1999	✓	✓
	ASTM D3410/B	×	✓
3-point flexion	ISO 14125:1998	✓	×
ILSS	ISO 14130:1997	✓	✓
IPS	ISO 14129:1997	×	✓
OHT	ASTM D5766M	×	✓
OHC	ASTM D6484M	×	✓
FHC	ASTM D6742M	×	✓
G_{IC}	EN 6033:2015	×	✓
G_{IIC}	EN 6034:2015	×	✓
T_g DSC	ISO 11357-2:2013	✓	✓
Fiber, resin and porosity content	UNE-EN 2564:2018	✓	×

3.4.2. Equipment

The HP-RTM mold integrated different sensors in order to monitor the process parameters in real time (on-line monitoring) while the materials are being processed. We used two types of sensors in the study: cavity pressure sensors and DEA cure monitoring sensors.

3.4.2.1. Cavity pressure sensors

We performed the monitoring of the injection pressure using piezoelectric sensors. These sensors have a natural high frequency that is capable to read changes in the cavity pressure at high speed, while being robust and stiff to hold the injection conditions. Piezoelectric sensors generate an electrical charge upon deformation or under thermal stresses, these deformations correspond to the sensor signal and with the sensor sensitivity, it is possible to convert the electric values into pressure measurements [176].

Two standard cavity pressure sensors (Priamus 6001B) were integrated inside the mold cavity. Each sensor integrated automatic detection systems of their specific sensitivity prior injection. Data acquisition was made with the BlueLine 5080-4p amplifier with four independent channels. These sensors could operate under mold temperatures up to 200° C and to a maximum cavity pressure of 20 MPa (200 bars). Sensors, equipment and software were provided by Priamus [177].

We applied corrections to the sensors signals as ghost measurements appeared without any force load. These ghost measurements were caused by the drift effect of the piezoelectric sensors [178]–[182]. It must be considered that this kind of pressure sensors are more suitable for short cycle – fast processing manufacturing methods as compression molding in plastics. So, in processes with longer manufacturing times (> 5 min) the signal contamination caused by drifting is more visible.

For the RTM and HP-RTM injections, we fixed the recording time for the pressure sensors to a maximum of 10 minutes in order to minimize drift effects. Before the injection, we let the sensors and the data acquisition system run until the mold had several minutes with a stable injection temperature, making acquisitions of the signal drift in order to verify that the ghost signals presented a total linear behavior for later subtraction to the measurements.

As sensors drift is different for any acquisition process, we decided to start the data acquisition 15 seconds before the actual injection in order to catch the drift tendency for that specific measure. In the final measurement, we took the linear tendency from those 15 seconds and subtracted it later to the entire measurement, erasing the drift effect to have a more realistic data.

The process is exemplified in Figure 3.17. We took the Trial 01 (HP-RTM 2 MPa) as an example. After the injection was performed, cavity pressure keeps increasing. This tendency does not describe the reality as the HP-RTM machine is no longer working, and it is expected to have a pressure decrease inside the mold cavity due to the shrinkage effect on the resin while curing.

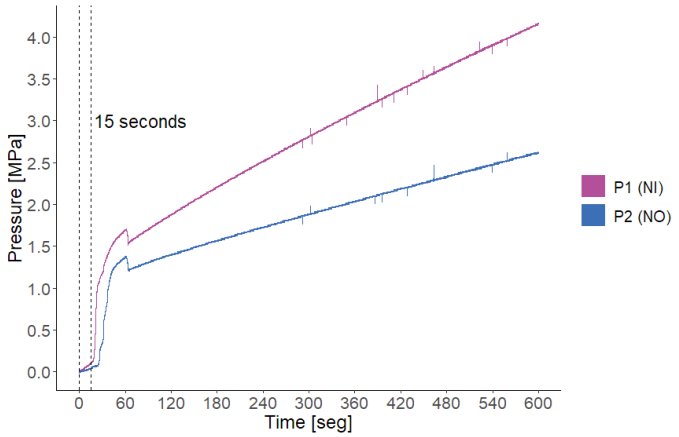

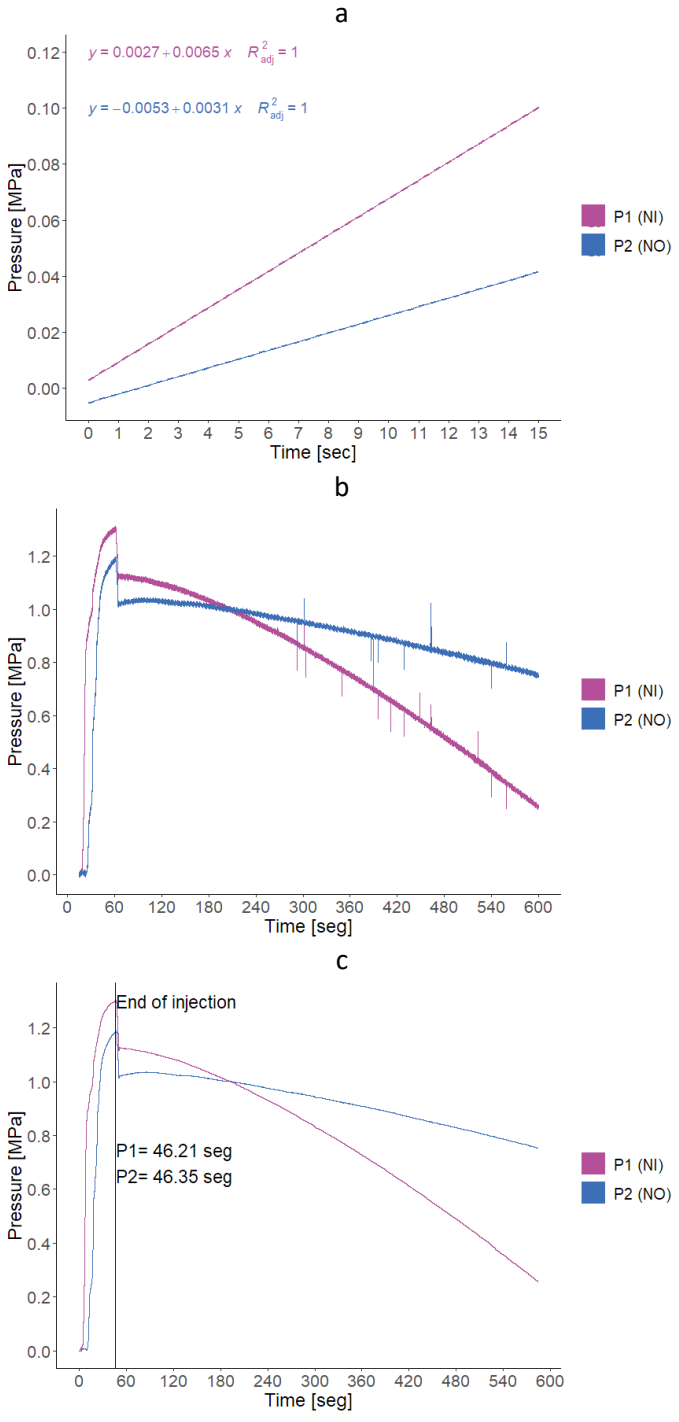

Figure 3.17. Removal of sensors drift and noise. P1 and P2 are the pressure sensors as (NI) stands for "near inlet", and "(NO) stands for "near outlet". a) original signal with drift contamination. b) Drift extracted from the first 15 seconds of the measurement. c) Pressure measurement without the drift effect. d) Final measure without signal noise.

We can see a more realistic approach of the cavity pressure after deleting the drift from the final signal. In addition to the drift, sensors also presented noise during the acquisition process (as random peaks in the signal, Figure 3.17 c). We erased that noise (Figure 3.17 d) using signal treatment options in a programmed R code (using signal filters contained in the "*Signal*" library as "*butterFilter*" and "*signal::filter*" from R-Studio) [183].)

The first 15 seconds of the measurement were only used for the determination of the drift tendency, so this part could be erased from the final data.

3.4.2.2. Cure monitoring sensors

Curing was monitored with dielectric (DEA) sensors. This type of sensors can measure changes in the material viscosity and thus, in its curing behavior. Resin acts a dielectric media in which its dipoles align, and ions try to move due to the stimuli applied by electrical currents in the sensors, the velocity of this movement is conditioned by the resin viscosity.

Dipole rotation and ion movement (ionic conductivity σ) are related to the dielectric properties of the measured resin by its complex permeability (equation 7), composed by its permittivity (ε') and loss factor (ε'') respectively. DEA sensors can read the curing state of the resin by dipole and ion movement. As the viscosity increases, dielectric movement reduces thus indicating the end of the curing process. Dipole movement is carried mainly at low temperatures, while ionic movement is done mainly under high temperatures. Ionic viscosity V_{ion} (equation 9) is directly related to the ionic conductivity [184]–[186].

$$\varepsilon^* = \varepsilon' - i\varepsilon'' \quad (7)$$

$$\tan\delta = \frac{\varepsilon''}{\varepsilon'} \quad (8)$$

$$V_{ion} = \frac{1}{\sigma} \quad (9)$$

Two Tool-mountable monotrode (TMM) 3c/3R DEA sensors were integrated in the mold cavity, each sensor integrated thermocouples in their surface area to measure the exothermic reactions in the curing material, and these sensors integrate a special coating to operate with conductive fibers as carbon. Data acquisition was carried out with the DEA 288 Ionic module with two individual channels. Sensors, equipment and software were provided by Netzsch [187].

The data measured with the dielectric sensors for each injection was the ion viscosity 9 (logarithmical) and the loss factor, defined in equation 8. Ion viscosity gives an idea the of the material softening, in this case the resin, after it has been injected inside the preheated mold cavity, in which reach its minimum ion viscosity value. And then following by a rise and stabilization of the viscosity, indicating the completion of the curing process (Figure 3.18). Ion viscosity is recommended to be measure in a logarithmical scale as the material conductance (G, equation 10) changes in several orders of magnitude during the curing process. Although the ion viscosity and the mechanical viscosity are different concepts, both are related, in a proportional way, to the polymer crosslinking density, which is a measure of the curing state [184]–[186], [188].

$$G = \frac{V}{I} \rightarrow \frac{Voltage}{Current} \quad (10)$$

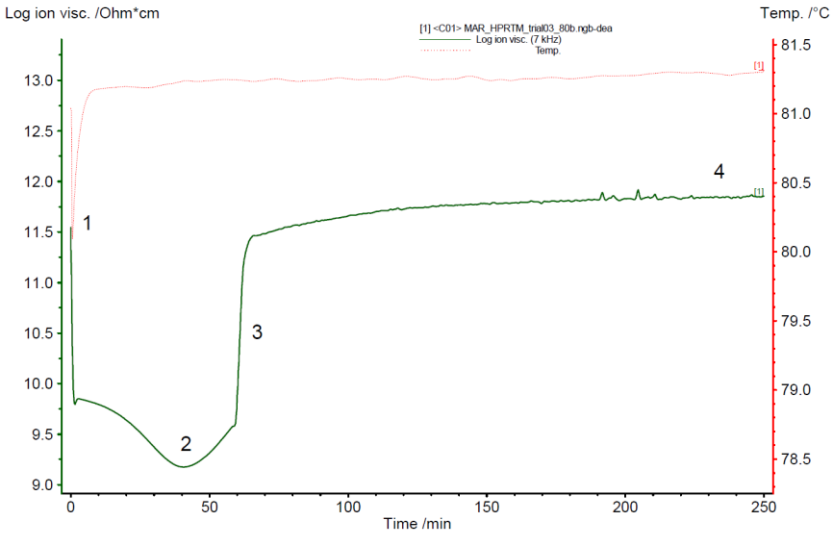

Figure 3.18. Example of a measurement for an epoxy-based component during manufacturing. 1) Flow front arrival at the sensor. 2) Minimum viscosity. 3) Curing phase. 4) Total end of cure. Adapted from [184], [185]

Changes in the dielectric loss factor are function of dipole motion and ionic conduction. The latter being more dominant and giving an indication of the ions mobility inside the resin, which is correlated to the resin viscosity and the degree of cure[189].

It is reported that dielectric measurements at low frequencies require long measurement times, and the final data is subjected to distortion by effects of electrode polarization. High frequencies (10 kHz to 100 kHz) are dominated by dipole rotation, giving an idea of the ion viscosity at the end of cure [188]. We performed a previous DEA analysis in one of the carbon fiber trials to test the stability of the new mixhead body core with the aim of stablishing an appropriate frequency range. In this test we placed the fibers as in the final configuration, with the same directions, ply number and injection conditions (resin and temperature). Frequencies used for the test were 1 Hz, 10 Hz, 100 Hz, 1kHz, 10 kHz, 100 kHz and 1 MHz (Figure 3.19). Recoding time was set to 4 hours as the injected resin (Sicomin) was cured at 80° C.

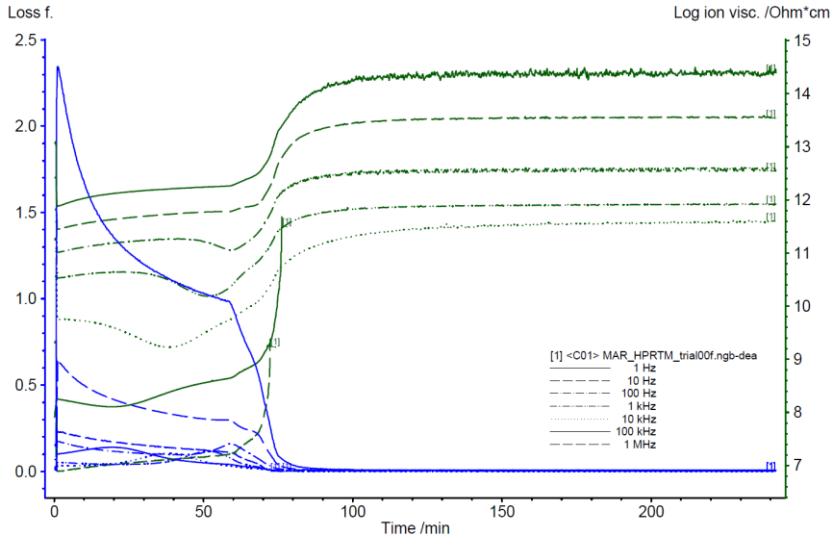

Figure 3.19. Establishment of frequency window for the CFRP samples manufactured with the HP-RTM machine (Injection pressure of 4 MPa)

Frequencies of 100 kHz and 1 MHz were lost after 70 minutes of measurement (Figure 3.20), possibly suggesting that the frequency of these signals was too high to give a proper measure.

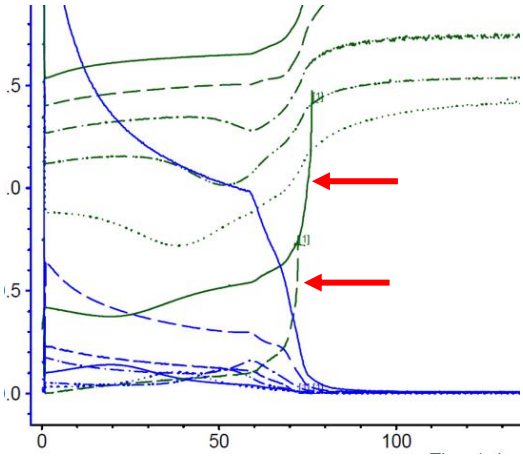

Figure 3.20. Detail of lost frequencies during DEA measurement (from Figure 3.19).

H. Lee [186] commented that material conductivity can be expressed my means of its frequency-independent σ_{DC} and frequency-dependent components σ_{DC} (equation 11). In thermosets, the early stage of the curing process tends to be dominated by the σ_{DC} component, making possible to describe the material loss factor in function of this parameter, being inversely proportional to the frequency (equation 12). In this case, at lower frequencies (1 Hz and 10 Hz), the loss factor is not proportional to the measured frequency, also limiting the measurement accuracy. In addition, we observed that the measure at 100 Hz is subjected to more noise than the other signals (Figure 3.21), so we decided to perform the following measurements only evaluating the range between 1 kHz to 10 kHz. (1kHz, 3 kHz, 5 kHz, 7 kHz and 10 kHz) (Figure 3.22).

$$\sigma = \sigma_{DC} + \sigma_{AC} \qquad 11$$

$$\varepsilon'' = \frac{\sigma_{DC}}{\omega \varepsilon_0} \rightarrow \varepsilon_0 \; Permitivity \; of \; free \; space \qquad 12$$

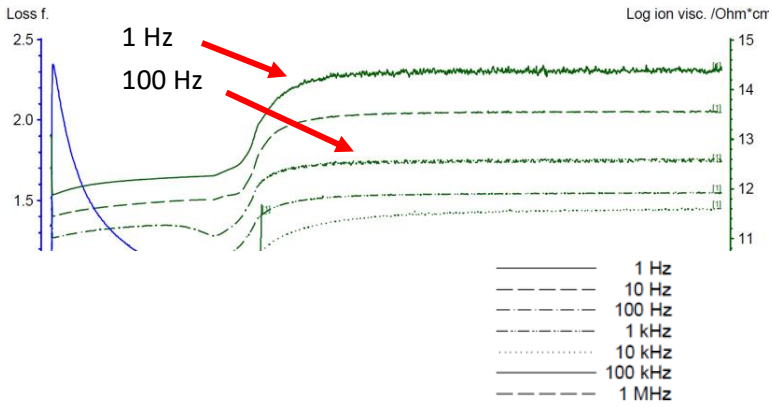

Figure 3.21. Detail of signals from DEA measurement (from Figure 3.19)

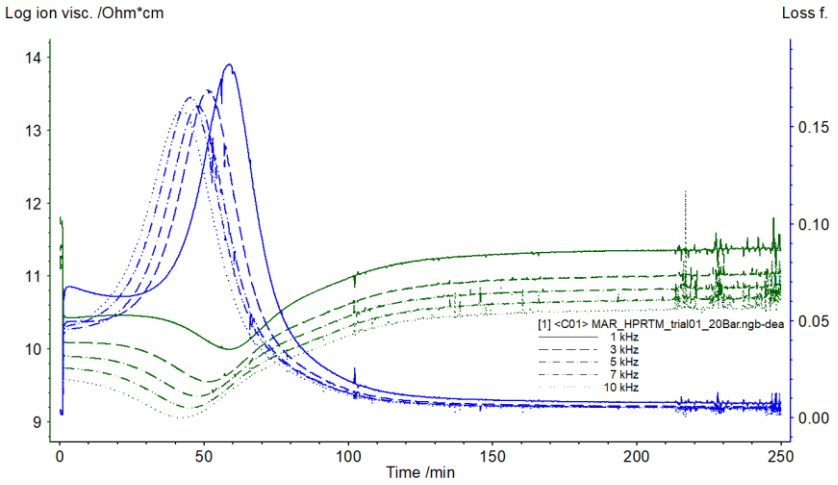

Figure 3.22. Frequency window for HP-RTM processing. Data gathered at 1 kHz, 3 kHz, 5 kHz, 7 kHz and 10 kHz. Sample measured at the 2 MPa injection under 80° C curing

Curing data was obtained from two points in the mold cavity: near to the resin inlet and near to vacuum ports (outlet). In the selected frequency range (1 to 10 kHz), we discarded the data from the 1 kHz and 10 kHz as these frequencies presented more noise than the other signals.

Comparing the remaining signals, measurements at 7 kHz were noisier than the 3 kHz and 5 kHz data. And between these two frequencies, no important differences were observed. So final comparisons between process parameters were performed at 5 kHz frequency. The Netzsch acquisition software allowed us to implement noise filters in order to soften the signals and make them easier to evaluate.

The information gathered in the DEA measurement was the minimum viscosity point (Figure 3.23, point 1), by evaluating the ion viscosity (minimum peak, Figure 3.23, point 2), end of the reaction by evaluating the intersection of the tangent lines between the reactivity slope and the baseline at the end of the measurement. Additionally, end of curing can be taken at the point where the loss factor starts to be constant (Figure 3.23, point 3) [184].

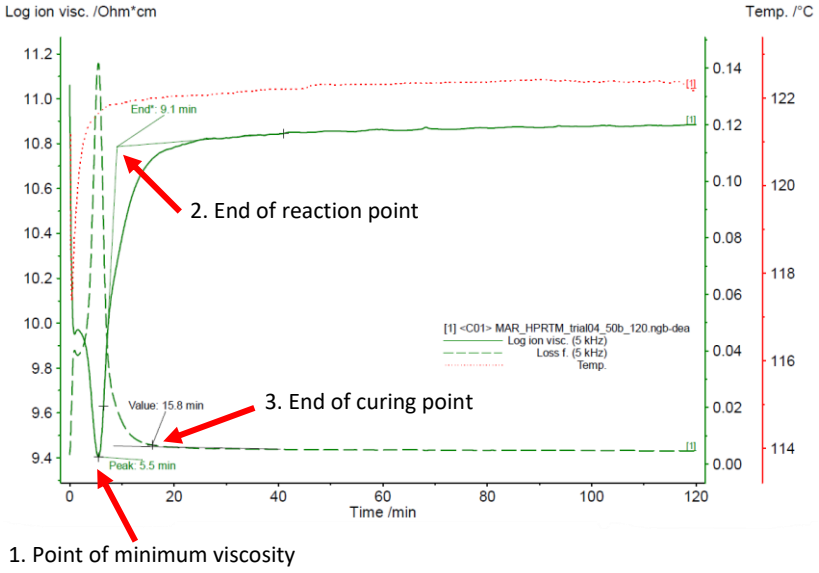

Figure 3.23. Evaluation of critical points of curing in the DEA measurements.

End of curing could be stablished as a critical point in where the slope of the reaction rate does not present significant changes or the measurement conductance is far below from its peak value (100 times or greater), but it can be a user-defined parameter depending on the applications. So it is possible to determine the end of cure by analyzing the loss factor to determine the point in which it reaches a constant value (meaning no further reactions)[186].

3.4.2.3. Sensors' position

Sensors' positioning was defined in order to have a contrast between the injection and vacuum points, thus reading the effect of the resin flow front. In this way is possible to analyze the resin flow front inside the mold cavity, in addition to the evolution of resin viscosity during the process. One pressure and one DEA sensors are located near to the injection point, the other sensors are located near to the vacuum area, as displayed in Figure 3.24.

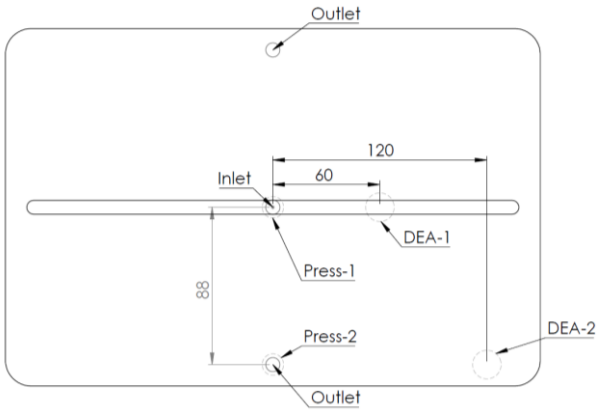

Figure 3.24 DEA and pressure sensors location in the mold cavity, dimensions in mm. (Press stands for pressure sensor, DEA are the cure monitoring sensors)

Mold structure was specifically machined to integrate the sensors and their connections. Steel mandrels were manufactured to protect the sensors' structure and facilitate their installation and removal if needed, each mandrel is placed by pressure in the mold cavity with O-rings to ensure sealing (Figure 3.25).

a b

Figure 3.25 Installation of cavity sensors. a) Sensors cavity in the mold structure (lower mold part). b) Sensors front and location in the mold cavity

3.4.2.4. Machines and other equipment

Conventional RTM samples for the HP-RTM study were manufactured on an Isojet DPE 2K + 1K Cuve 300 RTM machine [190].

Vitrimer composite samples were manufactured on a Coexpair Injector 5000cc RTM machine [191].

All the HP-RTM samples were manufactured using the Eurecat's Marieta HP-RTM machine. As the HP-RTM has not an integrated vacuum pump, leaks measurement and vacuum application was performed by using the Isojet machine.

Mold heating below 100° C was done with a water-based STL 1-9-B5/10-TK6 electric heater, provided by Single Temperiertechnik. This heater has a power capacity of 9 kW and could heat water until 90° C approx. [192] For higher temperatures, mold heating was performed with an oil-based Tool Temp TT-380 electric heater of 32 kW capacity using a non-toxic heating oil (Sil Baker AT). [193], [194]

Tension and flexural tests for neat vitrimer resin, and the tension tests for vitrimer composites were carried out in a Instron 5985 universal testing machine. A biaxial extensometer was applied in order to get strain measurements.

Compression, ILSS, IPS, OHT, OHC and FHC tests for vitrimer composites were carried out on an MTS series 332.31 dynamic testing machine. Two different load cells were used: MTS 661.19F-04 25 kN load cell for the ILSS test, and MTS 661.22D-01 250 for compression, IPS, OHT, OHC and FHC tests. [195]

Compression, flexion and ILSS tests for HP-RTM composites were performed on a Zwick-Roell Z050 TH electromechanic machine. Tests performed with a 50 kN load cell.

Interlaminar fracture toughness tests under mode I (G_{IC}) and II (G_{IIC}) for the vitrimer composites were performed in a Zwick-Roell Zwick 3 testing machine.

DSC tests were performed on a TA Instruments DSC Q20 machine.

FVF test were performed in a Combiplac sand bath from JP Selecta, with Duran No.4 filter elements with a capacity of 30 ml from Schott. Density measurements were carried on an AX 205-DR weight scale from Mettler-Toledo.

Ultrasonic inspections were carried with an Olympus OmniScan MX2 UT machine with a 5.0L64-NW1 phase-array probe of 5 MHz, having 64 individual elements. All inspections carried under immersion in water with a fixed velocity of 11 mm/s manually. Guiding marks were drawn on the composite panels to assist the inspections. System resolution was set to 0.5, other inspection parameters are summarized in Table 3.5. Thickness measurements were performed with an Oditest MD-01 manual caliper, with a measurement tolerance of 0.05 mm.

Table 3.5 Equipment parameters for UT inspection

Equipment:	Olympus OmniScan MX2 OMNI-M-PA16128
Probe	Olympus 5.0L64-NW1 5MHz
Wedge	Olympus SNW1-0L-IHC
Technique	Pulse-Eco (PE) Phase-Array 64 elements
Material velocity	2500 m/s
Resolution	0.5
Filter	None
Voltage:	40 V
Gain:	6 dB
Inspection velocity:	11 mm/s (manual inspection)
Inspection area	100% sample surface
Acceptance criteria	18 dB (Low TRL)
Thickness UT technique	A^-I/
Inspection mode	Immersion
Coupling agent	Water

For the high-temperature manufacturing tests during the HP-RTM manufacturing, we used a mobile extraction unit for the smoke that can be produced during the heating process. [196] And mold manipulation was carried using an hydraulic elevator of 1200 kg capacity [197].

Chapter 4: Implementation of the HP-RTM process

This chapter describes the design requirements for the HP-RTM prototype machine, its operational parameters, tunning and set-up process. Modifications on the machine structure are specified which were implemented to improve the machine operation to obtain proper materials. Additionally, this chapter describes the design of the HP-RTM mold, which is based on state of art considerations for HP-RTM processing, alongside structural and thermal FEM simulations. Then, the final mold construction and assembly is presented.

4.1. HP-RTM Machine

4.1.1. Machine considerations and design

A high-pressure resin mixing and injection prototype machine has been specifically designed and manufactured in Eurecat (Technological Center of Catalonia, Spain). The Composite Materials unit [198] was in charge of the process requirements, while the design, construction and final assembly was done by the Advanced Manufacturing Systems unit (AMS) [199], in collaboration with MSX Technology S.r.l, Italy [200]. This machine has the objective of reducing the injection time of the RTM process to accomplish the production-rate requirements for thermoset parts in the automotive industry.

Main operation parameters were defined as follows (Table 4.1):

Table 4.1. Design parameters for the HP-RTM machine operation

Requirement	Value/Range
Process control	By volumetric flux
Machine type	Bi-component (resin and hardener)
Tanks capacity	6000 cm^3/each
Maximum volumetric flux	200 cm^3/s
Maximum operative pressure	10 MPa (100 bar)
Allowable working viscosities	2 – 400 mPa-s
Injection temperatures	60 – 120° C
Pressure system	Hydraulic
Heating mechanisms	Electric, integrated with the structure and components (metallic components)
Connection to mold cavity	Integrated in the mold structure
Mixing mechanism	By fluids interaction (turbulent flow). As close of the injection cavity as possible to avoid curing in the injection cavities
Parameters control	Pressure and temperature in injection lines

This machine with model name “RTM-HP Marieta” is a two-component injection system where resin and hardener are pumped separately trough hydraulic driven axial pistons (syringes), and later combined into an external mixhead, where the mixture is injected inside the mold cavity

(Figure 4.1). The operational principle of the Eurecat's machine is similar to the commercially available HP-RTM machines using axial pistons [44]–[49]. Its differences stand on the structure, being simpler to operate for R+D purposes. The resin and hardener tanks are directly integrated in the pistons array, avoiding the need of external tanks and a distribution system, but in counterpart, making not possible to integrate recirculation lines or mixing devices on the fluids to maintain the operational temperatures. This machine also needs external devices to measure temperatures inside the resin and hardener tanks, alongside to apply vacuum by an externally connected pump.

The machine structure also integrates the hydraulic system, control and electrical panels, in addition to sensors and their acquisition system.

All the machine systems are enclosed into a metallic frame (Figure 4.1 a, Figure 4.2 b and c), at exception of the mixhead (mixing device), that is an independent system attached at the machine by the resin-hardener distribution system and their hydraulic connections (Figure 4.1 b, Figure 4.2 d).

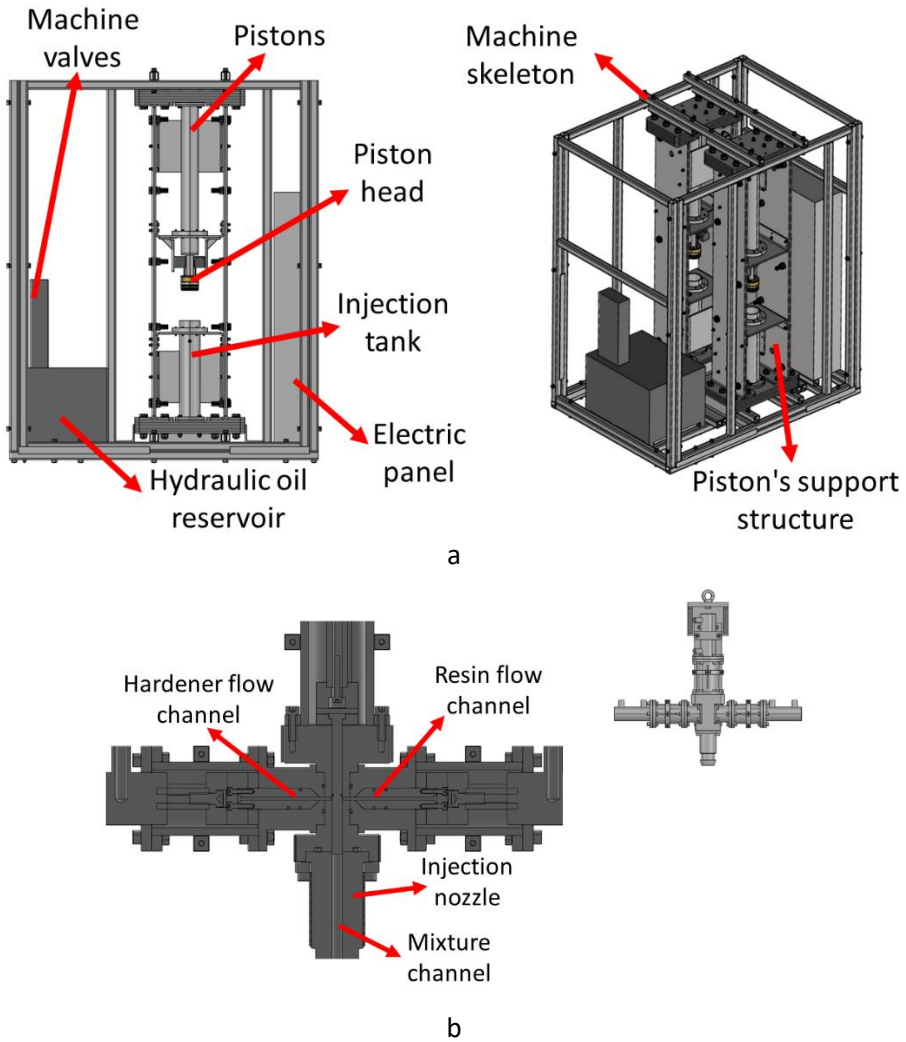

Figure 4.1. Eurecat's Marieta HP-RTM Machine and mixhead design. (a) Schematic view of the machine main frame with all the systems: pistons, hydraulic array and electric panel. (b) Schematic view of the mixhead and its subsystems

Figure 4.2. Machine construction and final assembly (Courtesy of MSX Tech.) (a) Axial pistons array and machine resin and hardener tanks. (b) Main machine frame with support plates (vertical) for the axial pistons and hydraulic array (pump and oil tank). (c) Final enclosure of the machine with security doors (lateral view axial pistons and electric panel). (d) Mixhead with dosing pistons (laterals), resin hoses and hydraulic conections (attached to the machine frame).

4.1.2. Function principle and operation

Resin and hardener channels are located inside the mixhead with two hydraulic pistons placed horizontally, one for each component. Before injection, these pistons are closed to prevent early resin and hardener interaction, causing premature curing. Once the injection starts, resin and hardener pistons retract, allowing both flows to enter in the mixing cavity colliding together inside the injection channel (mixture channel) and mixing in the process. Then, the mixture is directly injected into the mold cavity (Figure 4.1 b).

The mixhead also integrates a self-cleaning mechanism operated by a vertical hydraulic piston that closes the mixture channel and moves any residual mixture inside the mold cavity. This piston also integrates a second step that is activated once the curing process has been completed. In this step, the mold has to be detached, leaving only the injection nozzle connected to the mixhead. The cleaning piston is pushed at high-pressure in order to break and detach any solid residue of resin that might get trapped inside the mixture channel.

Electric heater cloths (Figure 4.3) were implemented in both machine tanks, injection lines and mixhead. In addition to temperature sensors in each induvial component to maintain a

predefined operational temperature. These cloths were manufactured by the Functional Textiles unit of Eurecat [201].

Figure 4.3. Sample of an electric cloth implemented in the machine components

Marieta HP-RTM machine is operated by a hydraulic pump that supplies movement to all the hydraulic driven components: injection pistons and mixhead pistons. Movement of each component (opening and closing independently) is controlled by electro valves (solenoids) that can be tunned manually to modify the hydraulic pressure of the specific component. Each component pressure can be read on the machine control panel. (Figure 4.4)

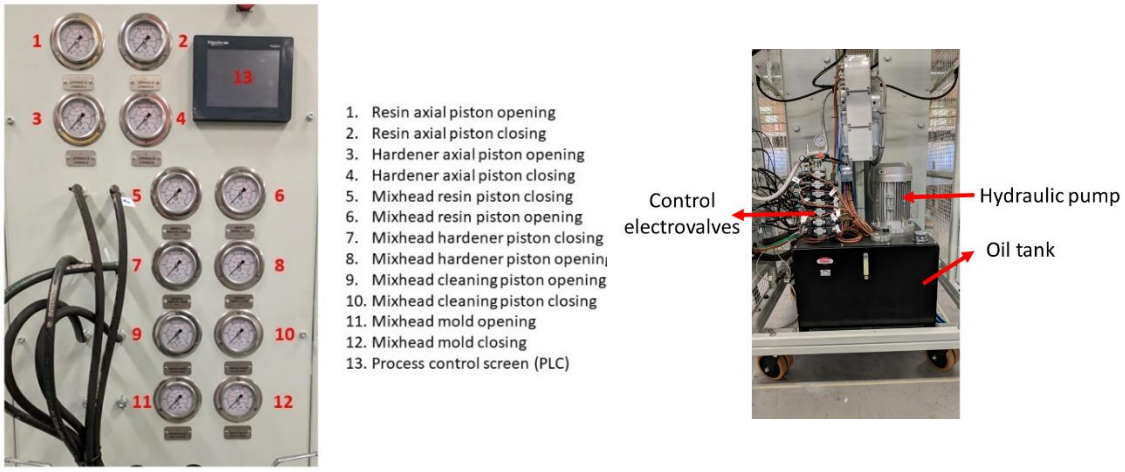

Figure 4.4. Electro valves system. a) Control panel for lecture of the machine components pressure. b) Hydraulic array and control valves

A PID control is responsible of the resin–hardener injection and ratio control. It acts directly onto two independent electrovalves (Figure 4.5). These valves control only the resin and hardener piston parameters in order to achieve the desired volume, mixture ratio and injection velocity (these valves are independent from the machine component valves mentioned before).

Figure 4.5. Injection electrovalves (for resin and hardener tanks)

The PID is programmed separately for the resin and hardener pistons through differentiated gain values.

The PID control reads the vertical position of both axial pistons by an electric longitudinal encoder (Figure 4.6, 1), that has a metallic wire (Figure 4.6, 2) directly attached to the piston head (Figure 4.6, 3). This measure helps to control the movement of the axial pistons, in addition to the vertical coordinates of the vacuum application port (located in the upper part of the tank), and the final displacement position (located at the bottom of the tank). The latter positions are known for the machine (set in the configuration panel), the machine uses the electric encoder to calibrate these positions in every injection.

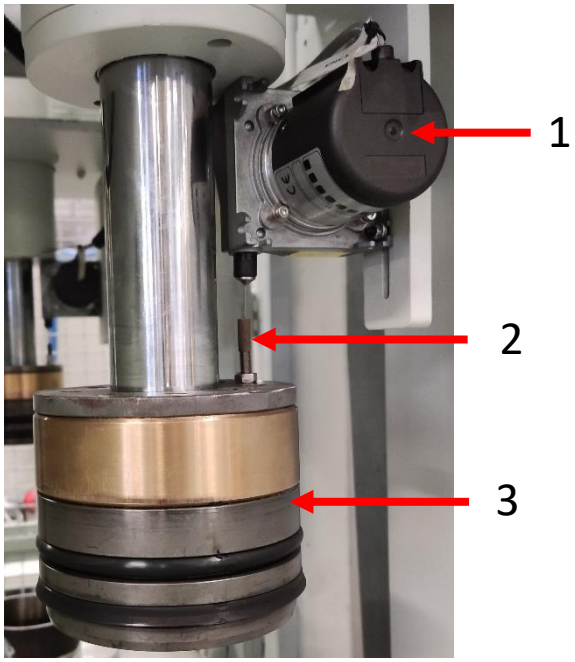

Figure 4.6. Injection piston and lineal transducer cable attached to the piston's head. 1. Linear electric encoder. 2. Connection wire. 3. Piston head

The PID control also accounts for the pistons transversal area, which is known and common for both components. In addition to the required injection mixture which the respective injection ratio between resin and hardener. Then, the PID control reads the pistons position before the injection begins and computes the required injection volume for resin and hardener, calculates the final pistons position, the time required for each piston to get to that position, and the velocity needed to move them by regulating the aperture of the injection electrovalves (Figure 4.7). PID control gains have to be manually adjusted to guarantee a correct components' mixture.

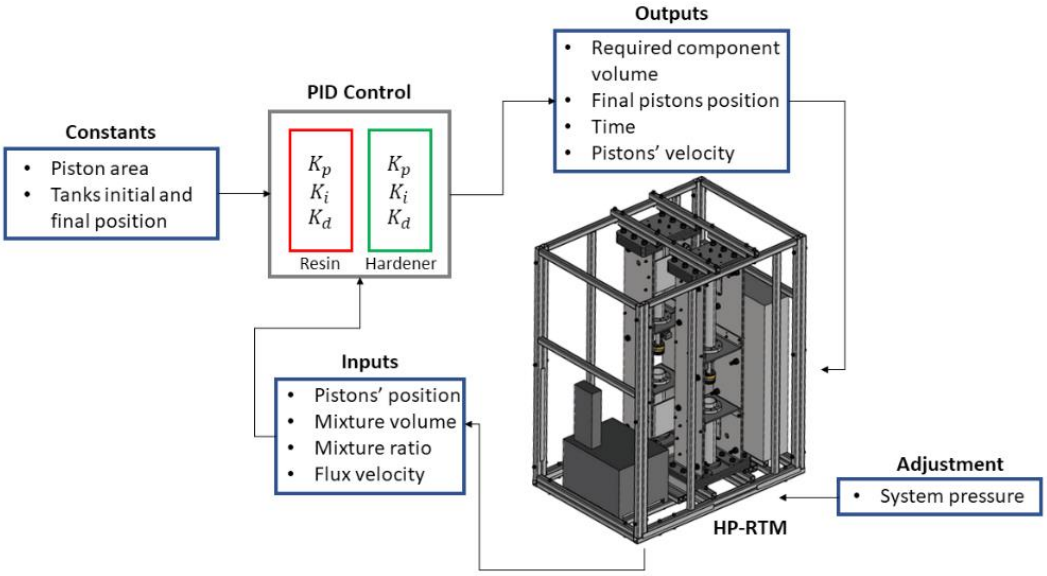

Figure 4.7. Scheme for the HP-RTM control system

To operate, the machine needs the desired injection volumetric flux (cm^3/s), vacuum time (s), intended mixture volume for injection (cm^3), injection ratio (% resin - % hardener) and the operation temperatures (° C) for tanks, injection lines and the mixhead, which are parameters defined by the user. Injection pressure can be regulated with the corresponding component electrovalves but is not a controlled process parameter, it acts more as a limitation parameter. If needed, corresponding electrovalves for both piston tanks can be manually tunned to reach the maximum pressure intended (Figure 4.8) and reading the injection pressure of the resin and hardener tanks in the control panel while the process is being carried.

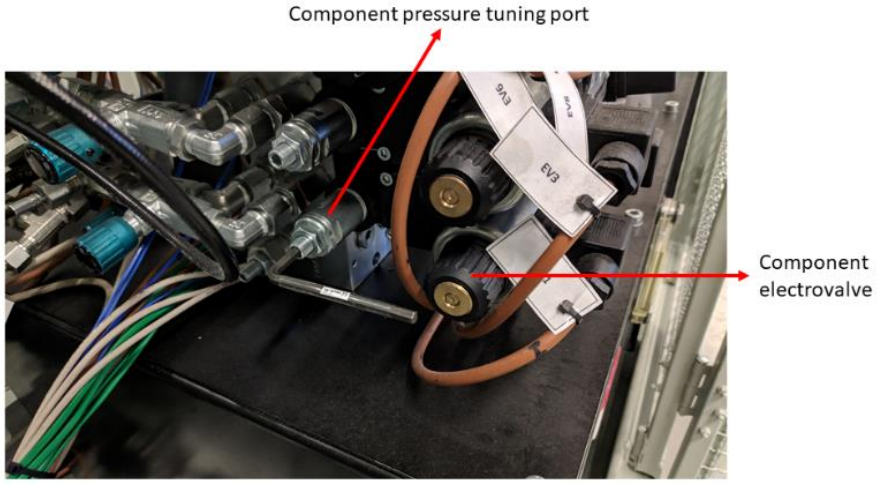

Figure 4.8. Pressure adjusting system for machine components

Resin and hardener are loaded in the machine tanks and the heating cloths are activated to the defined temperatures. Pistons move to vacuum position to start the degassing process, using an externally connected vacuum pump to each tank (Figure 4.9).

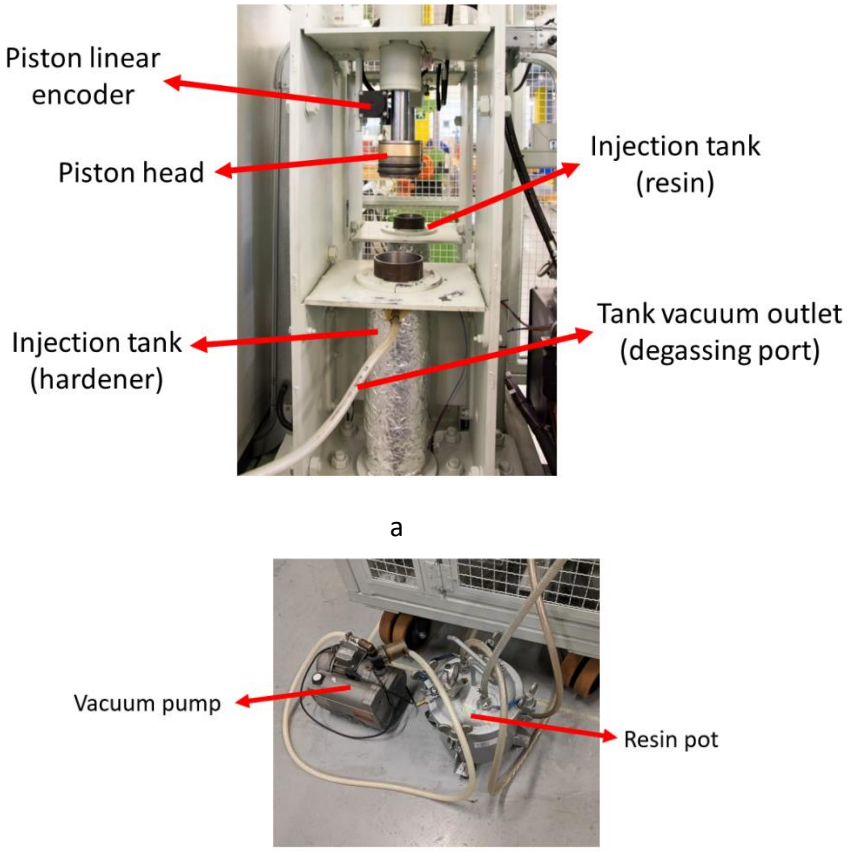

Figure 4.9. Detail of machine loading tanks and injection pistons. (a) Vacuum ports are located in the tanks side and connected to the vacuum pump and a resin trap by silicone hoses (b).

When the vacuum time is finished, injection pistons move to the initial tank position and the vacuum ports are no longer used. Then, each piston has to be moved manually to get in contact with the corresponding fluid to pressurize it. This is achieved by closing the dosage valves manually (located at the machine control panel, Figure 4.10) and tuning the pressure of the injection pistons, as displayed in Figure 4.8.

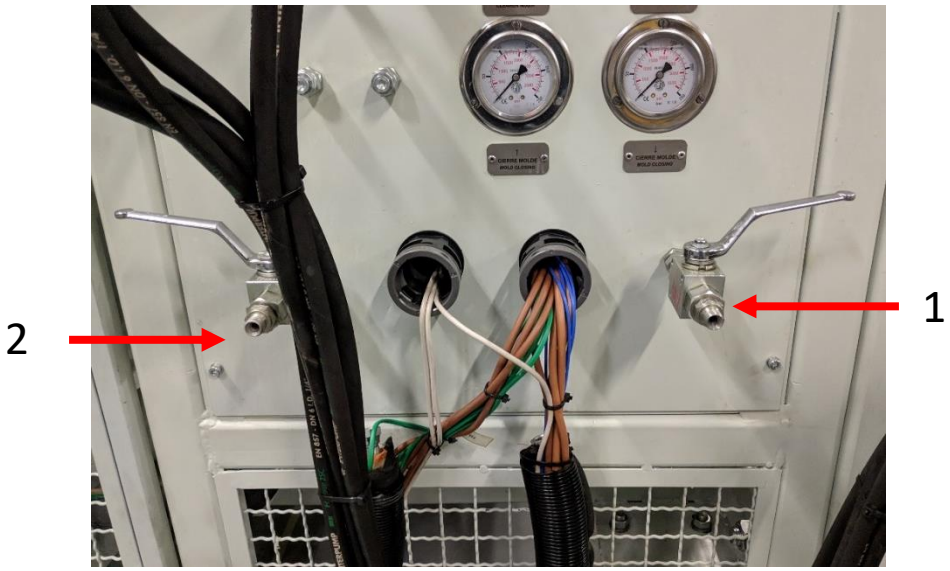

Figure 4.10. Machine dosage valves. Resin (1), hardener (2)

In this process, both resin and hardener channels in the mixhead are closed. We have to consider that the machine reads the injected fluids volume once they have left the tanks, so fluids inside the distribution and injection channels have to be accounted in the total injected volume.

When the injection order starts, resin and hardener channels open and the mixture is injected into the mold. After reaching the desired injection volume, these channels close and the cleaning piston moves down, sealing the injection channel. After curing, the machine is detached from the mold and the part is extracted.

This machine being a bi-component system, also serves as a monocomponent injector with specific resins (long pot life). When required, a mixture of resin and hardener can be loaded only in one of the thanks to make the injection inside the mold. For this, caution has to be made in order to control the mixture gel time to avoid curing inside the distribution channels. In the later configuration, injection also can be carried manually by operating the selected piston until the mold cavity is pressurized. In this case, the user defines when the injection has finished (by reading the system pressure).

As a summary, this machine is flux-controlled in which the user defines the desired resin quantity to be injected, in addition to the injection line temperatures and the resin-hardener ratio. Although pressure can be modified, it is not a process parameter (not possible to modify of the control panel), only acting as a limit for the machine operation. During the process, the machine is constantly measuring all the components temperatures, the resin and hardener pressure (injection lines) and the pistons velocity.

4.1.3. Machine tunning and set-up for HP-RTM operation

We must highlight that this machine is a first-stage prototype with unknown operation tolerances or limitations. Thus, our work started by understanding the machine behavior, its controllable parameters and possible deviations related to its operation.

As mentioned before, heating is performed by electric clothes that are directly in contact with the machine components. The injection thanks, that contain the resin and hardener are made of steel pipes of 6 mm thickness, each covered with an electric cloth, in addition to an isolation material to prevent heat dissipation during processing. There are no mixing elements inside the thanks, so the fluids are static until they reach the desired temperature.

We performed temperature measurements inside the machine tanks using a mixture of water and 5% cutting oil (to prevent water corrosion inside the tanks, as suggested by the manufacturer) in order to see the heating slope. Temperature readings were taken directly on the machine thermocouples. For the fluids, we placed thermocouples inside the tanks, making sure that both were located in the center of the fluid. By performing this study, we detected that between the tanks and the fluid there is a constant difference of ≈20° C with a slow heating slope of 0.2 – 0.3°C/min (Figure 4.11). So, when operating with a specific resin system, this difference must be considered to set the process parameters in the machine.

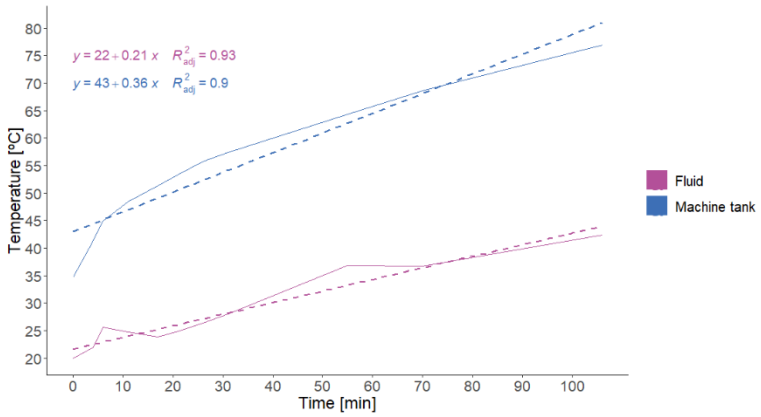

Figure 4.11. Heating slope of injection tanks and fluids. This may change depending on the thermal properties of the resin and hardener used.

In order to gain time, resin alone or resin mixture can be heated externally in an oven and then, poured inside the tanks while they are being heated prior to the injection test.

Heating temperatures are limited to 100° C by the manufacturer in order to prevent possible damage on the electrical components and their surrounding materials. Other control parameters can be modified as needed without any implication on the injection process. Different thermocouples are integrated through the machine tanks, distribution lines and mixhead for temperature monitoring (Figure 4.12). The machine also allows to heat a specific component if required.

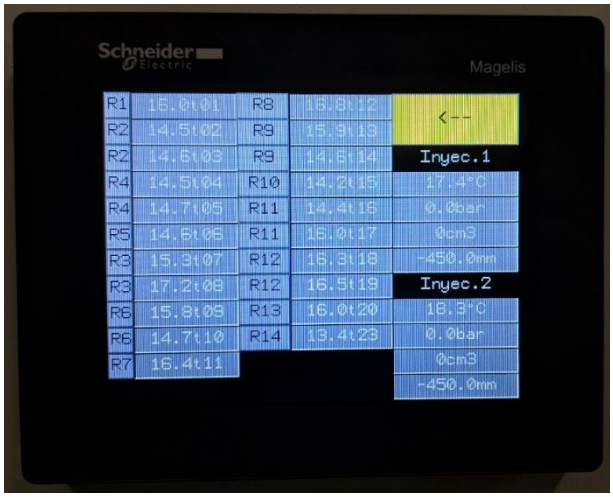

Figure 4.12. Machine heating monitoring and resin and hardener parameters control (pressure, flux and current position)

Fluids pressure is measured by two independent pressure sensors (Figure 4.13) attached to the resin and hardener fluid lines; pressure values also can be read in the control display.

Figure 4.13. Resin (left) and hardener (right) pressure sensors. Pressure for the injection lines

We detected some limitations with the injection volume by tunning the machine dosing ratio. A preliminary test consisted in the injection of 100 cm^3 of the water-oil mixture by changing the injection ratio (in percentage) into different possible values as: 100/0 (pure resin), 0/100 (pure hardener), 90/10, 80/20, 70/30, 60/40 and 50/50 (Figure 4.14). Both thanks were degassed for 5 minutes, and liquids injection was measured directly on the dosing valves located in the control panel by weighting the final quantities and calculating the volume by assuming a density of 1 g/m^3 (as pure water).

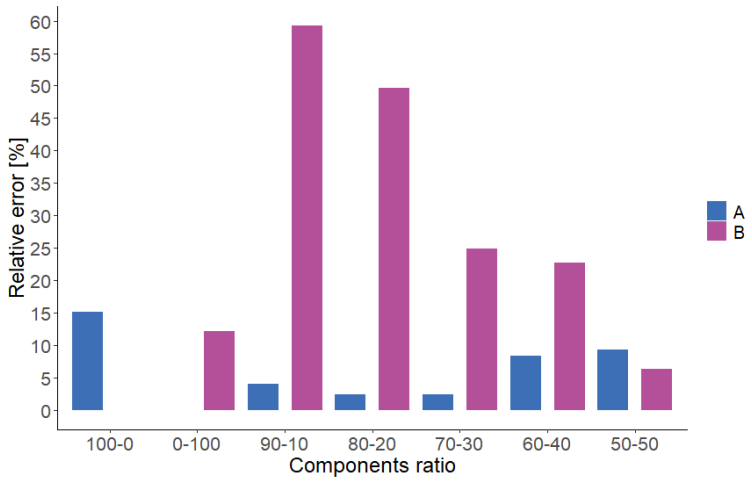

Figure 4.14. Relative error on the machine injection ratios for a constant fluid volume (100 cm^3). Quantities measured in the dosing points at the machine control panel

Other test consisted in selecting only one critical ratio value (as 90/10 where more of one component is required), and change the injection volume: 100, 200, 300, 400, 500 and 600 cm^3 (Figure 4.15).

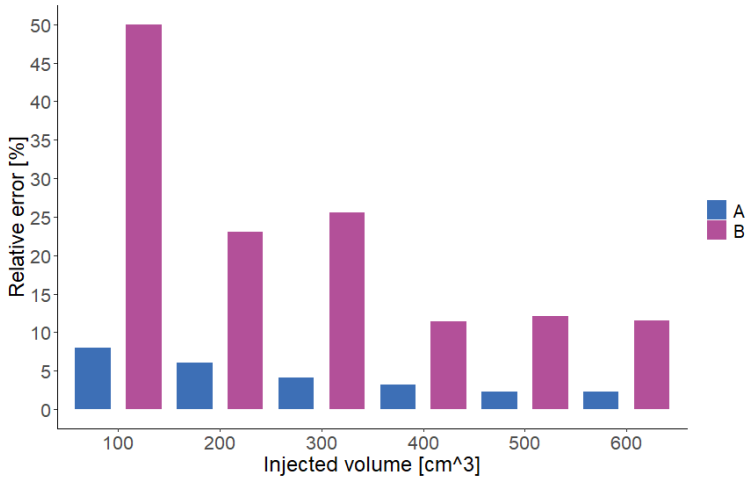

Figure 4.15. Relative error on the machine ratio by varying the injected volume quantity holding a fluid ratio of 90-10.

We found that the machine holds a tolerance around 10 cm^3 in the fluid's injection. Each tank has an injection error near to 14% when used independently and, as the fluid quantity is lower, the injection relative error increases until unreliable values, giving an idea of the machine operational limits.

We concluded that the minimum allowable injection quantity for each tank is about 50 cm^3, where the machine holds a maximum error of 10%. This quantity must be considered when using molds with small cavities (low internal volume), as well as using resin formulations with important differences in the mixing ratio, as in the case for 90/10 or 80/20 ratios. Being an early prototype, this machine is more appropriate for large injection quantities as an industrial environment, where its operational errors are less critical.

The calibration process of the machine is performed by changing the PID control gains manually for each component (resin and hardener). This calibration has to be performed at a specific resin temperature (affecting its viscosity), and a specific volumetric flux, making the process quite difficult to be implemented in a larger scale.

Resin and hardener have to be poured into their specific tank and have to be degassed and pressurized to avoid any interference with entrapped air inside the machine tanks and injection lines. Once the system is pressurized and the pistons are in contact with the fluids, the dossing valves are open to release the pressure, maintaining the fluids stable and contained inside the system (as in a syringe). The machine manufacturer recommended to use some initial values for the PID gains in order to start the calibration process, which are resumed in Table 4.2.

Table 4.2. Initial PID gain values for the calibration process

Control	Resin and hardener
kP (Proportional)	0.01
kI (Integrative)	5
kD (Derivative)	0

The calibration process of the PID parameters was implemented first, by regulating the resin gain values, and later the hardener gain values. Proportional control (kP) is set to the value that gives a closed approximation on the desired quantity, followed by the integrative control (kI). It was recommended to not tunning the derivative control (kD) unless some oscillations were appreciated in the piston's movement, but it was not the case.

4.1.4. Machine modifications

When received, this machine integrated a single PID control for both injection tanks, resulting in a very complex and unreliable calibration process. For this, we performed a modification on the machine software to allow both injection tanks to be controlled by independent PID controls (Figure 4.16).

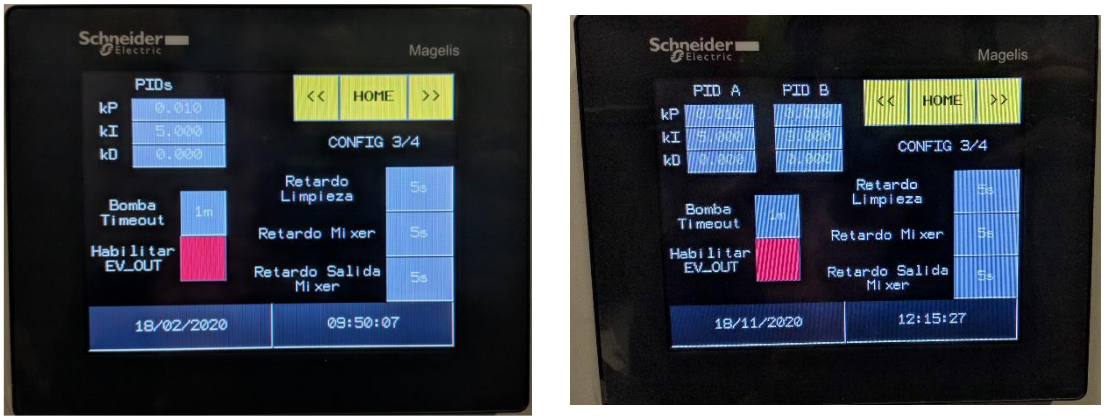

a b

Figure 4.16. Injection PID controls a) old single control. b) New independent control

For processing, we performed some initial injection trials in order to validate the machine behavior. The first trial was programmed as a simulation of the final composite part with a carbon fiber preform and the fast curing/high-reactivity resin intended to be used with this machine. The mixhead was directly attached to the mold as was described for the bi-component injection configuration, and resin and hardener mixture was carried out only by fluids interaction. When demolded, the final composite was not cured, and the resin and hardener were not mixed at all (Figure 4.17 a). For the second trial (Figure 4.17 b) we performed the injection using glass fiber instead of carbon fiber only with the purpose of material savings, and adding a metal mesh (Figure 4.18) inside the injection nozzle in order to create more turbulence in the fluids to improve their mixture. Other process parameters were maintained, but again the results were the same.

a b c

Figure 4.17. Initial injection trials for the 2K configuration. a) Test of a carbon fiber panel, having all fabric layers as the final composite material and using the high-reactivity resin. b) Injection trial using glass fiber in an equivalent volumetric fraction as the carbon fiber, injection carried out with a metal mesh inside the injection cavity to improve fluids interaction. c) Injection with glass fiber mat (single layer) and silicone hoses at the mold outputs to increase the available injection volume, metal mesh also integrated inside the injection cavity.

Figure 4.18. Metal mesh used to improve the mixture between the resin and hardener inside the machine injection nozzle.

At this point we detected that the problem relied on the machine injection tolerances: the corresponding HP-RTM mold have small cavity dimensions: 350 mm in length, 250 mm in width and a thickness of 2 mm, having only an available volume of 175 cm^3. Also, fibers correspond to almost the half of that volume (for an approximate of 50% in the volumetric fraction), so the required injection volumes were too low to be reliable.

We performed a third injection trial using only a layer of a glass fiber mat in order to have more volume available inside the injection cavity, adding reinforced silicon hoses on the mold output ports to increase the available cavity volume. Injection pressure was tuned down to 0.5 MPa (5 bar) for security reasons and the metal mesh was adapted in the injection nozzle again. This last trial was better than the last injections, but still some areas of the final panel were not properly cured (poor resin and hardener mixture, Figure 4.17 c).

Results from the last injection improved the first trials, but it still was required further development as some areas in the final composite were not completely cured. As further ideas, we proposed to use a commercially available static mixer (Figure 4.19) with the same dimensions as the cavity of the injection nozzle to improve the resin and hardener mixing. Reliying only on fluid interaction is not reliable in this machine.

Figure 4.19. Commercially available static mixer. Dimensions are the same as the injection nozzle cavity, material is compatible with the operative temperatures.

We also decided to change the resin system and continue the studies with a resin that has a more stable mixing ratio (near to 50/50) to improve the machine operation. In this way, both machine pistons could operate at similar parameters and the relative error could be improved as it was seen on the ratio test (Figure 4.14).

We performed modifications on the mixhead body: as conceived, the mixhead integrated the resin and hardener pistons directly opposed with a vertical piston for cleaning purposes (Figure 4.20). All three pistons are hold in place by the mixhead body core that is a solid metal block with a thigh fitting (g6/H7) between the cleaning piston and the injection cavity, integrating a rubber O-ring in the piston itself to maintain the system pressure.

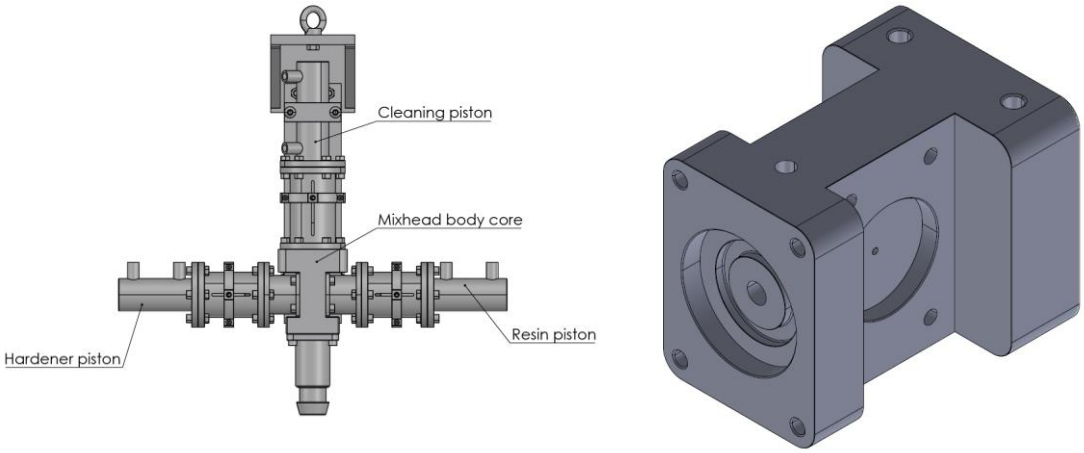

Figure 4.20. Machine mixhead. a) Detail of pistons position. b) detail of the mixhead body core

This modification responds to a failure detected during the bi-component injection trials. The cleaning piston was stuck in the closing position immediately after the injection (Figure 4.21), with no results after several attempts to retract it back. For this, we dismantled the entire mixhead and an important amount of force was required in order to release the cleaning piston form its position. Through closer inspections, we detected that the entrapment was originated by the O-ring cavity as its directly located at the resin and hardener exit ports, where resin fluids can filter and mix due their low viscosities at the operative temperatures, curing in the process and trapping the piston in its position.

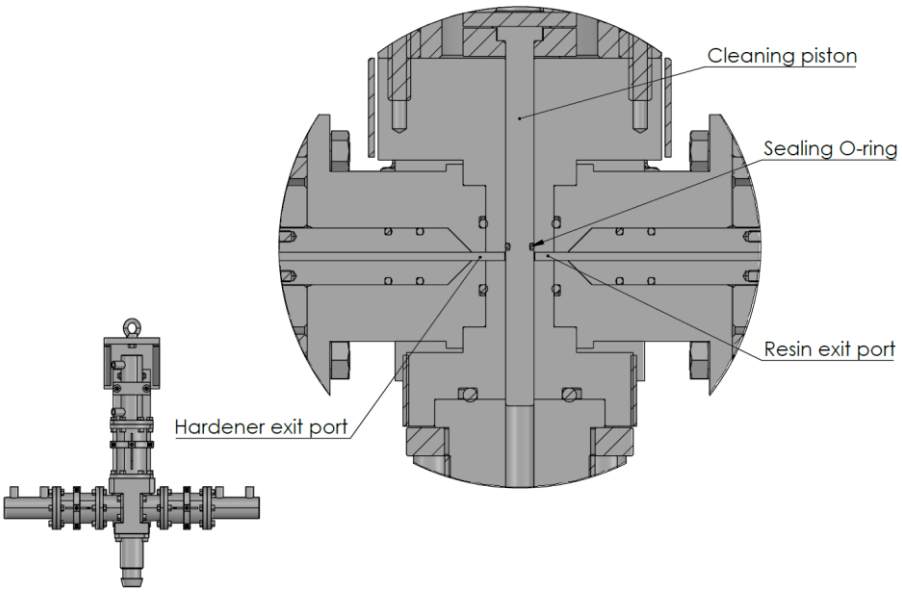

Figure 4.21. Detail of the mixhead assembly. View of the internal resin, hardener and cleaning channels with their corresponding pistons

Solidified resin was stuck on the piston cavity (Figure 4.22), holding it and preventing it to return to its initial position. The sealing strategy in the cleaning piston was not a suitable solution to maintain the system operative. Another factor that contributed to the failure was the use of high-reactivity resins, that give no time to act in the case of an injection failure.

a b

Figure 4.22. Failure of the cleaning piston. a) Stuck piston in the closed position inside the mixhead core. b) Piston after removal with the solidified O-ring

In this case, we proposed a redesign of the cleaning piston and the mixhead body core following the next considerations:

- The new mixhead body core must allow an easy access and dismantling in the case of future incidents, as for maintenance purposes.
- The cleaning piston must be as smooth as possible with no considerable geometry changes in order to prevent possible grips on solidified resin.
- Implementation of a new sealing method with the sealing cavity integrated in the body core, not on the piston as it is a moving component. As well as other complementary sealing methods to ensure that the entire body core is sealed for operation.
- To use scraper joints (piston joints) instead of conventional O-rings. In addition to use semi-permanent demolding solutions on the surfaces of the new body core, and the integration of additional sealing mechanisms to maintain the system sealed.

The new body core is composed by two opposed symmetrical parts (Figure 4.23) that are hold together mechanically through bolts (DIN 912 12.9). We decided to divide the body core transversally to the injection flows in order to prevent possible leaks during injection. We also implemented extraction threads in the center part of the body core to force opening in the case of possible leakages or entrapments.

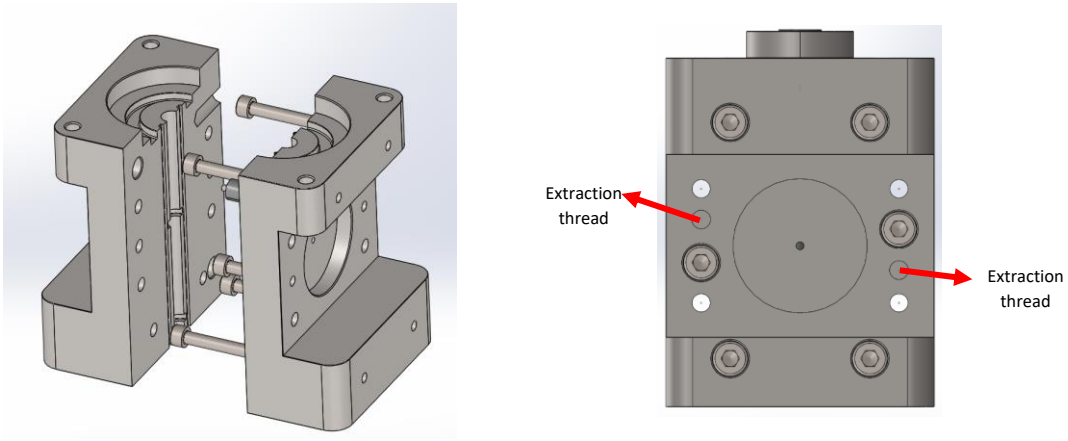

a b

Figure 4.23. New body core design. a) Detail of the two-half part and their union. b) Detail of threaded union and extraction threads in the body center

Between the body core parts we also implemented two vertical sealing cords made of rubber silicon to maintain the body union sealed. Additionally, we integrated a metal mandrel in the

upper part of the body core that has a plain joint made of compressed materials (Belpa CSA-90 [202]) and maintained in position also by a threaded connection. In the lower part of the body core is integrated a conventional O-ring that seals the connection between the mixhead body core and the machine injection nozzle. Finally, we added two scrapper joints (displayed in Figure 4.24) in the body core: one in the resin and hardener exit ports and another between the body core and the new upper mandrel in case of failure of the lower scrapper joint.

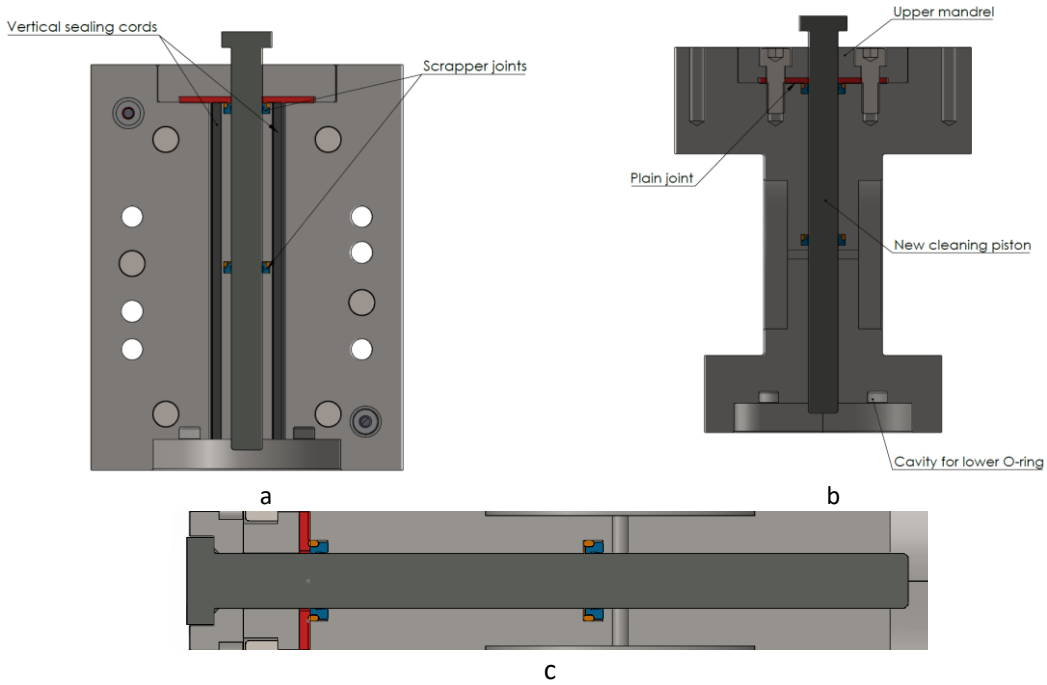

Figure 4.24. Detail of sealing mechanisms in the new body core. a) Contact surface between body core parts integrating the vertical silicone cords and detail of the upper mandrel with the plane joint. b) Detail of threaded connection of the upper mandrel. c) Scrapper joints (dynamic O-rings, blue) and the new cleaning piston

All sealing materials are commercially available, and the new body core was mechanized using high-strength steel (DIN 1.2738). Fittings were manually made between all the body core parts and the contact surfaces were polished and treated with semi-permanent demolding agents to continue with the machine operations (Figure 4.25).

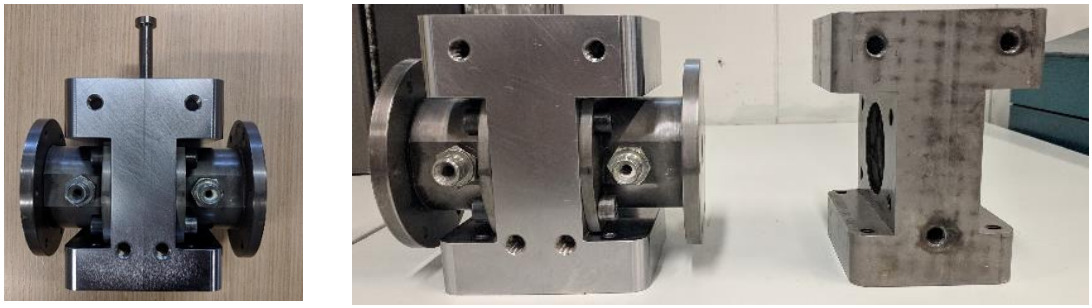

Figure 4.25. Assembly of the new mixhead body core and comparison with the original solid body core (right)

As conceived originally, the machine mixhead is directly attached to the injection mold by a specially designed holding plate (Figure 4.26) that maintains the mixhead in position by applying pressure on the injection nozzle though a metal ring (Figure 4.27) and by another nozzle directly integrated inside the mold (female nozzle) . The machine mixhead is additionally supported by two external plates that are attached in the resin and hardener pistons. In this configuration, the mixhead must remain attached to the mold until the composite is completely cured, making

unfeasible the injection of a mono-component resin or an already mixed resin using only one of the machine tanks.

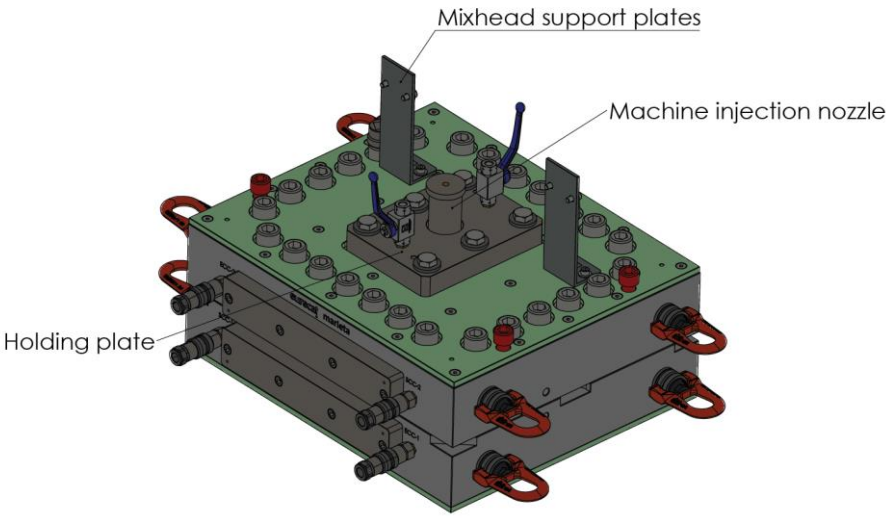

Figure 4.26. Mixhead connection system to HP-RTM mold

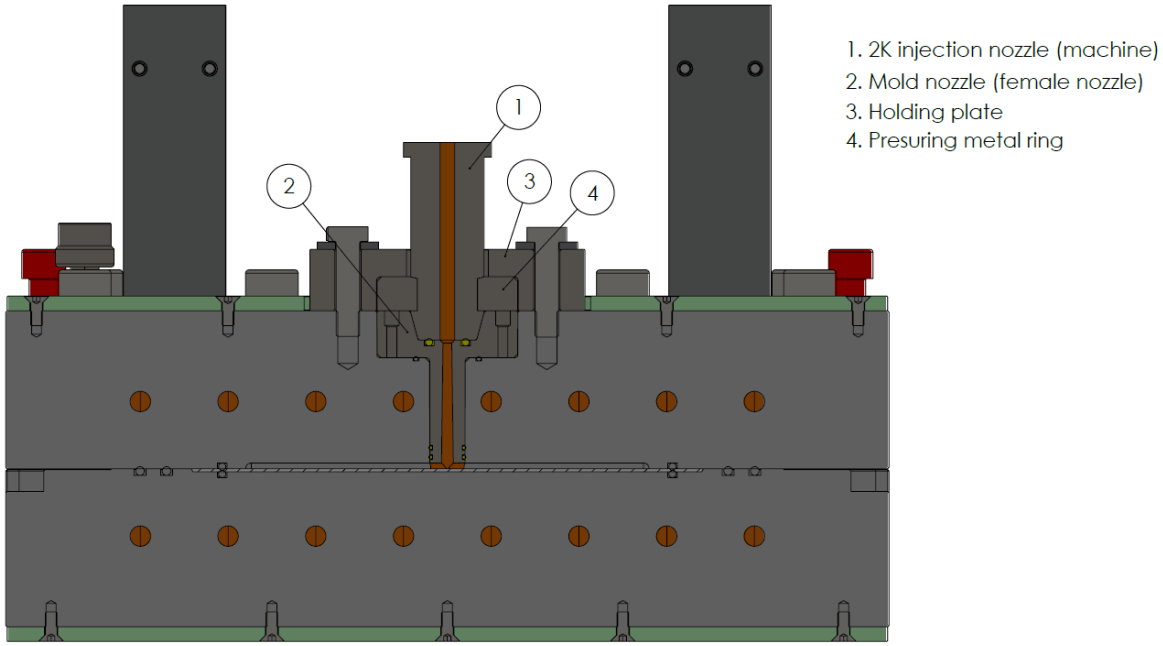

Figure 4.27. Detail of the mixhead connection into the mold. bi-component injection configuration

For this reason, we manufactured a variant of the injection nozzle (mono-component injection nozzle, Figure 4.28) that is shorter compared with the bi-component injection nozzle as no fluid's mixture is required. This new nozzle also integrates a threaded connection to attach the mixhead or the machine directly to the mold by using a high pressure-capable hose. Moreover, this new nozzle has the advantage to attach a 2-way ball valve that can be closed once the injection is finished and the mold pressurized to detach the machine and proceed with its cleaning process while the mold is being heated to cure the composite, preventing in this way possible mixture curing inside the injection lines.

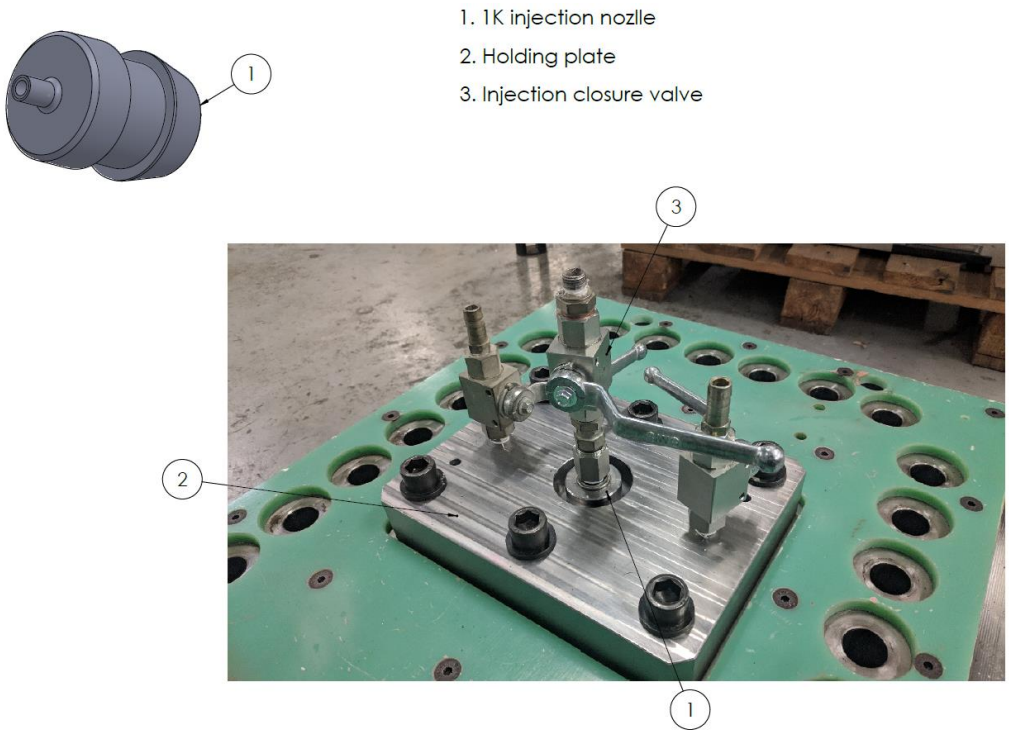

Figure 4.28. Detail of the mixhead connection into the mold. Mono-component injection configuration with inlet and outlet closure valves

After installing the new body core and using the new injection nozzle, we performed some injection trials using the machine in the mono-component configuration in order to validate the design reliability and the sealing capacity of all components without having issues with the mixing ratio. We tested different injection pressures: 1, 2 and 4 MPa (10, 20 and 40 bar, Figure 4.29). And all injections were successfully performed without any issues on the new mixhead assembly or its sealing mechanisms. The first injection (1 MPa) was made with a glass fiber mat, but other injections were performed with NCF carbon fiber to simulate final test conditions. In the latter, we detected a demolding issue in which the fabrics were trapped inside injection and vacuum ports of the mold, generating a superficial delamination in the composite. To prevent this, in the following injections we implemented a peel ply layer between the fabric preform and the mold surface to prevent fiber entrapment and possible delaminations.

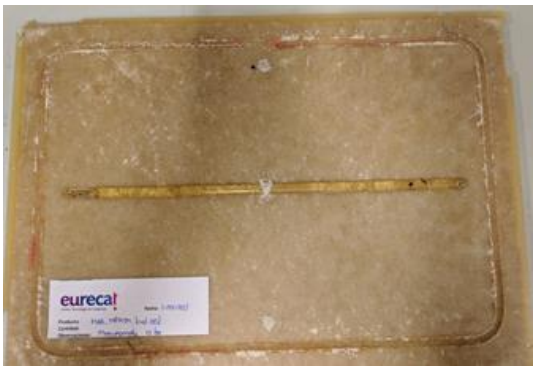

a

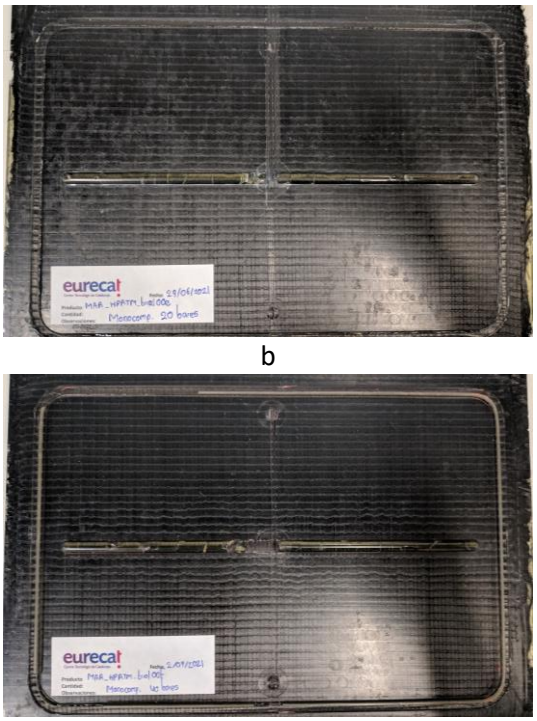

b

c

Figure 4.29. Validation of the new mixhead body core through mono-component injections. a) GF Mat 600 g/m2 at 1 MPa, testing of new mixhead stability. b) CF NFC 416 g/m2 at 2 MPa. c) CF NCF 416 g/m2 at 4 MPa

We detected a possible failure in another component using the new body core: the lateral pistons that close the resin and hardener channels started to operate at a lower velocity. By inspecting the body core, the resin mixture started to leak inside the piston mechanism, due to wearing of its sealing O-rings (Figure 4.30 a), thus lowering its operative velocity. For this, we proposed a modification on the lateral pistons to integrate PTFE support rings between the polymeric O-rings to prevent further wearing during operation (Figure 4.30 b).

a

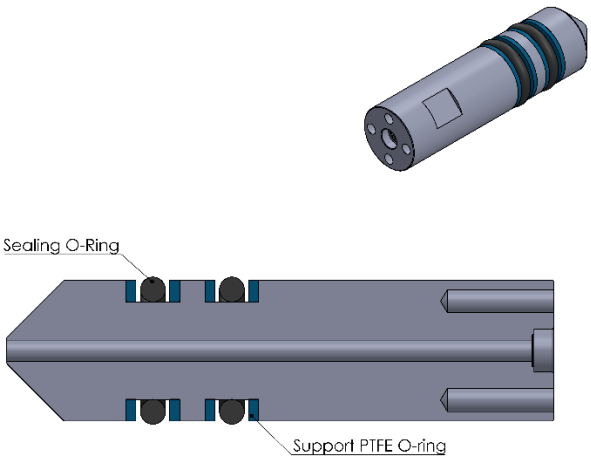

b

Figure 4.30 Proposed modification for the lateral pistons of the machine mixhead. a) Detail of the detected failure in the resin and hardener pistons, at the channel output was attached residues of the resin mixture. By opening the piston gasket was detected abrasion on the pistons O-rings. b) Proposed modifications

Nevertheless, the machine mixhead have proved to be complex and it was a high probability to present further issues related with its operation. Having this in mind, we decided to discard further bi-component injections to guarantee continuity on this study. Traditional resins systems were used instead of high-reactivity systems under mono-component injections, mixing manually the resin and hardener and injecting the mixture with only one of the machine tanks, in addition to attach the machine injection line directly to the mold without using the mixhead, finally not performing the intended modification.

4.2. HP-RTM Mold

The objective of this mold was to accomplish safe injections with the HP-RTM technology, minimizing or preventing possible issues related to high-pressure operations. As well, to allow conventional RTM injections. The mold considerations and design were based on the available information in the state of the art (thesis, publications, books, etc) for HP-RTM and conventional RTM processes [1], [6], [7], [27], [32], [37], [41], [54]–[56], [67].

4.2.1. Mold considerations and design

The injection pressure is the main parameter of the entire design. The mold structure had to sustain the maximum injection pressure without any important deformations in the injection cavity, while being safe for its operation.

This technology is mostly addressed to the automotive industry in which epoxy-based resins are mainly used, having curing temperatures near to 120° C. Aeronautic resins are considered as well, with curing temperatures near to 180° C, so mold materials and accessories have to operate under high-temperature conditions. Other aspects as mold weight, manipulation and ergonomics were also considered, as main testing operations are carried inside a laboratory with limited space.

We fixed the cavity thickness to 2 mm in order to extract coupons for materials testing. Maximum cavity length was defined having in mind the possibility to extract coupons for tensile tests, that are one of the largest for material testing (250 mm), and cavity width was considered with the possibility to extract a maximum of 4 coupons, also for tensile testing.

Design was kept simple and robust, we decided to not implement mold spacers or any other additional structure in order to prevent possible failure points. Other design parameters were defines as follows:

- Use of different polymeric materials in the sealing gaskets to overcome temperature and pressure conditions, as well as chemical compatibility with the resin systems and the cleaning solvents.
- To have a smooth surface finish in the injection cavity (N5/N6: non-perceptible marks) in order to avoid possible adhesions with the composite. Out of cavity areas were kept in a coarser finish (N7/N8) to reduce the overall mold cost [203].
- Dimension tolerances were defined to a maximum 7% deviation (fine - medium lineal dimensional tolerances) from the net cavity thickness (2 ± 0.14 mm) [204].
- Mold cavity flatness is defined between fine and medium tolerances (H – K), allowing deviations between 0.3 and 0.6 mm. [205]

Mold specifications are summarized in Table 4.3.

Table 4.3 Mold design specifications

Specifications	Dimensions
Net cavity dimensions	200 mm x 300 mm
Nominal thickness	2 mm
Working temperatures	120° C – 180° C
Max. Injection pressure	10 MPa (100 bar)
Heating mechanism	Oil/water circuit
Mold closure	Bolts
Mold fastening	Lifting eyebolts
Additional	Temperature measuring ports

We considered high-strength steel as the mold material: DIN 1.2311 or DIN 1.2312 steels as commonly used for injection molds. (Table 4.4)

Table 4.4 Selected materials for HP-RTM mold structure. [206], [207]

Material	Specifications
DIN 1.2311 F5303 (40CrMnMo7)	Standard steel for plastics and casting molds. Medium dimensions up to 400 mm cross-sections
DIN 1.2312 F5302 (40CrMnMoS8-6)	Standard steel for plastics and casting molds. Medium dimensions up to 400 mm cross-sections. Improved machinability

We decided to perform a central injection strategy. The mold nozzle integrates a conic cavity to allow cleaning and demolding after the resin has cured inside. As was described by Chaudhari et al. [6], in the design we integrated a distribution channel that is connected to the injection point, acting as a film gate injection strategy to reduce the local pressure in the preform and thus, reduce possible movement or waviness in the fibers.

Having a central injection strategy also contributes to a better distribution of the injection pressure across the mold structure. The injection channel had a diameter of 5 mm in a semispherical shape, where 20 mm are kept from the channel to the preform edge in order to avoid possible race tracking effects. Having in mind that this channel will remain in the final composite, we decided to extract the composite coupons avoiding the surrounding area of the distribution channel.

As mentioned before, mold connection with the mixhead was carried out through a compression plate that holds in place the injection nozzle with a steel ring. So, we adapted a female nozzle inside the mold that is connected to the machine injection nozzle, carrying the injected resin mixture to the preform. Detail of the joining mechanism is shown in Figure 4.31.

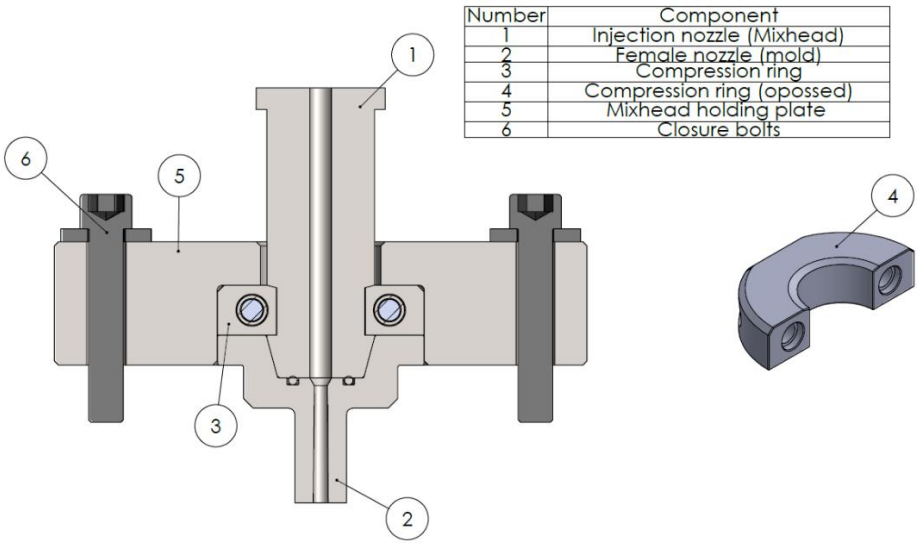

Figure 4.31. Detail of mixhead attaching mechanism into the mold.

Mold vacuum/venting ports were defined following the injection flow and placing them in the possible last filling points, as displayed in Figure 4.32. Symmetry was maintained in the mold design for simplicity. We implemented the vacuum/venting ports by using manual ball valves (2-way valves) to pressurize the injection cavity during the injection: the objective was to open the outlet valves and apply vacuum to evacuate the air trapped in the mold cavity. After this, the vacuum valves are closed and the injection progresses until the cavity is full and the mold pressurized.

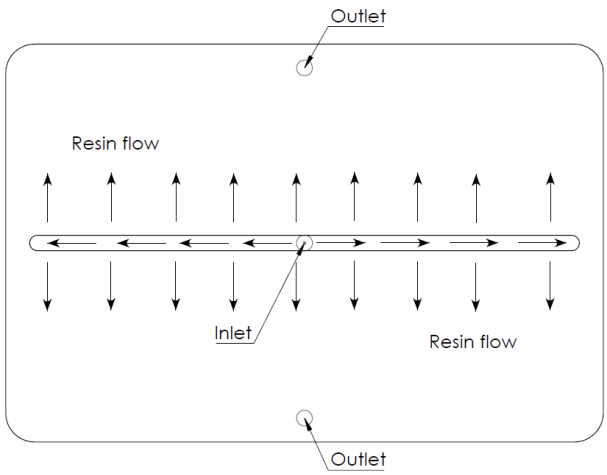

Figure 4.32. Injection flow pattern and location of the vacuum ports inside the mold cavity

The mold cavity and the vacuum valves are connected using metallic nozzles, similar to the in-mold injection nozzles. These nozzles were designed to be in contact with the mold holding plate (Figure 4.33).

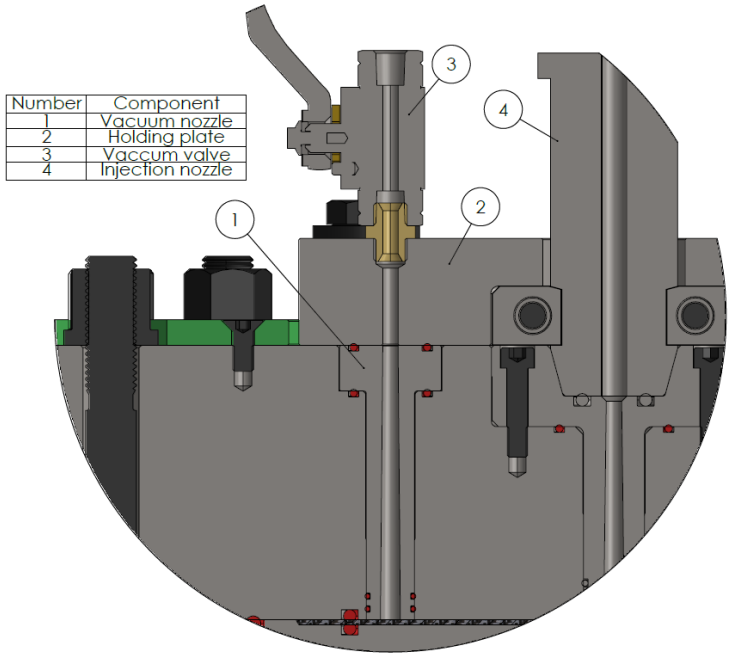

Figure 4.33 Detail of connection between vacuum nozzles and the closure valves

We implemented fiber clamping/pinch-off mechanisms using polymeric gaskets inside the mold cavity. Two symmetrical gaskets were located near the preform edges by over dimensioning the preform area to avoid any interference in the net final part. These gaskets have the purpose of avoiding preform movement during injections and possible dry zones caused by race tracking effects. Mold sealing was achieved by two polymeric gaskets located externally to the mold cavity: one serves as a selling method (inner gasket) while the other, (outer gasket) acts as security sealing method in the case of any failure (Figure 4.34).

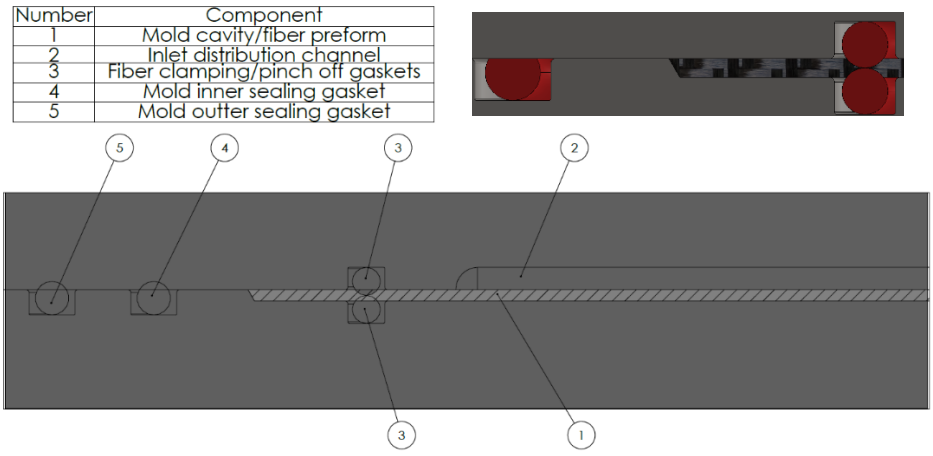

Figure 4.34 Detail of the fiber clamping and sealing gaskets located in the mold cavity (portion of the total area)

We considered O-rings for the mold sealing and fiber clamping rather than linear polymeric joints, that later are glued on the edges to close the sealing channel, as is commonly used for RTM process. The use of lineal sealing cords was discarded due to possible pressure failures in

the bonding points. Gasket cavities are designed with a rectangular shape, and dimensions are adjusted to achieve a nominal O-ring compaction of 25%. Moreover, we selected high-temperature silicon (VMQ/FVMQ) and fluorocarbon (FPM/FKM) materials (Table 4.5) for all the sealing and clamping O-rings inside the mold (Figure 4.35), operational temperatures and chemical compatibility were the main drivers for the materials selection [208].

Table 4.5. Material properties for O-ring sealing mechanisms. [208]

O-ring material	Temperature range [º C]	Advantages	Disadvantages
Silicone (VMQ o FVMQ)	-60 to 250 (VMQ) -55 to 225 (FVMQ)	High thermal strength and flexibility in cold environments. High strength under oxygen and ozone environments, oil resistance	Non-compatible with esters and ethers chemical species. Gas permeability, low strength to wearing and prune to be affected by acids and bases.
Viton (Fluorocarbon)	-20 to 250	Adequate for continuous use, non-flammable. Hydrocarbon, grease, and oil resistance.	Weak to organophosphates, ammonia, amines and solvents.

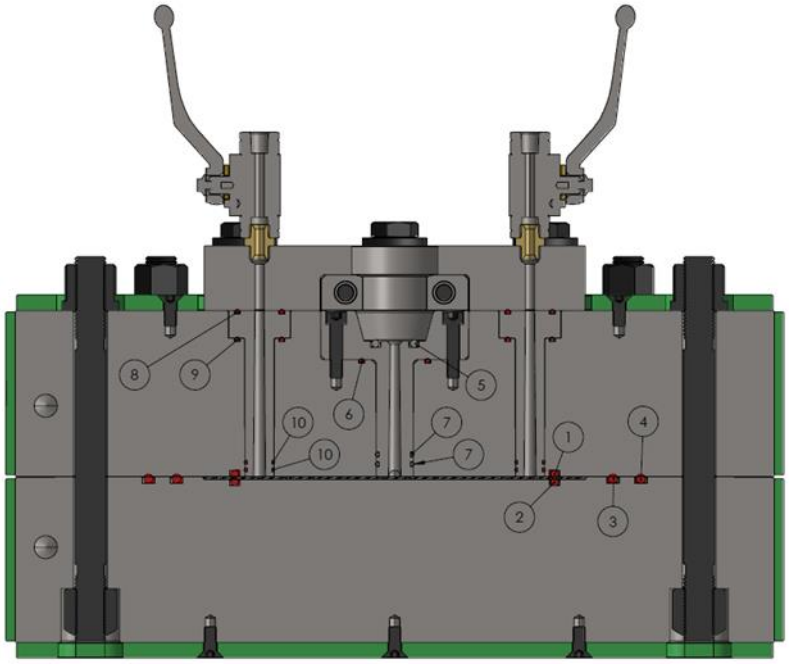

Figure 4.35. Array of mold sealing O-rings. 1) Upper clamping seal. 2) Lower clamping seal. 3) Mold cavity internal sealing O-ring. 4) Mold cavity external sealing O-ring. 5) Mold injection nozzle (male) sealing O-ring. 6) Mold injection nozzle (female) sealing O-ring. 7) Mold injection nozzle (female) cavity sealing O-ring. 8) Upper vacuum nozzle sealing O-ring. 9) Lower vacuum nozzle sealing O-ring. 10) Vacuum nozzle cavity sealing O-ring.

Initially, mold closure was intended to be done by using threaded stud bolts (DIN 940 M20 mm 12.9) with a total of 26 bolts located in all the mold area (Figure 4.36). Closure stability was verified considering the maximum injection pressure of 10 MPa (100 bar), and bolts number,

materials, bolts friction coefficient (0.2, lubricated), mold cavity area (86304 mm^2) and torque (500 Nm) [209].

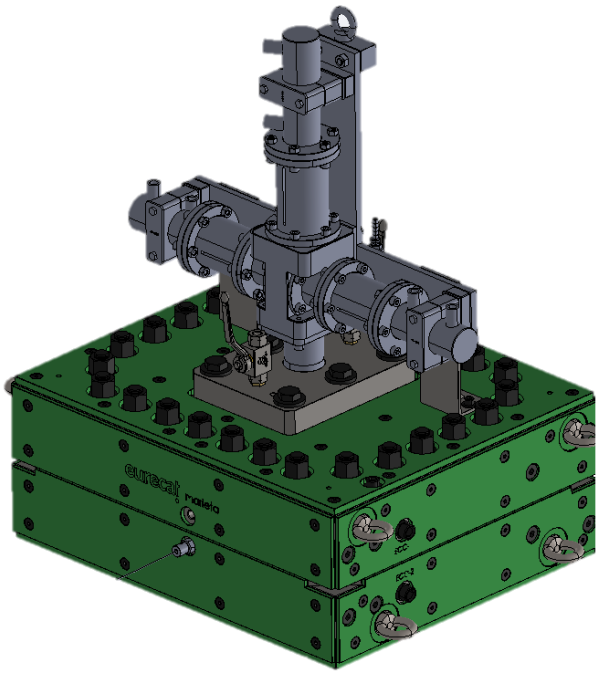

Figure 4.36. HP-RTM preliminary design

First, we calculated the total injection force ($F_{inj_{max}}$, equation 13) that the mold cavity will hold at maximum pressure (10 MPa) with the mold cavity area. Bolts' force (F_{bolts}, equation 14) can be calculated taking the maximum torque (M) considered for the mold, the friction coefficient factor (k) and the bolt's diameter (d). If we multiply that force to number of bolts, we obtain the total closing force that the bolts are applying to the mold structure.

$$F_{inj_{max}} = 10\ MPa = 10\frac{N}{mm^2} * 86304 mm^2 = 863040\ N * \frac{1\ kg}{9.8\ N} = 88065\ kg \quad (13)$$

$$F_{bolts} = \frac{M}{k * d} = \frac{500\ Nm}{0.2 * \left(20\ mm \frac{1\ m}{1000\ mm}\right)} = 125000\ \frac{N}{Bolt} = 12755\ \frac{kg}{Bolt} \quad (14)$$

At the end, knowing the injection force and the bolts force, we can obtain a security factor (S_{factor}, equation 15). Which has to be positive as the bolts must overcome the injection force to prevent mold opening during injection. Under these conditions our design is theoretically up to 3 times oversized, which let us know is safe.

$$S_{factor} = \frac{F_{bolts}}{F_{inj_{max}}} = \frac{125000\frac{N}{Bolt} * 26\ Bolts}{863040\ N} = 3.7 \quad (15)$$

4.2.2. Mold design validation trough FEM

This task was performed by the Product Development unit of Eurecat, Technological Center (simulation team) [210] to validate the mechanical and thermal performance of the HP-RTM mold. Simulations were carried out on the ANSYS Workbench software from ANSYS [211].

Boundary conditions for the mechanical simulations were defined knowing the mold material (steel DIN 1.2311), bolts material and number (steel, 26 bolts) and bolts force (125000 N/bolts). Mold geometry was simplified erasing all non-structural components, mold base was fixed (simulating its operational conditions), and a contact boundary condition was applied between mold parts. The mesh was constructed with tetrahedral elements, having a total of 1868094 elements. (Mechanical simulation boundaries summarized in Figure 4.37).

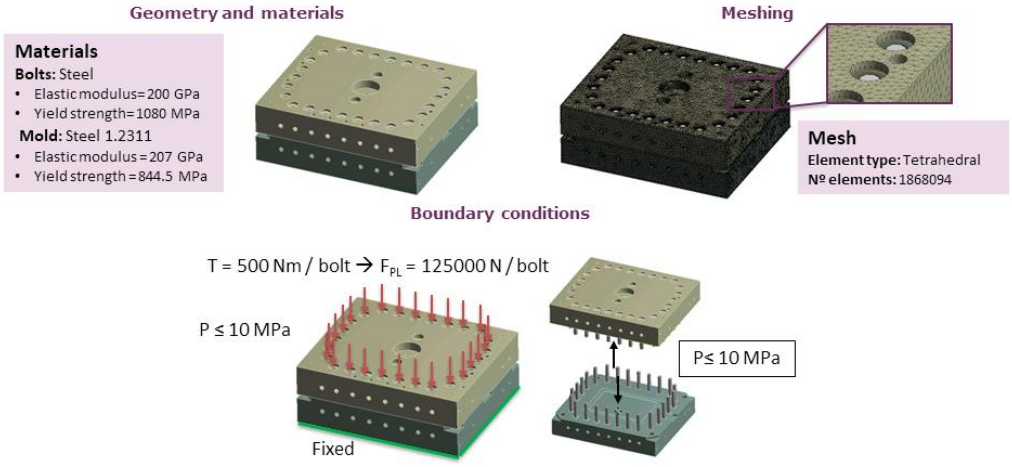

Figure 4.37 Boundary conditions for FEM validation of the mold structure. Adapted from [210]

With the simulation was possible to see that both mold parts maintain contact with each other at maximum pressure, without important changes in the pressure area (Figure 4.38 a). This means that the mold will not open or create gaps due to the injection pressure, as well as the mold structure has no important stresses. A maximum out-of-plane deformation of 0.037 mm in the upper mold part and -0.007 mm in the lower mold part is presented in the injection area (Figure 4.38 b), having a total deformation of 0.044 mm (2.2% with respect to the nominal dimensions), being inside the defined tolerances (7%) and validating the mold structural integrity.

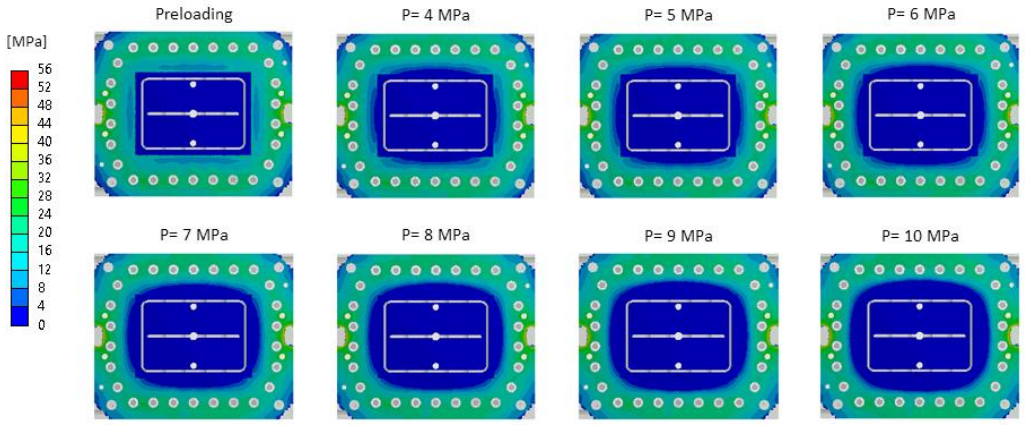

a

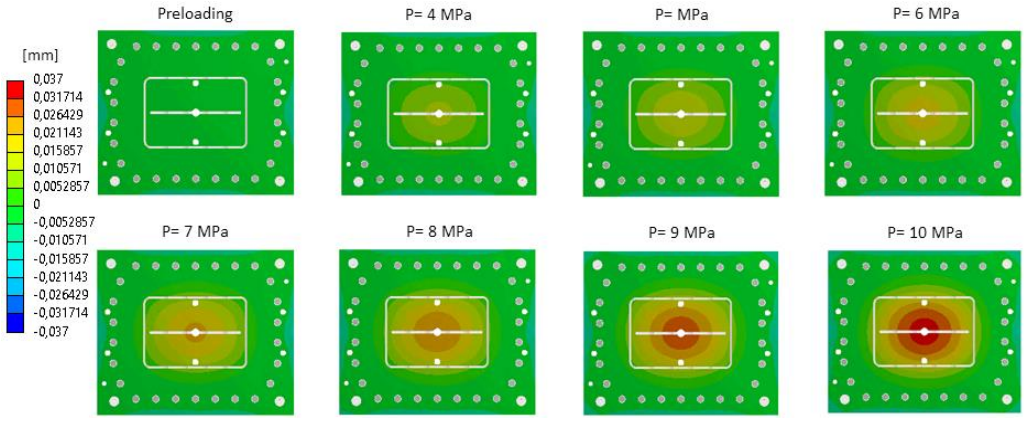

b

Figure 4.38 Structural FEM validation of the HP-RTM mold design. a) Contact pressure of mold parts under different injection pressures. b) Maximum out-of-plane deformations of the mold (upper part) under different pressures. Adapted from [210]

They also performed structural simulations on the mold bolts and their contact area (Figure 4.39). While the mold structure can hold stresses under its elastic limit, the bolts presented stresses near to plastic deformation at maximum injection pressure (Figure 4.39 b). The mesh was refined in the bolts and their contact areas.

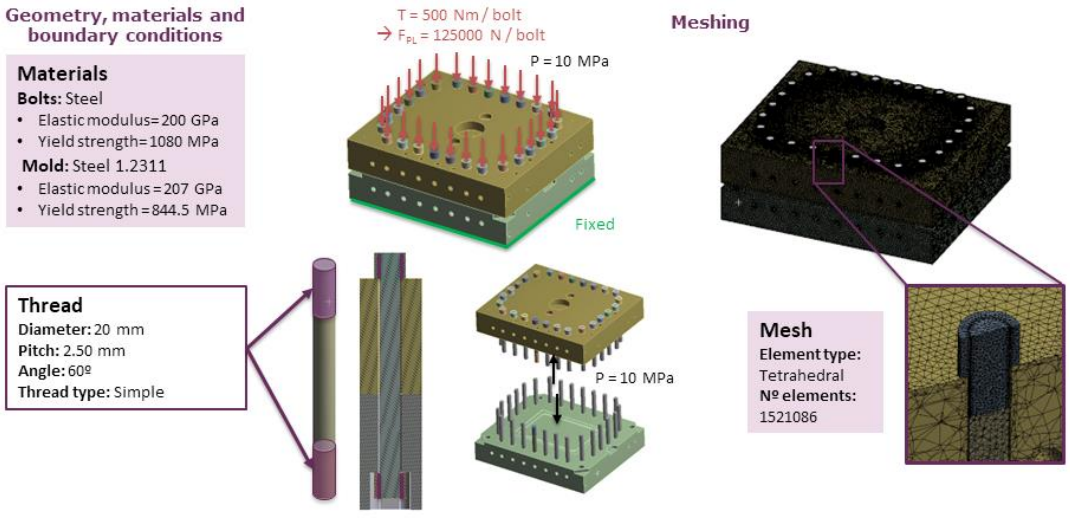

a

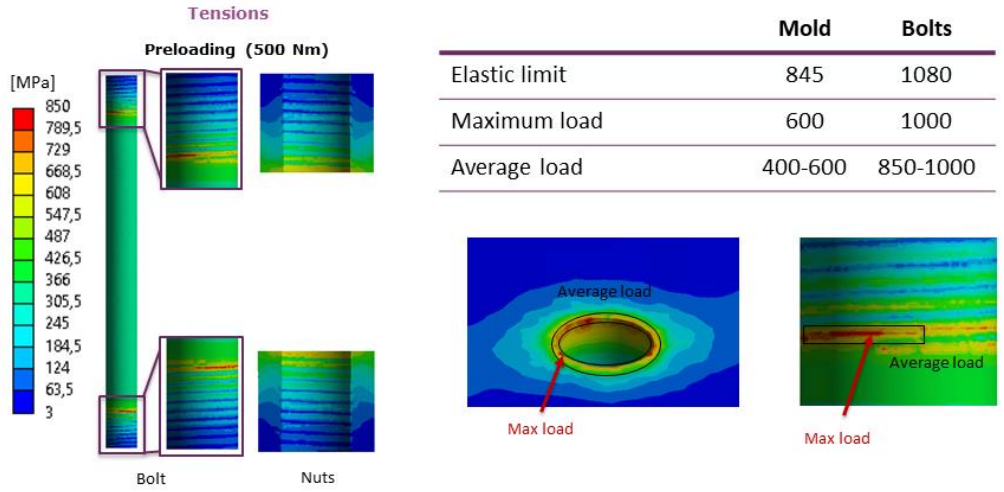

	Mold	Bolts
Elastic limit	845	1080
Maximum load	600	1000
Average load	400-600	850-1000

b

Figure 4.39. Structural FEM validation of the mold closure bolts. a) Simulation and boundaries definition. b) Presented stresses in the mold bolt area and bolts thread under maximum injection pressure. Adapted from [210]

Thermal simulations were performed in order to guarantee a uniform temperature distribution inside the injection cavity to avoid any curing differences in the final composite. The mold was designed to be heated by liquid (oil/water) using distribution channels machined directly inside the mold structure and interconnected through a hose between the two mold parts.

Water was selected as the heating media considering that the majority of injections would be carried at low curing temperature (80° C), using the water-based heater [192]. This heater has a capacity of 40 L/min, which was used to define the heating media velocity. Both mold parts were connected by a bridge (simulating a hose interconnecting both parts. Tetrahedral elements were also used, making the mesh finer at the heating channels and using a total of 1317541 elements. Thermal properties for the mold and the water are summarized in Figure 4.40 a.

Results show that the entire mold structure heats uniformly in an average time of 40 minutes. Maximum temperature differences inside the injection cavity are close to 0.18 °C. Thermal simulations were validated with experimental tests.

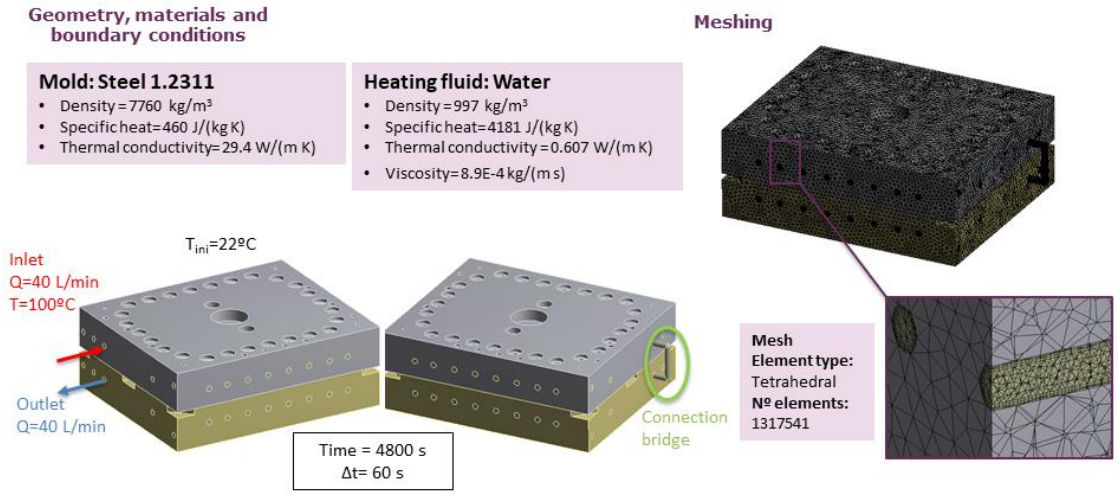

a

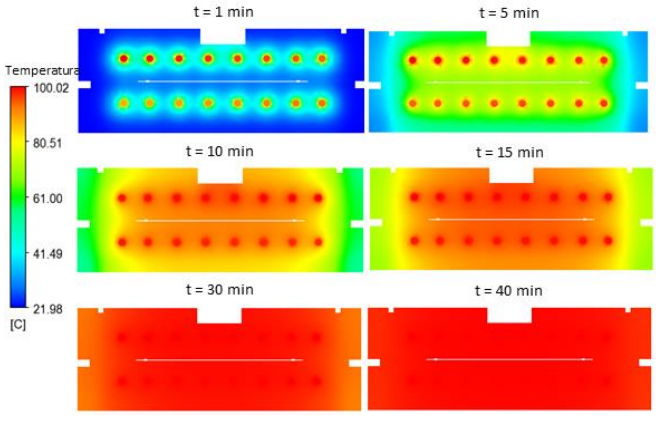

b

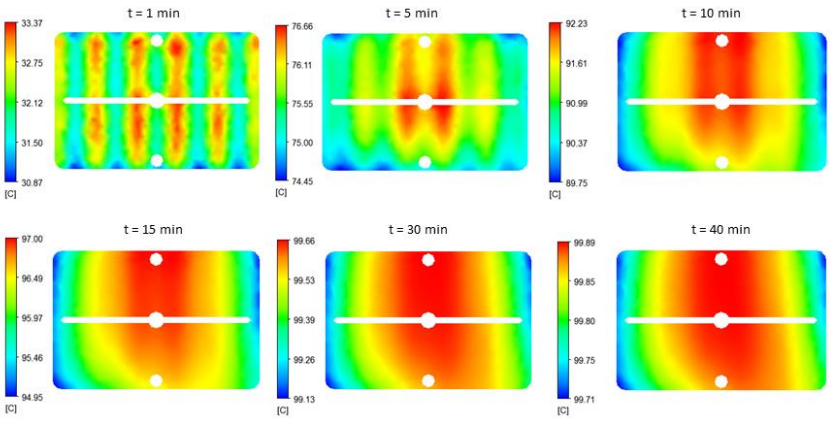

c

Figure 4.40 Heating FEM simulations for the mold structure. a) Boundary conditions. b) Heating of the mold parts until reaching injection/cure temperature. c) Heating evolution of the injection cavity area. Adapted from [212].

Considering all the data obtained in the simulations, we decide to modify the mold structure to prevent possible failures: bolts type was changed from stud bolts (DIN 940) to hexagonal socket cap head bolts (DIN 912), increasing the nominal bolt diameter from 20 to 24 mm to reduce the risk of bolts plasticity. We also redesigned the mold heating channels to simplify the overall structure, lowering the manufacturing costs. No further simulations were implemented.

We calculated again the bolts force (F_{bolts}, equation 16) and mold security factor (S_{factor}, equation 17) for the new design.

$$F_{bolts} = \frac{M}{0.2 * d} = \frac{500\ Nm}{0.2 * \left(24\ mm \frac{1\ m}{1000\ mm}\right)} = 104167\ \frac{N}{Bolt} = 10629\ \frac{kg}{Bolt} \qquad 16$$

$$S_{factor} = \frac{F_{bolts}}{F_{inj_{max}}} = \frac{104167 \frac{N}{Bolt} * 26\ Bolts}{863040\ N} = 3.14 \qquad 17$$

4.2.3. Final design and construction

Figure 4.41 shows the final mold design with all its injections accessories. Figure 4.42 presents the mold final structure and its connection with the HP-RTM mixhead.

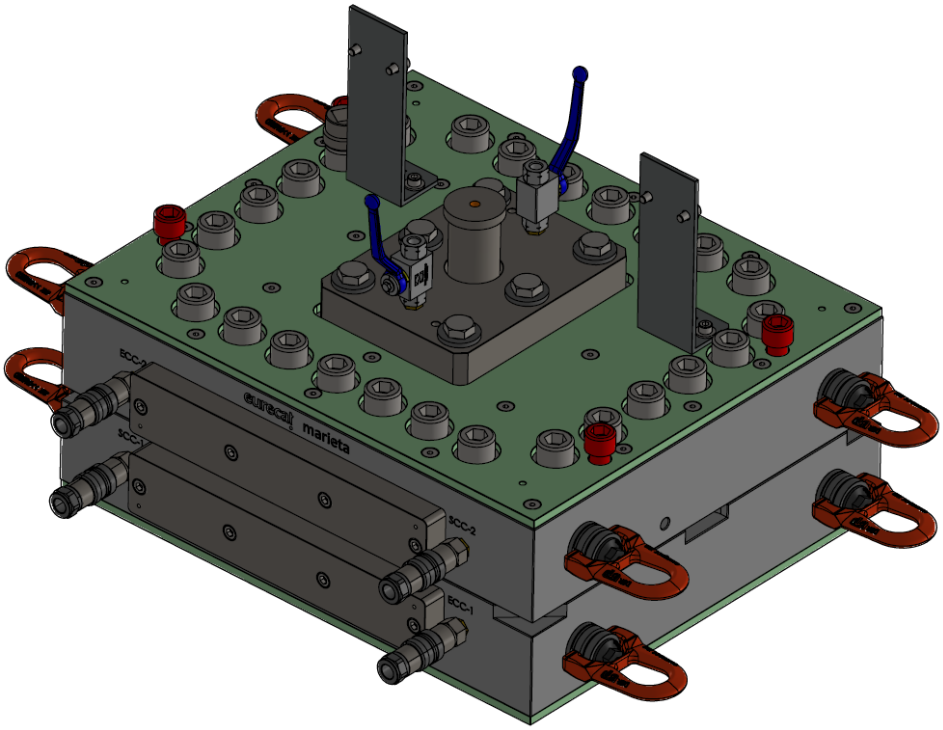

Figure 4.41 Final HP-RTM mold design

a

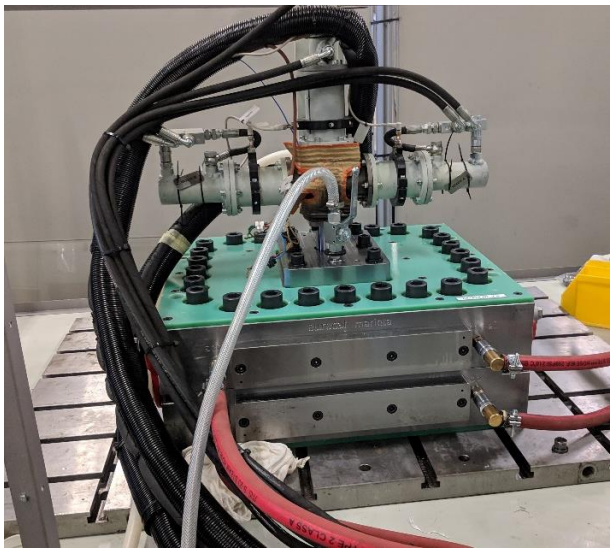

b

Figure 4.42 Mold construction. a) Detail of the mold structure. b) Detail of the machine mixhead integration and the heating and vacuum connections (configuration for bi-component injection)

The mold integrated isolation plates in the upper and lower mold surfaces to reduce heat leaks. Steel plates are located in the mold lateral faces to close and interconnect the heating channels. Mold cavity was directly machined in the mold structure (in the lower mold part) with angled edges at 45° to ease the demolding process. Injection tasks with the mold and the machine were carried in a modified structure, using a 1 Ton capacity manual crane. This structure integrates PMMA protection walls in case of a pressure failure (Figure 4.43).

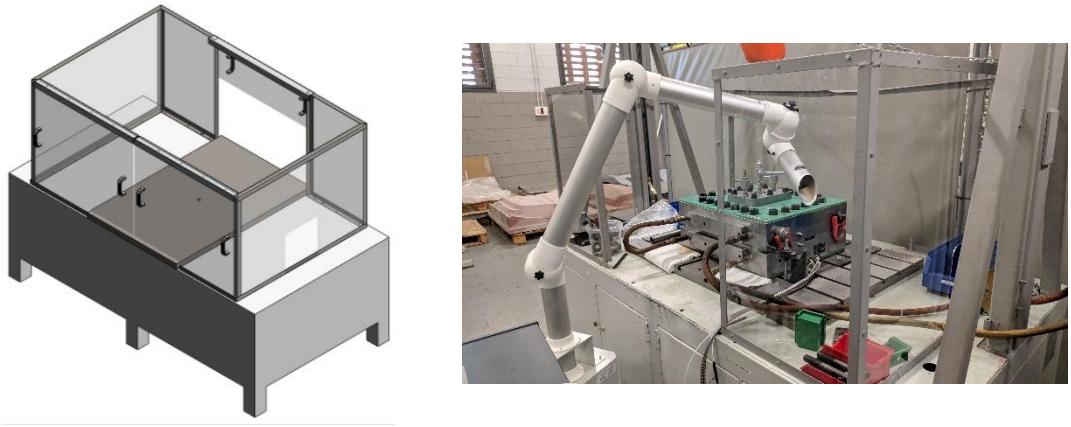

a b

Figure 4.43 Setup for injection operation. a) Design of the injection hoist with the PMMA protection walls. b) Final assembly with the HP-RTM mold.

4.3. Discussion on the HP-RTM technology

The Eurecat's HP-RTM prototype machine has proved to be capable to produce high-performance structural components based on continuous carbon fiber reinforcements. Its function principle is simple: the pressure is reached by using conventional hydraulic-driven axial pistons, as in other commercially available HP-RTM machines [44]–[49].

The machine operation is simple and easy to drive. But the ratio calibration proved to be complex, also needing future improvements on the injection volume, resin and hardener ratio and minimum operational tolerances.

Another aspect of the machine operation that has to be improved is the mixing quality of the resin and hardener inside the mixture channel. Early bi-component trials were not properly mixed as the mixture relies only on fluid dynamics. Chaudhari et al. [7] in their work used an injection pressure of 12 MPa (120 bar) at the mixing head of their machine to ensure resin and hardener proper mixture, which impacts directly on the fluid velocity and thus, the fluid dynamics (Reynolds number - turbulent state [213]). In our case, the maximum injection pressure was only 8 MPa, around 33% lower compared to their value. Additionally, we had to consider the machine minimum operational tolerances, the overall internal volume of our mold cavity and the volumetric fraction of the total resin mixture compared with the fabrics. There was a lot of parameters to manage in order to guarantee a proper turbulent flow and ensure resin and hardener mixture. If we increased the pressure, and consequently, the fluid velocity, we could had turbulent flow and a more optimal mixture, but as seen in the quality of the materials manufactured at 8 MPa, we increase the risk of presenting defects in the final component, something that already has been pointed by other authors, which recommend to use more gentle parameters [40]. So, the easiest way to improve the resin and hardener mixture

is by adding elements to create turbulent flows (static mixers), being a commercially available solution, also being disposable or exchangeable.

Moreover, we described that the focus on the machine issues relied on the mixhead itself. The mixhead operation is driven by mechanical components with constant movement having some implications: dimensional tolerances, sealing methods and the overall wearing of the parts during machine operation.

The use of the the high-reactivity resin system complicated the issues presented in the mixhead due to its very low viscosity [147] and its short-reactivity time, leaking between the mixhead components and curing instantly.

The mixhead was redesigned focusing on the system reliability and design simplicity to avoid moving parts as much as possible, and integrate static mechanisms to ensure the system sealing, cleanness and guarantee resin and hardener mixture. Factors as maintenance and easy access also were implemented, and the possibility to use exchangeable parts as nozzles to improve the system availability for line operation.

Reliability of the HP-RTM process is another factor to consider. In our case, we implemented HP-RTM injections using a mono-component configuration on a simple geometry that did not require the use of binder materials or specially designed injection ports to ensure the overall preform impregnation. We believe that in more complex geometries it would be difficult to ensure a proper injection.

Mold design and construction proved to be safe and reliable. The quality of the final materials was good in aspects as fibers impregnation, resin curing and dimensional tolerances. The mechanical and thermal simulations gave us enough information to know if the mold design was robust for the HP-RTM operation before even constructing it or proving the mold itself. Sealing strategy proved to be safe and robust, all the injections presented acceptable vacuum levels and vacuum leaks. Additionally, all sealing mechanisms contained the resin inside the mold cavity without any failure or pressure leaks inside the mold cavity

The injection strategy, using a center point with distribution channel (film injection strategy), proved to be an optimum solution to avoid fiber washout, which is one the main issues in the HP-RTM process [22], [37], [38], [54].

The composite samples manufactured with the mold at the different pressure values did not show any sign of washout at the inlet gate. Considering that in our study we used NCF instead of woven fabrics, having weaker bonds between fibers and being more sensitive to fibers sliding [38].

Previous authors as R. Chaudhari, P. Rosenberg, F. Henning or B. Thoma (Fraunhofer Institute for Chemical Technology ICT, [7], [27], [32], [41]) demonstrated that the film injection strategy helped to reduce the incident injection pressure over the fiber preform, minimizing the risk of movement. We also detected that the injection strategy helped to distribute the injection pressure over the mold structure, something that was visible in the mold simulations and the samples dimensional characterization (4.2.2, 5.1.1). The only possible issue with this strategy is that the distribution channel remains in the final piece, something that must be considered if we want to manufacture an element with exposed or visible surfaces. If the part allows it, the distribution channel can be hidden in a non-visible area.

Mold vacuum was also one key factor to the sample's final quality. In our case we did not prove the injection strategy without vacuum, but this has been tested by other authors as the vacuum helps to reduce the final porosity content in the composites, improving the final mechanical performance [4]. We found some issues on the vacuum strategy as the out ports were located over the composite sample. By having open vacuum channels, the incident force from the injection pressure, especially at the highest-pressure value, made the fibers break and deform, causing damage in the preform over the vacuum area, creating fiber bumps. This issue also influenced the composite entrapment at the upper mold part and causing superficial delaminations and thus requiring in our case, the use of the peel ply layer in order to avoid any possible damage during demolding.

In our case, mold manipulation was not intended for high-volume processing, being heavily manual. We would need the use of an hydraulic press to open and close the injection mold, in addition to intermediate steps to apply vacuum inside the mold cavity and seal it before injection, as the HP-CRTM process variant [6], [8], [24], [27], [40], [41]. Additionally, vacuum ports would need to be relocated outside the sample area to avoid marks on the samples surface.

Final composite samples did not present visible indications of race tracking. Albeit it has been reported that the fiber clamping/pinching-off mechanism is a good way to prevent it [54]–[56], our geometry was very simple, with any important geometry changes that could be affected by this defect. In addition, the mold internal pressure could have forced the resin to impregnate any defective area at the last stages of the injection.

Fiber clamping made necessary to trim the samples after cure, increasing the overall cycle time.

Moreover, we found that the clamping of the fibers created indentations in the mold surface, something that was mentioned previously by M. Bodaghi et al. [22]. This must be considered in a high-volume production environment.

The use of O-rings as sealing mechanism for HP-RTM processing, prove to be reliable and safe, we did not have any issue related with depressurization in the mold cavity. In conventional RTM process, we use conventional silicon cords bonding its edges, being simpler and cheaper, but sometimes creating issues with the injection, mold vacuum and resin leaks as the bonding points tend to separate. A similar case in the HP-RTM process would be more important as the internal pressure of the mold could create risks on a production environment. The O-rings used in this work were more expensive, if compared to traditional sealing solutions, but the materials selected (vulcanized silicon VMQ/FVMQ and fluorocarbon polymers FPM/FKM) proved to last longer, minimizing the operational cost.

Other aspects of the mold design as the heating strategy and the union mechanism to the machine mixhead and injection nozzles proved to be safe and reliable. Our design relied on bolts for the system closure, something that has to be considered also in a high-volume production environment, affecting the overall processing time.

Chapter 5: Results and discussion on HP-RTM performance

This chapter summarizes the performance of the HP-RTM composites by means of dimensional validations, non-destructive testing, and mechanical characterization. In addition, monitoring results from the pressure and cure monitoring sensors are presented, giving a discussion on the materials properties and process cycle and optimization.

5.1. Samples validation

5.1.1. Thickness measurement

We checked the thickness of the final composite samples in order to see if the mold structure presented any measurable deformation during the high-pressure injections. Thickness measurements for the RTM reference samples oscillated between 1.96 mm – 1.98 mm for the standard epoxy Sicomin resin, and 1.94 mm – 1.98 mm for the RTM6 resin, having some deviations. It was not possible to inject an RTM reference sample using the Airpoxy resin due to materials availability. Main deviations for the intended 2 mm thickness could be attributed to the use of the peel-ply layer used in the preform to avoid fiber gripping inside the injection and vacuum channels. Thickness maps for the base RTM samples are displayed in Figure 5.1.

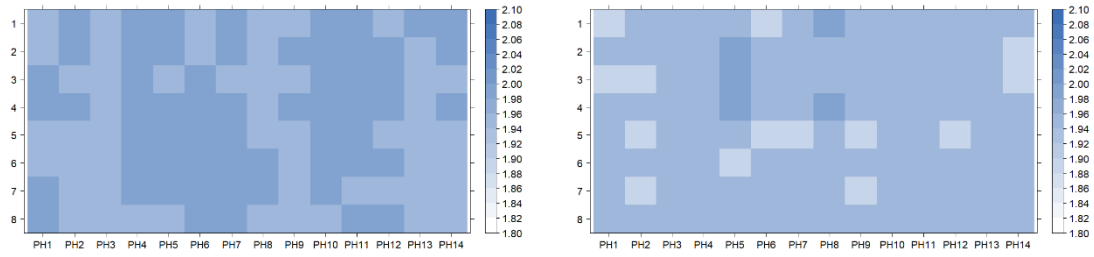

a b

Figure 5.1. Thickness map of the conventional RTM samples. a) Reference sample for the standard Sicomin resin. b) Reference sample for the aeronautic RTM6 resin. Measurements in mm

High-pressure samples were very stable, with thickness values around 1.94 mm and 1.96 mm. We detected that the overall thickness tends to increase as the injection pressure is higher, even at maximum pressure (8 MPa), two measurement points were near to 2.04 mm in the near to the injection area. In this way we confirm that the mold structure can hold the maximum injection pressure with any important deformations, samples thickness accomplished the defined mold tolerance. (2 ± 0.14 mm). Thickness maps for the HP-RTM samples are displayed in Figure 5.2.

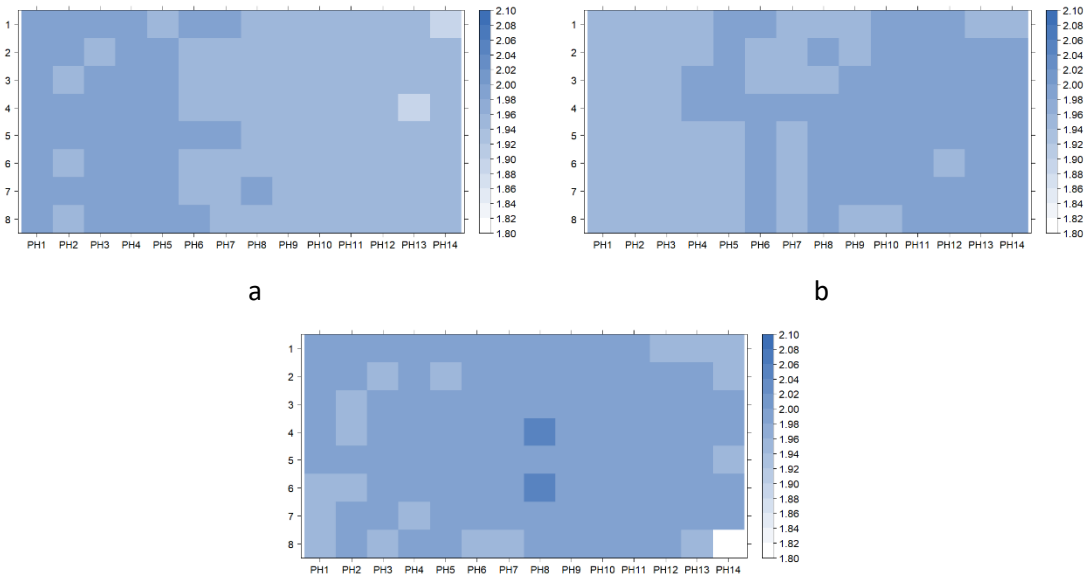

Figure 5.2. Thickness map of the Sicomin resin HP-RTM samples under a constant curing temperature (80° C). a) 2 MPa sample. b) 5 MPa sample. c) 8 MPa sample. Measurements in mm

Changing the injection temperature did not affect the thickness behavior of the composites as the tendency was like the reported in the samples manufactured at 5 MPa. We only found some deviations in the sample injected at 120° C (Figure 5.3).

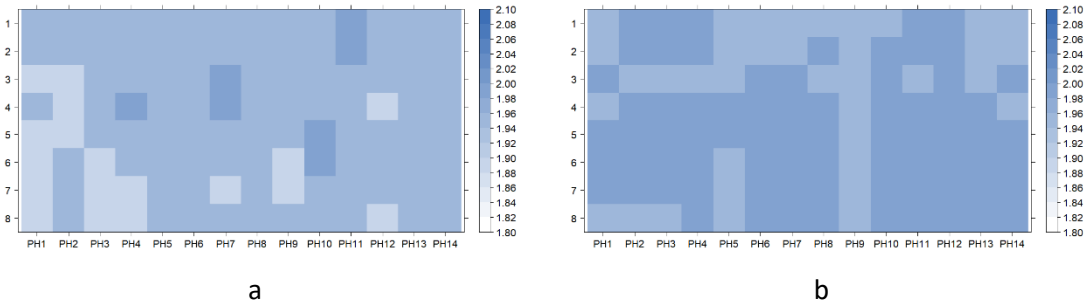

Figure 5.3. Thickness map of the Sicomin resin HP-RTM samples under a constant injection pressure. a) Sample injected at 120° C. b) Sample injected at 140° C. Measurements in mm

5.1.2. Visual inspection

In all cases, samples presented superficial marks related to the injection channel, fiber clamping and areas in contact with the pressure and curing sensors (Figure 5.4).

Figure 5.4. Visible superficial marks on the composite sample made by the sensors and the fiber clamping mechanism

Preform integrity during the injection was not compromised. At lower pressures we only detected some fibers misalignments, more related to the preform handling and positioning in the injection cavity, than to issues caused by the injection pressure (Figure 5.5). In the conventional RTM process, only the sample manufactured with the RTM6 resin presented a few porosity areas near the injection gate.

Figure 5.5. Process defects related to preform handling

At high-pressure (5 MPa and 8 MPa), the overall surface finish was better than conventional RTM samples. But we detected that the fibers tend to deform and enter inside the vacuum channels, leaving superficial bumps in the final composite. This fiber bump was bigger in the sample injected at 8 MPa, leaving some fibers inside the vacuum nozzle presumably due to damage in the preform (Figure 5.6).

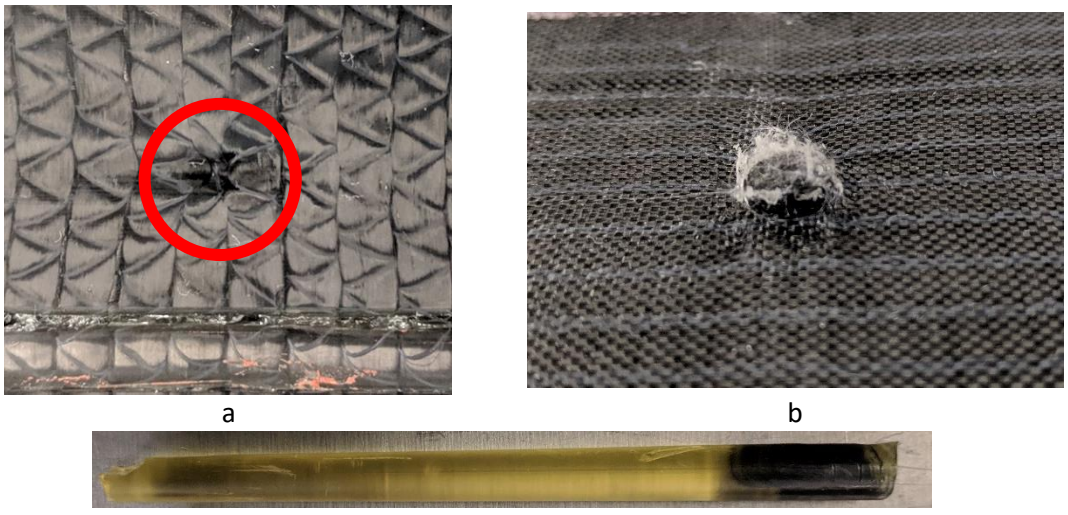

a b

c

Figure 5.6. Defects caused by the injection pressure, breaking and bumping the preform fibers at the molds vacuum ports. a) lower surface, wrinkled fibers. b) upper surface, bumping area. c) Remains of resin inside the vacuum nozzle channels, fibers trapped at the bottom of the channel.

Nevertheless, the strategy of implementing a distribution channel at the injection gate helped to reduce the incident pressure over the preform as no defects as fiber washout were found on this area (Figure 5.7).

a

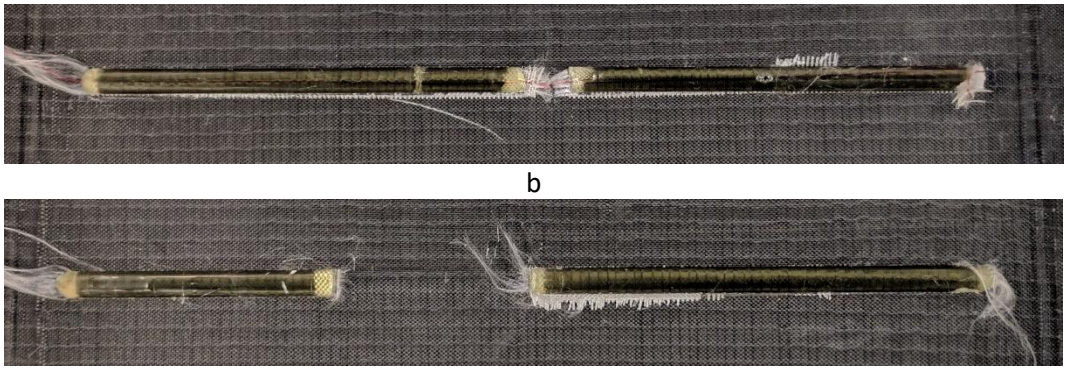

b

c

Figure 5.7. Samples area below the injection gate and distribution channel. a) 2 MPa sample. b) 5 MPa sample. c) 8 MPa sample

Samples injected at high temperature did not present issues related to the injection pressure. The sample injected at 120° C had some superficial porosity (Figure 5.8). Sealing issues were discarded as the vacuum leaks of the mold at this temperature was 4 x 10^{-5} MPa (0.4 mbar/min) and the vacuum level during injection was 2.3 x 10^{-4} MPa (2.3 mbar). Initially we considered that it was an effect of the injection velocity, being too low to fill the mold cavity before curing, since the Sicomin resin is a high-reactivity formulation. But we discarded this idea later as the sample injected at 140° C under the same pressure did not present visible porosity. Evaporation of resin volatiles was also discarded, so we believed that this might be caused by the mold demolding agents. As we used a semi-permanent solvent-based demolding agents, we only performed superficial cleaning of the mold surface between injections, reapplying a few more demolding layers. Maybe trapping residual materials as resin or changing the demolding behavior. After this, we decided to clean the mold surface with solvents and apply again pristine demolding layers, having care with the mold cleanness between injections. The following composite samples did not present this issue.

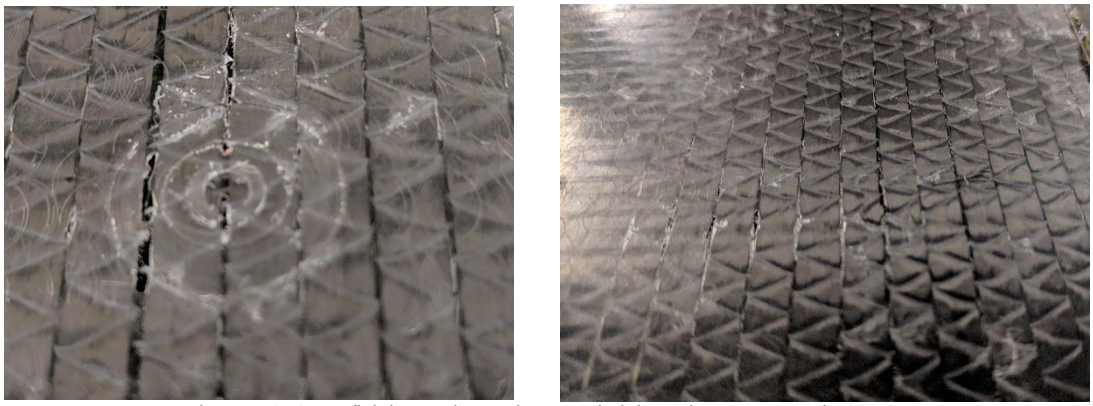

Figure 5.8. Superficial porosity on the sample injected at 5 MPa and 120° C

Vacuum levels and vacuum leaks were maintained inside the defined tolerances during all the injections (Table 5.1). We took measurements right after the mold closure under room temperature, and later, at the injection temperature for each trial. Sealing methods for this mold design were validated.

Table 5.1. Measurement of vacuum level and vacuum leaks during the injections. Data gathered at room temperature and at injection temperature

Injection trial	Vacuum level [MPa]	Mold vacuum leaks [MPa/min]	
		Room temperature	Injection temperature
Trial 01 2 MPa	1.6×10^{-4}	2.6×10^{-4}	4×10^{-5}
Trial 02 5 MPa	2.1×10^{-4}	3.9×10^{-4}	1.2×10^{-4}
Trial 03 8 MPa	2.3×10^{-4}	1.2×10^{-4}	5×10^{-5}
Trial 04 5 MPa +120° C	2.3×10^{-4}	1.2×10^{-4}	4×10^{-5}
Trial 05 5 MPa + 140° C	2.4×10^{-4}	9×10^{-5}	1×10^{-5}
Trial 06 RTM6 5 MPa	2.5×10^{-4}	1.6×10^{-4}	1×10^{-4}
Trial 07 RTM6 8 MPa	2.9×10^{-4}	-	1×10^{-4}
Trial 08 Airpoxy 8 MPa	3.8×10^{-4}	9×10^{-5}	1×10^{-5}
Trial 09 Airpoxy 5 MPa	3.4×10^{-4}	2.1×10^{-4}	4×10^{-5}
Trial 10 Sicomin base RTM	3×10^{-4}	2.2×10^{-4}	2.7×10^{-4}
Trial 11 RTM6 base RTM	2.1×10^{-4}	1.8×10^{-4}	6×10^{-5}

None of the injected trials presented evidence of race tracking or fiber washout. Apart from the distribution channel at the injection gate, the fiber clamping mechanism seem to help in preventing these issues. Despite the use of the fiber clamping method, resin was able to flow outside the clamping area, possibly caused by the internal cavity pressure. In just one case (Trial 05 with Sicomin resin at 5 MPa and 140° C, Figure 5.9), we ran out of the O-rings for clamping, as between injections we had to change it due to damage, in this case we used an O-ring with a bigger diameter (6 mm instead of 5 mm). The clamping area in the preform after the injection was dry, but the net area of the preform was not affected.

Figure 5.9. Detail of a dry zone under the clamping area for the trial injected with an O-ring with bigger diameter than the intended by design

5.1.3. Ultrasonic inspection

We performed ultrasonic inspections of all the composites made in the HP-RTM injections trials before cutting the coupons for characterization. All samples were inspected under the same conditions.

The reference RTM sample made with the Sicomin resin did not have any visible defects (Figure 5.10).

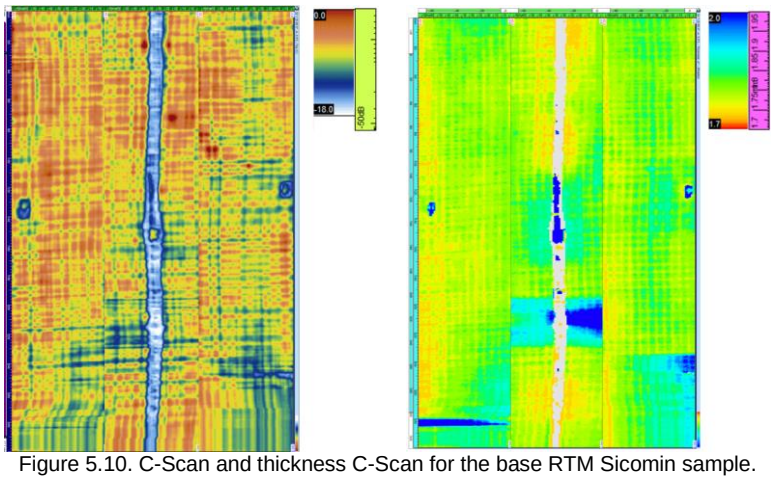

Figure 5.10. C-Scan and thickness C-Scan for the base RTM Sicomin sample.

Trials injected at 2, 5 and 8 MPa did not present any important defects, attenuation was below the defined thresholds withing limits, with no important thickness variation (≈1.75 mm to 1.95 mm, Figure 5.11).

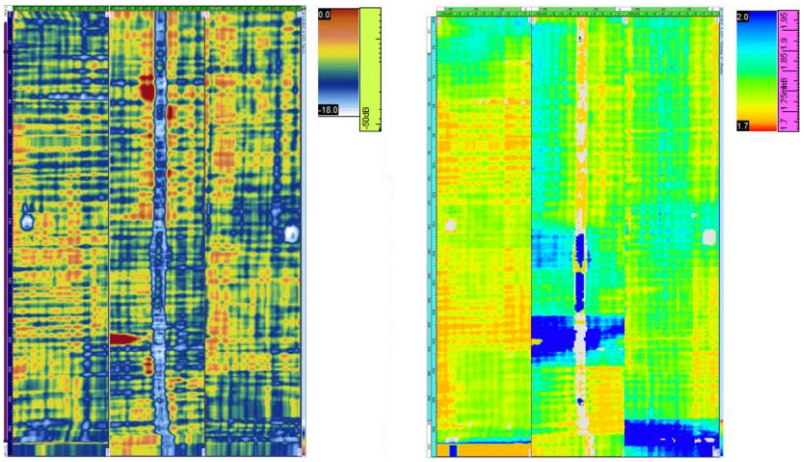

a

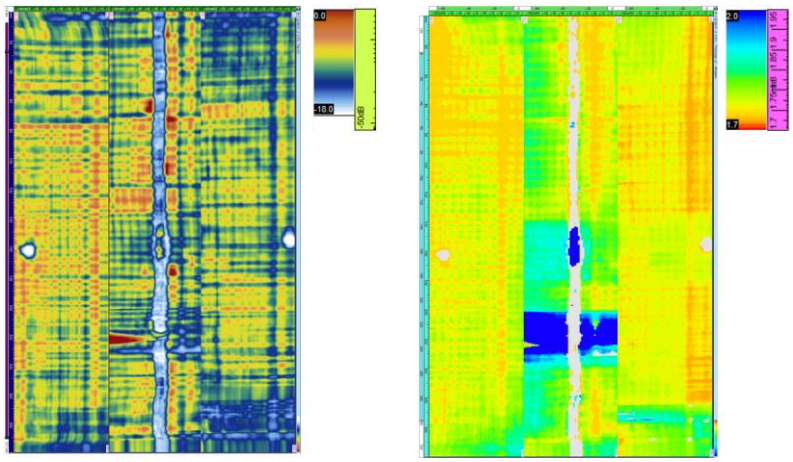

b

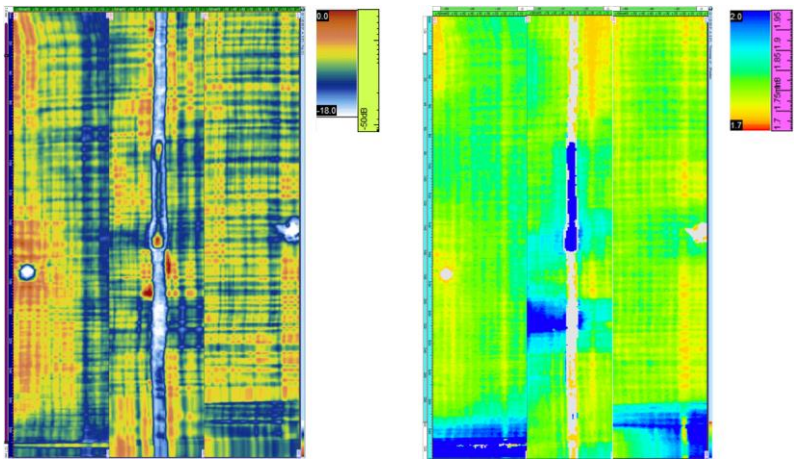

c

Figure 5.11. C-Scan and thickness C-Scan for the HP-RTM samples manufactured with the Sicomin resin at different injection pressures under constant temperature (80° C). a) 2 MPa. b) 5 MPa. c) 8 MPa

We detected signal attenuations in both high-temperature trials (trial 04 at 120° C, and trial 05 at 140° C), which appeared as possible dry zones near to a vacuum port (Figure 5.12), something that was not visible during the visual inspections.

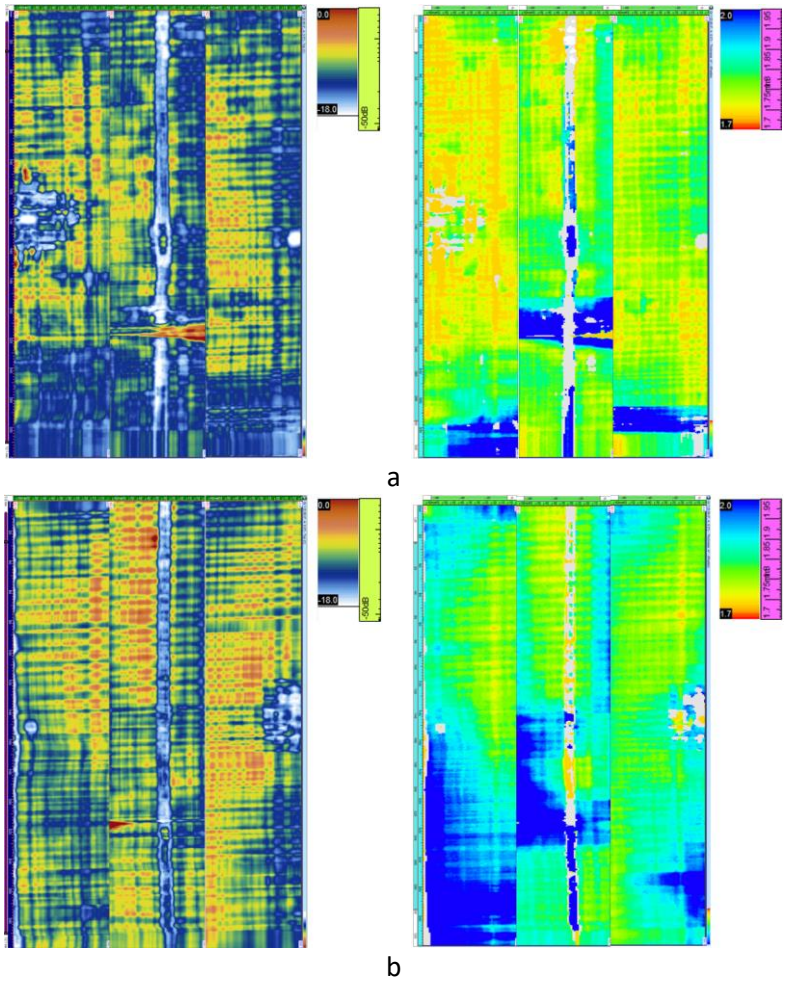

a

b

Figure 5.12. C-Scan and thickness C-Scan for the HP-RTM samples injected at high temperatures under constant pressure (5 MPa) using the Sicomin resin. a) Sample injected at 120° C. b) Sample injected at 140° C.

We believed that the injection pressure or injection velocity were not appropriate for fill the mold cavity before the resin starts its polymerization.

5.2. Mechanical properties of HP-RTM composites

We took the results from the base RTM samples as a baseline for all the HP-RTM samples, these properties are summarized in Table 5.2.

Table 5.2. Mechanical properties for base RTM Sicomin sample

Resin formulation	Flexural strength [MPa]	ILSS [MPa]	Compression strength [MPa]
Standard epoxy (Sicomin)	867.91 ± 108.31	47.59 ± 0.87	545.42 ± 34.98

5.2.1. T_g

Table 5.3 summarizes the DSC results from the samples injected at different injection temperatures.

Table 5.3. DSC characterization for the Sicomin resin manufactured at high-pressure under different curing temperatures

Sample	T_g [C]	Enthalpy [J/g]	Degree of cure
Uncured reference	-	222.02	-
5 MPa + 80° C	96.85	6.94	96.87%
5 MPa + 120° C	130.87	0	100%
5 MPa + 140° C	131.63	0	100%

There are not significant differences between the high temperature samples, but T_g is higher for the samples cured at 120° C and 140° C. We validate a proper curing time for all samples. It is clear that the injection temperature has a direct effect on the final glass transition temperature, possibly affecting the final properties of the composite materials.

Additionally, we performed DSC measurements for the HP-RTM injected under different pressures and cured at the same temperature (80° C). As was reviewed in the state-of-the-art chapter that pressure might have an incidence over the resin curing behavior. We demonstrated that is not the case. These results are summarized in Table 5.4.

Table 5.4. DSC characterization for the Sicomin resin manufactured under different injection pressures

Sample	T_g [C]	Enthalpy [J/g]	Degree of cure
Base RTM (0.1 MPa)	98.99	6.95	96.86%
HP-RTM 2 MPa	98.14	5.75	97.41%
HP-RTM 5 MPa	96.85	6.94	96.87%
HP-RTM 8 MPa	98.08	6.66	97.00%

5.2.2. Flexural strength

Samples tested under different injection pressures presented improvements to the base RTM properties (Figure 5.13): 1.43% at 2 MPa, 16.28% at 5 MPa and 16.34% at 8 MPa. In the latter case, variability was less than the other injection pressures.

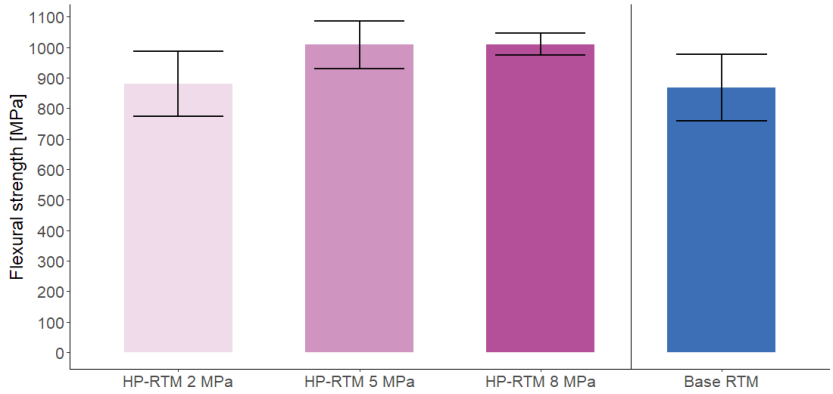

Figure 5.13. Comparative results in flexural strength for the standard epoxy formulation injected at different pressures. All samples cured at 80° C

We also detected improvements on the flexural strength by increasing the injection temperature compared with the base RTM data (Figure 5.14): 1.17% at 120° C and 7.02% at 140° C. The sample injected at 120° C presented higher variability, this could be related to the porosity found in the sample during the visual inspection. Nevertheless, the sample that was injected at 80° C under the same injection pressure had a higher flexural strength than the high temperature samples (9.41% more than the 120° C sample and 7.58% more than the 140° C sample). All samples injected at 5 MPa (50 bar).

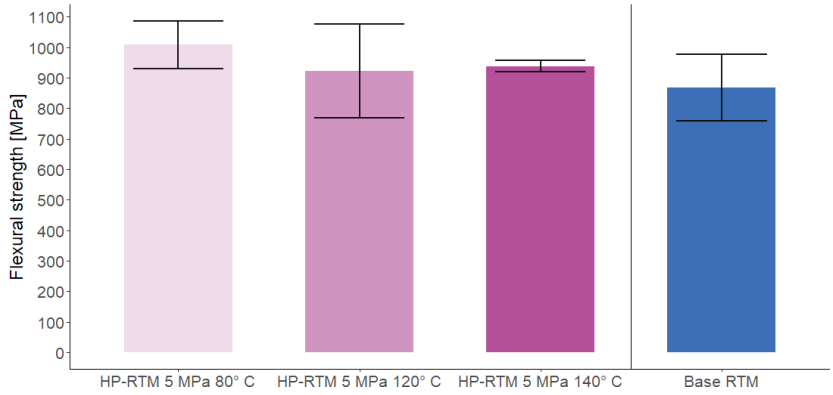

Figure 5.14. Comparative results in flexural strength for the standard epoxy formulation injected at different temperatures. 5 MPa injection pressure.

In general, most of the coupons failed under tensile stresses at the lower surface. Some failed by compressive stresses at the upper surface (Figure 5.15). We do not report invalid failure modes.

a

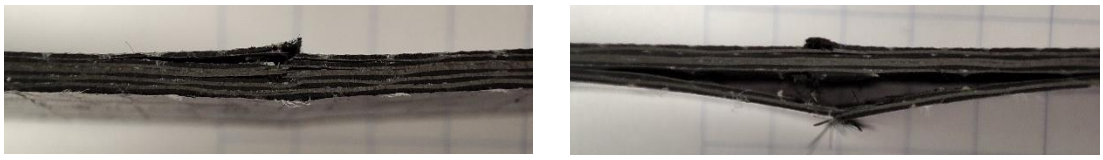

b c

Figure 5.15. Testing of HP-RTM samples under flexural stresses. a) Coupon being tested under 3-point load configuration. b) Example of a failure made mainly by compressive stresses on the coupon upper surface. c) Example of a failure made mainly by tensile stresses on the coupon lower surface.

5.2.3. Compression strength

Compression strength for the HP-RTM samples also presented improvements with respect to the base RTM properties. The injection pressure increased the compression strength by 0.68% at 2 MPa, 9.30% at 5 MPa and 13.47% at 8 MPa (Figure 5.16). Contrary to the flexural strength, further improvement is achieved at maximum pressure.

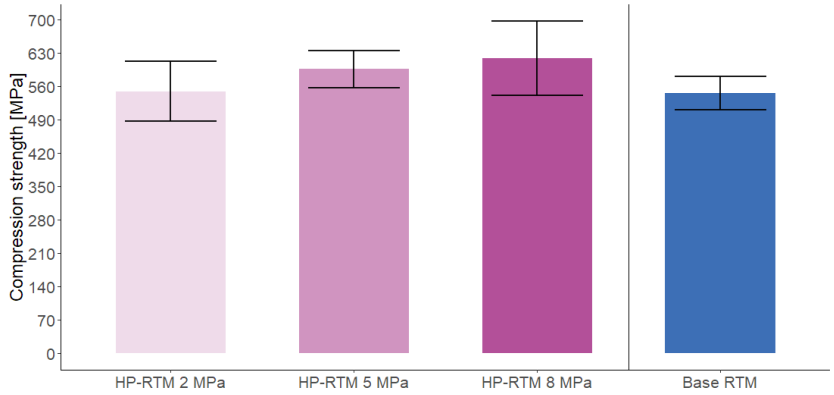

Figure 5.16. Comparative results in compression strength for the standard epoxy formulation injected at different pressures. All samples cured at 80° C

There were not sings of mechanical detriment as the pressure rises, this could be an indication that the compression properties could be further improved by rising the injection pressure. In this case we also considered the reduction of the internal porosity by the injection pressure.

High temperature samples also presented improvements of the compressive strength: 3.29% at 120° C, and 5.48% at 140° C. Likewise to the flexural properties, the sample injected at 80° C presented higher compressive strength: 5.82% more than the 120° C sample and 3.62% more than the 140° C sample (Figure 5.17). Equally to the flexural properties, the higher T_g and the reduced resin viscosity must be considered for the influence over the mechanical performance.

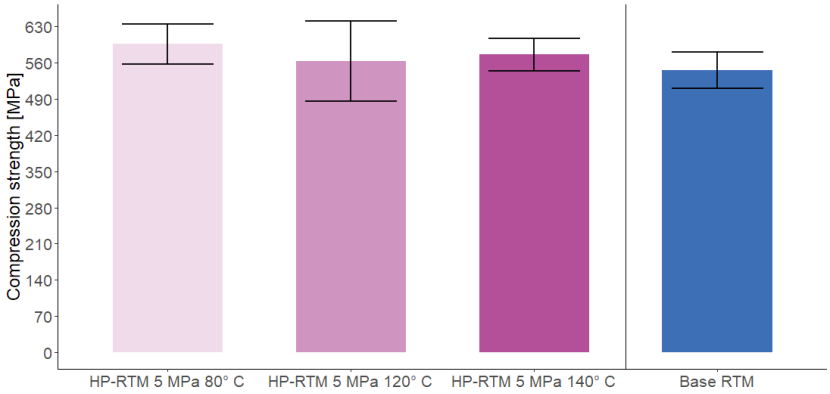

Figure 5.17. Comparative results in compression strength for the standard epoxy formulation injected at different temperatures. 5 MPa injection pressure.

None of the samples presented sliding during the testing. We believed that the implementation of the peel ply layer in the composite helped to create a rougher surface in which the coupons could attach to the ITTRI test fixture (that also has a rough surface). Most of the coupons presented complex failure morphologies (Figure 5.18).

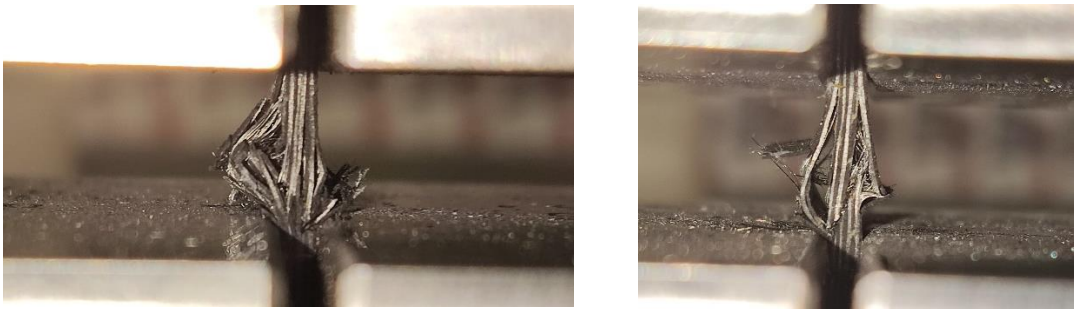

Figure 5.18. Failed compression coupons after testing

5.2.4. Interlaminar shear strength (ILSS)

Samples manufactured at 2 MPa and 8 MPa presented an improvement with respect to the base RTM values: 0.16% and 5.20% respectively. Only the sample manufactured at 5 MPa underperformed by -2.89%, although the differences between samples are minimal (Figure 5.19).

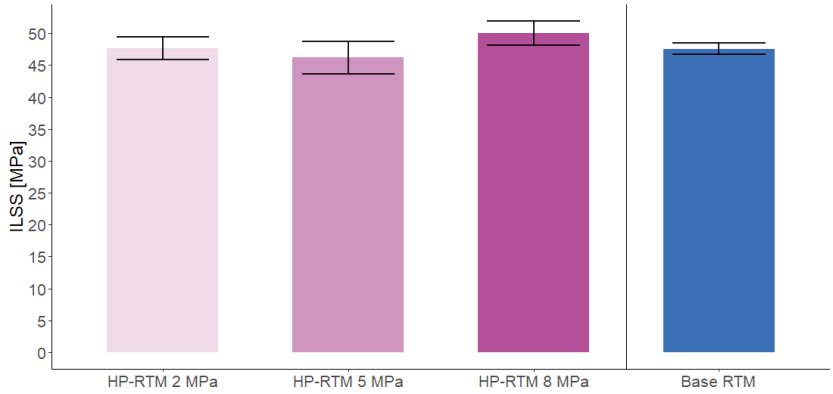

Figure 5.19. Comparative results in ILSS for the standard epoxy formulation injected at different pressures. All samples cured at 80° C

Samples manufactured at high temperatures also underperformed the baseline RTM values (-7.81% for 120° C and -5.89% for 140° C). Again, having a slightly better behavior on the low temperature sample (Figure 5.20).

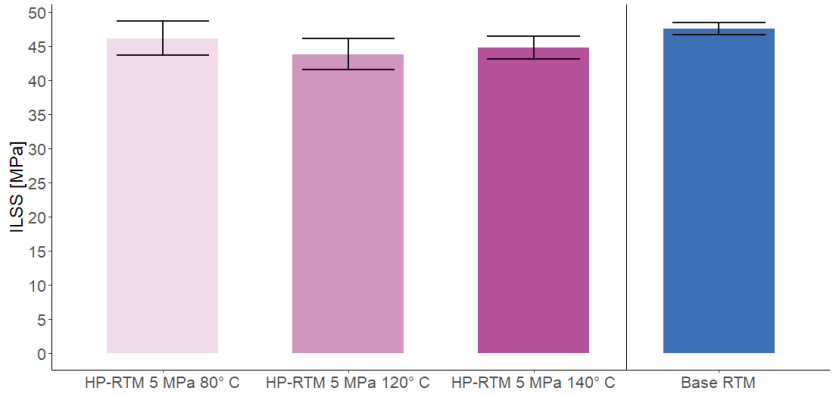

Figure 5.20. Comparative results in ILSS for the standard epoxy formulation injected at different temperatures. 5 MPa injection pressure.

Most of the ILSS samples presented non-acceptable failure modes as most of the coupons failed under “plasticity”, only a few coupons failed as expected (Figure 5.21).

a b

Figure 5.21. Examples of ILSS failures. a) Interlaminar shear failure. b) Plastic failure

5.2.5. Fiber, resin and porosity content

Fiber, resin and porosity content was measured only on the HP-RTM samples made with the standard Sicomin resin by evaluating only the effect of the injection pressure and comparing the results with the RTM baseline sample. Table 5.5 summarizes the most relevant results.

Table 5.5. Fiber mass, fiber volume and porosity content for base RTM sample and HP-RTM samples manufactured at different injection pressures (constant curing temperature)

Sample	Fiber mass Content [%]	Fiber volume Content [%]	Porosity Content [%]
Base RTM	66.30 ± 0.79	57.67 ± 0.74	4.22 ± 0.28
HP-RTM 2 MPa	67.28 ± 0.20	58.77 ± 0.15	4.26 ± 0.14
HP-RTM 5 MPa	65.63 ± 0.79	57.17 ± 0.85	3.78 ± 0.10
HP-RTM 8 MPa	64.02 ± 0.53	55.44 ± 0.67	3.60 ± 0.11

The intended fiber volumetric fraction for the HP-RTM samples was 58%, as a function of the fabrics aerial weight, the number of layers and the nominal thickness. Most of the samples reach that value with some deviations: 0.56% for the base RTM sample, 1.34% for HP-RTM at 2 MPa, 1.43% for HP-RTM at 5 MPa, and 4.42%for the HP-RTM sample at 8 MPa. The porosity content of the 2 MPa sample is quite similar to the base RTM, having a difference of 0.95%. But there is an improvement on the 5 MPa and the 8 MPa samples, having a reduction of 10.43% and 14.69% respectively.

Table 5.6 summarizes the mechanical properties of the composite's samples manufactured with the HP-RTM process.

Table 5.6. Summary of the mechanical properties for the HP-RTM composites. Injection pressure and temperature as study parameters

Pressure [MPa]	Temperature [C]	Flexural strength [MPa]	Compression Strength [MPa]	ILSS [MPa]
2	80	880.34 ± 105.58	549.16 ± 62.51	47.66 ± 1.81
5		1009.19 ± 77.85	596.16 ± 38.87	46.21 ± 2.54
8		1009.69 ± 36.10	618.88 ± 78.12	50.06 ± 1.88
5	120	922.35 ± 154.01	563.35 ± 77.41	43.87 ± 2.28
	140	938.07 ± 18.28	575.31 ± 31.18	44.79 ± 1.67

5.3. Process monitoring and cycle optimization

5.3.1. Filling time and cavity pressure monitoring

We measured the injection time for the mold cavity under RTM and HP-RTM processes. In this case we consider that standard RTM is implemented by doing the injection at low pressure, usually to allow good fibers impregnation, and then could be implemented a post-filling step, increasing the injection pressure once the mold cavity is full [151]. In the case of HP-RTM, the injection pressure is maintained until the mold cavity is full and pressurized, forcing the resin to impregnate the preform fibers. In comparison with the base RTM process, filling times in the HP-RTM process were highly reduced: 73.88% at 2 MPa, 79.33% at 5 MPa and 88.89% at 8 MPa (Table 5.7).

Table 5.7. Comparison of the filling time depending on the injection pressure. Time recorded manually

Process	Injection pressure [MPa]	Filling time [seg]
RTM	0.1	180
HP-RTM	2	47
	5	37.2
	8	20

We did not measure the injection pressure of the base RTM process as the injection time was close to the total measurement time (10 minutes). In this case the measurement data would be highly influenced by the sensors drift.

The following figures display the pressure inside the mold cavity under the different injection pressures (2 MPa, 5 MPa and 8 MPa). In the 2 MPa injection (Figure 5.22), the maximum pressure was reached at 46.21 seconds, which happens to be the measured time for injection. We could see that after the injection stops, there is rapid drop on the cavity pressure followed by a slow decrease of the internal pressure. There is also a delay of 0.14 seconds between the mold inlet and outlet.

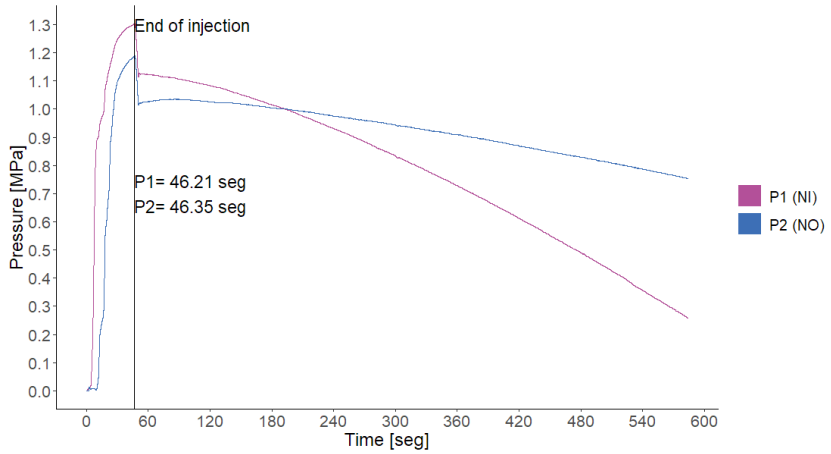

Figure 5.22. Internal cavity pressure of the HP-RTM mold under 2 MPa injection. P1 (NI) “near inlet”, and P2 (NO) “near outlet”. Injection temperature fixed at 80° C.

Maximum pressures recorded at the mold inlet and outlet were 1.31 MPa and 1.19 MPa respectively, having a difference of 0.11 MPa in the total impregnation distance (88 mm). Comparing the values with the machine pressure (2 MPa), at the inlet we only have 65.67% of the total pressure, and 59.95% at the outlet.

Injection at 5 MPa (Figure 5.23) reached the maximum pressure at 30.03 seconds with a delay of 0.16 seconds between the inlet and outlet. Maximum pressures inside the mold cavity were 2.95 MPa for inlet and 2.91 MPa at the outlet, with a difference with the machine pressure of 58.92% and 58.22% respectively. In this case, the pressure drop after the injection is not as pronounced as in the 2 MPa injection, but the drop tendency is similar in the measured time.

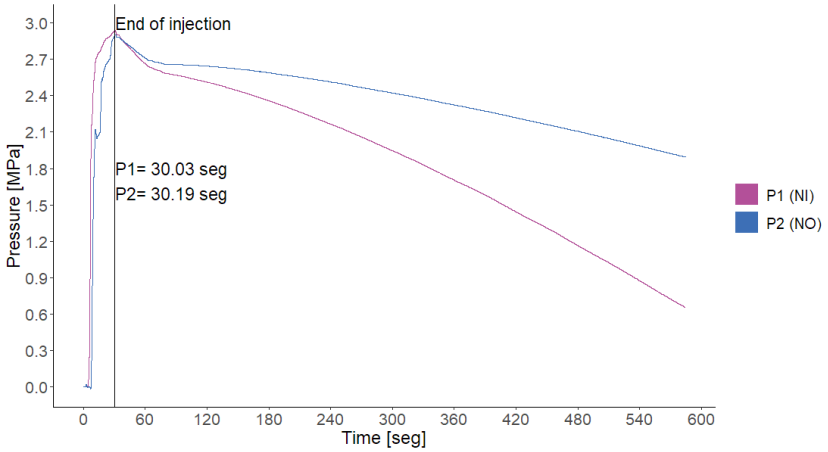

Figure 5.23. Internal cavity pressure of the HP-RTM mold under 5 MPa injection. P1 (NI) “near inlet”, and P2 (NO) “near outlet”. Injection temperature fixed at 80° C.

For the 8 MPa injection (Figure 5.24), the sensor at the outlet appeared to reach its maximum pressure before the inlet sensor: 16.05 seconds and 16.76 seconds respectively. At this point, it was not possible to reach further cavity pressure as the machine reached the maximum pressure at the injection line (8 MPa). After the injection, the cavity pressure presents a slight rise maintained during the curing process. Pressure values for the injection cavity were 4.5 MPa at the inlet and 4.47 MPa at the outlet, being 56.26% and 55.85% respectively of the injection line pressure (8 MPa).

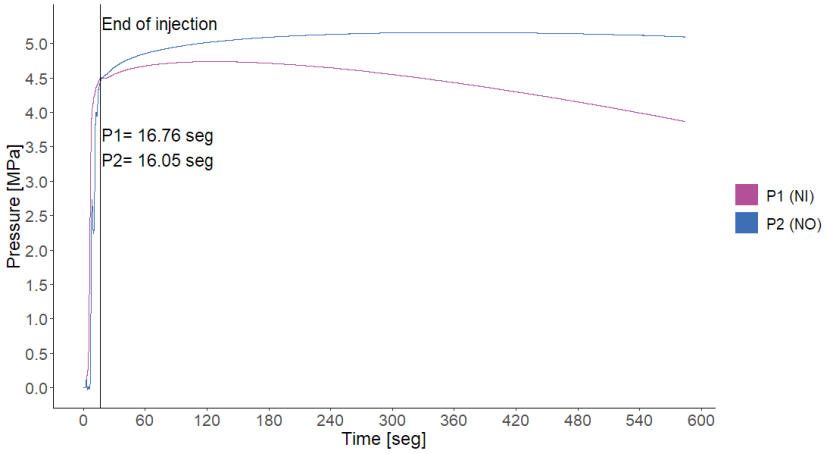

Figure 5.24. Internal cavity pressure of the HP-RTM mold under 8 MPa injection. P1 (NI) “near inlet”, and P2 (NO) “near outlet”. Injection temperature fixed at 80° C.

It must be considered that in these injections, the curing temperature was fixed at 80° C with a slow curing rate, so the pressure changes after the injection must be caused by the mold structure responding to the pressure stresses, rather than curing shrinkage. The behavior of the internal pressure of the mold cavity was different in the high temperature injections, both 120° C and 140° C injections were carried out at an injection pressure of 5 MPa. In both cases we recorded a rapid drop in the mold cavity pressure.

In the injection carried at 120° C (Figure 5.25), filling time was 15.5 seconds at the inlet and 15.6 seconds at the outlet, which is faster that the injection carried at 80° C (30 seconds). Rather than a viscosity effect, we believed that this injection time resulted from a wrong configuration of the machine set-up, despite the machine pressure was fixed at 5 MPa. In this measurement, internal cavity pressure was lost between 120 and 180 seconds after the injection. We had to treat the

sensor raw data as beyond this point, pressure started to become negative which is physically impossible.

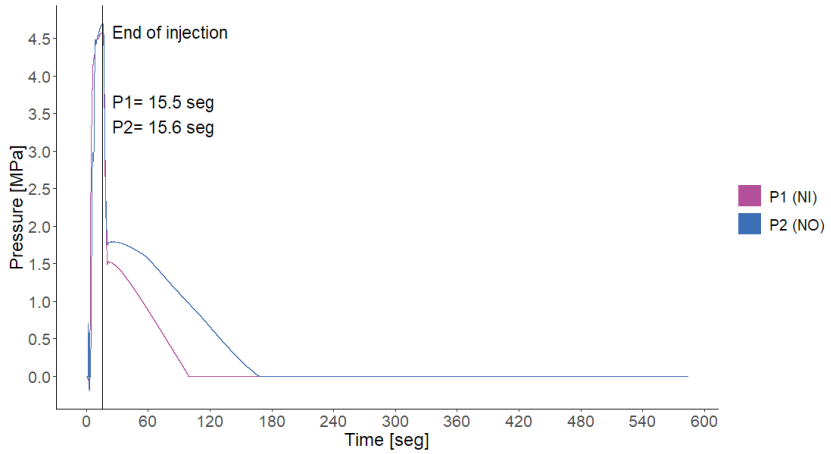

Figure 5.25. Internal cavity pressure of the HP-RTM mold under 5 MPa injection. P1 (NI) “near inlet”, and P2 (NO) “near outlet”. Injection temperature fixed at 120° C.

The injection at 140° C (Figure 5.26) was longer than in the other cases. In this injection we were not able to see a clear indication of the moment when the mold cavity was completely pressurized. (In the other injections there was a point in which the machine was not able to inject more resin as the mold cavity was completely full and pressurized). After curing and opening the mold, we could not see any indication of resin leaks or any mold-related issue. Similarly, to the 120° C, after the injection, there is a rapid drop in the internal cavity pressure.

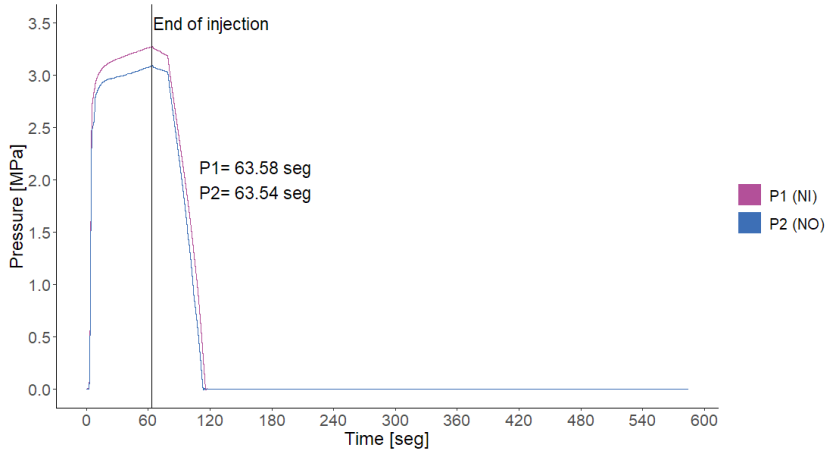

Figure 5.26. Internal cavity pressure of the HP-RTM mold under 5 MPa injection. P1 (NI) “near inlet”, and P2 (NO) “near outlet”. Injection temperature fixed at 140° C.

One possible explanation is that the machine axial pistons use hydraulic O-rings to seal and pressurize the resin inside the tanks. These O-rings suffered from constant wearing and degradation by temperature, in some cases we found remains of the O-ring materials inside the tanks, possibly creating leak points between the pistons and the tank wall, loosing pressure in the process. We changed the pistons O-Rings frequently to prevent further issues.

5.3.2. Monitoring of curing time

Ion viscosity and loss factor were measured in all the injections near to the resin inlet and vacuum ports (outlet) in order to see if there was a difference between these spots. End of reaction was obtained from the ion viscosity data and the end of cure was obtained by the loss factor data.

DEA curing data from the baseline RTM injection is displayed in Figure 5.27. The DEA measurement started when the mold was being heated from room temperature in order to measure the total heating time that this mold requires to reach the injection temperature and heating slope. Heating started 3.6 minutes after the measure was set on at 15.4 °C of room temperature, and reached 80° C after 61.1 minutes, having a heating slope of 1.06° C/min. DEA curing data was measured at 126 minutes, when the mold had a stable curing temperature. Minimum viscosity points for this injection were reached at 39.2 minutes at the resin inlet, and 40.3 minutes at the resin outlet. End of reaction was reached at 87.4 minutes at the resin inlet and 84.9 minutes at the resin outlet. End of curing could be considered at 103.1 minutes and 112.7 minutes at the resin inlet and outlet respectively, representing a reduction up to 57.04%, considering that this resin formulation (Sicomin) is meant to be cured at 80° C for 4 hours. This data is presented having in consideration that it is only valid for this specific curing thickness and fiber volumetric fraction, other types of fabric or thicknesses may have another DEA behavior.

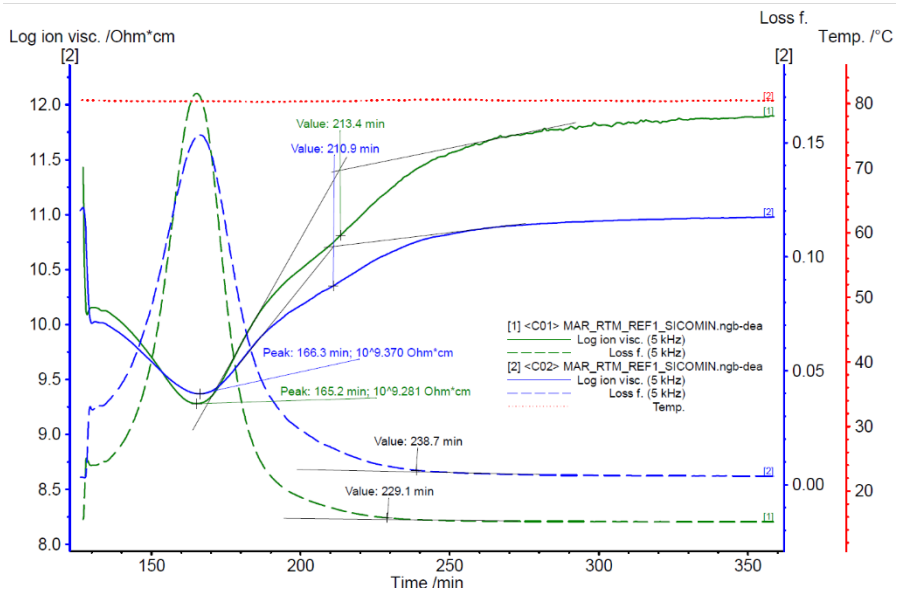

Figure 5.27. DEA curing analysis for the base RTM injection (0.1 MPa injection + 0.6 MPa post filling compaction) carried out at 80° C using the Sicomin resin. [1] refers to the sensor located near to the inlet (NI), and [2] the sensor located near to the outlet (NO).

Figure 5.28 describes the curing behavior for the sample injected at 2 MPa and cured at 80° C. At this temperature we could see that the resin reached it minimum viscosity value at 47.7 minutes near the inlet and 43.1 minutes near the outlet. This could make sense as the resin located at near the outlet point spent more time inside the mold cavity, as the resin near the inlet was injected towards the end of the injection. Although we can validate this behavior, the time difference between the two points is big considering that this injection took 47 seconds to fill the mold cavity.

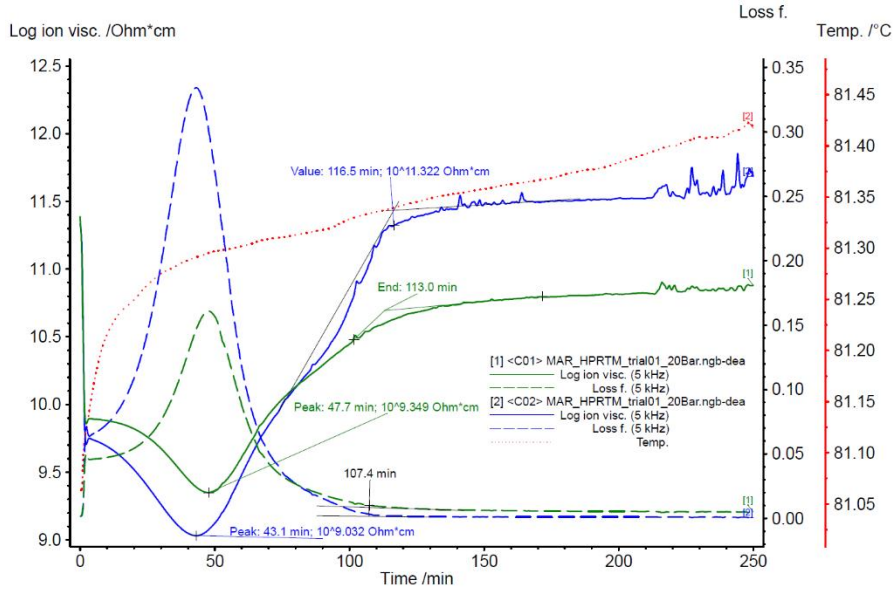

Figure 5.28. DEA curing analysis for the 2 MPa injection carried out at 80° C. [1] refers to the sensor located near to the inlet (NI), and [2] the sensor located near to the outlet (NO)

End of reaction was reached at 113 minutes near the inlet and 116.5 near the outlet. By analyzing the loss factor, both sensors display an end of the cure near to 107 minutes, which is more or less at the end of the reaction. Considering that this resin formulation (Sicomin) is meant to be cured at 80° C for 4 hours (datasheet information), using the DEA sensors allow us to have a reduction in the curing time about 55.25%. We can highlight that there is a slight reduction on the resin temperature at the beginning of the injection, considering that the injection temperature was set to be 60° C.

Under 5 MPa (Figure 5.29) there are no significant changes at the lowest viscosity points (45.1 and 43.4 minutes for near the injection and near the outlet respectively). Although one of the end of reaction points happens to be earlier (87.8 minutes at the inlet), the other sensor gives a time value closer to the 2 MPa injection (111 minutes). End of curing could be considered at 111.8 minutes for the sensor located near to the inlet, and 92.9 minutes for the sensor near to the outlet, giving a cure time reduction of 53.42% and 61.29% respectively.

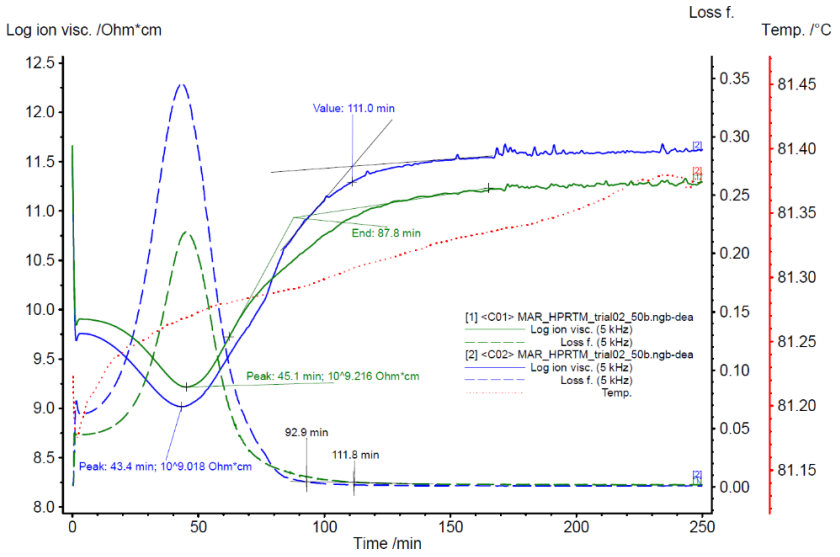

Figure 5.29. DEA curing analysis for the 5 MPa injection carried out at 80° C. [1] refers to the sensor located near to the inlet (NI), and [2] the sensor located near to the outlet (NO)

Figure 5.30 describe the DEA analysis for the sample injected at 8 MPa at 80° C. During the DEA monitoring we observed that the DEA data from the sensor number 1 (near inlet) was displaying an abrupt change in the ion viscosity near 60 minutes after the injection. At first we believed that it could be related to the injection pressure as has been reported before [26], but it made no sense as the reactivity slope was almost vertical, meaning an instant curing. By closer inspection after demolding, we detected that it was generated a porosity defect in this particular point, changing in this way the dielectric readings in the sensor. Sample quality for this injection was good compared with the others, in the ultrasonic inspection (Figure 5.11 c) we did not detect particular indications near to the sensor area (Figure 5.31), so we considered this as a superficial defect and we did not take this sensor data for curing analysis.

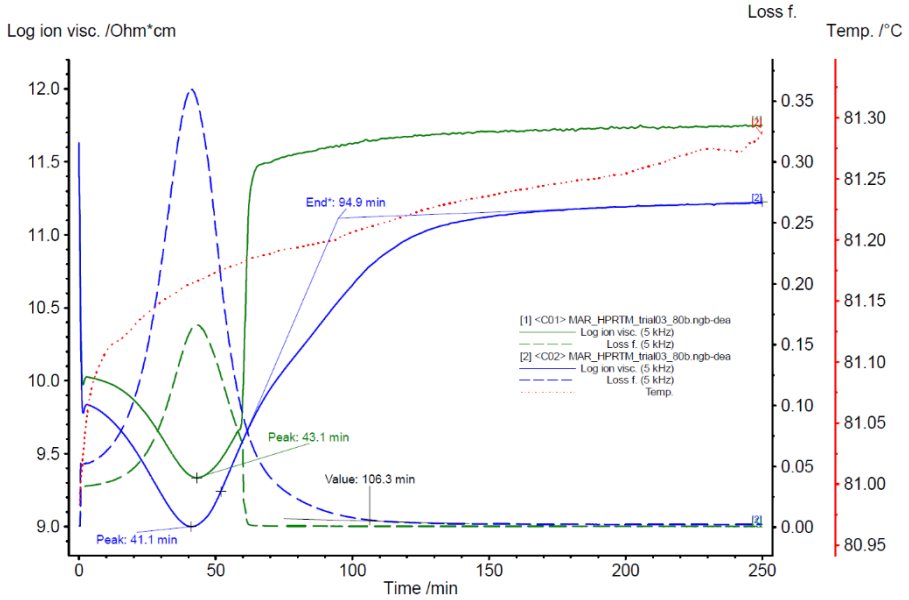

Figure 5.30. DEA curing analysis for the 8 MPa injection carried out at 80° C. [1] refers to the sensor located near to the inlet (NI), and [2] the sensor located near to the outlet (NO)

Figure 5.31. Superficial defect found at the sample injected at 8 MPa and 80° C. Close up to the local defect at the sensor location

In this injection, resin reached its minimum viscosity value at 41.1 minutes, the end of reaction is set at 94.9 minutes and the end of curing could be considered at 106.3 minutes, having a reduction of 55.7% in the total curing time.

Considering that the injections with the pressure parameter were cured under the same temperature and time, we can summarize the DEA analysis as follows (Table 5.8):

Table 5.8. Summary of the curing parameters for the HP-RTM samples manufactured at 80° C varying the injection pressure and compared with the base RTM sample. Data obtained from the DEA sensors

Pressure [MPa]	Time for minimum viscosity [min]		End of reaction [min]		End of curing [min]	
	Inlet	Outlet	Inlet	Outlet	Inlet	Outlet
Base RTM (0.1 + 0.6)	39.2	40.3	87.4	84.9	103.1	112.7
2	47.7	43.1	113	116.5	107.4	
5	45.1	43.4	87.8	111	111.8	92.9
8	43.1	41.1	-	94.9	-	106.3

In the high temperature injections, sample injected at 120° C (Figure 5.32) was left 120 minutes in order to guarantee full curing as the resin data sheet did not present information about curing time at this temperature. The sensor located near the resin outlet did not provide curing information, so we analyzed only the data from the inlet sensor. At this temperature, resin reached its minimum viscosity at 5.5 minutes and the end of reaction is measured at 9.1 minutes. End of curing was set to 15.8 minutes, having a reduction of 93.42% with respect to the baseline curing cycle.

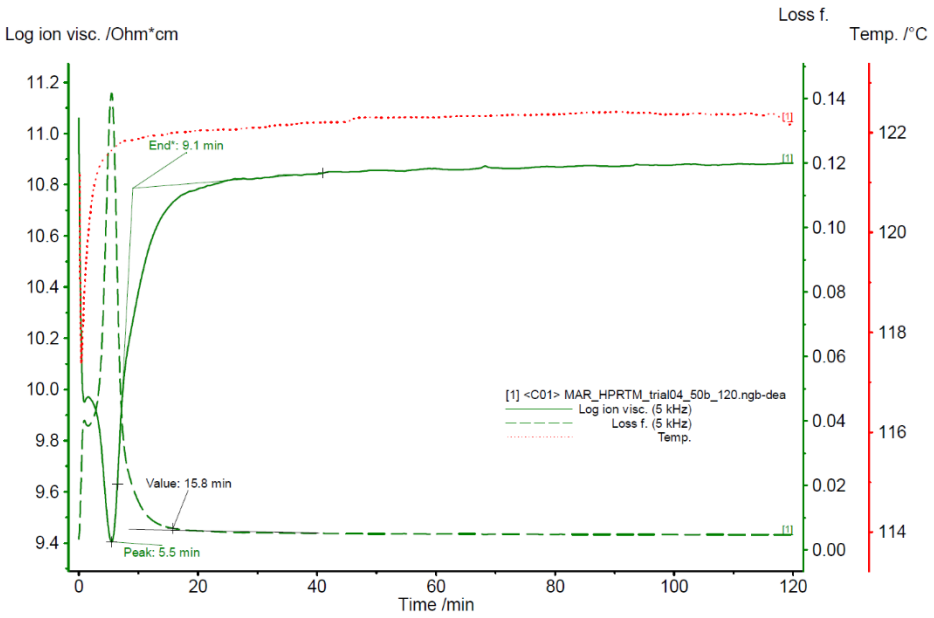

Figure 5.32. DEA curing analysis for the 5 MPa injection carried out at 120° C. [1] refers to the sensor located near to the inlet (NI).

For the 140° C injection (Figure 5.33) we also had issues with the sensor located at the resin outlet. Minimum viscosity point was reached at 3 minutes after the injection started, and the end of reaction was set to 3.8 minutes. End of curing could be measured near to 7 minutes, representing a reduction of 97.08 minutes from the baseline curing cycle, and being in this case the shortest cycle time. We observed a slight temperature peak (about 2° C) at the minimum viscosity point, possible related to the exothermic reaction of the curing process for this resin.

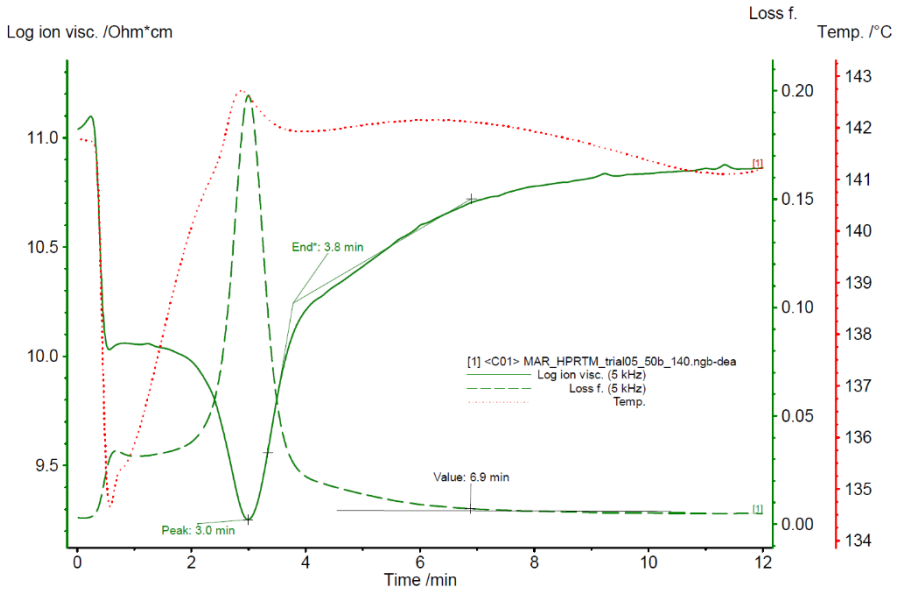

Figure 5.33. DEA curing analysis for the 5 MPa injection carried out at 140° C. [1] refers to the sensor located near to the inlet (NI).

Table 5.9 summarizes the DEA analysis for the HP-RTM samples (5 MPa) cured at 120° C and 140° C, compared with the baseline RTM sample cured at 80° C, and the HP-RTM (5 MPa) also cured at 80° C.

Table 5.9. Summary of the curing parameters for the HP-RTM samples manufactured at 5 MPa varying the injection temperature and compared with the base RTM sample and the HP-RTM sample cured at 80° C (also at 5 MPa). Data obtained from the DEA sensors

Injection temperature [C]	**Time for minimum viscosity [min]**		**End of reaction [min]**		**End of curing [min]**	
	Inlet	Outlet	Inlet	Outlet	Inlet	Outlet
Baseline RTM (80)	39.2	40.3	87.4	84.9	103.1	112.7
HP-RTM (80)	45.1	43.4	87.8	111	111.8	92.9
HP-RTM 120	5.5	-	9.1	-	15.8	-
HP-RTM 140	3	-	3.8	-	6.9	-

5.3.3. Process optimization

Considering the filling time and curing time at the different process parameters, injection and curing times can be summarized as follows:

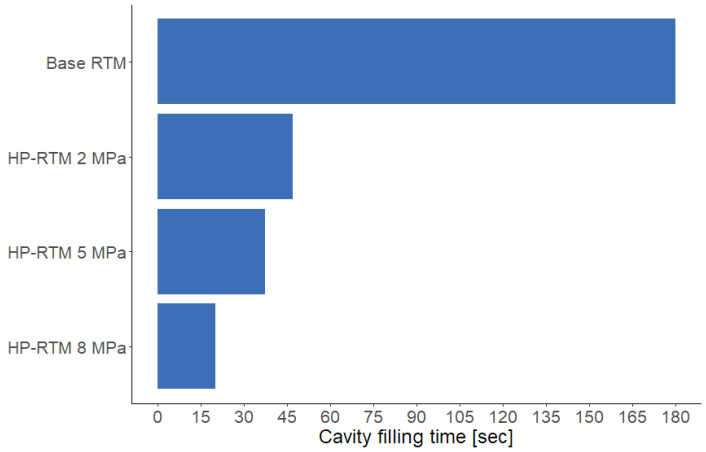

Figure 5.34. Mold cavity filling time for the base RTM sample and the HP-RTM samples under constant temperature (80° C)

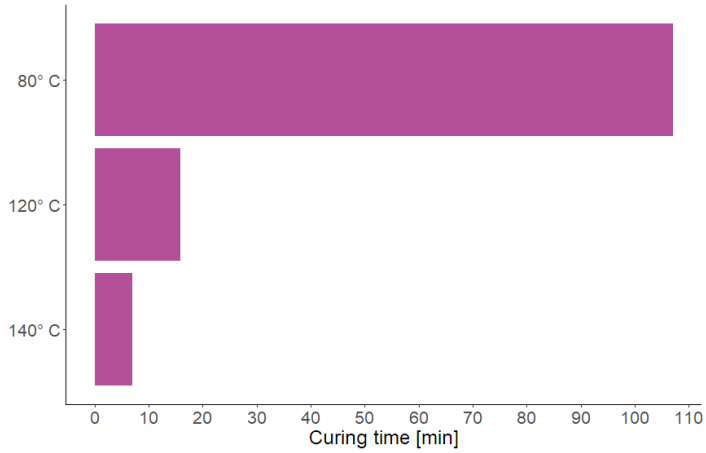

Figure 5.35. Curing time for the high-reactivity resin (Sicomin) under constant pressure (5 MPa)

Samples manufactured at high pressures presented important improvements in the mold filling time, up to 20 seconds (Figure 5.34). But the cycle time was dominated by the resin curing time (Figure 5.35). Combining the injection at the highest pressure with a curing temperature of 140° C will reduce further the total process cycle (around 7 minutes for this resin formulation). Considering the filling time for the base RTM (3 minutes) and the curing time at low temperature (around 107 minutes), we can have a process cycle reduction up to 93.64%.

5.4. Discussion on HP-RTM composites performance

Flexural properties as function of the injection pressure presented an overall improvement over the conventional RTM process, in this case having the best properties at the maximum injection value (8 MPa). The improvement of the mechanical properties by increasing the injection pressure relies on the reduction of the material internal porosity, something that was explained by M. Bodaghi et al. [25] or R. S. Davé [54], and by the studies of R. Chaudhari [7] as they proved that materials with less void content have better flexural and shear strengths. The injection pressure creates compaction forces over the voids inside the laminate, reducing the their size and thus, their overall void content [36], [214].

By analyzing the injection pressures used in this study. Improvements of the flexural strength of the 8 MPa injection were not that important from the 5 MPa injection. While there was a notable difference between the 2 MPa injection pressure to the 5 MPa. Suggesting that there is a point in the process in which it would not be possible to have further improvements. This was discussed by I. Swentek et al. [40] as they mentioned that the increase of the internal pressure leads to a reduction of the fiber volumetric fraction (possibly due to deformations in the mold cavity), and consequently, to the mechanical properties. We also must consider if the increment of the injection pressure creates local deformation of the reinforcement fibers. Thickness measurements from the HP-RTM samples (Figure 5.2) showed that at 8 MPa, there is a slight increase on the local thickness about 0.08 mm at least in the center area (near to the injection gate), which represents a change of the theoretical volumetric fraction from 59.43% to 57.09%, corroborated by the fiber and resin content test. In counterpart, compression strength was not affected by this difference as the samples manufactured at 8 MPa presented an improvement from the 5 MPa samples. Compression test with an injection pressure beyond 8 MPa would be necessary in order to stablish a maximum improvement point.

The evaluation of the glass transition temperature proved that the materials injected and cured at higher temperatures presented higher T_g (up to 26.42%) which led to an increase of the flexural strength (up to 7.02% at 140° C) due to a higher polymer crosslinking density [215]–[217]. Also having benefits on the total curing time, with a reduction of more than 96%. We found that comparing the samples under the different curing temperatures, the flexural strength slightly lowers as the T_g increases, this could be an indication of brittleness as the polymer with higher T_g present a stiffer behavior, reducing its fracture toughness [217]. Other epoxy resin from Sicomin, as the one used in this study [218], presented the mechanical characterization of the net resin under different curing temperatures (40° C, 60° C and 80° C). The higher curing temperature presents a higher T_g (13.41%), but lower flexural modulus (-14.98) and flexural strength (-7.33%), like in our case.

The effect of the injection pressure and temperature on the shear properties was not clear. The variations in the mechanical properties compared with the base RTM were very low (5.2% max) without a clear tendency, as the 2 MPa and 8 MPa presented a mechanical improvement, while the 5 MPa presented a slight detriment on the material performance.

Moreover, the high temperature samples presented slightly less performance than the RTM baseline sample. We believe that rather than a material or process influence, the final performance of the ILSS samples was influenced by the test setup itself. Just a few samples presented acceptable failure modes, as most of the coupons presented a pseudo-plastic failure. For the HP-RTM samples, we performed the ILSS test out of standard conditions: loading element radius of 3 mm, instead of 5 mm, and support element radius of 3 mm, instead of 2 mm. A. Nishimura et al. [219] studied the effect of the loading and support radius on the ILSS test performance for a GFRP (under ASTM D2344 standard [220], samples of 15 mm x 10 mm x 2.5 mm), the fracture behavior and the shear strength tend to change depending of the load and support radius. Larger support radius and smaller loading radius (as our case, comparing with the standard recommended dimensions) tend to create translaminar shear fractures focused on the loading element area (high stresses) and presenting early failure. Also, this fracture mode tends to create non-linear responses in the ILSS sample, visible as a curvature tendency in the load graph. Failed samples under this fracture mode presented triangular shapes. Varying the loading and support radius also creates bending on the tested samples, evidenced by the test curve behavior (Figure 5.36, Figure 5.37).

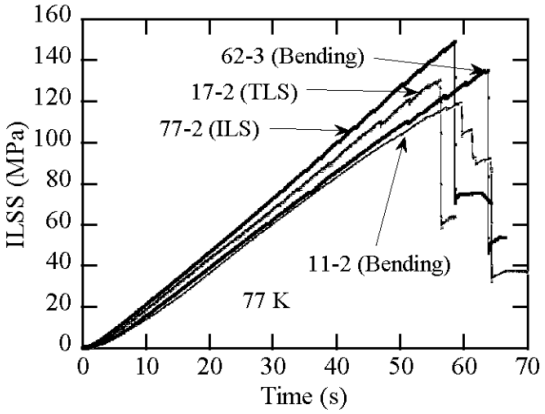

Figure 5.36. Examples of ILSS test curves depending on the loading and support radius. 11-2 curve gives the case of bending fracture in smaller radius. 17-2 curve is an example of translaminar failure, and 77-2 curve of an interlaminar shear failure. [219]

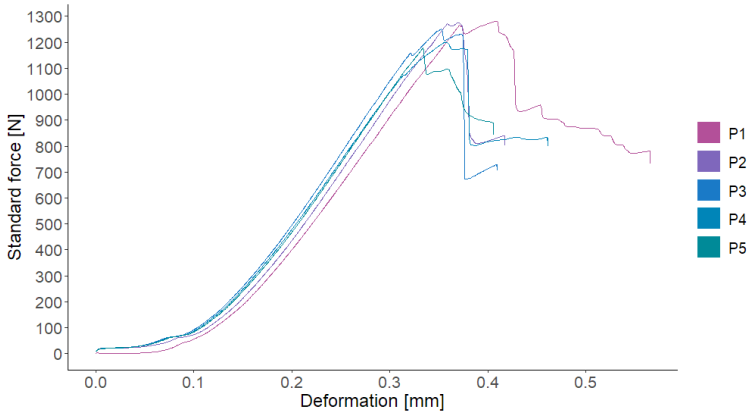

Figure 5.37. Example of the ILSS test for the 2 MPa HP-RTM injection. Detail of failure mode of each tested coupon

There is not a big difference between the base RTM sample and the low and medium HP-RTM samples, but it is interesting that the sample manufactured at higher pressure presented less fiber volume. As mentioned before, rising the injection pressure could create gaps or separation between the mold surfaces, lowering the FVF [40]. Particularly, samples for this test were extracted from points near to the distribution channel in the inlet point, being located at the high-pressure zone of the mold cavity, as was detected with the FEM simulations, being thicker than other zones. Something that was corroborated with the dimensional analysis of the samples extracted from the mold (Figure 5.2) and by individual measurements of the coupons used in the test.

It could be possible that this thickness difference had some interference over the mechanical response of the materials, especially with the samples manufactured at 8 MPa, having less fiber content. Something that has been reported by other authors, where the FVF has a direct impact on the modulus of elasticity, yield stress, composite failure mode, ultimate strength and to specific properties as tensile of flexural strength [221]–[224].

We also detected a tendency in the samples porosity content as a function of the injection pressure, where it decreases as the pressure rises, thanks to the compaction forces of the injection pressure [36]. Megdikhani et al. [214] reported that the void content has some influence over the mechanical properties of FRP, specially on matrix dominated properties such as compression or ILSS. The latter presenting variations between 5% and 10% with void content

variations of 1% for UD ply and woven FRP, voids in compression facilitate instability failure modes, slightly affecting the compression strength by a 1% of void content, and under flexural strength, variations of 1% in the void content could affect the material up to 10%. Similar conclusions made X.Liu et al. [225]. In our study, we can conclude that the injection pressure helped to increase the mechanical performance of the samples by the reduction of the composite's internal porosity content, especially in the compression strength being a matrix dominated property, flexural strength was also improved by this effect.

M. Bodaghi et al [36] reported void content for HP-IRTM being less than 2% at 2 MPa, which is far less than our outcome. We can consider possible causes as the degassing time of the resin (10 minutes in our case), air entrapment during injection or deviations from the determination of the resin and fiber density prior the porosity content test.

The use of the cavity pressure sensors and DEA sensors was a key factor on the HP-RTM process monitoring. Our mold cavity was relatively small, but the use of the pressure sensors gave us an idea of the filling tendency by evaluating the time delays between the maximum pressure points. In larger or more complex mold cavities, it would be useful to place different pressure sensors between the inlet and outlet ports of the mold, and across the cavity width, as made by the previous studies in the Fraunhofer institute [7], [27], [32], [41]. Pressure sensors could give information about the advance of the resin frontline, also giving information if there are risk of race tracking zones or dry zones by comparing the local cavity pressure in different points, as well, giving an idea of the sample curing by the pressure behavior inside the mold cavity [226]. An example in our case was the evidence of injection issues at the 140° C injection, as it did not reach the maximum pressure at the expected time.

We also evidenced pressure release after injection, especially at the 2 MPa and 5 MPa, as the cavity pressure slowly reduced in the 10 minutes after the injection stopped. In this case, we can discard resin shrinkage effects as the DEA sensors proved that curing started around 40 minutes after injection (curing at 80° C), and the 8 MPa injection retain most of the cavity pressure after the injection. We believed that this behavior was influenced by the mold structure itself as it relaxes and distribute the pressure forces after finishing the injection, especially at the lower pressure values (2 – 5 MPa). The pressure inside the mold cavity were lower than the net injection pressure (≈ 55% – 65%), possible because of the effects of pressure distribution inside the mold cavity. Similar differences on the cavity pressure was found by R. Chaudhari et al. [7] in their process.

In the high temperature trials, we detected a fast drop on the cavity pressure after the injection. Curing data from the DEA sensors revealed that at 120° C, the resin started to cure after 5.5 minutes, and 3 minutes at 140° C. The pressure sensors detected almost a complete loss of the cavity pressure at 3 minutes (120° c curing) and 1 minute (140° C). Comparing with the pressure profile of the 80° C cured sample at the same injection pressure, this could be attributed to the resin shrinkage as it is reported that this effect can cause volumetric contractions up to 6% [227].

Apart from cycle time, piezoelectric sensors also have sensibility to temperature, being another cause of drift. [179]–[181], [228]. In this case we made some sensor runs prior the injection while the mold was being heated until reaching a stable temperature and the 15 seconds recorded prior the injection already had the influence of the injection temperature. So, it is possible that during the injection measurements the sensors also had drift influence by the injection temperature. Although the sensors manufacturer guarantees that this kind of sensors could work under high-temperature environments [177], [229]. In overall, these sensors have the

advantage of being small enough to fit into any mold cavity without affecting the mold structure considerably and its operation is relatively simple, despite of the signal corrections due to drift.

The increase of the injection pressure had the most impact on the injection time, as from conventional RTM, we had an injection time of 3 minutes that was reduced to only 20 seconds (≈89%) at the highest injection pressure in the HP-RTM samples. Filling time is very important when using high-reactivity formulations as the ultrasonic inspections of the high-temperature plates (Figure 5.12) presented evidence of dry spots/high-porosity areas near the vacuum ports, indicating a possible premature curing before filling all the mold cavity. A possible cause is insufficient pressure.

The use of the DEA cure monitoring sensors gave us information about the resin arrival and impregnation, minimum viscosity points, start of curing and the end of curing from the resin inside the mold cavity. By analyzing the DEA data from the HP-RTM samples manufactured at different temperatures, we observed that there are differences between the DEA data at the resin inlet and outlet ports (2 – 4 minutes), usually starting first at the outlet port as the resin located near these ports have been inside the mold cavity longer that the resin near the inlet port as being the last to be injected inside the mold cavity.

In the state-of-the-art chapter, we discussed that the injection pressure has an impact of the curing time [26], [61] of the resin by incrementing the reaction rate, but in this study we did not detected a clear indication of this behavior (Table 5.9). The end of curing data from the sensors has no significant fluctuations (about a maximum of 14 minutes between measurement at the three injection pressures). Moreover, the minimum viscosity points at the three injection pressures had only a difference of 5 minutes approximately, understanding the injection pressure as a non-dominant factor for the resin curing time, as was explained by J. Ramos et al. [62].

We must remark that this time reduction is related only to the injection and curing time. Other times as mold preparation before injection (≈ 120 minutes if demolding agents must be applied), mold opening and closing (≈ 20 minutes each considering that the mold is closed by bolts), preform manufacture (≈ 30 minutes), mold heating (≥ 60 minutes), sample demolding and mold cleaning (≈ 40 minutes) are not considered. So, automation of those process parameters is necessary to make the process reliable and profitable [5], [23], [43], [230].

Chapter 6: Results and discussion on the vitrimer composites processed by RTM and HP-RTM

As we mentioned in previous chapters, thermoset composite materials offer many advantages over traditional structural materials, but in counterpart, they present many challenges in order to be repaired and recycled.

The introduction of vitrimers offer new possibilities in the composite materials market by presenting mechanical performance as thermosets, while offer the possibilities to be reshaped. repaired and recycled. The H2020 project Airpoxy [127] was developed to introduce the advantages of vitrimers in the aeronautical industry, offering high-performance and sustainability.

In this chapter we present the characterization of the high-performance vitrimer composites, developed under the Airpoxy project, meant to be used as an alternative to structural thermosets, being processed by the RTM process.

Additionally, we explored the possibility to combine this vitrimer with a high-volume manufacturing method as HP-RTM to evaluate its possible advantages in the automotive industry.

6.1. Mechanical properties of vitrimer composites processed by RTM

6.1.1. Neat vitrimer properties

6.1.1.1. T_g

The T_g of the AIR-3R vitrimer obtained by DSC was 170°C ± 3°C, which is equal to the baseline requirement (3.3.2). The DSC showed that of current curing process (3.2.2) led to a degree of complete curing.

Moisture influence over the T_g was evaluated by Cidetec [31], having a mass gain of 2.3% after being conditioned at 70° C - 85% RH by 30 days until equilibrium. The measured T_g after this conditioning was 155° C, having a reduction of 8.8% of the pristine value.

6.1.1.2. Tensile strength

The AIR-3R net vitrimer resin presented better tensile modulus and tensile strength (Figure 6.1) compared with the net baseline properties, having an improvement of 15% and 10.71% respectively.

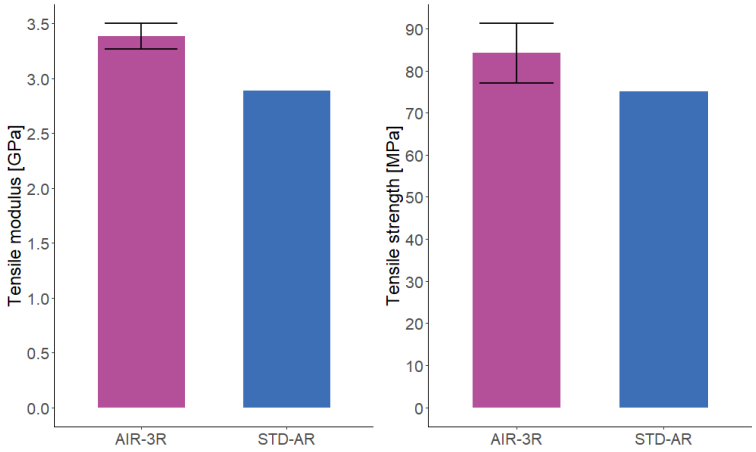

Figure 6.1. Tensile modulus and strength for the neat vitrimer and baseline reference

6.1.1.3. Flexural strength

The flexural modulus of the AIR-3R formulation was similar to the baseline, albeit the flexural strength was slightly lower, having a difference of -11.3%. Still having comparable mechanical behavior (Figure 6.2).

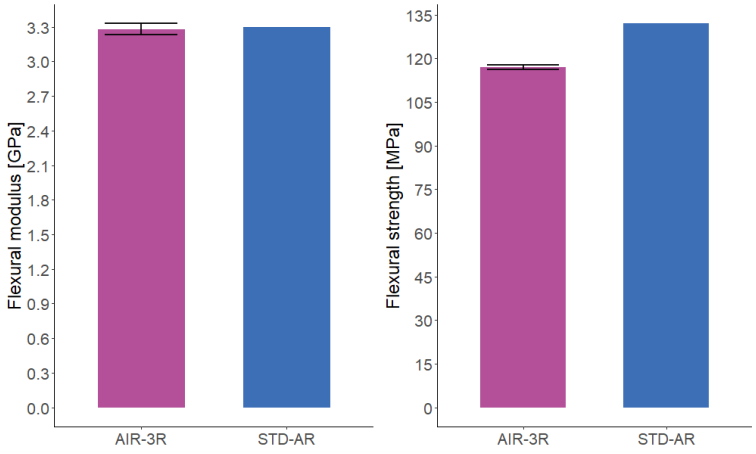

Figure 6.2. Flexural modulus and strength for the neat resin vitrimer and baseline reference

6.1.2. Mechanical properties of the carbon fiber reinforced vitrimer

The characterization performed in this section differs from the HP-RTM composites on section (6.2), and the characterization of vitrimers manufactured by the HP-RTM process on section 6.2. All the samples were manufactured by conventional RTM process using reinforcements from Chomarat: T800HB 6K 5HS satin woven fabric of 280 g/m^2, and the T800H 24K UD reinforcement of 284 g/m^2, both references having a custom-made PA stabilization veil (binder) of 8 g/m^2.

Composites samples were tested on RT condition, as well as the temperature-humidity conditions HW70 and HW120. Specific details of the materials and testing conditions were previously described in Chapter 2.

6.1.2.1. Tensile strength

Figure 6.3 and Figure 6.4 show a comparison of the modulus and tensile strength of the carbon composites studied under the different test conditions. For CP and UD 0° reinforcements, tensile modulus performed slightly better in the three different conditions than the aeronautic thermoset baseline: 8.7% and 1.3% at RT, 7% and 1.9% at HW70 and 6.6% and 11.9% at HW120, respectively. The same tendency is observed for tensile strength, with increments of 8.2% (CP) and 5.4% (UD 0°) for RT, and 1.8% (CP) and 5.8% (UD 0°) for HW70. In the highest temperature condition (HW120), AIR-3R performed slightly worst: -2.9% (CP) and -6.7% (UD 0°); this could be related on the moisture condition.

However, the UD 90° fabric's performance was different: the relative variation of the modulus was 4.7%, -7% and -28.2% for RT, HW70 and HW120, respectively. The tensile strength decreased by -31.1%, -54% and -60.3% for RT, HW70and HW120, respectively.

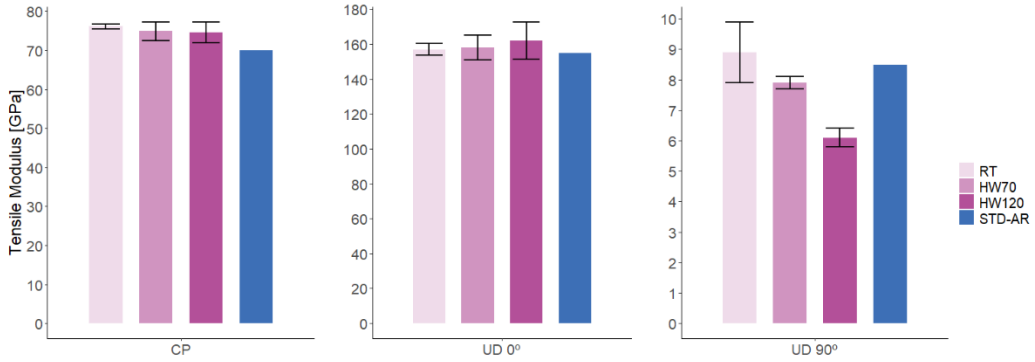

Figure 6.3. Comparative results in tensile modulus for AIR-3R vitrimer. CP and UD fabrics tested at the temperature-moisture conditions. STD-AR values are equivalent in the three different temperature conditions (as displayed in Table 2)

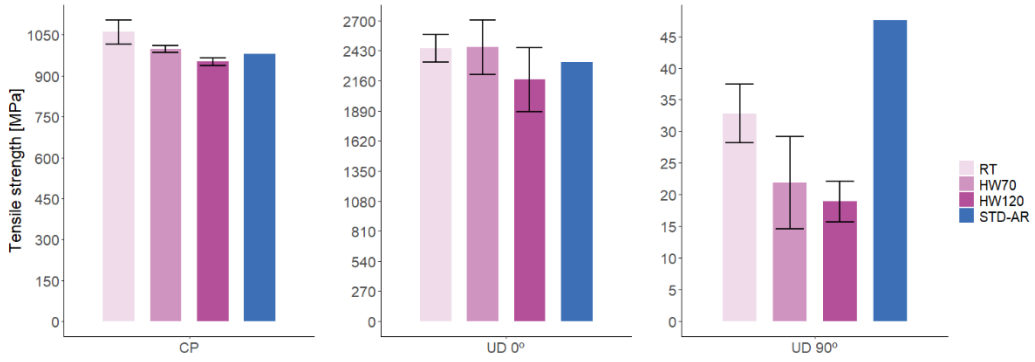

Figure 6.4. Comparative results in tensile strength for AIR-3R vitrimer. CP and UD fabrics tested at the temperature-moisture conditions.. STD-AR values are equivalent in the three different temperature conditions (as displayed in Table 2).

6.1.2.2. Compression strength

Compression test results presented a high variability, inherent to the test setup. About 50% of the samples tested had to be discarded because of invalid failure modes, having percent bending strain values (PBS) superior to 10% (Equation 5).

Compression modulus (Figure 6.5) of CP fabric composites with AIR-3R vitrimer was higher than the defined baseline by 8.8% in RT and HW70, and 11.9% HW120. For the UD 0° composite, the compression modulus was within 1% above the reference. In the UD 90° fabric, at RT, AIR-3R overpassed the thermoset formulation, but under temperature and humidity it presented a slightly inferior response, albeit still comparable with the thermoset counterpart: 22.2% in RT, -3.5% in HW70 and -5.9% in HW120.

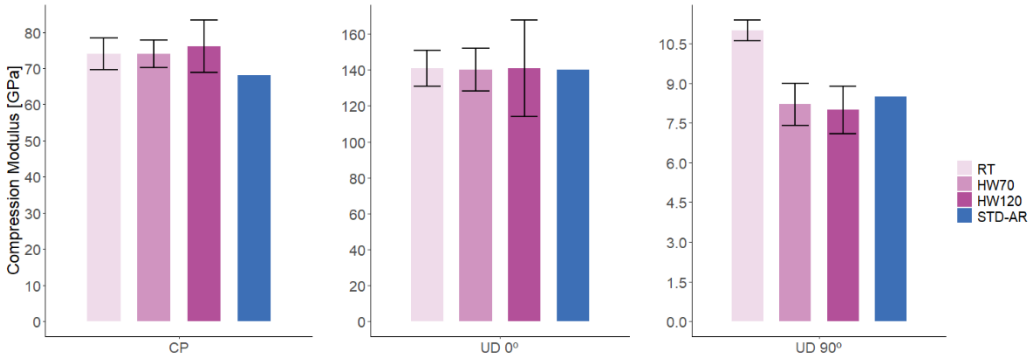

Figure 6.5. Comparative results in compression modulus for AIR-3R vitrimer. CP and UD fabrics tested at the temperature-moisture conditions. STD-AR values are equivalent in the three different temperature conditions (as displayed in Table 2)

Compression strength (Figure 6.6) of the vitrimer composites presented an abrupt drop in most of the conditions: -24.8% in RT, -26.3% in HW70 and -25.6% in HW120 for CP; -40.6% in RT, -44.9% in HW70 and -35.3% in HW120 for UD 0°; and -24.2% in RT, -39.3% in HW70, and -11.8% in HW120 for UD 90°.

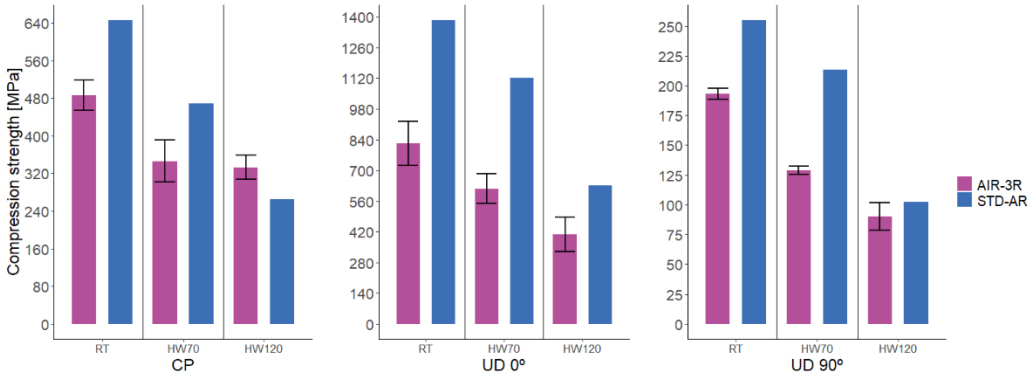

Figure 6.6. Comparative results in compression strength for AIR-3R vitrimer. CP and UD fabrics tested at the temperature-moisture conditions. Samples with the PA veil

Optical micrographies (Figure 6.7) of the AIR-3R sample revealed some gray-rounded areas appear between the fiber layers corresponding to the thermoplastic PA veil initially included in the CF fabrics. According to the manufacturer, this veil has a melting temperature close to 180° C that corresponds to the in-mold post curing temperature of the AIR-3R vitrimer formulation. In the first curing step (130 °C), the vitrimer starts to polymerize, embedding the

veil structure inside the laminate. Therefore, even if this veil later melts, it is trapped by the already frozen structure of the vitrimer matrix, possibly acting as a contaminant or stress concentrator.

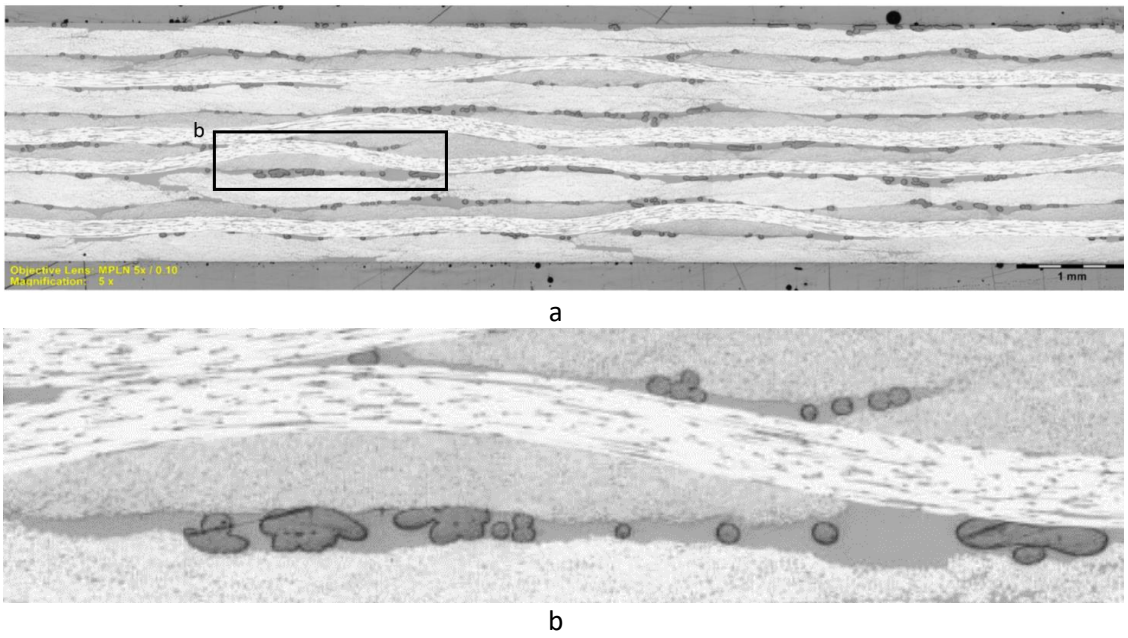

Figure 6.7. Micrographies of AIR-3R composite sample. a) panel cross-section. b) Detail of layers interface in the laminate. Objective lens MPLN 5X/0.10

6.1.2.3. Interlaminar shear strength (ILSS)

In all temperature conditions, the interlaminar shear strength of the AIR-3R vitrimer was comparable to the baseline (Figure 6.8). The CP fabric response was comparable to the baseline thermoset. Only at RT did it slightly underperform: -10% in RT, 7.1% in HW70 and 0% in HW120. For UD, shear performance was superior to the baseline, even reaching an outstanding performance at the higher temperature condition: 20% in RT, 40% in HW70 and 43.3% in HW120.

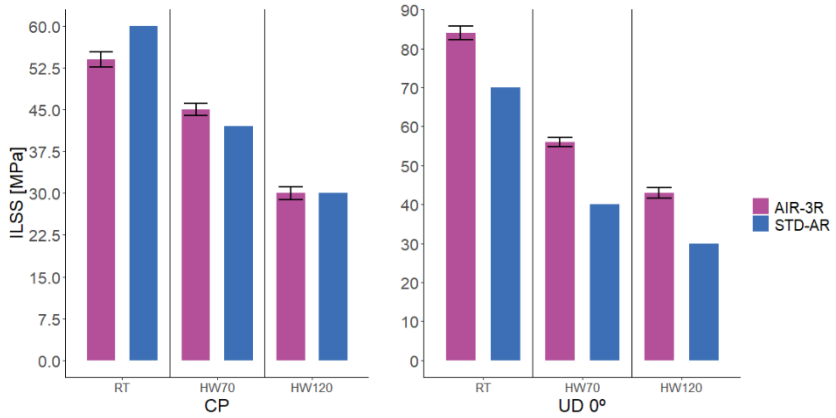

Figure 6.8. ILSS shear performance of the AIR-3R vitrimer. CP and UD fabrics tested at the temperature-moisture conditions.

6.1.2.4. In-Plane shear strength (IPS)

The IPS modulus for the vitrimer composite was generally better than the thermoset based composite in both CP and UD, particularly in high temperature conditions (Figure 6.9): -2.2% in RT, 5.5% in HW70 and 17.4% in HW120 for CP fabric, and 2.3% in RT, 8.6% in HW70 and 22.7% in HW120 for UD.

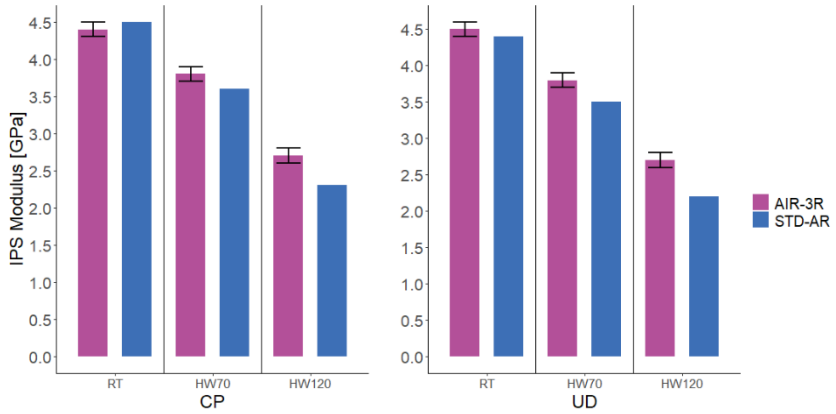

Figure 6.9. In-Plane Shear modulus of the AIR-3R vitrimer. CP and UD fabrics tested at the temperature-moisture conditions.

Regarding the in-plane shear strength (Figure 6.10), the vitrimer composite underperformed the baseline, particularly in the CP fabric: -10% in RT, -17.7% in HW70 and -21.5% in HW120 for CP, and -17.1% in RT, -11.5% in HW70 and -10.5% in HW120 for UD.

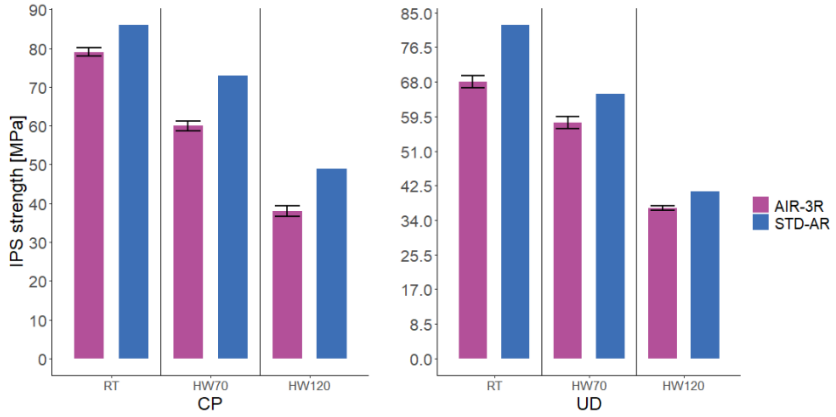

Figure 6.10. In-Plane Shear strength of the AIR-3R vitrimer. CP and UD fabrics tested at the temperature-moisture conditions.

6.1.2.5. Open Hole Tension (OHT), Compression (OHC) and Filled Hole Compression (FHC)

OHT strength at RT conditions, the AIR-3R formulation is comparable to the base thermoset resin (Figure 6.11). After moisture saturation, testing at 70° C presented a superior strength:

4.5% and 29.8%, respectively. All specimens presented good failure modes (Figure 6.12). Again, fibers carry most of the load indicating no alternations in composite behavior.

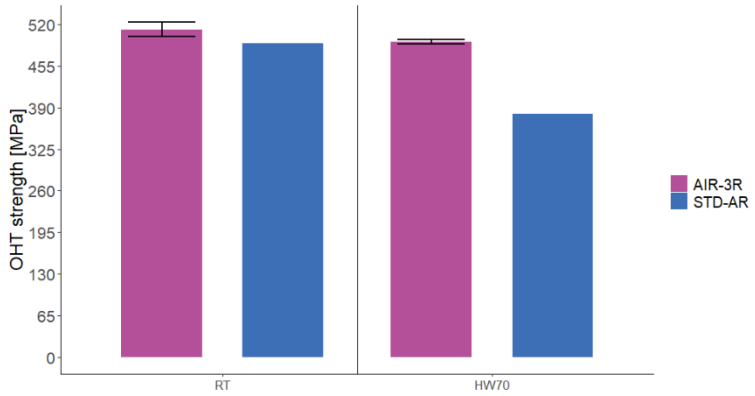

Figure 6.11. OHT test for the AIR-3R vitrimer tested at the temperature-moisture conditions.

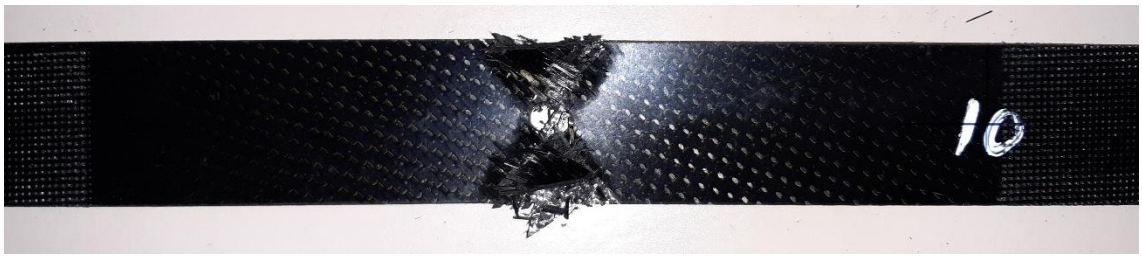

Figure 6.12. AIR-3R failed specimen under OHT test

OHC specimens had a proper failure mode under the specified standard. The AIR-3R vitrimer had a slightly lower compressive strength than the thermoset baseline (Figure 6.13). The PA veil is likely behind these results, considering the results of the compression and shear tests.

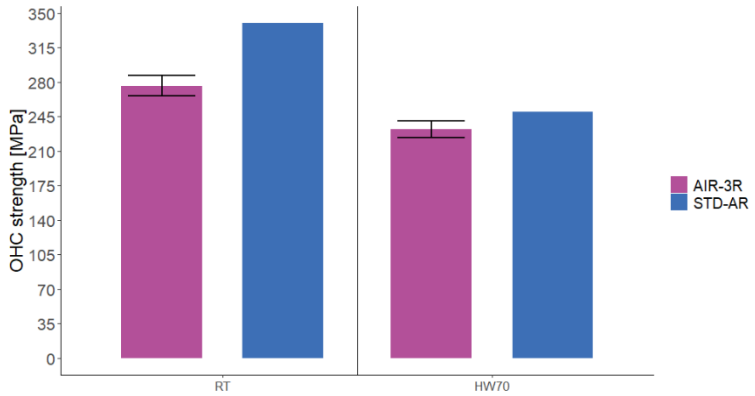

Figure 6.13. OHC test for the AIR-3R vitrimer tested at the temperature-moisture conditions.

The FHC strength for the AIR-3R vitrimer composite was slightly lower (-13.6%) than the baseline at RT and reached the same value for the HW70 condition (Figure 6.14). All the specimens presented non-valid failure modes as they failed outside the bolt area (Figure 6.15). The attempts to improve this issue by tightening the jig bolts and by ensuring a correct alignment of the sample and parallelism of the loading plates did not succeed.

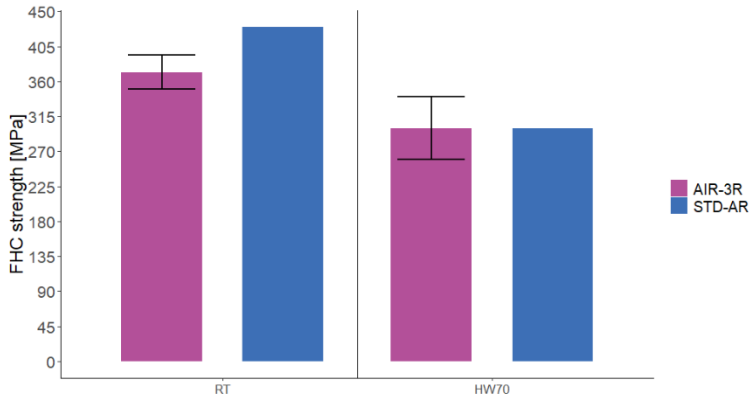

Figure 6.14. FHC test for the AIR-3R vitrimer tested at the temperature-moisture conditions.

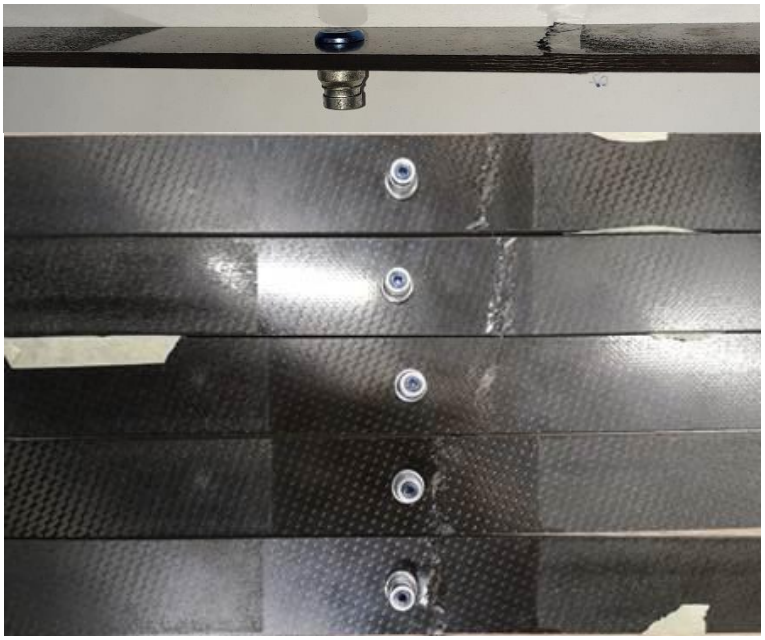

Figure 6.15. Failed FHC specimens

6.1.2.6. Interlaminar fracture toughness

The AIR-3R vitrimer specimens presented lower fracture toughness under mode I (G_{IC}) at RT but were still comparable to the base thermoset resin in that they exhibited a 11.4% difference (Figure 6.16).

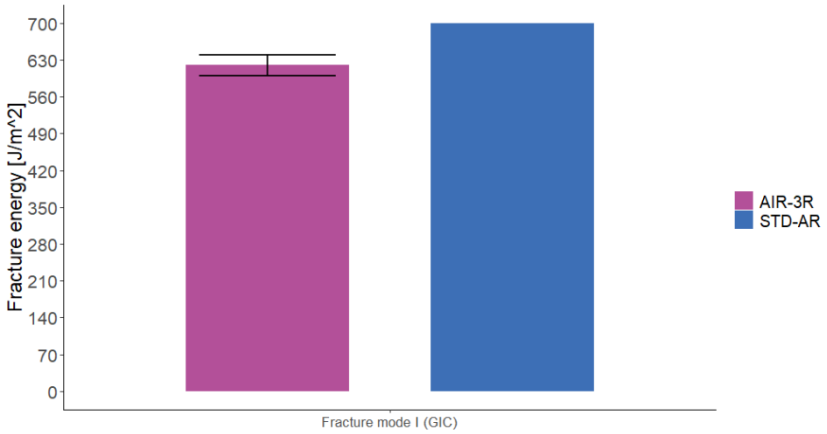

Figure 6.16. Fracture toughness for AIR-3R vitrimer composite

A baseline value for the fracture toughness under mode II (G_{IIC}) was not defined. The AIR-3R vitrimer composite presented a mean G_{IIC} value of 876.19 J/m^2.

6.2. Properties of vitrimer composites processed by HP-RTM

In chapter 5 we evaluated the capabilities of our HP-RTM machine and the properties of the materials produced with it. In section 6.1 we described the benefits of vitrimers over a thermoset baseline. In this section (6.2), we aim to combine both topics.

After evaluating the capabilities of our HP-RTM machine and the mechanical characterization of the composite materials produced by it. And after evaluating the benefits of vitrimers with respect to traditional thermoset resin formulations, we wanted to see if both topics (high-speed processing and vitrimer composites) could be combined in order to have more improvements as reduction of the total process time while generating sustainable composite materials.

We injected the high-performance resins for aeronautics (RTM6 thermoset epoxy and the AIR 3R) on the HP-RTM machine to see if this could affect their final performance.

6.2.1. Samples validation

6.2.1.1. Thickness measurement

RTM6 resin samples were more stable than the Sicomin samples. At 5 MPa pressure, the sample thickness oscillated between 1.94 mm and 1.96 mm, with the latter in the center area. At 8 MPa, thickness was stable at 1.96 mm with some points near to the injection port with thickness of 2.04 mm. Thickness maps for the RTM6 HP-RTM samples are displayed in Figure 6.17.

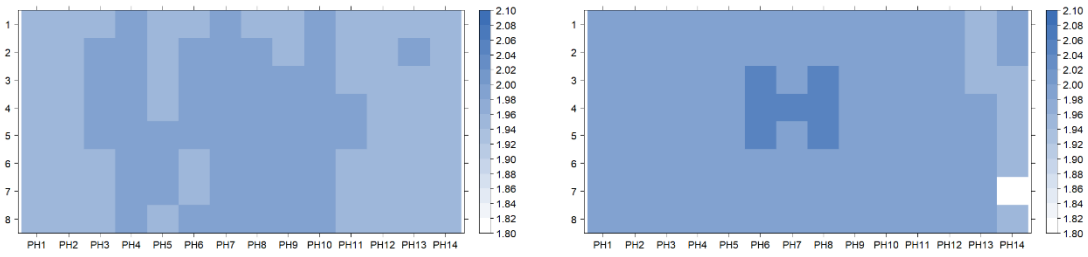

a b

Figure 6.17. Thickness map of the aeronautic RTM6 resin injected at high-pressure. a) 5 MPa sample. b) 8 MPa sample. Measurements in mm

AIR-3R vitrimer samples had similar tendencies as described before (Figure 6.18).

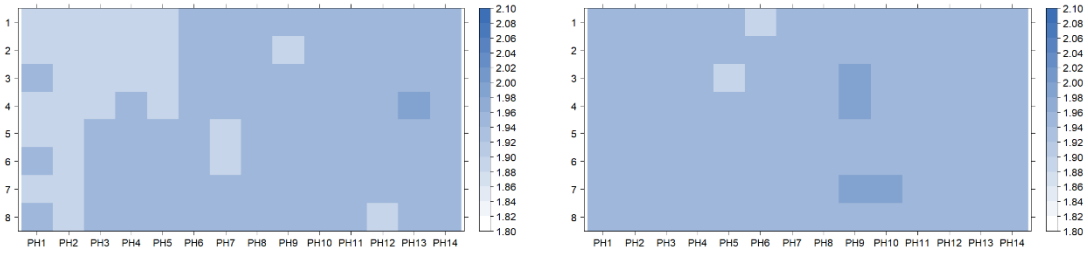

a b

Figure 6.18. Thickness map of the vitrimer Airpoxy resin injected at high-pressure. a) 5 MPa sample. b) 8 MPa sample. Measurements in mm

6.2.1.2. Visual inspection

Samples manufactured with the RTM6 resin presented similar issues as the traditional resin related to the injection pressure (fiber bumps at the vacuum gates), with no further issues related to the mold or the resin formulation.

With the AIR-3R resin, only the 5 MPa samples presented issues related to the resin system itself. This particular injection was the last done using the AIR-3R resin, as the 8 MPa sample was manufactured before. In this case, the remaining dynamic hardener was insufficient for the sample, so we mixed it with another batch of hardener.

Normally, this hardener has a powdery morphology, but this batch was solidified and presented a different color than normal. We believed that this particular pot was not properly stored, changing its properties. In the composite sample it was possible to see some areas with a different tone (Figure 6.19) and some superficial porosity, corresponding to the hardener that was not fully dissolved in the resin. It was not possible to repeat this panel as we did not have more vitrimeric resin available. The sample injected at 8 MPa presented also bumps in the vacuum area with no issues related to the formulation.

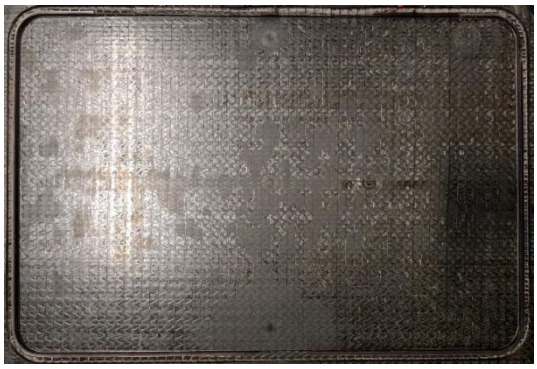

Figure 6.19. Surface of the composite sample injected at 5 MPa using the Airpoxy vitrimer formulation. Darker areas related to possibly undissolved hardener

6.2.1.3. Ultrasonic inspection

In the base RTM6 sample (Figure 6.20), the attenuation of the ultrasonic signal was very high under the defined criteria. In both cases, the injection channel and vacuum ports area are marked on the inspections.

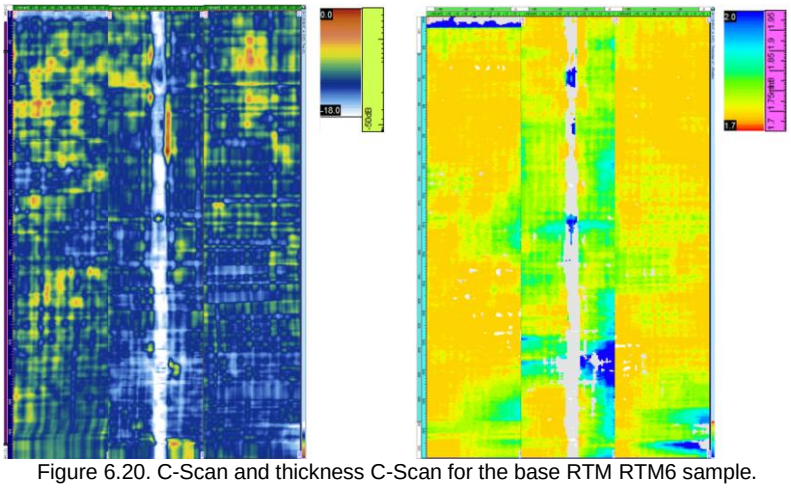

Figure 6.20. C-Scan and thickness C-Scan for the base RTM RTM6 sample.

The RTM6 resin samples (Figure 6.21) did not present any important defects. For the AIR-3R resin (Figure 6.22), the sample that had the issue with the hardener (Trial 09) presented high values of signal attenuation, but it was still on the limits.

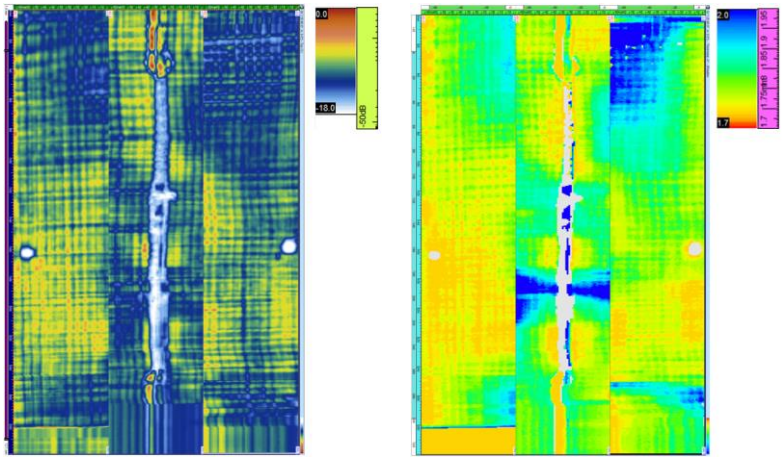

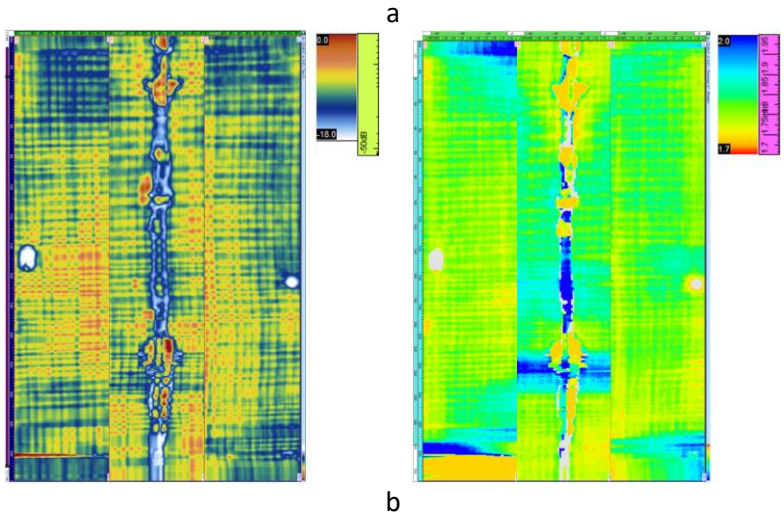

Figure 6.21. C-Scan and thickness C-Scan for the HP-RTM samples manufactured with the RTM6 resin. a) 2. b) 5 MPa c) 8 MPa

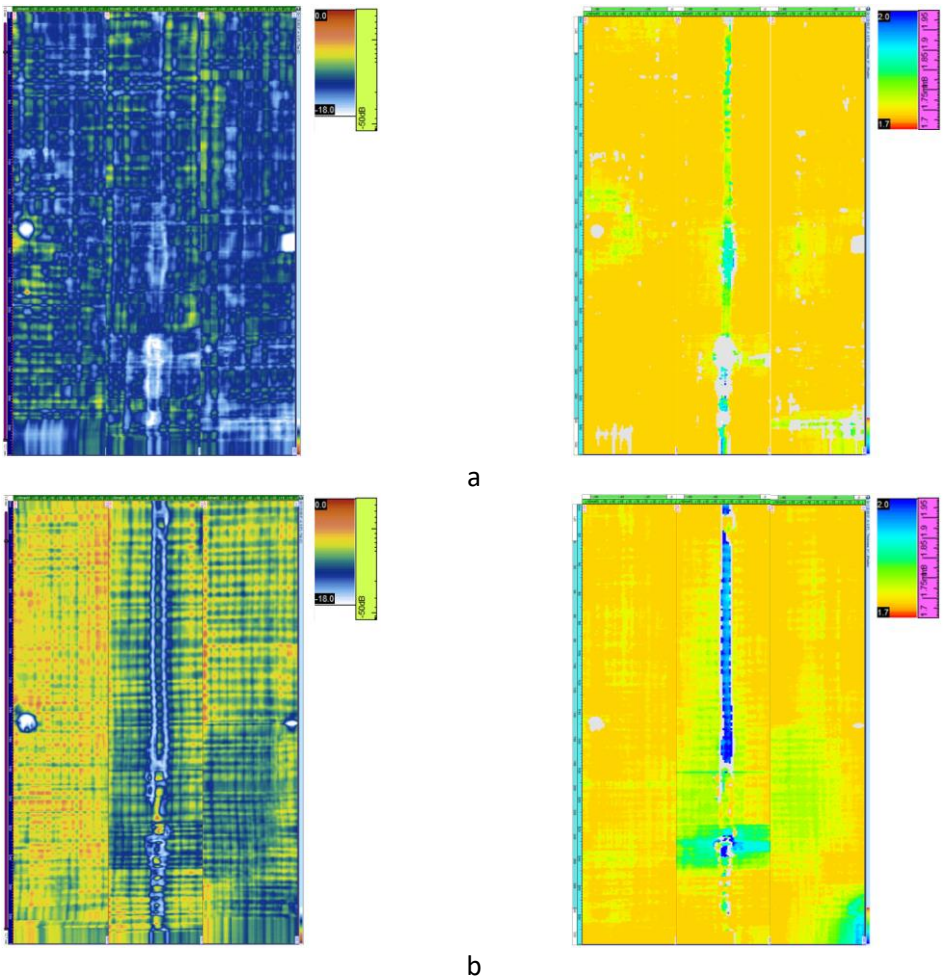

Figure 6.22. C-Scan and thickness C-Scan for the HP-RTM samples manufactured with the vitrimer AIR-3R resin. a) 2 MPa. b) 5 MPa c) 8 MPa

6.2.2. Mechanical characterization of high-performance resins processed by HP-RTM

Table 6.1 present the properties for the thermoset baseline resin processed by RTM.

Table 6.1. Mechanical properties for base RTM RTM6 sample

Resin formulation	Flexural strength [MPa]	ILSS [MPa]	Compression strength [MPa]
Aero epoxy (RTM6)	938.46 ± 55.73	49.48 ± 3.01	514.77 ± 31.85

6.2.2.1. Flexural strength

RTM6 resin manufactured with HP-RTM in the upper pressure values presented improvements over the base RTM sample: and 7.02% at 5 MPa and 8 MPa respectively (Figure 6.23). Again, showing that there are no further improvements beyond 5 MPa. At 2 MPa injection, the flexural strength was similar to the base RTM process: 1.17%.

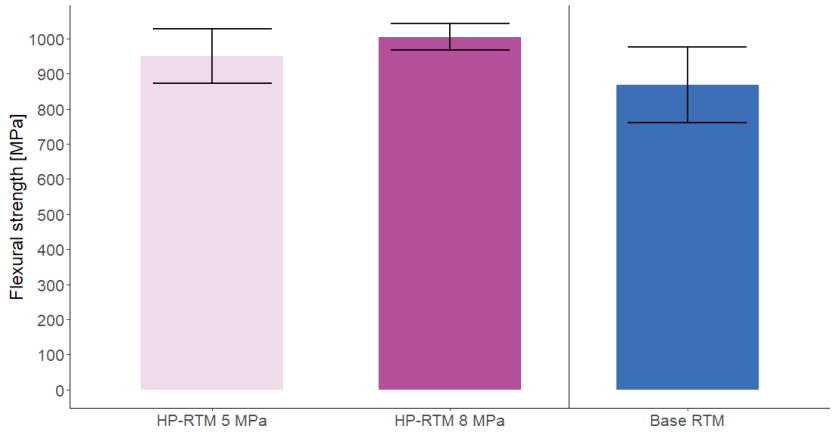

Figure 6.23. Comparative results in flexural strength for the aeronautical epoxy formulation (RTM6) injected at different pressures.

The AIR-3R vitrimer presented a flexural strength of 718.74 ± 119.99 MPa at 5 MPa, and 889.04 ± 130.24 MPa at 8 MPa (19.15% respect to the latter). If compared with the aero RTM6 resin, AIR-3R vitrimer underperformed -24.29% at 5 MPa and -11.48% at 8 MPa. In this case we must consider that the injection carried at 5 MPa was affected by the undissolved hardener in the cured sample, affecting the final properties. The flexural properties of the vitrimer HP-RTM composites are comparable with the RTM6 if it is only taken the 8 MPa injection. Figure 6.24 compares both RTM6 and AIR-3R performance under flexion.

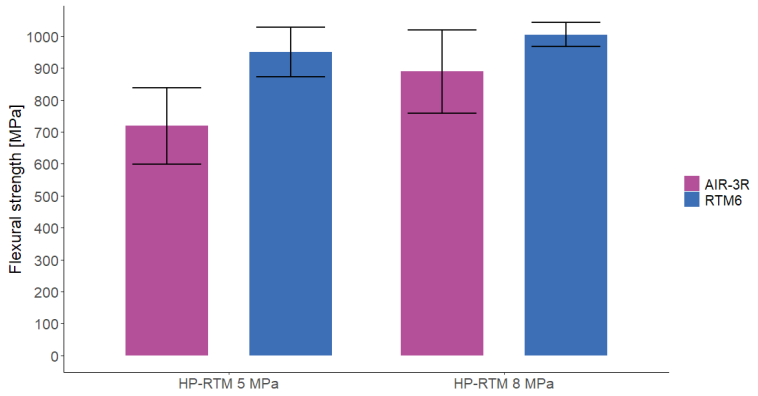

Figure 6.24. Comparative results in flexural strength for the aeronautical epoxy thermoset (RTM6) and the vitrimer (AIR-3R) processed by HP-RTM.

6.2.2.2. Compression strength

RTM6 resin also presented improvements in its compression response, but there are no significant differences compared with the base RTM sample (Figure 6.25): 3.99% improvement at 5 MPa, and 5.33% at 8 MPa. For this formulation, pressure appears to not lead to important improvements over the compressive response.

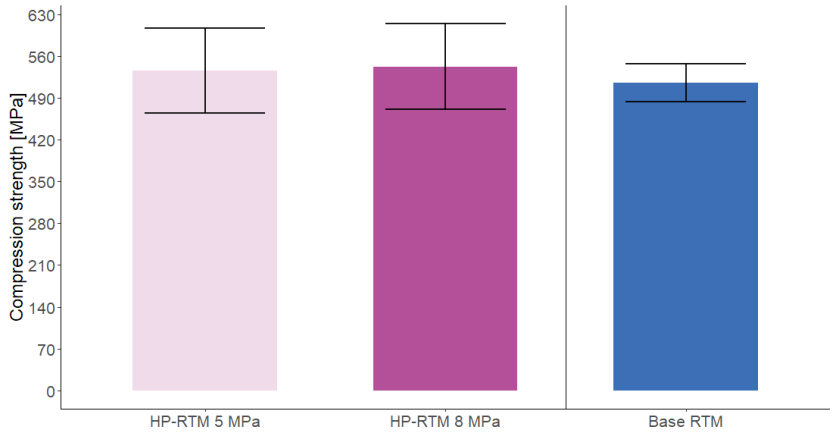

Figure 6.25. Comparative results in compression strength for the aeronautical epoxy formulation (RTM6) injected at different pressures. Injection and curing temperatures were maintained for all cases

For comparison, samples manufactured with the RTM6 resin in the study of the mechanical properties of the aeronautic vitrimer (section 6.1) presented a compression strength of 646 ± 32 MPa manufactured with conventional RTM, being 20.3% higher than the base RTM samples used in the HP-RTM study.

AIR-3R HP-RTM samples presented a compression strength of 435.40 ± 32.10 MPa at 5 MPa, and 525.73 ± 73.31 MPa at 8 MPa (improvement of 17.18% at the highest pressure). Again, comparing to the RTM6 resin, the vitrimer underperformed by 15.30% at 5 MPa (caused by the hardener issue). But at 8 MPa, the mechanical response was similar, only with a difference of 3.04% (similarly to the conventional RTM vitrimer composites without the PA veil). Comparing the compression strength of the highest-pressure sample with the sample manufactured with conventional RTM in the vitrimer study (paragraph 6.1), the latter has an improvement of

16.28%. Being the fabric used the only difference in this case. Figure 6.26 compares both RTM6 and AIR-3R performance.

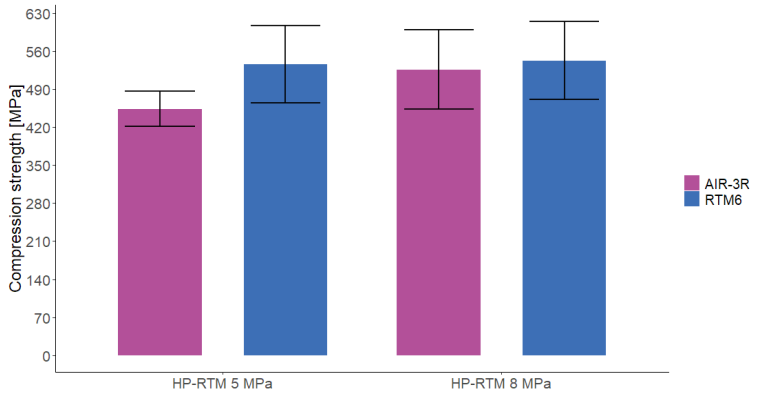

Figure 6.26. Comparative results in compression strength for the aeronautical epoxy thermoset (RTM6) and the vitrimer (AIR-3R) processed by HP-RTM.

6.2.2.3. Interlaminar Shear Strength (ILSS)

The RTM6 resin samples manufactured at high-pressure underperformed the base RTM mechanical response: -16.77% and -15.67% at 5 MPa and 8 MPa respectively. As it was presented on the ILSS samples for the standard epoxy formulation, most of the failure modes did not correspond to the expected outcome, affecting the mechanical behavior (Figure 6.27). These results are -17.53% under the performance from the baseline values in the vitrimer composite characterization.

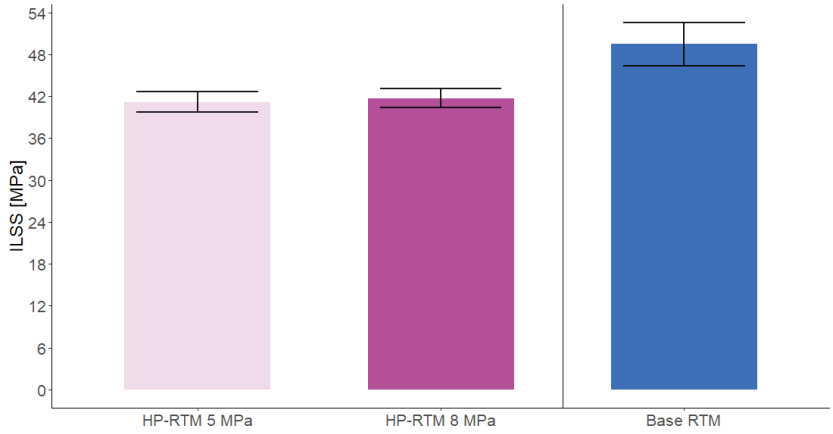

Figure 6.27. Comparative results in ILSS for the aeronautical epoxy formulation (RTM6) injected at different pressures. Injection and curing temperatures were maintained for all cases

The HP-RTM samples from the AIR-3R vitrimer had a different behavior than the standard epoxy (Sicomin) and the aeronautical epoxy (RTM6). For this case, the 5 MPa sample had better mechanical response than the 8 MPa sample, knowing that the undissolved hardener affected the other mechanical properties: 33.38 ± 1.1 MPa at 5 MPa, and 30.93 ± 2.4 MPa at 8 MPa (a difference of 7.21%).

The 8 MPa sample, that did not have issues with the formulation, the shear strength from the vitrimer HP-RTM sample is about 25.88% below the RTM6 HP-RTM sample (Figure 6.28).

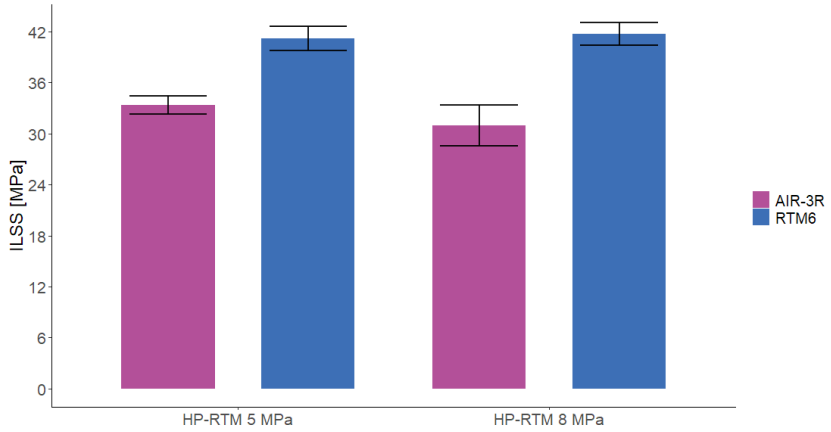

Figure 6.28. Comparative results in ILSS for the aeronautical epoxy thermoset (RTM6) and the vitrimer (AIR-3R) processed by HP-RTM.

Temperature effects on the cycle time was not tested as these resins are not meant to cure as the high-reactivity resins, being this the real issue on the HP-RTM processing of this kind of formulations.

6.3. Discussion on high-performance vitrimer composites

By comparing the T_g of AIR-3R vitrimer with the reported vitrimers by other authors, this formulation is above most of them [29], [78], [79], [87], [99], [100], [105], [108], [112], [113]. In particular, the vitrimer formulation from S. Wang et al. [95] which is a bio-based Vanillin epoxy - Diamine 4,4'-methyl-enebiscyclohexanamine, had a slightly better T_g value (1.16%). The authors proved to be effect of the high rigidity Schiff-based structure, as the cross-linking density was proved to be low. Similarly, the Poly(hexahydrotriazine) - 2,2-bis[4-(4-aminophenoxy)phenyl]propane vitrimer from Y. Yuan et al. [73] has a superior T_g compared with the AIR-3R vitrimer (14.22%), being more equivalent to some aeronautical thermoset formulations [73], [129]–[131]. Their polymer is based on C-N strong covalent structures. A similar case was found in the phenolic – urethane formulation from X. Liu et al. [109]

T_g value of the AIR-3R vitrimer under moisture conditions agrees with related findings on the effects of moisture in the glass transition temperature of epoxies [231], [232]. The T_g value of the aged AIR-3R vitrimer is still above the highest temperature and humidity condition, meaning that it should not affect its final performance under these conditions. Polymer matrices are sensible to water absorption (hygroscopic), especially epoxies, swelling and softening in the process thus reducing its mechanical properties [233], [234].

In terms of the neat resin properties, the AIR-3R vitrimer performs similarly to the baseline aeronautic resin. Other reported vitrimer formulations have quite similar tensile properties, most being slightly under this formulation [29], [78], [79], [82], [95], [235]. Only the Imine-Amine based vitrimer formulation from H. Liu et al. [70], and the 2,2-bis[4-(4-aminophenoxy)phenyl]propane formulation from Y. Yuan et al. [73] presented better tensile properties related to the high rigidity of their polymer networks. The latter author also having better flexural properties. I. Aranberri et al. [123] reported similar flexural properties on a DGEBA-disulfide vitrimer formulation. The overall mechanical properties of the AIR-3R

formulation are quite similar to the thermoset baseline, meaning that the use of this dynamic formulation would not affect the performance of structural components.

Tensile properties from the AIR-3R vitrimer composites were comparable or slightly superior than the baseline values for the cross-ply and 0° unidirectional (fiber direction) fabrics. In these cases, the load is mainly sustained by the reinforcement, demonstrating that this vitrimeric formulation does not interfere with the final composite performance [78].

The tensile strength of the unidirectional fabric in the matrix direction (90°) were lower than expected. We must consider that this is a matrix dominated load case. Related to this, H. Hamada et al. [236], and later R. Maurin et al. [237], reported that tensile properties on UD CF in 90° are complex to determine. Fiber presence acts as a stress concentrator inside the matrix, so the matrix is a dominant factor, but the strength also depends on the fibers nature, chemistry and their interfacial properties and quality. Effects of the decreased T_g caused by the water uptake also has to be considered in this case. Fracture analysis in the samples would be necessary in order to understand the dominant effect on the AIR-3R transverse tensile properties.

Compression properties proved to be highly affected by the added binder material. The PA veil was included in the AIR-3R vitrimer composite in order to enhance the interlaminar toughness and impact resistance, as has been demonstrated in several studies addressing interleaving thermoplastic veils [238]–[247]. The presence of the PA veil caused a decrement in the compressive response of the vitrimer composite. Related publications detail that thermoplastic veils acting as interleaves often increase the fracture toughness by serving as an obstacle to crack propagation but, as a countereffect, lowering the composite's in-plane properties [240]. Thermoplastic veils that do not melt during the manufacturing process have more permeability than the fibers, thus creating resin rich zones and promoting voids. The higher the veil's aerial weight, the greater the detrimental effect on the mechanical response is accentuated [241], [243], [248]–[250]. One of these studies reports that with a 4 g/m^2 co-PA veil the compression strength decreases by 9%. In this work, the PA veil had double the aerial weight which negatively impacted the compression strength by 22.6% (Figure 6.29).

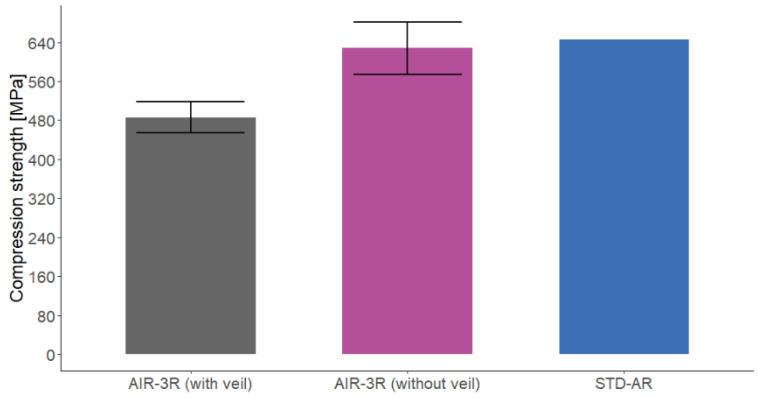

Figure 6.29. Comparison of the compressive strength for the AIR-3R vitrimer with and without the PA veil, and the base thermoset reference. CP fabric under RT condition

In view of the results with and without veil, it is concluded that the AIR-3R vitrimer formulation has no detrimental effect on the compressive strength of the final composite, thus being mechanically comparable to the thermoset baseline resin (-2.8%).

When comparing it to the vitrimers reported in the literature, AIR-3R has a superior compressive strength in reference to the 2,2-bis[4-(4-aminophenoxy)phenyl]propane-based formulation from Y. Yuan et al [73]. In this point, we have to highlight that their neat vitrimer properties were higher that the AIR-3R formulation. The difference could be related to the lower fiber content in their composites (50.1% for a plane-weave fabric in a cross-ply configuration).

In view of the influence of the PA veil in the compression response, another batch of ILSS samples was manufactured with the CP fabric without the PA veil and it was tested at RT. These samples showed better performance than the original testing set, surpassing the baseline thermoset by 20% (Figure 6.30) and demonstrating than the presence of the PA veil in the laminate causes a 24.89% loss in the interlaminar shear performance.

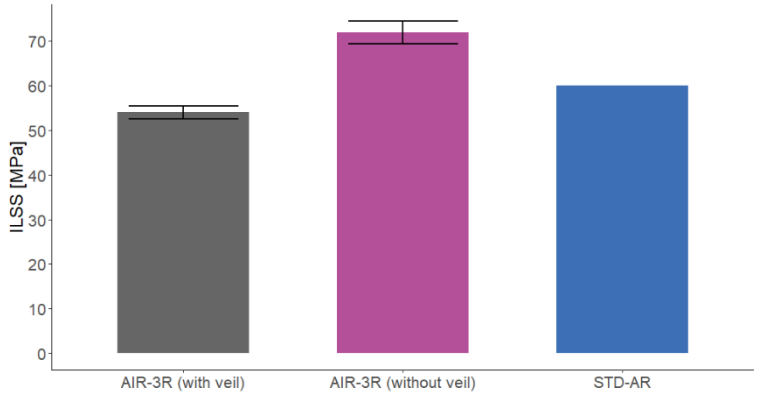

Figure 6.30. Comparison of the interlaminar shear strength for the AIR-3R vitrimer with and without the PA veil, and base thermoset reference. CP fabric under RT condition

Shear properties of the AIR-3R vitrimer, at least under interlaminar tests (ILSS) proved to be also influenced by the presence of the un-melted PA veil, having an important detrimental effect on the material strength (up to 25% approximately). The in-plane shear strength from the AIR-3R composites was also lower than the thermoset baseline. We believe that the PA veil influences over these results as was proved for the compression and ILSS test, in which the fiber/matrix interaction is an important parameter in the material performance. But in overall, the ILSS shear strength and IPS shear modulus suggest that the AIR-3R vitrimer has good toughness, good adhesion to the reinforcements, good adhesion between layers and good shear resistance, even after hot wet conditioning of the specimens.

As explained in the compression properties of the AIR-3R vitrimer composites, some authors have studied the effect of the binder materials on composites performance. This also has to be considered as in the HP-RTM process. The use of binders have been implemented as a way to overcome the possible washout or fiber deformations caused by the incident resin pressure and velocity [34], [35]. In counterpart, presenting detrimental effects over the fabrics permeability [6], [38] and the mechanical performance of the composites affecting tensile and flexural properties [8].

Open hole tension and compression, and filled hole compression are tests meant to assess the performance of composite materials in presence of stress concentrations. These tests were specially developed by the aeronautical industry as composite materials are more susceptible of damage under this kind of load [251]–[253]. The AIR-3R project was developed to impact the aeronautical industry, so the vitrimer composites were tested under these standards. In the OHT test, the load is sustained by the reinforcements and the results were similar to the thermoset

baseline, corroborating that the matrix change does not affect the mechanical properties of the final composites, as in the tensile tests. But the OHC and FHC tests underperformed the thermoset baseline. Again, we believe that the influence of the PA binder material has to be considered in the vitrimer performance by testing later these properties on samples with no binder material added. Unfortunately, there are no other publications, at least at the time that this work was written, that evaluate other vitrimer composite performance under OHT, OHC and FHC tests.

Interlaminar fracture toughness under mode I (G_{IC}) was comparable to other reported thermoset composites toughened with thermoplastic veils: T300 UD CF 167 g/m^2 – Epoxy RTM6-2 with 20 wt% PAEK veil [254], UD CF 350 g/m^2 – Epoxy L160 with 17 g/m^2 PA-66 veil [238], Epoxy MTM57/T700S (24K) UD prepreg with 4.5 g/m^2 and 9 g/m^2 PA-66 veils [255]. Despite the differences of the veil materials, toughening mechanisms and mechanical responses were similar. Factors such as veil polymer type and aerial weight were more important in the performance of the final laminate.

Mode II (G_{IIC}) interlaminar fracture toughness was lower than in similar thermoset composites toughened with thermoplastic veils. [242], [254]–[256]. Toughening mechanisms in mode II (G_{IIC}) are more complex than mode I (G_{IC}), depending most on the neat properties of the matrix and the architecture of the reinforcement, rather than the fiber bridging effect. The clarification of this topic deserves further research.

Previously we have discussed the benefits of the CFRP on the automotive industry over the overall weigh reduction of automotive structures, and the related benefits on the CO_2 emissions. But current industrial trends require the use of more sustainable materials as thermoset materials have issues on reparability, reprocessability and recyclability, with current disposal solutions also having environmental issues. Several reported vitrimers have presented the ability to overcome these issues, even some formulations being formulated from renewable or “green” resources [28], [29], [95], [99], [100], [104]–[106], [108]–[111], [69], [112], [113], [115], [122], [70]–[74], [79], [87]. In this work we have demonstrated that this particular vitrimer formulation is mechanically comparable with current aeronautical thermoset resins, also with the advantage of being formulated by commercially available resources, possibly influencing the final material cost. But the vitrimeric (dynamic) properties of the AIR-3R formulation are yet to be studied. At this moment, S. Weidmann et al. [91], also under the Airpoxy project [127], studied the thermoforming characteristics of the AIR-3R formulation. They reported that the vitrimer density at the forming temperatures is very high, making it difficult to do without any process-generated defects.

The RTM6 and the Airpoxy vitrimer are not designed to be high-reactivity formulations, making unprofitable to use the HP-RTM process. We demonstrated that we can highly reduce the mold filling times (up to 20 seconds in our mold cavity), while offering improvements over the mechanical performance by the effect of pressure. But the curing time for both resins are far from the injection value: 1.5 hours for the AIR-3R vitrimer and 2 hours for the RTM6 resin. In this case it would be necessary to have high reactivity – high performance vitrimer formulation that could be injected with HP-RTM and cured in a shot amount of time: 5 minutes or even 10 minutes, and still maintain high performance for structural applications. For our knowledge (at least at this work has been written), there are no reports of those kinds of vitrimer formulations yet. Some vitrimers are formulated to be a catalyst free polymers, as the AIR-3R resin, but external additives could be added to the formulation to accomplish requirements as fast curing [257].

Chapter 7: General discussion

High-Pressure Resin Transfer Molding technology (HP-RTM) is a capable out-of-autoclave process variation that have advantages over conventional RTM processing of composite materials as reduced mold filling times, with the possibility to use high reactivity – fast curing resin systems, improving productivity. Automation is necessary to improve production chain in order to make it reliable and profitable (preform construction, handling, mold operation and cleaning).

Process monitoring is a key factor to study and understand the phenomenology during the injection, and predict accurately the final component quality, the curing state of the resin and determine when to open or demold the final part to optimize the process, as well as predict possible failures and reject components even before mold opening and part inspection.

The Eurecat's Marieta HP-RTM machine is capable to produce high performance composites, needing improvements on its components, its operation and the overall performance. The HP-RTM mold also proved to be reliable as the injection strategies as the central film injection (distribution channel), the vacuum strategy and the fiber clamping mechanism helped to avoid commonly related HP-RTM issues such as fiber movement, preform washout or dry zones.

Sample defects were more defined at higher pressures due to the design of the vacuum ports of the mold, the preform fibers deformed and entered inside the vacuum channel as it was an open cavity. Placement of the vacuum ports over the sample area also influenced the preform defects, we must consider move the ports outside the component area in future designs, maintaining the clamping mechanisms. For complex geometries we would need to study of the material permeability and implement filling simulations in order to define the best injection strategy and ports placement.

The injection pressure proved to be a determinant factor to improve the mechanical properties of the composite material, specially flexural and compression strength, when compared with the standard RTM process. These improvements are an effect of the reduction of the porosity content inside the laminate, as the incident cavity pressure compress the voids reducing their content. There is a point in which is not possible to increase more the material performance by rising the injection pressure, having the risk of having detrimental effects instead by the reduction of the fiber volumetric fraction caused by mold deflections at high-pressure. Information summarized in Figure 7.1.

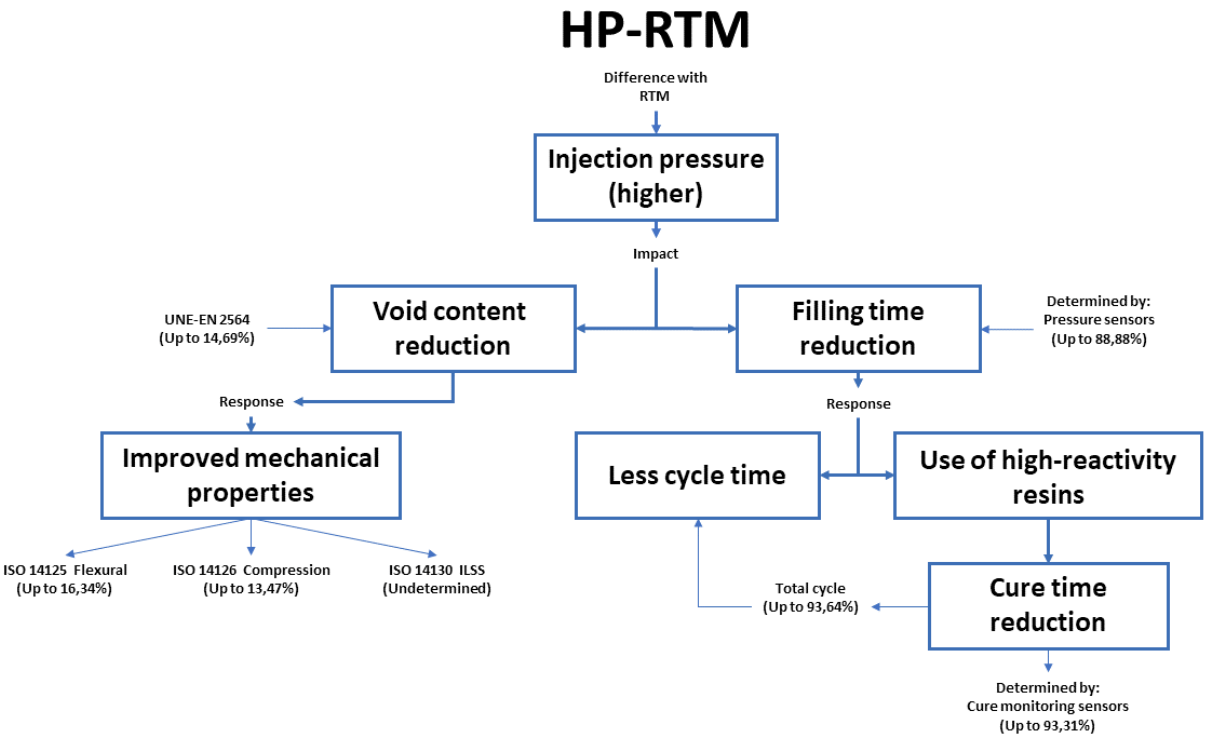

Figure 7.1. Improvements of HP-RTM process over conventional RTM

Rising the injection temperature also had an improvement in the flexural and compression properties, drove by the higher T_g of the final composites. The reduction of the resin viscosity is another improvement factor as the resin tend to impregnate better the preform, but further analysis' have to be made in order to determine the degree of influence of both parameters.

Increasing the injection temperature also helped to reduce the curing time of the high-reactivity resin (Sicomin), presenting an important improvement in the total process cycle. Factors as cavity size and injection pressure must be considered in order to fill the mold cavity without having premature curing in the sample. Both process parameters led to a significant reduction of the total process time, where the pressure helped to reduce the cavity filling time, and the temperature reduced the curing time. Further improvements have to be made on the HP-RTM sub-processes as preform cutting and placement, and mold operation and cleaning.

The effect of the injection pressure and temperature on the shear performance was not clear for the HP-RTM samples, as there is not a tendency that explain the influence over the material. We suspect that the test setup is responsible for this outcome as most of the ILSS failed in undesired conditions or presented non-linear behavior.

Process monitoring by using cavity pressure and DEA curing sensors was a key factor in order to understand the injection and curing phenomena inside the mold cavity. Cavity pressure and ionic viscosity could give indications of resin frontline, possible race tracking or dry zones, resin arrival time, minimum viscosity points and end of curing, helping to improve and optimize the process. We demonstrated that is possible to know when an injected part has issues before even opening the mold, in this way we could set minimum operational parameters in order to accept or discard samples while processing. Piezoelectric pressure sensors require signal treatment after the injection as these devices have signal drifting caused the sensor itself, factors as temperature also affect the sensor response.

Vitrimers offer advantages over traditional thermosets as reparability, reprocessability and recyclability while maintaining a frozen topology in their operational temperatures, presenting thermoset-like performance.

The neat vitrimer properties of the AIR-3R demonstrate that this formulation can be replaced as a matrix for high-performance structural components, having similar properties to the thermoset baseline and thus not affecting their performance. This new epoxy-disulfide vitrimer composites presented good in-plane stiffness under tension and compression, and good shear stiffness, denoting good adhesion between fibers at the interface. Vitrimer composite strength under compression and interlaminar shear proved to be highly influenced by the presence of the un-melted thermoplastic veil, which had been intended to enhance the fracture toughness.

Micrography analysis and comparison to related studies show that the un-melted veil created brittle resin-rich zones. Compression samples without the PA veil demonstrated that this trapped interface in the laminate reduces the compressive strength by 22.6%, while the ILSS samples presented reductions of 24.89%. The interlaminar veils could also have influenced the tension strength at UD 90º, in-plane shear strength, OHC and FHC strength, all of which were lower than the base thermoset formulation.

Fracture toughness in mode I (GIC) was comparable to reported thermoset formulations with toughening thermoplastic veils. Mode II appears to be lower than the references with and without the thermoplastic veils. Further research should be carried out to clarify the micro-mechanisms behind the fracture behavior of this vitrimer formulation, as well as the impact of the thermoplastic veils, their melting temperature and aerial weight on the in-plane vitrimer composite properties.

The mechanical properties of the AIR-3R and the composites prepared with this new vitrimer formulation were comparable to the aeronautical resin. Vitrimer dynamic properties have to be studied in order to establish a processing window in which this formulation could be reprocessed, while maintaining the overall composite properties. Summary presented on Figure 7.2.

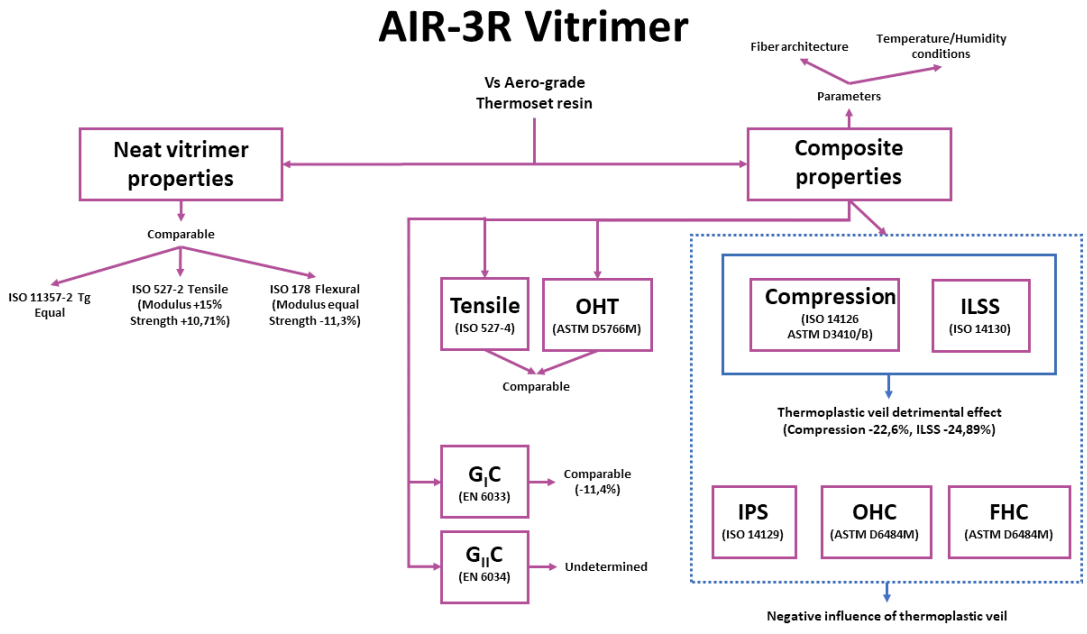

Figure 7.2. Summary of vitrimer properties over aero-grade thermoset reference

Both topics: HP-RTM processing and vitrimer composites demonstrated to be compatible as the material samples of the vitrimer composites made under HP-RTM presented similar properties to the current aerospace thermoset resin, while reducing the mold filling times and improving the mechanical properties by processing at high pressures.

Albeit the Airpoxy formulation is not a high reactivity resin, the development of a new variant of this vitrimer could be studied to improve its reactivity, possibly introducing vitrimer advantages in the automotive industry, being capable to be injected at higher pressures. This would impact on the process cycle (filling and curing times), increasing the overall production rate. Due to its dynamic characteristics, the elements produced with this formulation could be welded, repaired, reformed or recycled, reducing further the operative or maintenance costs of the component, while being an environmentally friendly solution. In addition to the composites advantages in the transport industry: weight reduction reducing the amount of CO_2 during operation.

Chapter 8: Conclusions

The HP-RTM prototype machine prove to be capable to produce high-performance materials in cycle times affordable to high-volume production environments. The difference of this machine with commercially available alternatives is its target, being more appropriate for research and low production environments. Although, the Marieta Machine needs further improvements regarding functioning, calibration and the modification to make bi-component injections reliable. Future machine versions can be oriented towards reduced volumes for small pieces, and mono-component injections.

By evaluating the pressure parameter, the mold structure tends to expand more at higher values, reducing the overall fiber volume fraction. While the baseline samples presenting thicknesses rounding 1.94 – 1.98 mm, the sample injected at the maximum pressure (8 MPa), had 2.04 mm. Temperature parameter help to reduce the curing time and the overall cycle time.

Temperature influenced the glass transition temperature (T_g) of the HP-RTM samples, improving it by 26.42%. Pressure had no effects on the T_g.

Injection pressure is the main process parameter as we improved the flexural strength up to 16.28% at 8 MPa, and compression strength up to 13.47% at the same pressure. Although, for flexural strength, the improvements between 5 MPa and 8 MPa are similar. We had not representative results on the shear strength as most of the samples presented non-valid failures.

Temperature improved the flexural strength up to 7.02% at 140° C, and the compression strength up to 5.48% at the same temperature. Improvements come from the higher T_g, having in the polymer better cross-linking density, and better degree of curing as we measured a 100% cure at 140° C.

In the fiber, resin and porosity content evaluation, the 2 MPa and 5 MPa samples presented comparable fiber volume content as the baseline RTM (≈57%), the 8 MPa sample had less fiber volume content (a 4.42% less) due to mold deflections, corroborated by the samples thickness measurements. Porosity content was improved by the injection pressure, having a reduction of 14.69% at 8 MPa thanks to the effect on the cavity pressure. We confirm that the injection pressure improves mechanical properties by reducing the void content inside the composites. The reduction of the fiber volume content affected the flexural strength at 8 MPa.

Using the on-line monitoring sensors, we detected that the mold cavity pressure values oscillated between 55% and 60% of the injection pressure by the force distribution inside the mold cavity. In addition, the pressure sensors show us that the mold filling times are reduced by increasing the injection pressure. Having reductions up to 73.88% at 2 MPa, 79.33% at 5 MPa and 88.88% at 8 MPa. Moreover, we detected abrupt changes in the mold cavity pressure at the samples injected at high-temperature due to resin shrinkage of the high-reactivity Sicomin resin.

With the DEA curing sensors, we detected that pressure did not affect the curing process, reinforcing the DSC results. But temperature reduced the curing time, having a reduction of 85.87 % at 120° C, and 93.83% at 140° C. Pressure and temperature improved the general RTM cycle time up to 93.64%.

For the vitrimer composites topic, we found that neat vitrimer properties are comparable to the thermoset counterpart, having the same T_g (170° C), comparable flexural modulus, and better tensile modulus and strength (15% and 10.71% respectively). Flexural strength of the neat vitrimer underperformed the thermoset baseline by 11.3%.

For the composites manufactured with the epoxy vitrimer formulation, we found that the tensile strength and modulus were mostly comparable to the thermoset baseline for the 5HS woven and the UD 0°, slightly underperforming at the highest temperature/moisture condition (-2.9% for the satin, and -6.7% for the UD at 0°). Samples made with the UD reinforcement at 90° presented worst tensile modulus and strength (up to -28.2% and -60.3% respectively), requiring further analysis to stablish the cause.

The PA binder veil had a detrimental effect on the compression and shear properties. The veil did not melt during processing, being trapped inside the laminated and creating fragile resin rich zones. This impacted directly over the compression strength, reducing it by a 22.6%, and the interlaminar shear strength, by a 24.89%. Samples manufactured without the PA veil proved to be comparable with the thermoset baseline.

Open hole tension strength of the vitrimer composites was comparable with the thermoset baseline, performing better at the 70° C/85% RH condition (29.8%). The open hole and filled hole compression strength was also affected by the inclusion of the PA veil.

The interlaminar fracture toughness of the vitrimer composites under mode I (G_{IC}) was comparable to the thermoset baseline, only having a difference of -11.4%. But we detected that the interlaminar fracture toughness under mode II (G_{IIC}) was lower than other reported thermoset materials (as not having a thermoset baseline). Further research is needed to understand the toughening mechanisms.

For the high-performance resin formulations processed by HP-RTM, injection pressure also improved the flexural strength of the RTM6 samples, having an increment of 7.02% at 5 MPa and 8 MPa. Although the fiber volume content was not measured for these samples, mold deflections due to internal pressure is likely to be the cause. Pressure also improved the compression strength of the RTM6 samples, having a maximum of 5.33% at 8 MPa.

RTM6 composites presented equal interlaminar shear strength at 5 MPa and 8 MPa injection pressures. But both were lower than the RTM baseline (-17.53%), due to the non-valid failure modes in the tests.

The flexural strength of the AIR-3R composites under HP-RTM process was -11.48% lower than the RTM6 samples at the same injection pressures. The un-dissolved hardener on the 5 MPa sample presented a detriment of -24.29% on the flexural strength. The compressive strength of the AIR-3R composites was comparable with the RTM6 samples, but the sample injected at 5 MPa underperformed by 15.67% due to the hardener.

In addition, we found that the interlaminar shear strength of the AIR-3R HP-RTM samples were lower than the RTM6 in both injection pressures. We also consider the non-valid failures in the test.

By injecting both aeronautic thermoset resin and AIR-3R vitrimer resin, we demonstrated that the HP-RTM process also can improve the processing time and mechanical performance, but all efforts had no meaning on the overall cycle time as these resins are not meant to cure in short times.

Combining both thesis topics can create a new research area for fast-processing sustainable materials. Further research must be oriented towards fast-curing dynamic polymers in order to make them feasible to be processed by HP-RTM.

Future work

The Eurecat's HP-RTM machine will need short – mid future modifications to adapt static mixers inside the machine injection nozzle, and the implementation of the PTFE support ring on the resin and hardener piston to prevent wearing of the mixhead O-rings and resin leaks. Alternative designs can be researched for implementing the mixing mechanisms inside the mold rather than in a specific mechanical component. Other machine versions can be proposed to be suitable for small laboratory-scale testing or for mono-component resins.

The machine capabilities have to demonstrated in a full-scale demonstrator. This would validate the Eurecat's machine as a capable and feasible alternative for the high-volume processing.

The HP-RTM mold design need some improvements to avoid injection issues related to the vacuum ports placement. Future plane and complex geometries would require placing the vacuum ports outside the preform area, while maintaining the sealing and fiber clamping mechanisms.

Effects on the resin viscosity and the fabrics permeability need to be study. Shear properties of the HP-RTM composites need further research as the current tests did not present a clear influence of the process parameters in comparison with the base RTM process and failure modes did not correspond with the expected outcome.

Process monitoring could be improved by implementing more sensors inside the mold cavity. Further studies could be made with more types of pressure sensors due to the required post-processing in the pressure signal.

The AIR-3R vitrimeric formulation proved to be mechanically comparable with the current aeronautic thermoset formulation. Although the in-plane properties demonstrated to be highly affected by the PA toughening veil inside the laminates. More test without the PA would be required in aims to know the real performance of this vitrimeric formulation. And future formulations of the resin could be formulated to have a fast-curing process in order to enhance the system productivity and complement it with the benefits of the HP-RTM processing.

References

[1] A. Cherniaev, Y. Zeng, D. Cronin, and J. Montesano, "Quasi-static and dynamic characterization of unidirectional non-crimp carbon fiber fabric composites processed by HP-RTM," *Polym. Test.*, vol. 76, no. December 2018, pp. 365–375, 2019, doi: 10.1016/j.polymertesting.2019.03.036.

[2] A. Martin, "Vehículos de baja emisión de carbono: beneficios para los conductores, la economía y el medio ambiente," *Transp. Enviroment*, 2012, [Online]. Available: https://www.transportenvironment.org/node/3345

[3] F. Rondina *et al.*, "Development of full carbon wheels for sport cars with high-volume technology," *Compos. Struct.*, vol. 192, no. January, pp. 368–378, 2018, doi: 10.1016/j.compstruct.2018.02.083.

[4] B. J. Han, Y. C. Jeong, C. M. Kim, R. W. Kim, and M. Kang, "Forming characteristics during the high-pressure resin transfer molding process for CFRP," *Adv. Compos. Mater.*, vol. 28, no. 4, pp. 365–382, 2019, doi: 10.1080/09243046.2018.1556236.

[5] K. Jacques, L. Bax, H. Vasiliadis, I. Magallon, and K. Ong, "Polymer composites for automotive sustainability," *Eur. Technol. Platf. Sustain. Chem.*, p. 56, 2015, [Online]. Available: http://www.suschem.org/cust/documentrequest.aspx?DocID=998%5Cnhttp://www.suschem.org/publications.aspx

[6] R. Chaudhari, "Characterization of high-pressure resin transfer molding process variants for manufacturing high-performance composites," Karlsruhe Institute of technology, 2013.

[7] R. Chaudhari, P. Rosenberg, M. Karcher, S. Schmidhuber, P. Elsner, and F. Henning, "High-pressure RTM process variants for manfuacturing of carbon fiber reinforced composites," *ICCM Int. Conf. Compos. Mater.*, vol. 2013-July, pp. 1560–1568, 2013.

[8] L. Khoun, D. Maillard, and M. N. Bureau, "Effect of process variables on the performance of glass fibre reinforced composites made by high pressure resin transfer moulding," *SPE Automot. Compos. Div. - 12th Annu. Automot. Compos. Conf. Exhib. 2012, ACCE 2012 Unleashing Power Des.*, pp. 380–392, 2012.

[9] M. S. Sarfraz, H. Hong, and S. S. Kim, "Recent developments in the manufacturing technologies of composite components and their cost-effectiveness in the automotive industry: A review study," *Compos. Struct.*, vol. 266, no. February, p. 113864, 2021, doi: 10.1016/j.compstruct.2021.113864.

[10] "Automotive lightweight material market to grow by 5%," *Met. Powder Rep.*, vol. 75, no. 6, pp. 319–319, Nov. 2020, doi: 10.1016/j.mprp.2020.10.047.

[11] J. Zhang, V. S. Chevali, H. Wang, and C. H. Wang, "Current status of carbon fibre and carbon fibre composites recycling," *Compos. Part B Eng.*, vol. 193, no. December 2019, p. 108053, 2020, doi: 10.1016/j.compositesb.2020.108053.

[12] E. Ghassemieh, "Materials in Automotive Application, State of the Art and Prospects," in *New Trends and Developments in Automotive Industry*, InTech, 2011. doi: 10.5772/13286.

[13] E. Pakdel, S. Kashi, R. Varley, and X. Wang, “Recent progress in recycling carbon fibre reinforced composites and dry carbon fibre wastes,” *Resour. Conserv. Recycl.*, vol. 166, no. November 2020, p. 105340, 2021, doi: 10.1016/j.resconrec.2020.105340.

[14] D. Borjan, Ž. Knez, and M. Knez, “Recycling of carbon fiber-reinforced composites—difficulties and future perspectives,” *Materials*, vol. 14, no. 15. pp. 1–13, 2021. doi: 10.3390/ma14154191.

[15] M. Harris, “Carbon fibre: the wonder material with a dirty secret,” *The Guardian*, 2017. https://www.theguardian.com/sustainable-business/2017/mar/22/carbon-fibre-wonder-material-dirty-secret (accessed Mar. 23, 2022).

[16] S. Hernández, F. Sket, C. González, and J. Llorca, “Optimization of curing cycle in carbon fiber-reinforced laminates: Void distribution and mechanical properties,” *Compos. Sci. Technol.*, vol. 85, pp. 73–82, 2013, doi: 10.1016/j.compscitech.2013.06.005.

[17] P. Wang, S. Drapier, J. Molimard, A. Vautrin, and J. C. Minni, “Characterization of Liquid Resin Infusion (LRI) filling by fringe pattern projection and in situ thermocouples,” *Compos. Part A Appl. Sci. Manuf.*, vol. 41, no. 1, pp. 36–44, 2010, doi: 10.1016/j.compositesa.2009.09.007.

[18] A. Anil Kumar and R. Sundaram, “Cure cycle optimization for the resin infusion technique using carbon nanotube additives,” *Carbon N. Y.*, vol. 96, pp. 1043–1052, 2016, doi: 10.1016/j.carbon.2015.09.044.

[19] E. Poodts, G. Minak, L. Mazzocchetti, and L. Giorgini, “Fabrication, process simulation and testing of a thick CFRP component using the RTM process,” *Compos. Part B Eng.*, vol. 56, pp. 673–680, 2014, doi: 10.1016/j.compositesb.2013.08.088.

[20] D. Abraham, S. Matthews, and R. McIlhagger, “A comparison of physical properties of glass fibre epoxy composites produced by wet lay-up with autoclave consolidation and resin transfer moulding,” *Compos. Part A Appl. Sci. Manuf.*, vol. 29, no. 7, pp. 795–801, 1998, doi: 10.1016/S1359-835X(98)00055-4.

[21] R. Hillermeier, T. Hasson, L. Friedrich, and C. Ball, “Advanced thermosetting resin matrix technology for next generation high volume manufacture of automotive composite structures,” *SAE Tech. Pap.*, vol. 2, no. Step 4, pp. 1–9, 2013, doi: 10.4271/2013-01-1176.

[22] M. Bodaghi, P. Simacek, S. G. Advani, and N. C. Correia, “A model for fibre washout during high injection pressure resin transfer moulding,” *J. Reinf. Plast. Compos.*, vol. 37, no. 13, pp. 865–876, 2018, doi: 10.1177/0731684418765968.

[23] F. Henning, L. Kärger, D. Dörr, F. J. Schirmaier, J. Seuffert, and A. Bernath, “Fast processing and continuous simulation of automotive structural composite components,” *Compos. Sci. Technol.*, vol. 171, no. December 2018, pp. 261–279, 2019, doi: 10.1016/j.compscitech.2018.12.007.

[24] M. Deléglise, P. Le Grognec, C. Binetruy, P. Krawczak, and B. Claude, “Modeling of high speed RTM injection with highly reactive resin with on-line mixing,” *Compos. Part A Appl. Sci. Manuf.*, vol. 42, no. 10, pp. 1390–1397, 2011, doi: 10.1016/j.compositesa.2011.06.002.

[25] M. Bodaghi, C. Cristóvão, R. Gomes, and N. C. Correia, “Experimental characterization of voids in high fibre volume fraction composites processed by high injection pressure RTM,” *Compos. Part A Appl. Sci. Manuf.*, vol. 82, pp. 88–99, 2016, doi: 10.1016/j.compositesa.2015.11.042.

[26] R. W. Kim, C. M. Kim, K. H. Hwang, and S. R. Kim, “Embedded based real-time monitoring in the high-pressure resin transfer molding process for CFRP,” *Appl. Sci.*, vol. 9, no. 9, 2019, doi: 10.3390/app9091795.

[27] P. Rosenberg, R. Chaudhari, P. Albrecht, M. Karcher, and P. F. Henning, “Effects of Process Parameters on Cavity Pressure and Component Performance in High-Pressure Rtm Process Variants,” no. August 2015, p. 16, 2014.

[28] A. Dorigato, “Recycling of thermosetting composites for wind blade application,” *Adv. Ind. Eng. Polym. Res.*, 2021, doi: 10.1016/j.aiepr.2021.02.002.

[29] H. Memon, Y. Wei, L. Zhang, Q. Jiang, and W. Liu, “An imine-containing epoxy vitrimer with versatile recyclability and its application in fully recyclable carbon fiber reinforced composites,” *Compos. Sci. Technol.*, vol. 199, no. June, p. 108314, 2020, doi: 10.1016/j.compscitech.2020.108314.

[30] S. Black, “Composites recycling: Gaining traction,” *Composites World*, 2017. https://www.compositesworld.com/articles/composites-recycling-gaining-traction (accessed Mar. 25, 2022).

[31] Cidetec, “3R leading technology Reprocessable, Repairable and Recyclable: materials with an endless lifespan.” https://www.cidetec.es/en/top-achievements/3r-leading-technology

[32] P. Rosenberg, R. Chaudhari, M. Karcher, F. Henning, and P. Elsner, “Investigating cavity pressure behavior in high-pressure RTM process variants,” *AIP Conf. Proc.*, vol. 1593, no. 2014, pp. 463–466, 2014, doi: 10.1063/1.4873822.

[33] S. H. Han, E. J. Cho, H. C. Lee, K. Jeong, and S. S. Kim, “Study on high-speed RTM to reduce the impregnation time of carbon/epoxy composites,” *Compos. Struct.*, vol. 119, pp. 50–58, 2015, doi: 10.1016/j.compstruct.2014.08.023.

[34] J. Wang, P. Simacek, and S. G. Advani, “Use of medial axis to find optimal channel designs to reduce mold filling time in resin transfer molding,” *Compos. Part A Appl. Sci. Manuf.*, vol. 95, pp. 161–172, 2017, doi: 10.1016/j.compositesa.2017.01.003.

[35] H. Salek and P. Trudeau, “Development of Low Cost Fuselage Frames by Resin Transfer Molding,” *SAE Tech. Pap. Ser.*, vol. 1, 2013, doi: 10.4271/2013-01-2325.

[36] M. Bodaghi, R. Costa, R. Gomes, J. Silva, N. Correia, and F. Silva, “Experimental comparative study of the variants of high-temperature vacuum-assisted resin transfer moulding,” *Compos. Part A Appl. Sci. Manuf.*, vol. 129, no. July 2019, p. 105708, 2020, doi: 10.1016/j.compositesa.2019.105708.

[37] S. Nonn, C. Kralovec, and M. Schagerl, “Damage mechanisms under static and fatigue loading at locally compacted regions in a high pressure resin transfer molded carbon fiber non-crimp fabric,” *Compos. Part A Appl. Sci. Manuf.*, vol. 115, no. May, pp. 57–65, 2018, doi: 10.1016/j.compositesa.2018.09.011.

[38] M. Bodaghi, P. Simacek, N. Correia, and S. G. Advani, “Experimental parametric study of flow-induced fiber washout during high-injection-pressure resin transfer molding,” *Polym. Compos.*, no. October, pp. 1–13, 2019, doi: 10.1002/pc.25437.

[39] P. K. Mallick, *Thermoset matrix composites for lightweight automotive structures*. LTD, 2021. doi: 10.1016/b978-0-12-818712-8.00006-9.

[40] I. Swentek, B. Beck, V. Ugresic, T. Potyra, and F. Henning, “Impact of HP-RTM process

parameters on mechanical properties with epoxy and polyurethane systems," *SAMPE J.*, vol. 53, no. 3, pp. 20–25, 2017.

[41] P. Rosenberg, B. Thoma, P. F. Henning, F. C. Technologie, I. Fahrzeugsystemtechnik, and K. Institut, "Characterization of Epoxy and Polyurethane Resin Systems for Manufacturing of High - Performance Composites in High - Pressure Rtm Process," *SPE Automot.*, no. September, pp. 1–18, 2015.

[42] G. Gardiner, "HP-RTM on the rise : CompositesWorld," Apr. 14, 2015. https://www.compositesworld.com/articles/hp-rtm-on-the-rise (accessed Mar. 12, 2020).

[43] E. Tempelman, B. N. van Eyben, and H. Shercliff, "Manufacturing and Design: Understanding the principles of how things are made," in *Manufacturing and Design: Understanding the principles of how things are made*, 2014, p. 172. doi: 10.1016/C2011-0-08438-7.

[44] "Our Products - KraussMaffei." https://www.kraussmaffei.com/en/our-products/metering-systems (accessed Mar. 12, 2020).

[45] "KraussMaffei RimStar Nano, Compact and Modular," *Direct Industry*. https://pdf.directindustry.es/pdf-en/krauss-maffei-injection-moulding-technology/rimstar-nano-compact-modular/20425-281939.html (accessed Apr. 06, 2020).

[46] "E-System| High pressure dosing machine for HP RTM Process | Cannon Plastec." https://www.cannonplastec.com/products/machinery/dosing-machine/e-system/ (accessed Mar. 12, 2020).

[47] "Cannon E-System Enhanced: the New Generation of Dosing Units for HP-RTM," *Direct Industry*. https://pdf.directindustry.com/pdf/cannon-spa/e-system-enhanced-new-generation-dosing-units-hp-rtm/61208-606900.html (accessed Apr. 06, 2020).

[48] "The Cannon News," *Cannon*, 2016. https://www.cannon.com/wp-content/uploads/CN_K2016_-Oct.pdf

[49] "STREAMLINE MK2 - High-pressure metering machines for HP-RTM." https://www.hennecke.com/us/products/dosing/hp/streamline (accessed Mar. 12, 2020).

[50] B. M. Simonet Suau and M. Galan Vallejo, "Procedimiento de fabricación automática y rápida de estructuras de composite mediante multi-inyección y moldeo por compresión," ES2463890A2, 2012 [Online]. Available: https://patents.google.com/patent/ES2463890A2/es?oq=ES2463890

[51] Airtificial, "RMCP," 2018. https://www.airtificial.com/pagina/rmcp/ (accessed Apr. 23, 2020).

[52] "Sinatec Electronics." http://sinatec.es/ (accessed Sep. 01, 2022).

[53] Airtificial, "Mobility. Descripción." http://carbures.com/index.php/2-uncategorised/572-mobility-descripcion (accessed Apr. 23, 2020).

[54] R. S. Davé and A. C. Loos, Eds., *Processing of composites*. Munich: Hanser, 2000. [Online]. Available: https://www.hanserpublications.com/Products/204-processing-of-composites.aspx

[55] C. Alabau Perich, "RTM MOULD DESIGN AND CONSTRUCTION FOR A DN 50 PN 16 RTM

mould design and construction for DN 50 PN 16 flansch," University of Girona, 2007. [Online]. Available: https://dugi-doc.udg.edu/bitstream/handle/10256/7492/1Projekt-Alabau.pdf?sequence=1&isAllowed=y

[56] C. D. Rudd, A. C. Long, K. N. Kendall, and C. G. E. Mangin, "Liquid moulding technologies : resin transfer moulding, structural reaction injection moulding, and related processing techniques," Woodhead Publishing Limited, 1997, pp. 38–41, 346. [Online]. Available: https://www.elsevier.com/books/liquid-moulding-technologies/rudd/978-1-85573-242-1

[57] M. Stute, "Darcy's law." https://www.ldeo.columbia.edu/~martins/climate_water/lectures/darcy.html

[58] T. S. Lundström and B. R. Gebart, "Influence from process parameters on void formation in resin transfer molding," *Polym. Compos.*, vol. 15, no. 1, pp. 25–33, 1994, doi: 10.1002/pc.750150105.

[59] S. Bickerton and S. G. Advani, "Characterization and modeling of race-tracking in liquidcomposite molding processes," *Compos. Sci. Technol.*, vol. 59, no. 15, pp. 2215–2229, Nov. 1999, doi: 10.1016/s0266-3538(99)00077-9.

[60] C. Kaynak and Y. O. Kas, "iga," *Polym. Polym. Compos.*, vol. 14, no. 1, pp. 55–64, 2006, doi: 10.1177/096739110601400105.

[61] G. P. Johari, J. G. McAnanama, and D. A. Wasylyshyn, "The effects of pressure and temperature on molecular dynamics during linear-chain polymerization by dielectric measurements," *J. Chem. Phys.*, vol. 105, no. 23, pp. 10621–10631, 1996, doi: 10.1063/1.472948.

[62] J. A. Ramos, N. Pagani, C. C. Riccardi, J. Borrajo, S. N. Goyanes, and I. Mondragon, "Cure kinetics and shrinkage model for epoxy-amine systems," *Polymer (Guildf).*, vol. 46, no. 10, pp. 3323–3328, 2005, doi: 10.1016/j.polymer.2005.02.069.

[63] J. C. Cruz and T. A. Osswald, "Monitoring epoxy and unsaturated polyester reactions under pressure-Reaction rates and mechanical properties," *Polym. Eng. Sci.*, vol. 49, no. 11, pp. 2099–2108, Nov. 2009, doi: 10.1002/pen.21448.

[64] Y.-J. Huang, T.-J. Lu, and W. Hwu, "Curing of unsaturated polyester resins - effects of pressure," *Polym. Eng. Sci.*, vol. 33, no. 1, pp. 1–17, Jan. 1993, doi: 10.1002/pen.760330102.

[65] C. D. Han, "Effect of Pressure on the Curing of Unsaturated Polyester," in *Rheology and Processing of Polymeric Materials: Volume 2: Polymer Processing*, 2007, pp. 555–556.

[66] N. Gushurst, T. Frerich, and A. S. Herrmann, "Investigations on the Influence of High Pressures on the Curing Behaviour and Material Properties of Composite Structures for the Development of a Material Model," in *Advances in Polymer Processing 2020*, Berlin, Heidelberg: Springer Berlin Heidelberg, 2020, pp. 313–323. doi: 10.1007/978-3-662-60809-8_26.

[67] F. Behnisch, P. Rosenberg, A. K. Weidenmann, and F. Henning, "Investigation of the matrix influence on the laminate properties of epoxy- and polyurethane-based CFRPs manufactured with HP-RTM-process," *AIP Conf. Proc.*, vol. 1914, 2017, doi: 10.1063/1.5016789.

[68] M. Etchells and C. Lira, "Online Viscosity and Tg Measurement of CFRP Manufactured Using High-Pressure RTM (HP-RTM)," *SAMPE J.*, pp. 24–33, 2020, [Online]. Available:

https://www.researchgate.net/publication/337482625_Online_Viscosity_and_Tg_Measurement_of_CFRP_manufactured_using_High-Pressure_RTM

[69] Y. Yang, Y. Xu, Y. Ji, and Y. Wei, "Functional epoxy vitrimers and composites," *Prog. Mater. Sci.*, no. February, p. 100710, 2020, doi: 10.1016/j.pmatsci.2020.100710.

[70] H. Liu, H. Zhang, H. Wang, X. Huang, G. Huang, and J. Wu, "Weldable, malleable and programmable epoxy vitrimers with high mechanical properties and water insensitivity," *Chem. Eng. J.*, vol. 368, no. February, pp. 61–70, 2019, doi: 10.1016/j.cej.2019.02.177.

[71] W. Denissen, J. M. Winne, and F. E. Du Prez, "Vitrimers: Permanent organic networks with glass-like fluidity," *Chem. Sci.*, vol. 7, no. 1, pp. 30–38, 2016, doi: 10.1039/c5sc02223a.

[72] R. A. Witik, R. Teuscher, V. Michaud, C. Ludwig, and J. A. E. Månson, "Carbon fibre reinforced composite waste: An environmental assessment of recycling, energy recovery and landfilling," *Compos. Part A Appl. Sci. Manuf.*, vol. 49, pp. 89–99, 2013, doi: 10.1016/j.compositesa.2013.02.009.

[73] Y. Yuan *et al.*, "Multiply fully recyclable carbon fibre reinforced heat-resistant covalent thermosetting advanced composites," *Nat. Commun.*, vol. 8, no. 1, p. 14657, Apr. 2017, doi: 10.1038/ncomms14657.

[74] I. Azcune and I. Odriozola, "Aromatic disulfide crosslinks in polymer systems: Self-healing, reprocessability, recyclability and more," *Eur. Polym. J.*, vol. 84, pp. 147–160, 2016, doi: 10.1016/j.eurpolymj.2016.09.023.

[75] D. Montarnal, M. Capelot, F. Tournilhac, and L. Leibler, "Silica-like malleable materials from permanent organic networks," *Science (80-.).*, vol. 334, no. 6058, pp. 965–968, 2011, doi: 10.1126/science.1212648.

[76] J. Han, T. Liu, C. Hao, S. Zhang, B. Guo, and J. Zhang, "A Catalyst-Free Epoxy Vitrimer System Based on Multifunctional Hyperbranched Polymer," *Macromolecules*, vol. 51, no. 17, pp. 6789–6799, 2018, doi: 10.1021/acs.macromol.8b01424.

[77] J. M. Winne, L. Leibler, and F. E. Du Prez, "Dynamic covalent chemistry in polymer networks: A mechanistic perspective," *Polym. Chem.*, vol. 10, no. 45, pp. 6091–6108, 2019, doi: 10.1039/c9py01260e.

[78] A. Ruiz de Luzuriaga *et al.*, "Epoxy resin with exchangeable disulfide crosslinks to obtain reprocessable, repairable and recyclable fiber-reinforced thermoset composites," *Mater. Horizons*, vol. 3, no. 3, pp. 241–247, 2016, doi: 10.1039/C6MH00029K.

[79] H. Si *et al.*, "Rapidly reprocessable, degradable epoxy vitrimer and recyclable carbon fiber reinforced thermoset composites relied on high contents of exchangeable aromatic disulfide crosslinks," *Compos. Part B Eng.*, vol. 199, no. June, p. 108278, 2020, doi: 10.1016/j.compositesb.2020.108278.

[80] D. A. Kissounko, P. Taynton, and C. Kaffer, "New material: vitrimers promise to impact composites," *Reinf. Plast.*, vol. 62, no. 3, pp. 162–166, 2018, doi: 10.1016/j.repl.2017.06.084.

[81] Y. Yang, G. Peng, S. Wu, and W. Hao, "A repairable anhydride-epoxy system with high mechanical properties inspired by vitrimers," *Polymer (Guildf).*, vol. 159, no. November, pp. 162–168, 2018, doi: 10.1016/j.polymer.2018.11.031.

[82] Q. Yu *et al.*, "Vanillin-based degradable epoxy vitrimers: Reprocessability and mechanical

properties study," *Eur. Polym. J.*, vol. 117, no. 1, pp. 55–63, 2019, doi: 10.1016/j.eurpolymj.2019.04.053.

[83] F. Ji, X. Liu, D. Sheng, and Y. Yang, "Epoxy-vitrimer composites based on exchangeable aromatic disulfide bonds: Reprocessibility, adhesive, multi-shape memory effect," *Polymer (Guildf).*, vol. 197, no. April, p. 122514, 2020, doi: 10.1016/j.polymer.2020.122514.

[84] X. Feng and G. Li, "Catalyst-free β-hydroxy phosphate ester exchange for robust fire-proof vitrimers," *Chem. Eng. J.*, vol. 417, p. 129132, Aug. 2021, doi: 10.1016/j.cej.2021.129132.

[85] B. Krishnakumar *et al.*, "Catalyst free self-healable vitrimer/graphene oxide nanocomposites," *Compos. Part B Eng.*, vol. 184, p. 107647, Mar. 2020, doi: 10.1016/j.compositesb.2019.107647.

[86] W. Zhao, L. An, and S. Wang, "Recyclable high-performance epoxy-anhydride resins with DMP-30 as the catalyst of transesterification reactions," *Polymers (Basel).*, vol. 13, no. 2, pp. 1–18, 2021, doi: 10.3390/polym13020296.

[87] Y. Liu *et al.*, "Catalyst-free malleable, degradable, bio-based epoxy thermosets and its application in recyclable carbon fiber composites," *Compos. Part B Eng.*, vol. 211, no. 1219, p. 108654, 2021, doi: 10.1016/j.compositesb.2021.108654.

[88] J. Zheng *et al.*, "Vitrimers: Current research trends and their emerging applications," *Mater. Today*, vol. xxx, no. xx, 2021, doi: 10.1016/j.mattod.2021.07.003.

[89] N. J. Van Zee and R. Nicolaÿ, "Vitrimers: Permanently crosslinked polymers with dynamic network topology," *Prog. Polym. Sci.*, vol. 104, p. 101233, 2020, doi: 10.1016/j.progpolymsci.2020.101233.

[90] W. Alabiso and S. Schlögl, "The impact of vitrimers on the industry of the future: Chemistry, properties and sustainable forward-looking applications," *Polymers (Basel).*, vol. 12, no. 8, 2020, doi: 10.3390/POLYM12081660.

[91] S. Weidmann, P. Volk, P. Mitschang, and N. Markaide, "Investigations on thermoforming of carbon fiber reinforced epoxy vitrimer composites," *Compos. Part A Appl. Sci. Manuf.*, vol. 154, no. September 2021, p. 106791, 2022, doi: 10.1016/j.compositesa.2021.106791.

[92] R. Martin *et al.*, "Dynamic sulfur chemistry as a key tool in the design of self-healing polymers," *Smart Mater. Struct.*, vol. 25, no. 8, 2016, doi: 10.1088/0964-1726/25/8/084017.

[93] B. Wang, S. Ma, S. Yan, and J. Zhu, "Readily recyclable carbon fiber reinforced composites based on degradable thermosets: A review," *Green Chem.*, vol. 21, no. 21, pp. 5781–5796, 2019, doi: 10.1039/c9gc01760g.

[94] Y. Zhu, F. Gao, J. Zhong, L. Shen, and Y. Lin, "Renewable castor oil and DL-limonene derived fully bio-based vinylogous urethane vitrimers," *Eur. Polym. J.*, vol. 135, no. May, p. 109865, 2020, doi: 10.1016/j.eurpolymj.2020.109865.

[95] S. Wang *et al.*, "Facile: In situ preparation of high-performance epoxy vitrimer from renewable resources and its application in nondestructive recyclable carbon fiber composite," *Green Chem.*, vol. 21, no. 6, pp. 1484–1497, 2019, doi: 10.1039/c8gc03477j.

[96] E. Chabert, J. Vial, J. P. Cauchois, M. Mihaluta, and F. Tournilhac, "Multiple welding of

long fiber epoxy vitrimer composites," *Soft Matter*, vol. 12, no. 21, pp. 4838–4845, 2016, doi: 10.1039/c6sm00257a.

[97] A. Ruiz De Luzuriaga *et al.*, "Transient mechanochromism in epoxy vitrimer composites containing aromatic disulfide crosslinks," *J. Mater. Chem. C*, vol. 4, no. 26, pp. 6220–6223, 2016, doi: 10.1039/c6tc02383e.

[98] J. C. Markwart *et al.*, "Intrinsic flame retardant phosphonate-based vitrimers as a recyclable alternative for commodity polymers in composite materials," *Polym. Chem.*, vol. 11, no. 30, pp. 4933–4941, 2020, doi: 10.1039/d0py00275e.

[99] W. Denissen, I. De Baere, W. Van Paepegem, L. Leibler, J. Winne, and F. E. Du Prez, "Vinylogous Urea Vitrimers and Their Application in Fiber Reinforced Composites," *Macromolecules*, vol. 51, no. 5, pp. 2054–2064, 2018, doi: 10.1021/acs.macromol.7b02407.

[100] I. De Baere, W. Denissen, W. Van Paepegem, J. Winne, and F. Du Prez, "Assessement of urea based vitrimers as a new matrix material for fibre reinforced polymers," in *ECCM18 - 18th European Conference on Composite*, 2018, p. 7. [Online]. Available: http://hdl.handle.net/1854/LU-8569138

[101] K. Yu, Q. Shi, M. L. Dunn, T. Wang, and H. J. Qi, "Carbon Fiber Reinforced Thermoset Composite with Near 100% Recyclability," *Adv. Funct. Mater.*, vol. 26, no. 33, pp. 6098–6106, Sep. 2016, doi: 10.1002/adfm.201602056.

[102] R. Martin, A. Rekondo, A. Ruiz De Luzuriaga, G. Cabañero, H. J. Grande, and I. Odriozola, "The processability of a poly(urea-urethane) elastomer reversibly crosslinked with aromatic disulfide bridges," *J. Mater. Chem. A*, vol. 2, no. 16, pp. 5710–5715, 2014, doi: 10.1039/c3ta14927g.

[103] Z. Zhou, Y. Zeng, C. Yu, Q. Li, and F. Zhang, "Intrinsically self-healing and stretchy poly(urethane-urea) elastomer based on dynamic urea bonds and thiol-ene click reaction," *Mater. Chem. Phys.*, vol. 267, no. August 2020, p. 124642, Jul. 2021, doi: 10.1016/j.matchemphys.2021.124642.

[104] M. K. Bangash, A. Ruiz de Luzuriaga, J. Aurrekoetxea, N. Markaide, H. J. Grande, and M. Ferraris, "Development and characterisation of dynamic bi-phase (epoxy/PU) composites for enhanced impact resistance," *Composites Part B: Engineering*, vol. 155. pp. 122–131, 2018. doi: 10.1016/j.compositesb.2018.08.039.

[105] P. Taynton *et al.*, "Repairable woven carbon fiber composites with full recyclability enabled by malleable polyimine networks," *Adv. Mater.*, vol. 28, no. 15, pp. 2904–2909, 2016, doi: 10.1002/adma.201505245.

[106] "MALLINDA vitrimer matrix composites for the circular economy." https://www.mallinda.com/

[107] L. Yu *et al.*, "Rapid Fabrication of Fiber-Reinforced Polyimine Composites with Reprocessability, Repairability, and Recyclability," *ACS Appl. Polym. Mater.*, vol. 3, no. 11, pp. 5808–5817, 2021, doi: 10.1021/acsapm.1c01027.

[108] S. Wang, X. Xing, X. Zhang, X. Wang, and X. Jing, "Room-temperature fully recyclable carbon fibre reinforced phenolic composites through dynamic covalent boronic ester bonds," *J. Mater. Chem. A*, vol. 6, no. 23, pp. 10868–10878, 2018, doi: 10.1039/c8ta01801d.

[109] X. Liu, Y. Li, X. Xing, G. Zhang, and X. Jing, "Fully recyclable and high performance phenolic

resin based on dynamic urethane bonds and its application in self-repairable composites," *Polymer (Guildf).*, vol. 229, no. April, 2021, doi: 10.1016/j.polymer.2021.124022.

[110] T. Liu *et al.*, "Carbon Fiber Reinforced Epoxy Vitrimer: Robust Mechanical Performance and Facile Hydrothermal Decomposition in Pure Water," *Macromol. Rapid Commun.*, vol. 42, no. 3, pp. 1–6, 2021, doi: 10.1002/marc.202000458.

[111] H. Wang *et al.*, "A Triple Crosslinking Design toward Epoxy Vitrimers and Carbon Fiber Composites of High Performance and Multi-shape Memory," *Chinese J. Polym. Sci. (English Ed.*, 2021, doi: 10.1007/s10118-021-2538-7.

[112] Y. Y. Liu, J. He, Y. D. Li, X. L. Zhao, and J. B. Zeng, "Biobased epoxy vitrimer from epoxidized soybean oil for reprocessable and recyclable carbon fiber reinforced composite," *Compos. Commun.*, vol. 22, no. August, p. 100445, 2020, doi: 10.1016/j.coco.2020.100445.

[113] Y. Y. Liu, G. L. Liu, Y. D. Li, Y. Weng, and J. B. Zeng, "Biobased High-Performance Epoxy Vitrimer with UV Shielding for Recyclable Carbon Fiber Reinforced Composites," *ACS Sustain. Chem. Eng.*, 2021, doi: 10.1021/acssuschemeng.1c00231.

[114] X. Liu, E. Zhang, Z. Feng, J. Liu, B. Chen, and L. Liang, "Degradable bio-based epoxy vitrimers based on imine chemistry and their application in recyclable carbon fiber composites," *J. Mater. Sci.*, vol. 56, no. 28, pp. 15733–15751, 2021, doi: 10.1007/s10853-021-06291-5.

[115] Y. Xu, S. Dai, L. Bi, J. Jiang, H. Zhang, and Y. Chen, "Catalyst-free self-healing bio-based vitrimer for a recyclable, reprocessable, and self-adhered carbon fiber reinforced composite," *Chem. Eng. J.*, vol. 429, no. September 2021, p. 132518, 2022, doi: 10.1016/j.cej.2021.132518.

[116] P. Li *et al.*, "Degradable benzyl cyclic acetal epoxy monomers with low viscosity: Synthesis, structure-property relationships, application in recyclable carbon fiber composite," *Compos. Sci. Technol.*, vol. 219, no. October 2021, p. 109243, 2022, doi: 10.1016/j.compscitech.2021.109243.

[117] X. An, Y. Ding, Y. Xu, J. Zhu, C. Wei, and X. Pan, "Epoxy resin with exchangeable diselenide crosslinks to obtain reprocessable, repairable and recyclable fiber-reinforced thermoset composites," *React. Funct. Polym.*, vol. 172, no. January, p. 105189, 2022, doi: 10.1016/j.reactfunctpolym.2022.105189.

[118] Y. Wang, B. Jin, D. Ye, and Z. Liu, "Fully recyclable carbon fiber reinforced vanillin-based epoxy vitrimers," *Eur. Polym. J.*, vol. 162, no. November 2021, p. 110927, 2022, doi: 10.1016/j.eurpolymj.2021.110927.

[119] T. Liu *et al.*, "A Self-Healable High Glass Transition Temperature Bioepoxy Material Based on Vitrimer Chemistry," *Macromolecules*, vol. 51, no. 15, pp. 5577–5585, 2018, doi: 10.1021/acs.macromol.8b01010.

[120] Y. Y. Liu, J. He, Y. D. Li, X. L. Zhao, and J. B. Zeng, "Biobased, reprocessable and weldable epoxy vitrimers from epoxidized soybean oil," *Ind. Crops Prod.*, vol. 153, no. February, p. 112576, 2020, doi: 10.1016/j.indcrop.2020.112576.

[121] X. Yang, L. Guo, X. Xu, S. Shang, and H. Liu, "A fully bio-based epoxy vitrimer: Self-healing, triple-shape memory and reprocessing triggered by dynamic covalent bond exchange," *Mater. Des.*, vol. 186, p. 108248, Jan. 2020, doi: 10.1016/j.matdes.2019.108248.

[122] P. Taynton, K. Yu, R. K. Shoemaker, Y. Jin, H. J. Qi, and W. Zhang, “Heat- or water-driven malleability in a highly recyclable covalent network polymer,” *Adv. Mater.*, vol. 26, no. 23, pp. 3938–3942, 2014, doi: 10.1002/adma.201400317.

[123] I. Aranberri, M. Landa, E. Elorza, A. M. Salaberria, and A. Rekondo, “Thermoformable and recyclable CFRP pultruded profile manufactured from an epoxy vitrimer,” *Polym. Test.*, vol. 93, no. October 2020, p. 106931, Jan. 2021, doi: 10.1016/j.polymertesting.2020.106931.

[124] F. Zhou *et al.*, “Preparation of self-healing, recyclable epoxy resins and low-electrical resistance composites based on double-disulfide bond exchange,” *Compos. Sci. Technol.*, vol. 167, no. July, pp. 79–85, Oct. 2018, doi: 10.1016/j.compscitech.2018.07.041.

[125] H. Fang, W. Ye, K. Yang, K. Song, H. Wei, and Y. Ding, “Vitrimer chemistry enables epoxy nanocomposites with mechanical robustness and integrated conductive segregated structure for high performance electromagnetic interference shielding,” *Compos. Part B Eng.*, vol. 215, p. 108782, 2021, doi: 10.1016/j.compositesb.2021.108782.

[126] X. Li, J. Zhang, L. Zhang, A. Ruiz de Luzuriaga, A. Rekondo, and D.-Y. Wang, “Recyclable flame-retardant epoxy composites based on disulfide bonds: Flammability and recyclability,” *Compos. Commun.*, vol. 25, p. 100754, Jun. 2021, doi: 10.1016/j.coco.2021.100754.

[127] “AIRPOXY - ThermoformAble, repaIrable & bondable smaRt ePOXY-based composites for aero structures.” https://www.airpoxy.eu/

[128] European Commision, “ThermoformAble, repaIrable and bondable smaRt ePOXY based composites for aero structures,” 2018. https://cordis.europa.eu/project/id/769274

[129] Hexcel Corporation, “HexPly® 8552,” 2020. https://www.hexcel.com/user_area/content_media/raw/HexPly_8552_eu_DataSheet.pdf

[130] Hexion, “EPIKOTE™ Resin 475 and EPIKURE™ Curing Agent 375 and HELOXY™ Additive 575,” 2021. https://www.hexion.com/CustomServices/PDFDownloader.aspx?type=tds&pid=77f8c63d-5814-6fe3-ae8a-ff0300fcd525

[131] U. Beier, F. Fischer, J. K. W. Sandler, V. Altstädt, C. Weimer, and W. Buchs, “Mechanical performance of carbon fibre-reinforced composites based on stitched preforms,” *Compos. Part A Appl. Sci. Manuf.*, vol. 38, no. 7, pp. 1655–1663, 2007, doi: 10.1016/j.compositesa.2007.02.007.

[132] J. Juan, A. Silva, J. A. Tornero, J. Gámez, and N. Salán, “Void content minimization in vacuum infusion (VI) via effective degassing,” *Polymers (Basel).*, vol. 13, no. 17, pp. 1–23, 2021, doi: 10.3390/polym13172876.

[133] H. Jeong, “Effects of Voids on the Mechanical Strength and Ultrasonic Attenuation of Laminated Composites,” *J. Compos. Mater.*, vol. 31, no. 3, pp. 276–292, Feb. 1997, doi: 10.1177/002199839703100303.

[134] A. R. Chambers, J. S. Earl, C. A. Squires, and M. A. Suhot, “The effect of voids on the flexural fatigue performance of unidirectional carbon fibre composites developed for wind turbine applications,” *Int. J. Fatigue*, vol. 28, no. 10 SPEC. ISS., pp. 1389–1398, 2006, doi: 10.1016/j.ijfatigue.2006.02.033.

[135] DowAksa, “12K A-42 Technical Data Sheet,” 2016. https://www.dowaksa.com/wp-

content/uploads/2016/03/12K-A-42S.pdf (accessed Oct. 27, 2021).

[136] S. G. & Co., "Saertex B-C-416g/m2-1270mm." [Online]. Available: https://www.saertex.com/en

[137] Chomarat, "C-WEAVE™ 280SA5 T800HB 6K." https://composites.chomarat.com/en/product/c-weave-280sa5-t800hb-6k/

[138] A. De Fontgallant and D. Calderón, "AIRPOXY Deliverable 1.3: Report on the preliminary analysis and definition of specifications for the raw materials," 2019. https://www.airpoxy.eu/wp-content/uploads/AIRPOXY-D1.3-Preliminary-specifications-for-the-raw-materials_R1.0.pdf

[139] D. Calderón, R. González, and A. De Fontgallant, "AIRPOXY Deliverable 1.1: Report on the preliminary specifications for demonstrators," 2019. https://www.airpoxy.eu/wp-content/uploads/AIRPOXY-D1.1-Preliminary-specifications-for-demonstrators_R1.0.pdf

[140] Sicomin, "Pultrusion and filament winding," 2014. http://sicomin.com/products/epoxy-systems/pultrusion-filament-winding

[141] Hexcel Corporation, "HexFlow® RTM6," 2018. https://www.hexcel.com/user_area/content_media/raw/RTM6_DataSheetPDF.pdf

[142] I. Odriozola *et al.*, "Thermomechanically reprocessable epoxy composites and processes for their manufacturing," WO2015181054 A1, 2015 [Online]. Available: https://patents.google.com/patent/CA2949583A1/ja

[143] I. Odriozola *et al.*, "Composites de epoxi reprocesables termomecánicamente y procedimientos para su fabricación," ES2682954 T3, 2015 [Online]. Available: https://patents.google.com/patent/ES2682954T3/es?assignee=cidetec&oq=cidetec

[144] INP96, "INFUSIÓN DE RESINA Y MOLDEO POR VACÍO," 2021. https://inp96.es/infusion-y-vacio/ (accessed Sep. 08, 2021).

[145] GAZECHIM COMPOSITES IBÉRICA, "DESMOLDEANTES." https://www.gazechim.es/category/productos/desmoldeantes/

[146] A. S. Chemicals, "Antala Automoción." https://www.antala.es/sector/automocion/

[147] Huntsman, "Araldite® composite solutions provide fast curing where high productivity is required." https://www.huntsman-transportation.com/automotive-composites/body-in-white.html

[148] Cronaser, "Corium Lubricants." https://cronaser.com/grasas-corium/?highlight=antiseize (accessed Sep. 06, 2022).

[149] Horizon 2020, "Out of autoclave processes development for composite frames manufacturing with high production rate and low cost (COFRARE 2.0)," 717070, 2018 [Online]. Available: https://cordis.europa.eu/project/id/717070

[150] Horizon 2020, "Out of autoclave technologies for frame and shear tie of Regional Aircraft (COFRARE 2020)," 821261, 2020 [Online]. Available: https://cordis.europa.eu/project/id/821261

[151] P. Simacek, Ö. Eksik, D. Heider, J. W. Gillespie, and S. Advani, "Experimental validation of post-filling flow in vacuum assisted resin transfer molding processes," *Compos. Part A Appl. Sci. Manuf.*, vol. 43, no. 3, pp. 370–380, 2012, doi: 10.1016/j.compositesa.2011.10.002.

[152] K. A. Olivero, H. J. Barraza, E. A. O'Rear, and M. C. Altan, "Effect of Injection Rate and Post-Fill Cure Pressure on Properties of Resin Transfer Molded Disks," *J. Compos. Mater.*, vol. 36, no. 16, pp. 2011–2028, Aug. 2002, doi: 10.1177/0021998302036016244.

[153] W. C. Lyons, "Basic Principles, Definitions, and Data," in *Working Guide to Reservoir Engineering*, Elsevier, 2010, pp. 1–95. doi: 10.1016/B978-1-85617-824-2.00001-0.

[154] Y. Matsuhisa and A. R. Bunsell, "Tensile failure of carbon fibers," in *Handbook of Tensile Properties of Textile and Technical Fibres*, Elsevier, 2009, pp. 574–602. doi: 10.1533/9781845696801.2.575.

[155] Y.-P. Jeon, R. Alway-Cooper, M. Morales, and A. A. Ogale, "Carbon Fibers," in *Handbook of Advanced Ceramics*, Elsevier, 2013, pp. 143–154. doi: 10.1016/B978-0-12-385469-8.00009-5.

[156] 900GPa, "HEXCEL HexForce ® G0926 D 1304 TCT." https://www.900gpa.com/es/product/fabric/WovenCombo_00A23AD07F?u=metric

[157] Teijin, "Tenax Filament yarn." https://www.teijincarbon.com/fileadmin/PDF/Datenblätter_en/Product_Data_Sheet_TSG01en__EU_Filament_.pdf

[158] International Organization for Standardization, "Plastics — Determination of tensile properties — Part 2: Test conditions for moulding and extrusion plastics," ISO 527-2:2012, 2012 [Online]. Available: https://www.iso.org/standard/56046.html

[159] International Organization for Standardization, "Plastics — Determination of flexural properties," ISO 178:2019, 2019 [Online]. Available: https://www.iso.org/standard/70513.html

[160] International Organization for Standardization, "Plastics — Determination of tensile properties — Part 4: Test conditions for isotropic and orthotropic fibre-reinforced plastic composites," ISO 527-4:1997, 1997 [Online]. Available: https://www.iso.org/standard/4595.html

[161] International Organization for Standardization, "Fibre-reinforced plastic composites — Determination of compressive properties in the in-plane direction," ISO 14126:1999 [Online]. Available: https://www.iso.org/standard/23638.html

[162] ASTM International, "Standard Test Method for Compressive Properties of Polymer Matrix Composite Materials," ASTM D3410 / D3410M, 2016 doi: 10.1520/D3410_D3410M-16E01.

[163] International Organization for Standardization, "Fibre-reinforced plastic composites — Determination of flexural properties," ISO 14125:1998, 1998 [Online]. Available: https://www.iso.org/standard/23637.html

[164] International Organization for Standardization, "Fibre-reinforced plastic composites Determination of apparent interlaminar shear strength by short-beam method," ISO 14130:1997 [Online]. Available: https://www.iso.org/standard/23642.html

[165] International Organization for Standardization, "Fibre-reinforced plastic composites — Determination of the stress / shear strain response , including the in-plane shear modulus and strength by the ± 45 ° tension test method," ISO 14129:1997, 1998 [Online]. Available: https://www.iso.org/standard/23641.html

[166] ASTM International, "Standard Test Method for Open-Hole Tensile Strength of Polymer

Matrix Composite Laminates," ASTM D5766 / D5766M-11(2018), 2008 doi: 10.1520/D5766_D5766M-11R18.

[167] ASTM International, "Standard Test Method for Open-Hole Compressive Strength of Polymer Matrix," ASTM D6484 / D6484M-20 doi: 10.1520/D6484_D6484M-20.

[168] ASTM International, "Standard Practice for Filled-Hole Tension and Compression Testing of Polymer Matrix Composite Laminates," ASTM D6742 / D6742M-17 doi: 10.1520/D6742_D6742M-17.

[169] UNE, "Aerospace series - Carbon fibre reinforced plastics - Test method - Determination of interlaminar fracture toughness energy - Mode I - GIC," UNE-EN 6033:2015 [Online]. Available: https://www.aenor.com/normas-y-libros/buscador-de-normas/une/?c=N0055912

[170] UNE, "Aerospace series - Carbon fibre reinforced plastics - Test method - Determination of interlaminar fracture toughness energy - Mode II - GIIC (Endorsed by AENOR in January of 2016.)," UNE-EN 6034:2015 [Online]. Available: https://www.une.org/encuentra-tu-norma/busca-tu-norma/norma?c=N0055913

[171] International Organization for Standardization, "Plastics — Differential scanning calorimetry (DSC) — Part 2: Determination of glass transition temperature and step height," ISO 11357-2:2020 [Online]. Available: https://www.iso.org/standard/77310.html

[172] S. Saseendran, M. Wysocki, and J. Varna, "Evolution of viscoelastic behavior of a curing LY5052 epoxy resin in the glassy state," *Adv. Manuf. Polym. Compos. Sci.*, vol. 2, no. 2, pp. 74–82, Apr. 2016, doi: 10.1080/20550340.2016.1236223.

[173] Asociación Española de Normalización, "Aerospace series - Carbon fibre laminates - Determination of the fibre, resin and void contents," UNE-EN 2564:2018, 2018 [Online]. Available: https://www.une.org/encuentra-tu-norma/busca-tu-norma/norma?c=N0060716

[174] ASTM International, "Standard Test Methods for Constituent Content of Composite Materials," ASTM D3171-06, 2006 doi: 10.1520/D3171-06.

[175] International Organization for Standardization, "Plastics — Methods for determining the density of non-cellular plastics — Part 1: Immersion method, liquid pycnometer method and titration method," ISO 1183-1:2019, 2019

[176] PRIAMUS SYSTEM TECHNOLOGIES, "GLOSSARY IMPORTANT TERMS FROM PROCESS TECHNOLOGY." https://www.priamus.com/en/services/glossary

[177] PRIAMUS SYSTEM TECHNOLOGIES, "PRIAMUS PRODUCTS." https://www.priamus.com/en/products

[178] O. Mack, "New procedures to characterize drift and non-linear effects of piezoelectric force sensors," *17th IMEKO TC3 Conf. Force, Mass Torque 2001*, pp. 141–148, 2001.

[179] R. Otmani, N. Benmoussa, and B. Benyoucef, "The thermal drift characteristics of piezoresistive pressure sensor," *Phys. Procedia*, vol. 21, pp. 47–52, 2011, doi: 10.1016/j.phpro.2011.10.008.

[180] S. Costa, P. F. Teixeira, J. A. Covas, and L. Hilliou, "Assessment of piezoelectric sensors for the acquisition of steady melt pressures in polymer extrusion," *Fluids*, vol. 4, no. 2, 2019, doi: 10.3390/fluids4020066.

[181] D. A. Van Den Ende, W. A. Groen, and S. Van Der Zwaag, “Development of temperature stable charge based piezoelectric composite quasi-static pressure sensors,” *Sensors Actuators, A Phys.*, vol. 163, no. 1, pp. 25–31, 2010, doi: 10.1016/j.sna.2010.06.010.

[182] L. Quagliarella, N. Sasanelli, and V. Monaco, “Drift in posturography systems equipped with a piezoelectric force platform: Analysis and numerical compensation,” *IEEE Trans. Instrum. Meas.*, vol. 57, no. 5, pp. 997–1004, 2008, doi: 10.1109/TIM.2007.913833.

[183] D. Harvey, “10.4: Using R to Clean Up Data,” 2021. https://chem.libretexts.org/Bookshelves/Analytical_Chemistry/Chemometrics_Using_R_(Harvey)/10%3A_Cleaning_Up_Data/10.4%3A_Using_R_to_Clean_Up_Data (accessed Feb. 02, 2022).

[184] NETZSCH-Gerätebau GmbH, “DEA 288 Ionic - Dielectric Analyzer Opening a New World of Cure Monitoring.”

[185] NETZSCH-Gerätebau GmbH, “Curing of Thermosetting Resins for Fiber-Reinforced Parts,” 2011. [Online]. Available: https://d2brmtk65c6tyc.cloudfront.net/media/thermal-analysis/white-paper/White_Paper_Curing_of_Thermosetting_Resins_for_Fiber-Reinforced_Parts.pdf?1426281757&Policy=eyJTdGF0ZW1lbnQiOlt7IlJlc291cmNlIjoiaHR0cHM6XC9cL2QyYnJtdGs2NWM2dHljLmNsb3VkZnJvbnQubmV0XC

[186] H. L. Lee, *The Handbook of Dielectric Analysis and Cure Monitoring*, 1st ed. Cambridge: Lambient Technologies LLC, 2017. [Online]. Available: https://static1.squarespace.com/static/59627b143e00be4fb1e3aed9/t/59b9c58f18b27db13da22af4/1505346973511/DielectricAnalysisCureMonitoringHandbook.pdf

[187] “NETZSCH Group.” https://www.netzsch.com/

[188] J. Gotro, “Dielectric Cure Monitoring Part 13: Equipment for Dielectric Cure Monitoring,” *Polymer Innovation Blog*, 2015. https://polymerinnovationblog.com/dielectric-cure-monitoring-part-13-equipment-for-dielectric-cure-monitoring/ (accessed Feb. 14, 2022).

[189] B. Z. Jang and W. K. Shih, “Techniques for cure monitoring of thermoset resins and composites - a review,” *Mater. Manuf. Process.*, vol. 5, no. 2, pp. 301–331, 1990, doi: 10.1080/10426919008953248.

[190] Isojet Equipements, “INJECTION RTM & INFUSION UNIT”, [Online]. Available: https://www.isojet.com/en/machine-en/injection-rtm-infusion-unit-9.html

[191] Coexpair, “Production workstation,” 2021. http://coexpair2.com.apache11.hostbasket.com/#production-workstation (accessed Sep. 21, 2021).

[192] Single Temperiertechnik GmbH, “Compact water tank TK,” 2020. https://single-temp.de/en/products/water-operated/wassertemperiersysteme/33/compact-water-tank-tk?c=24

[193] “Tool Temp Ltd.” https://www.tool-temp.net/

[194] Dilube SA, “THERMAL OILS.” http://dilube.com/en/product/thermal-oils-2/ (accessed Oct. 15, 2021).

[195] MTS Systems, “Series 322 Test Systems,” 2021. https://www.mts.com/en/products/materials/dynamic-materials-test-systems/series-322-test-systems (accessed Sep. 21, 2021).

[196] ULT AG, “ACD 200.1 A6 – compact extraction unit for odors, gases and vapors.”

https://www.ult.de/en/products-and-services/process-solutions/odour-gas-vapour/acd-200-a6-compact-extraction-unit.html (accessed Oct. 04, 2021).

[197] Novodinámica, “Apiladores eléctricos y manuales. Ref: 16018.” http://www.novodinamica.com/es/apiladores/apiladores-electricos-y-manuales/apilador-eleva-1200-kg-a-3580-mm/4/25/143 (accessed Oct. 04, 2021).

[198] Eurecat, “Materials Compòsits,” 2015. https://eurecat.org/ambits-de-coneixement/materials-composits/ (accessed Oct. 28, 2021).

[199] Eurecat, “Nous Processos de Fabricació,” 2015. https://eurecat.org/ambits-de-coneixement/nous-processos-fabricacio/ (accessed Oct. 28, 2021).

[200] “MSX Technology S.r.l.,” 2020. http://www.msxtec.com/

[201] Eurecat, “Functional Textiles,” 2015. https://eurecat.org/en/field-of-knowledge/functional-textiles/ (accessed Sep. 09, 2021).

[202] Montero Sealing and Insulation Technology, “BELPA ® MATERIALES PARA JUNTAS /BELPA ® CSA 90.” https://www.monterofye.com/materiales-para-juntas/belpa-csa-90/ (accessed Jan. 13, 2022).

[203] CNC Cookbook, “Complete Guide to Surface Finish Symbols, Charts, RA, RZ, Measurements, and Callouts.” https://www.cnccookbook.com/surface-finish-chart-symbols-measure-calculators/

[204] UNE, “General tolerances - Part 1: Tolerances for lineal and angular dimensions without individual tolerance indications (ISO 2768-1:1989),” UNE-EN 22768-1:1994, 1994 [Online]. Available: https://www.une.org/encuentra-tu-norma/busca-tu-norma/norma?c=N0010984

[205] UNE, “General tolerances - Part 2: Geometrical tolerances for features without individual tolerance indications (ISO 2768-2:1989),” UNE-EN 22768-2:1994, 1994 [Online]. Available: https://www.une.org/encuentra-tu-norma/busca-tu-norma/norma/?c=N0010985

[206] Stahlhandel Gröditz GmbH, “1.2311 (40CRMNMO7) QUENCHED AND TEMPERED 280 - 325 HB.” https://www.stahlportal.com/en/stock/12311-40crmnmo7-quenched-and-tempered-280-325-hb/

[207] Stahlhandel Gröditz GmbH, “1.2312 (40CRMNMOS8-6) MATERIAL DATA SHEET.” https://www.stahlportal.com/en/stock/12312-40crmnmos8-6-quenched-and-tempered-280-325-hb/

[208] Epidor, “O-Ring Catalogue,” 2020.

[209] J. E. Shigley, L. D. Mitchell, and H. Saunders, “Mechanical Engineering Design (4th Ed.),” *J. Mech. Transm. Autom. Des.*, vol. 107, no. 2, pp. 145–145, Jun. 1985, doi: 10.1115/1.3258702.

[210] R. Busqué and A. Brigido, “Internal report: VERIFICACIÓ MECÀNICA DE L’ESTABILITAT DEL MOTLLO, MITJANÇANT SIMULACIÓ ESTRUCTURAL,” Cerdanyola del Vallès, 2020. [Online]. Available: https://eurecat.org/en/field-of-knowledge/product-development/

[211] ANSYS, “ANSYS Workbench.” https://www.ansys.com/products/ansys-workbench (accessed Sep. 06, 2022).

[212] R. Busqué and A. Brigido, “Internal report: VERIFICACIÓ MECÀNICA DE L’ESTABILITAT DEL

MOTLLO, MITJANÇANT SIMULACIÓ ESTRUCTURAL. (Simulació d'escalfament)," 2020. [Online]. Available: https://eurecat.org/es/ambitos-de-conocimiento/desarrollo-de-producto/

[213] E. Shashi Menon, "Fluid Flow in Pipes," in *Transmission Pipeline Calculations and Simulations Manual*, Elsevier, 2015, pp. 149–234. doi: 10.1016/B978-1-85617-830-3.00005-5.

[214] M. Mehdikhani, L. Gorbatikh, I. Verpoest, and S. V Lomov, "Voids in fiber-reinforced polymer composites: A review on their formation, characteristics, and effects on mechanical performance," *J. Compos. Mater.*, vol. 53, no. 12, pp. 1579–1669, May 2019, doi: 10.1177/0021998318772152.

[215] M. Michel and E. Ferrier, "Effect of curing temperature conditions on glass transition temperature values of epoxy polymer used for wet lay-up applications," *Constr. Build. Mater.*, vol. 231, p. 117206, 2020, doi: 10.1016/j.conbuildmat.2019.117206.

[216] D. S. Kumar, M. J. Shukla, K. K. Mahato, D. K. Rathore, R. K. Prusty, and B. C. Ray, "Effect of post-curing on thermal and mechanical behavior of GFRP composites," *IOP Conf. Ser. Mater. Sci. Eng.*, vol. 75, p. 012012, Feb. 2015, doi: 10.1088/1757-899X/75/1/012012.

[217] G. Levita, S. De Petris, A. Marchetti, and A. Lazzeri, "Crosslink density and fracture toughness of epoxy resins," *J. Mater. Sci.*, vol. 26, no. 9, pp. 2348–2352, 1991, doi: 10.1007/BF01130180.

[218] Sicomin, "SR InfuGreen 810 / SD 882X", [Online]. Available: http://sicomin.com/datasheets/product-pdf1243.pdf

[219] A. Nishimura *et al.*, "EFFECT OF RADIUS OF LOADING NOSE AND SUPPORTS IN SHORT BEAM TEST FIXTURE ON FRACTURE MODE AND INTERLAMINAR SHEAR STRENGTH OF GFRP AT 77 K," in *AIP Conference Proceedings*, 2008, vol. 986, pp. 50–59. doi: 10.1063/1.2900391.

[220] ASTM International, "Standard Test Method for Short-Beam Strength of Polymer Matrix Composite Materials and Their Laminates," ASTM D2344/D2344M-16, 2016 doi: 10.1520/D2344_D2344M-16.

[221] E. Elkazaz, W. A. Crosby, A. M. Ollick, and M. Elhadary, "Effect of fiber volume fraction on the mechanical properties of randomly oriented glass fiber reinforced polyurethane elastomer with crosshead speeds," *Alexandria Eng. J.*, vol. 59, no. 1, pp. 209–216, Feb. 2020, doi: 10.1016/j.aej.2019.12.024.

[222] H. H. K. Xu, C. P. Ostertag, L. M. Braun, and I. K. Lloyd, "Effects of Fiber Volume Fraction on Mechanical Properties of SiC-Fiber/Si3N4-Matrix Composites," *J. Am. Ceram. Soc.*, vol. 77, no. 7, pp. 1897–1900, Jul. 1994, doi: 10.1111/j.1151-2916.1994.tb07068.x.

[223] J. I. P. Singh, S. Singh, and V. Dhawan, "Influence of fiber volume fraction and curing temperature on mechanical properties of jute/PLA green composites," *Polym. Polym. Compos.*, vol. 28, no. 4, pp. 273–284, May 2020, doi: 10.1177/0967391119872875.

[224] H. He and F. Gao, "Effect of Fiber Volume Fraction on the Flexural Properties of Unidirectional Carbon Fiber/Epoxy Composites," *Int. J. Polym. Anal. Charact.*, vol. 20, no. 2, pp. 180–189, Feb. 2015, doi: 10.1080/1023666X.2015.989076.

[225] X. Liu and F. Chen, "A review of void formation and its effects on the mechanical performance of carbon fiber reinforced plastic," *Eng. Trans.*, vol. 64, no. 1, pp. 33–51, 2016.

[226] C. Pasco, “Characterisation of the Thermoset Prepreg Compression Moulding Characterisation of the Thermoset Prepreg Compression Moulding Process,” no. July, 2018.

[227] R. Gonzalez Henriquez and P. Mertiny, “3.21 Filament Winding Applications,” in *Comprehensive Composite Materials II*, Elsevier, 2018, pp. 556–577. doi: 10.1016/B978-0-12-803581-8.10313-3.

[228] S. Y. Kim, K. H. Kim, and Y. Kim, “Comparative study on pressure sensors for sloshing experiment,” *Ocean Eng.*, vol. 94, pp. 199–212, 2015, doi: 10.1016/j.oceaneng.2014.11.014.

[229] PRIAMUS SYSTEM TECHNOLOGIES, “Data sheet: Standard and Miniature Cavity Pressure Sensors.” https://www.priamus.com/sites/default/files/2021-10/DS094e Standard and Miniature Cavity Pressure Sensors Ed 10_21.pdf

[230] G. Gardiner, “The rise of HP-RTM,” 2015. https://www.compositesworld.com/articles/the-rise-of-hp-rtm (accessed Apr. 06, 2020).

[231] R. Delasi and J. Whiteside, “Effect of Moisture on Epoxy Resins and Composites,” in *Advanced Composite Materials—Environmental Effects*, 100 Barr Harbor Drive, PO Box C700, West Conshohocken, PA 19428-2959: ASTM International, pp. 2-2–19. doi: 10.1520/STP34855S.

[232] J. I. Cauich-Cupul, E. Pérez-Pacheco, A. Valadez-González, and P. J. Herrera-Franco, “Effect of moisture absorption on the micromechanical behavior of carbon fiber/epoxy matrix composites,” *J. Mater. Sci.*, vol. 46, no. 20, pp. 6664–6672, 2011, doi: 10.1007/s10853-011-5619-0.

[233] E. Toumpanaki, J. M. Lees, M. Barbezat, and G. P. Terrasi, “Effect of internal moisture content on the TG values of CFRP rods,” *9th Int. Conf. Fibre-Reinforced Polym. Compos. Civ. Eng. CICE 2018*, vol. 2018-July, pp. 112–118, 2018.

[234] N. Sharp, C. Li, A. Strachan, D. Adams, and R. B. Pipes, “Effects of water on epoxy cure kinetics and glass transition temperature utilizing molecular dynamics simulations,” *J. Polym. Sci. Part B Polym. Phys.*, vol. 55, no. 15, pp. 1150–1159, 2017, doi: 10.1002/polb.24357.

[235] T. Liu *et al.*, “Fully recyclable, flame-retardant and high-performance carbon fiber composites based on vanillin-terminated cyclophosphazene polyimine thermosets,” *Compos. Part B Eng.*, vol. 224, no. June, p. 109188, 2021, doi: 10.1016/j.compositesb.2021.109188.

[236] H. Hamada, N. Oya, K. Yamashita, and Z.-I. Maekawa, “Tensile Strength and its Scatter of Unidirectional Carbon Fibre Reinforced Composites,” *J. Reinf. Plast. Compos.*, vol. 16, no. 2, pp. 119–130, Jan. 1997, doi: 10.1177/073168449701600202.

[237] R. Maurin, P. Davies, N. Baral, and C. Baley, “Transverse Properties of Carbon Fibres by Nano-Indentation and Micro-mechanics,” *Appl. Compos. Mater.*, vol. 15, no. 2, pp. 61–73, Mar. 2008, doi: 10.1007/s10443-008-9057-3.

[238] B. Beylergil, M. Tanoğlu, and E. Aktaş, “Effect of polyamide-6,6 (PA 66) nonwoven veils on the mechanical performance of carbon fiber/epoxy composites,” *Compos. Struct.*, vol. 194, no. February, pp. 21–35, 2018, doi: 10.1016/j.compstruct.2018.03.097.

[239] B. Beylergil, M. Tanoğlu, and E. Aktaş, “Enhancement of interlaminar fracture toughness

of carbon fiber–epoxy composites using polyamide-6,6 electrospun nanofibers," *J. Appl. Polym. Sci.*, vol. 134, no. 35, pp. 1–12, 2017, doi: 10.1002/app.45244.

[240] D. Quan, F. Bologna, G. Scarselli, A. Ivankovic, and N. Murphy, "Interlaminar fracture toughness of aerospace-grade carbon fibre reinforced plastics interleaved with thermoplastic veils," *Compos. Part A Appl. Sci. Manuf.*, vol. 128, no. June 2019, p. 105642, 2020, doi: 10.1016/j.compositesa.2019.105642.

[241] S. M. García-Rodríguez, J. Costa, K. E. Rankin, R. P. Boardman, V. Singery, and J. A. Mayugo, "Interleaving light veils to minimise the trade-off between mode-I interlaminar fracture toughness and in-plane properties," *Compos. Part A Appl. Sci. Manuf.*, vol. 128, p. 105659, Jan. 2020, doi: 10.1016/j.compositesa.2019.105659.

[242] D. Quan, F. Bologna, G. Scarselli, A. Ivanković, and N. Murphy, "Mode-II fracture behaviour of aerospace-grade carbon fibre/epoxy composites interleaved with thermoplastic veils," *Compos. Sci. Technol.*, vol. 191, no. February, p. 108065, 2020, doi: 10.1016/j.compscitech.2020.108065.

[243] C. Monteserín *et al.*, "Effect of Different Types of Electrospun Polyamide 6 Nanofibres on the Mechanical Properties of Carbon Fibre/Epoxy Composites," *Polymers (Basel).*, vol. 10, no. 11, p. 1190, Oct. 2018, doi: 10.3390/polym10111190.

[244] D. Quan, R. Alderliesten, C. Dransfeld, N. Murphy, A. Ivanković, and R. Benedictus, "Enhancing the fracture toughness of carbon fibre/epoxy composites by interleaving hybrid meltable/non-meltable thermoplastic veils," *Compos. Struct.*, vol. 252, p. 112699, Nov. 2020, doi: 10.1016/j.compstruct.2020.112699.

[245] D. Quan *et al.*, "The influence of interlayer/epoxy adhesion on the mode-I and mode-II fracture response of carbon fibre/epoxy composites interleaved with thermoplastic veils," *Mater. Des.*, vol. 192, p. 108781, Jul. 2020, doi: 10.1016/j.matdes.2020.108781.

[246] C. Cheng *et al.*, "Simultaneously improving mode I and mode II fracture toughness of the carbon fiber/epoxy composite laminates via interleaved with uniformly aligned PES fiber webs," *Compos. Part A Appl. Sci. Manuf.*, vol. 129, p. 105696, Feb. 2020, doi: 10.1016/j.compositesa.2019.105696.

[247] L. Daelemans, S. van der Heijden, I. De Baere, H. Rahier, W. Van Paepegem, and K. De Clerck, "Nanofibre bridging as a toughening mechanism in carbon/epoxy composite laminates interleaved with electrospun polyamide nanofibrous veils," *Compos. Sci. Technol.*, vol. 117, pp. 244–256, Sep. 2015, doi: 10.1016/j.compscitech.2015.06.021.

[248] V. A. Ramirez, P. J. Hogg, and W. W. Sampson, "The influence of the nonwoven veil architectures on interlaminar fracture toughness of interleaved composites," *Compos. Sci. Technol.*, vol. 110, pp. 103–110, Apr. 2015, doi: 10.1016/j.compscitech.2015.01.016.

[249] L. Zhu, "Investigations on damage resistance of carbon fiber composite panels toughened using veils," *Chinese J. Aeronaut.*, vol. 26, no. 3, pp. 807–813, 2013, doi: 10.1016/j.cja.2013.05.006.

[250] S. M. García-Rodríguez, J. Costa, V. Singery, I. Boada, and J. A. Mayugo, "The effect interleaving has on thin-ply non-crimp fabric laminate impact response: X-ray tomography investigation," *Compos. Part A Appl. Sci. Manuf.*, vol. 107, no. November 2017, pp. 409–420, 2018, doi: 10.1016/j.compositesa.2018.01.023.

[251] S. Yu and J. S. Colton, "A compact open-hole compression test fixture for composite materials," *Compos. Part B Eng.*, vol. 223, p. 109126, Oct. 2021, doi:

10.1016/j.compositesb.2021.109126.

[252] Instron, “Composites Test Fixtures Open-Hole Compression.” https://www.instron.com/-/media/literature-library/products/2014/03/composites-test-fixtures-open-hole-compression.pdf

[253] Intertek, “Tensile Strength (Open Hole) of Polymer Matrix Composite Laminates Testing.” https://www.intertek.com/polymers/tensile-testing/open-hole/#:~:text=Open Hole Tensile ASTM D5766,sectional area%2C disregarding the hole.

[254] Z. Wu, X. S. Yi, and A. Wilkinson, “Interlaminar fracture toughness of carbon fibre/RTM6-2 composites toughened with thermoplastic-coated fabric reinforcement,” *Compos. Part B Eng.*, vol. 130, pp. 192–199, 2017, doi: 10.1016/j.compositesb.2017.08.003.

[255] G. W. Beckermann and K. L. Pickering, “Mode I and Mode II interlaminar fracture toughness of composite laminates interleaved with electrospun nanofibre veils,” *Compos. Part A Appl. Sci. Manuf.*, vol. 72, pp. 11–21, 2015, doi: 10.1016/j.compositesa.2015.01.028.

[256] M. Kuwata and P. J. Hogg, “Interlaminar toughness of interleaved CFRP using non-woven veils: Part 2. Mode-II testing,” *Compos. Part A Appl. Sci. Manuf.*, vol. 42, no. 10, pp. 1560–1570, 2011, doi: 10.1016/j.compositesa.2011.07.017.

[257] G. Gardiner, “Reprocessable, repairable and recyclable epoxy resins for composites,” *Composites World*, 2021. https://www.compositesworld.com/articles/reprocessable-repairable-and-recyclable-epoxy-resins-for-composites